University of Naples Federico II

Polytechnic and Basic Sciences School

Department of Chemical Sciences

neapōlis

Ph.D. in Chemical Sciences

Nature-inspired antioxidants and redox-active organic systems for biomedical research and applications

Maria Laura Alfieri

Advisor

Prof. Alessandra Napolitano

Examiner

Prof. Marina Della Greca

XXXII Cycle 2017 – 2020

Coordinator: prof. Angela Lombardi

Index

ABSTRACT

The imitation of Nature's chemical principles and logics has emerged as a competitive strategy for the design and implementation of functional molecular systems and biomaterials for innovative technological and biomedical applications. A unique source of inspiration in this context is offered by phenols, polyphenols and especially catechols, in view of their various biological roles.

In this frame the present project addressed structure-property-function relationships in synthetic eumelanin and polydopamine by a biomimetic chemistry and modeling approach and in particular:

a) the elucidation of the main structural components of polydopamine and their role in wet adhesion and film-forming properties;

b) preparation of model eumelanins at high degree of regioregularity and comparative evaluation of their chromophoric and antioxidant properties;

c) design and implementation of novel fluorescence turn-on systems for sensing applications or alternative mussel-inspired systems for technological applications;

d) preparation and characterization (NMR, mass spectrometry, UV-visible, particle and film morphology, antioxidant properties) of novel adhesive polymers based on control of monomer structure, functional groups and deposition conditions.

Main outcomes can be summarized as follows:

1) PDA film deposition: a) requires high dopamine concentrations (>1 mM); b) is not attributable to cyclized 5,6-dihydroxyindole (DHI) intermediates produced by dopamine autoxidation; c) is accelerated by equimolar amounts of periodate causing fast conversion to the *o*-quinone; d) is enhanced by the addition of hexamethylenediamine (HMDA) and other

long chain aliphatic diamines even at low dopamine concentrations (<1 mM);

2) a pH-sensitive fluorescent thin film was obtained by optimization of the strongly fluorogenic reaction between dopamine and resorcinols. This fluorogenic reaction is efficient and may be exploited for the sensing of volatile amines;
3) enzymatic oxidation of tyramine proved a practical procedure for surface functionalization and coating at neutral pH and at much lower substrate concentration compared to standard autoxidative PDA coating protocols;
4) eumelanin precursors, 5,6-dihydroxyindoles, can form adhesive films under dip-coating conditions in the presence of HMDA;
5) synthetic eumelanin pigments prepared from biosynthetic precursors, DHICA and its methyl ester, are of particular interest due to their strong antioxidant properties and the intense absorption in the UVB/UVA region.

Research work on related topics has also been carried out showing that:

- gelatin-based hydrogels are able of incorporating and releasing under controlled conditions DHICA and MeDHICA. Chemical assays confirmed the antioxidant power of the indoles incorporated into the gelatin network;
- new 1,4-benzothiazine based chromophores prepared from 3-substituted 1,4-benzothiazines show a peculiar acidichromic behaviour hinting to their exploitation as pH sensors or related applications;
- melanins feature a reversible redox behavior as evidenced by electrochemistry-based reverse engineering methods exchanging

electrons with various reductants and oxidants, including drugs and neurotoxicants;

- biomimetic phenolic polymers exhibit correlations between the electron-transfer or hydrogen atom transfer capacity and EPR indices of π-electron spin delocalization highlighting specific structural determinants of the antioxidant activity;
- 3-hydroxytyrosol and even more its 5-S-lipoyl conjugate are able to counteract Hg-induced cytotoxicity in human erythrocytes. Sulfated derivatives of tyrosol polymers proved to be highly efficient as antioxidants and as anticoagulant agents in *in vitro* assays.

Overall, these results fulfil the main objectives of the PhD project and expand the current repertoire of functional nature-inspired materials and systems.

List of publications

1. E. Kim, W.T. Leverage, Y. Liu, L. Panzella, **M.L. Alfieri**, A. Napolitano, W.E. Bentley, G.F. Payne "Paraquat−melanin redox-cycling: evidence from electrochemical reverse engineering" *ACS Chemical Neuroscience*, 7 (**2016**), 1057-1067; doi:10.1021/acschemneuro.6b00007.

2. Z. Temoçin, E. Kim, J. Li, L. Panzella, **M.L. Alfieri**, A. Napolitano, D.L. Kelly, W.E. Bentley, G.F. Payne "The analgesic acetaminophen and the antipsychotic clozapine can each redox-cycle with melanin" *ACS Chem. Neuroscience*, 8 (**2017**), 2766-2777; doi:10.1021/acschemneuro.7b00310.

3. **M.L. Alfieri**, R. Micillo, L. Panzella, O. Crescenzi, S.L. Oscurato, P. Maddalena, A. Napolitano, V. Ball, M. d'Ischia "Structural basis of polydopamine film formation: probing 5,6-dihydroxyindole-based eumelanin type units and the porphyrin issue" *ACS Appl. Mater. Interfaces*, 10 (**2018**), 7670-7680; doi: 10.1021/acsami.7b09662.

4. A. Officioso, L. Panzella, F. Tortora, **M.L. Alfieri**, A.Napolitano, C. Manna "Comparative analysis of the effects of olive oil hydroxytyrosol and its 5-S-lipoyl conjiugate in protecting human erythrocytes from mercury toxicity" *Oxid Med Cell Longev.*, (**2018**), 1-9; doi:10.1155/2018/9042192.

5. M. Iacomino, **M. L. Alfieri**, O. Crescenzi, M. d'Ischia, A. Napolitano. "A unimolecular variant of the fluorescence turn-on oxidative coupling of

catecholamines with resorcinols" *ACS OMEGA*, 4 (**2019**), 1541-1548; doi.org/10.1021/acsomega.8b02778.

6. **M. L. Alfieri**, L. Panzella, S.L. Oscurato, M. Salvatore, R. Avolio, M.E. Errico, P. Maddalena, A. Napolitano, M. d'Ischia. "The chemistry of polydopamine film formation: the amine-quinone interplay" *Biomimetics*, 3 (**2018**), 26; doi:10.3390/biomimetics3030026. Cover art "Mussel-Inspired Polydopamine Adhesion: Amines and Quinones as Key Players" Volume 3, issue 3, September 2018.

7. L. Panzella, G. D'Errico, G. Vitiello, M. Perfetti, **M. L. Alfieri**, A. Napolitano, M. d'Ischia "Disentangling structure-dependent antioxidant mechanisms in phenolic polymers by multiparametric EPR analysis" *Chem. Commun.*, 54 (**2018**), 9426; doi: 10.1039/c8cc05989f.
8. **M.L. Alfieri**, M. Iacomino, A. Napolitano, M. d'Ischia "Reaction-based, fluorescent film deposition from dopamine and a diamine-tethered, bis-resorcinol coupler" *Int J Mol Sci.*, 20 (**2019**), E4532; doi: 10.3390/ijms20184532.

9. **M. L. Alfieri**, L. Panzella, S.L. Oscurato, M. Salvatore, R. Avolio, M.E. Errico, P. Maddalena, A. Napolitano, V. Ball, M. d'Ischia "Hexamethylenediamine-mediated polydopamine film deposition: inhibition by resorcinol as a strategy for mapping quinone targeting mechanisms" *Front Chem.*, 7 (**2019**), 407; doi:10.3389/fchem.2019.00407.

Manuscripts in preparation

1. **M.L. Alfieri**, L. Panzella, A. Youri, A. Napolitano, V. Ball, M. d'Ischia "Pseudo-polydopamine (ψ-PDA) thin films by tyrosinase-controlled oxidation of tyramine: a mild, versatile and no-waste mussel-inspired coating technology".

2. **M.L. Alfieri**, L. Panzella, L. Cipolla, A. Napolitano "Gelatin-based systems for the controlled release of 5,6-dihydroxyindole-2-carboxylic acid, a melanin-related metabolite with potent antioxidant activity".
3. **M.L. Alfieri**, L. Panzella, M. Correia da Silva, A. Napolitano "Sulfated tyrosol polymers: antioxidant and anticoagulant activity".

Chapter 1

Introduction

1.1 Nature-inspired functional systems: state of the art

The imitation of Nature's chemical principles and logics has emerged as a competitive strategy for the design and implementation of functional molecular systems and biomaterials for innovative technological and biomedical applications.[1-4] Tissue engineering and regenerative medicine have been taking great inspiration from the natural world. Of particular interest are biopolymeric matrices and bioactive nanosized fillers that thanks to their biodegradability, high mechanical strength, and similarities with extracellular matrices help in repair and regenerate damaged tissues and organs, especially to obtain bone-like implantable materials.[5-9] Surface modification with biocompatible smart materials capable to improve cell attachment, proliferation and adhesion to tissues is an important issue in the context of biomedical applications because the biological response is often determined by biointerfacial interactions.[10] Likewise, the design and realization of materials and coatings with tailored hydrophilicity/hydrophobicity properties is currently a hot topic of great technological relevance, and nature represents in this connection a uniquely rich source of inspiration for innovative solutions.[11] An example is represented by the lotus leaf surface that possesses a typical superhydrophobic ability and self-cleaning property due to branch-like nanostructures on top of the micropapillae.[12] Besides hydrophobicity, optical properties are often associated with structured molecular architectures. Color through structure can be found in a significant number of animals, particularly those living in poorly illuminated environments[13] and, they find relevant

technological applications such as, light manipulation, optical sensors, light–energy conversion, plasmonic materials with ultrahigh surface plasmon resonance (SPR) efficiency and metamaterials.[14,15] Many examples of environment-friendly energy-storage materials have also been reported.[16] For example, inspired by the electron shuttles functioning in extracellular electron transfer via reversible redox-cycling, electrode materials with similar active functional groups have been explored.[17] Nature inspired frameworks for the development of solar cells,[18] photovoltaic materials,[19] and systems for artificial photosynthesis[20] also represent a highly active field of research. Based on these examples it is apparent that all of the above mentioned properties and functions depend in most cases on the dynamic interplay of interacting molecular systems endowed with great chemical versatility and responsiveness.

A unique source of inspiration in this context is offered by phenols, polyphenols and especially catechols that provide the core reactive unit in a number of bioactive compounds and biopolymers and are attracting growing interest in view of their diverse biological roles, *e.g.* as physiological mediators and messenger molecules in the nervous system, photoprotective pigments, structural components, metal chelating agents and reactive components in adhesive organisms (Figure 1.1.1).

Natural catechol-based systems and derivatives can be classified in two main groups:

1. *Small molecules* as molecular mediators and messengers, including: catecholamine neurotransmitters and hormones, such as dopamine, norepinephrine and epinephrine and their metabolites and conjugates; products of metabolic transformation of steroids, such as the catecholestrogens; active

structural components as N-acetyldopamine in the insect cuticle sclerotization; pigments as anthocyanines and flavonoids that confer to fruits and flowers their characteristic colours;[21] anti-oxidants and free radical scavengers as hydroxytyrosol, pyrogallol, gallic, caffeic and chlorogenic acid derivatives, epicatechins, curcumin and anthocyanines;[22-24]

2. *Polyphenolic polymers* of plant origin as lignins, tannins, characterized by a marked structural diversity.[25] Lignins derive from coniferyl and p-coumaryl alcohols and are investigated for their fuel value as well as to produce plastic-like materials.[26] Tannins and related substances are used as clarifying agents in alcoholic drinks and as aroma ingredient in both alcoholic and soft drinks or juices, and find extensive uses in the wine industry.[27,28] Polyphenolic polymers can also be found in animals in which noticeable examples include the melanins, the black (eumelanin) or reddish-brown (pheomelanin) pigments of human skin and hair, mammalian fur, bird feathers, cephalopod ink.[29,30]

During the past decade considerable attention has been directed to implement synthetic mimics of natural phenolic compounds for a broad range of applications, including hydrogels, biocompatible and biomimetic glues and synthetic adhesives, nanostructures for drug delivery, sensors, semiconductors, photo- and thermostabilizing agents, antioxidants and other functional systems for biomedicine and organic electronics.[31-37]

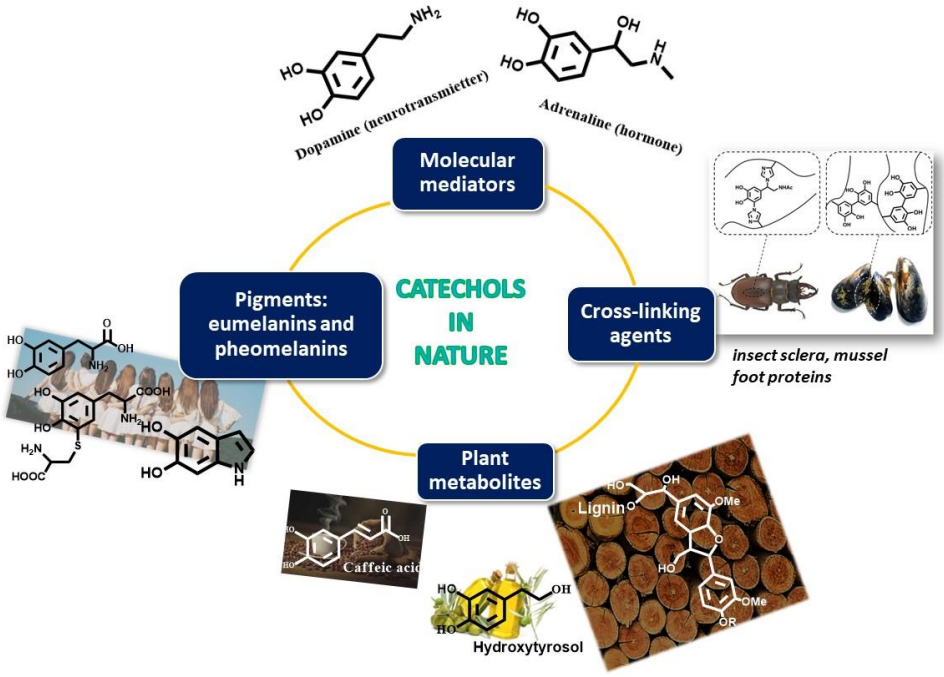

Figure 1.1.1 Representative biological roles of catechols, *e.g.* as physiological mediators and messenger molecules in the nervous system (dopamine and other catecholamines), structural components (lignins), photoprotective pigments (melanins) and reactive components in adhesive organisms (dopa residues in mussel byssus proteins).

Natural phenolic compounds with their carbogenic diversity and tunable redox behavior due to variable oxygenation patterns also provide an important source of inspiration for novel free radical scavengers to mitigate oxidative stress correlates of several pathological conditions, including cardiovascular diseases, neurodegeneration and cancer.[38-41] Oxidative stress refers to elevated intracellular levels of reactive oxygen species (ROS), small and highly reactive molecules such as singlet oxygen, peroxyl radicals, superoxide radicals, hydroxyl radicals but also non-radical oxidizing agents such as hydrogen peroxide and ozone that can easily

be converted into oxygen radicals. When maintained at proper cellular concentrations ROS can function as “redox messengers” in intracellular signaling and regulation though, when exceeding physiological levels cause damage to lipids, proteins and DNA and cell death.

Production of ROS is a consequence of cellular metabolism and inflammatory processes or derive from exposure to exogenous pollutants or ingestion of environmental toxicants. Living organisms are endowed with antioxidant systems either to eliminate ROS or minimize their negative effects such as vitamins C and E, carotenoids, anthocyanins, polyphenols and uric acid, that can be obtained by humans through the diet. Glutathione, a low-molecular-weight tripeptide and one of the most important natural antioxidant, is synthesized by living organisms and used to control ROS level either via direct interaction with them or serving as a cofactor for ROS-detoxifying enzymes.[42]

In human skin, redox homeostasis is usually controlled by black eumelanin pigments derived from tyrosine and endowed with antioxidant properties. Mutation-dependent incorporation of cysteine leads conversely to reddish-brown prooxidant pheomelanins in the UV susceptible red-haired phenotype. Because of their ability to respond dynamically to light and redox stimuli, melanins attract growing biomedical interest.[43] However, the extreme heterogeneity of their molecular systems and practical difficulties in their extraction and purification processes from natural sources, made their structural characterization and the definition of structure-properties relationships a most difficult task. To this aim, synthetic mimics of natural melanins that can be obtained by oxidative polymerization of dopamine (DA), 3,4-dihydroxy-L-phenylalanine (DOPA), 5-S-cysteinyldopamine (CDA), 5,6-dihydroxyindole (DHI) or 5,6- dihydroxyindole carboxylic acid (DHICA) hold much promise for technological applications due

to their peculiar properties which include a broad-band UV and visible absorption profile, redox properties, free radical scavenging ability and water-dependent hybrid electronic-ionic semiconduction.[44-49]

Among the various approaches that can be used to modify material surfaces, the most suitable and convenient in terms of time and ease of execution and relevance for technological purposes are those based on wet adhesion technologies. The mimicry of mussel strategy for underwater adhesion is exemplified by the development of polydopamine (PDA) as a highly adhesive biomaterial for surface functionalization and coating incorporating the key catechol and amine functionalities of byssal proteins.[32,50-52] This black synthetic eumelanin-like polymer displays intriguing physicochemical properties similar to those of natural and synthetic melanins,[49] including a broad band visible absorption,[53] an intrinsic free radical character,[54,55] and a water-dependent, ionic-electronic hybrid conductor behaviour.[56] Because of its robustness, universal adhesion properties, biocompatibility, reversible and pH-switchable permselectivity for both cationic and anionic redox-active probe molecules, PDA-based coating technology has opened up the doorway to novel opportunities in the fields of bioengineering, nanomedicine, biosensing and organic electronics,[32,57–65] for example, for the development of nanoparticles with free radical scavenging properties or for drug delivery,[61,66,67] in the setup of new systems for energy conversion (*e.g.* artificial photosynthetic mimics)[68] or as biointerface.[7,59,60] The detailed factors and mechanisms underlying the adhesion properties of PDA and related catechol-based coatings have been addressed in several studies also using model systems to probe the critical structural elements.

Promising opportunities may derive from the design of PDA-based composites mimicking hierarchical self assembly in nacre, *e.g.* the recently reported graphene

oxide–PDA nanocomposites shown to have higher tensile strength and toughness compared to natural nacre.[36]

Also, the possibility to impart film forming ability to natural polymers including eumelanins and polyphenol plant materials endowed with other important biological activity/functional properties has represented a focus of intense research. Studies toward next generation mussel-inspired catechol-amine systems have led to the development of a) polyphenol/polyamine combinations, giving uniform nanoscale adhesive aggregates via robust bonding effects; b) the use of catechol, gallic acid or caffeic acid combined with hexamethylenediamine (HMDA).[69-73]

So far, however, progress in polyphenol-, catecholamine- and melanin-based functional materials and systems has been hindered by several gaps and issues.[74,75] For example, polydopamine and synthetic melanin properties have been based more on empirical approaches than on rational strategies. Moreover, the exploitation of catecholamine chemistry for bioadhesion has suffered from the lack of systematic studies of catecholamine redox chemistry including functionalization at the quinone moiety.

1.2 Catechol chemistry

The variety of biological roles played by catechols can be explained by the versatility of their chemistry.

The presence of an *ortho* diphenol group confers to catechols a high oxidizability, slightly acidic properties under specific conditions, an electron-rich aromatic ring for reactions with electrophiles allowing functionalization and an ideal disposition

for bidentate coordination and hydrogen bonding. As a result, catechol chemistry is largely dominated by metal chelating properties and redox equilibria.

The catecholic ortho hydroxyl groups can in fact donate non-bonding electron pair to many metal ions such as Fe^{2+}/Fe^{3+}, Cu^{2+}, Co^{2+}, Ni^{2+}, V^{3+}, Ga^{3+} to form reversible non-covalent complexes (chelates). The coordinative chemistry of catechols with iron (III) has been deeply investigated as it seems to play a fundamental role in the underwater adhesion mechanism of mussels.[76–79] It has been found that catechol coordination chemistry is strictly controlled by pH via the deprotonation of the catecholic hydroxyl groups and depends also on Fe^{3+} concentration. The mono catechol-Fe^{3+} complexes dominate at pH lower than 5.6 and high iron (III) concentrations, bis complexes at pH between 5.6 and 9.1, and tris complexes at pH higher than 9.1 and low Fe^{3+} concentrations.

Catechol redox systems involves the formation of quinone and hydroquinone type equilibrium species. The pH dependence of the catechol redox process can be ascribed to a two proton−two electron ($2H^+$ $2e^-$) transfer, commonly known as a proton-coupled electron transfer reaction (Scheme 1.2.1). Under biological conditions, the redox reaction between catechol and oxygen, typically referred to as "autoxidation", is thermodynamically unfavorable because of the high activation energy barrier (530 mV), but this obstacle can be overcome by the presence of enzymes (*e.g.* tyrosinase, horseradish peroxidase/H_2O_2) or metal ions (*e.g.* Fe^{3+}).[80]

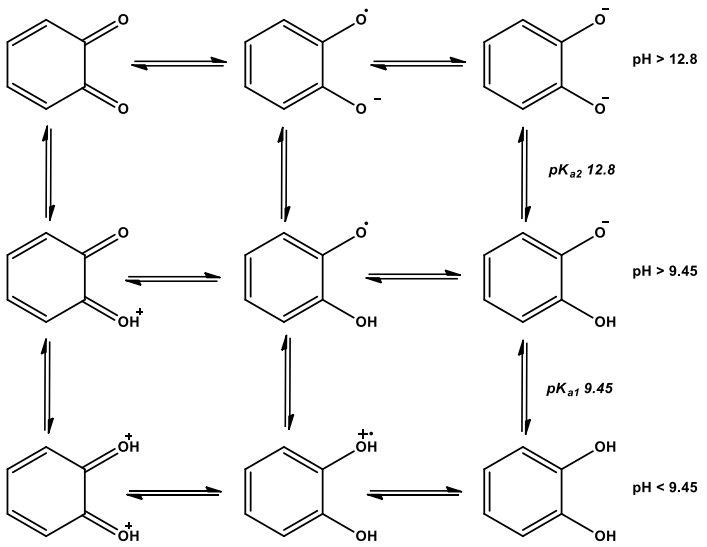

Scheme 1.2.1. Redox and protonation equilibria of catechols.

Characteristic features of the catechol chemistry is oxidation to semiquinone and quinone derivatives, a process in which catechols can turn into free radical and highly electrophilic species, respectively, becoming available for efficient coupling processes and for nucleophilic attack by functional groups of biomolecules such as thiols, amines, as well as carbon nucleophiles including phenolic and catecholic rings, allowing for conjugation, polymerization, cross-linking and coupling even under mild biologically-relevant conditions (Scheme 1.2.2).

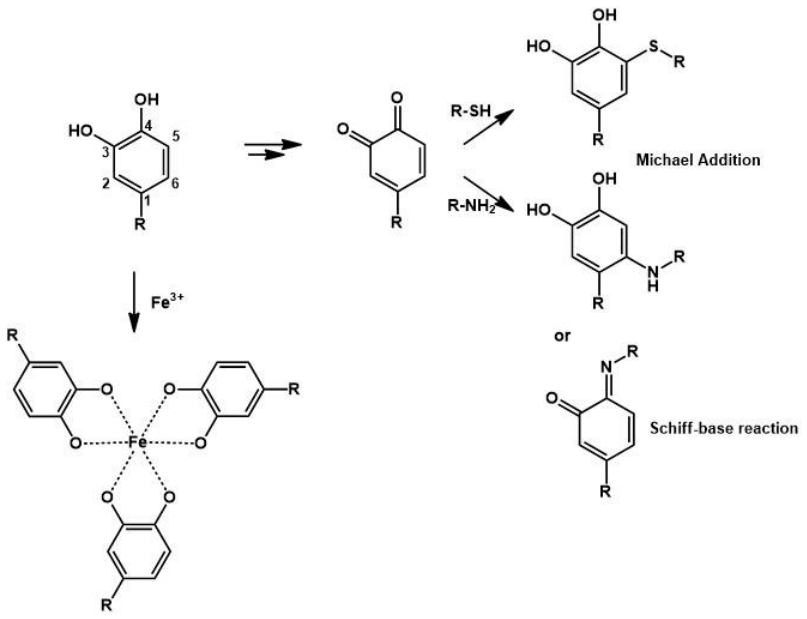

Scheme 1.2.2. Overview of the chemistry of catechol systems.

As mentioned above, the reaction between catechols and amines is of critical importance in many natural biological processes, such as the cross-linking of adhesive proteins by marine organisms,[81] the formation of cytoskeleton by insects[82] and the biosynthesis of melanin.[46] For instance in mussel byssus, a proteinaceous fibrous material produced by mussels to anchor to hard substrates and resist lift and drag forces from waves,[83] byssal proteins, particularly mussel foot proteins (Mfp), are rich in DOPA and lysine (Lys) amino acids.[84] Particularly foot proteins Mfp-3 and Mfp-5, which are located at plaque-substrate interface, exhibit a high DOPA content approaching 30 mol %,[85] suggesting a relation between DOPA and the remarkable mussel wet adhesion capability, and in particular the abundance and proximity of DOPA and Lys residues in many Mfp's have long suggested their synergistic role in adhesion on to a wide spectrum of materials (Figure 1.2.1).

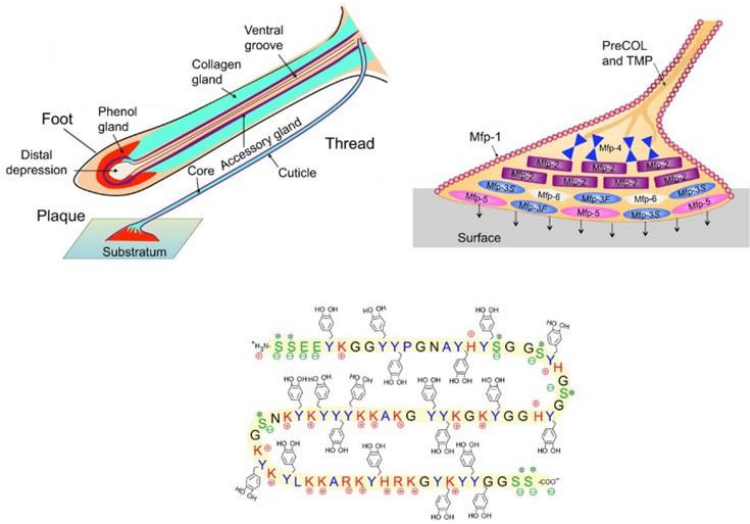

Figure 1.2.1. Mussel foot, byssus plaque structure and sequence of Mfp-5 from *Mytilus edulis*.[86]

Amines may react with *o*-quinones to form adducts either by addition or Schiff base formation. The factor that mainly determines which of these reaction types will predominate, is the type of amine. In a Michael type addition, an amine is attached to the catechol ring at the 6- position (see Scheme 1.2.2) to form amino-catechol coupling product depending on the pH, the type of catechol substituents and the basicity of the nucleophilic amines. Catechols with a substituent on the aromatic ring, have a reduced reactivity when compared to unsubstituted catechol, mostly dependent on the steric effect of the group. A third factor is the basicity of the nucleophilic amines: a more basic amine results in a higher reaction rate. In a Schiff base reaction, that is affected mainly by the pH, the amine attacks the 1- or 2- position and an imine is created. In the same way thiols can react with *o*-quinones by regioselective nucleophilic attack in the 2/5-position of the ring as shown in Scheme 1.2.2.

Because of their chemically versatile structure, catechols and related systems are intensively investigated in the frame of supramolecular structures, metal chelating or cross-linking systems and polymers. Recent studies reported the design and biomimetic use of natural and synthetic catechols in biomedicine, analytical chemistry, nanotechnology and materials science, offering promising candidate structures for various technological applications.[87]

1.3 Aims of the PhD project

Within the frame briefly described in the previous paragraph, the present PhD project is aimed at exploiting or mimicking natural molecular systems, both phenolic and heteroaromatic, to translate their UV-absorbing, metal binding, redox and free radical scavenging properties into new functional soft, robust, adhesive, multifunctional and fully biocompatible materials and molecular systems for various biomedical and technological applications, including thermo- and oxidative stabilization of polymers, metal chelation, tissue engineering, anticoagulants, antioxidants, food supplements and functional biocompatible components for hydrogels, sensors, and other functional systems.

To pursue this general aim the present project addresses the structure-property-function relationships in synthetic eumelanin and polydopamine by a biomimetic chemistry and modeling approach based on: a) the elucidation of the main structural components of polydopamine and their role in wet adhesion and film-forming properties; b) preparation of different model eumelanins in order to get a higher degree of regioregularity and comparative evaluation of their chromophoric and antioxidant properties; c) investigation of the effects of additives particularly diamines, metal cations and other conditions of the oxidative

polymerization process on the film forming and other properties of the final polymers; d) characterization (NMR, mass spectrometry, UV-visible, particle and film morphology, antioxidant and anticoagulant properties and biocompatibility) of novel mussel-inspired adhesive polymers based on control of monomer structure, functional groups and deposition conditions. Other research topics concern the elucidation of the structural determinants of the antioxidant activity in phenolic polymers from naturally occurring precursors, and the preparation of sulfated polyphenols either monomeric or polymeric whose antifouling and anticoagulant activity was also evaluated.

Specific aims of the project include:

a) The definition of structure-property-function relationships in synthetic eumelanin and polydopamine;
b) The rational design of novel fluorescence turn-on systems for sensing applications based on catecholamine oxidation chemistry and coupling with nucleophiles;
c) The development of alternative mussel inspired systems for various applications based on tyrosinase-catalyzed oxidation of tyramine for technological applications;
d) Preparation of eumelanin precursors like 5,6-dihydroxyindole derivatives including ester for adhesion and amide/diamide derivatives of 5,6-dihydroxyindole-2-carboxylic acid and regioisomeric dimers for preparation of model pigments by oxidative polymerization;
e) Investigation of the properties of melanins obtained from the two main oligomers intermediates *i.e.* the 4,4' biindolyl and 4,7' biindolyl dimers from DHICA and DHICA methyl ester (MeDHICA);

f) The design of gelatin-based hydrogels to trap bioactive molecules for drug delivery, tissue engineering and other biomedical applications;
g) The design of unconventional benzothiazine-based H-atom donor antioxidants exploiting the potential of the bioinspired -N=CR-CH_2-S- push-pull system;
h) Elucidation of the structural determinants of the antioxidant activity in phenolic polymers;
i) The development of sulfur-containing antioxidants with multi-defense activity, catechols conjugated with lipoic acid, and sulfate esters of phenolic polymers for anticlotting applications.

Part of the work described under research line (c) was carried out during a one-month stage in the laboratory of Professor Vincent Ball at the Faculty of Chirurgie Dentarie and at the Institut National de la Santè et de la Recherche Médicale (University of Strasbourg, France).

Part of the work described under research line (f) was carried out during a one-month stage in the laboratory of Professor Luisa De Cola at the Institut de Science et d'Ingénierie Supramoléculaires (ISIS) (University of Strasbourg, France).

Part of the work described under research line (i) was carried out during a one-month stage in the laboratory of Organic and Pharmaceutical Chemistry of Assistant Professor Marta Correia da Silva at the Faculty of Pharmacy, University of Porto (FFUP), Portugal.

Overall, the results described in this thesis have led to significant advances in our understanding of eumelanin, polydopamine and phenolic polymers

properties and have disclosed novel bioinspired functional materials and systems of potential technological and biomedical relevance.

Chapter 2

The chemistry of polydopamine film formation

2.1 Introduction

As previously mentioned the development of innovative and versatile dip-coating technologies for surface functionalization has been a very active issue over the past decade[34,88] following the discovery in 2007 of the extraordinary wet adhesion properties of polydopamine (PDA), a black insoluble and structurally disordered eumelanin-like material produced by the oxidative polymerization of dopamine under alkaline conditions and inspired by the robust adhesion properties of catechol- and amine-rich mussel byssus proteins (Figure 2.1.1).[57,75]

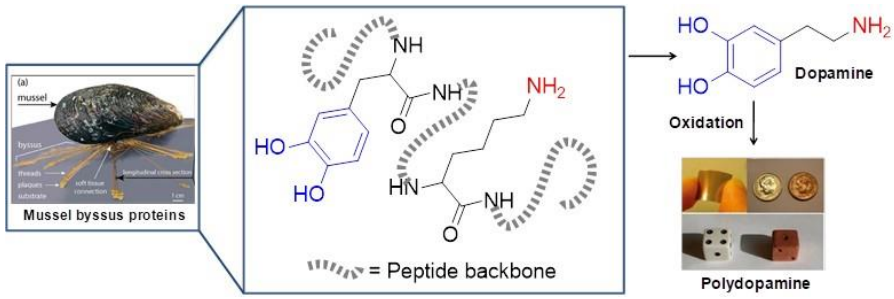

Figure 2.1.1. Catechol and amino groups are the core reactive unit in mussels' and PDA adhesion mechanisms.

PDA film properties, including hydrophilicity and thickness, can be finely tuned by a variety of experimental parameters including dopamine concentration,[89] nature of the buffer,[90] oxidant,[91-93] and pH.[89]

However, despite increasing importance in materials science, the development of a mature and multivalent PDA-based technology is hindered by current limitations

in the control, optimization and tailoring of surface and mechanical properties. To overcome these and related scientific and technological issues, elucidation of the structure of PDA films represents a crucial goal of research.

Extensive work in the field has demonstrated that PDA formation shares many characteristics with melanin biosynthesis pathways (Scheme 2.1.1). In particular, eumelanins derive from tyrosinase-catalyzed oxidation of tyrosine or 3,4-dihydroxy-L-phenylalanine (DOPA) *via* 5,6-dihydroxyindole intermediates, namely DHI and the major circulating melanogen DHICA, that in the later stages of the process undergoes oxidative polymerization leading ultimately to the pigments. The decarboxylation of DOPA to dopamine assisted by DOPA decarboxylase is, indeed, the initiating step of the biosynthesis of catecholamine neurotransmitters. Within the dopaminergic neurons of substantia nigra dopamine undergoes a slow non enzymatic oxidation to give dopamine-quinone which leads to the accumulation of neuromelanin. As with eumelanin, it appeared that neuromelanin and PDA can thus be described in terms of complex structural properties arising from the involvement of various intermediates including uncyclized and cyclized DHI-based units, including partly dimers, trimers, tetramers, and their resulting aggregates.[33,94]

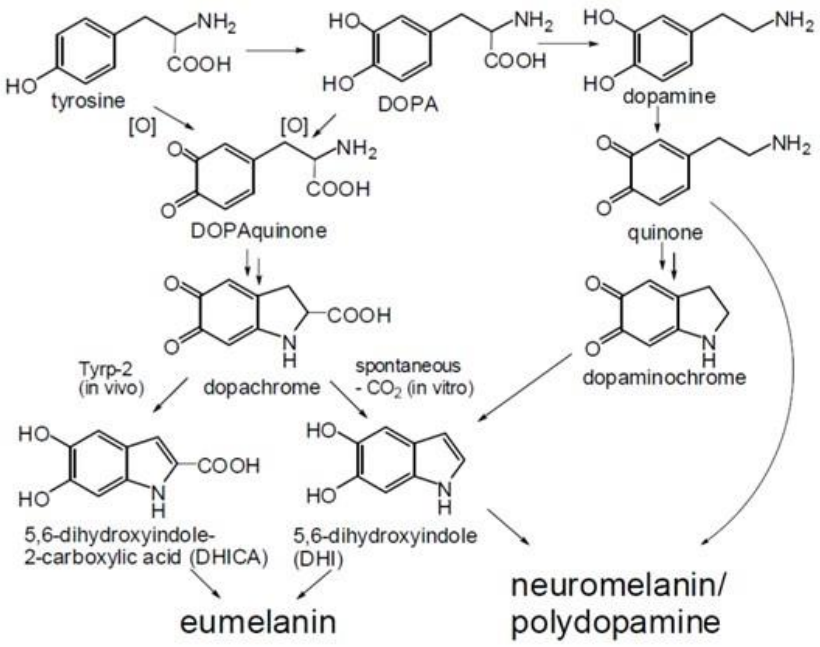

Scheme 2.1.1. Biosynthetic and synthetic pathways for eumelanin, neuromelanin and PDA.

Until 2012 two different speculative PDA structural models were commonly proposed: the "open-chain polycatechol/quinone" model, based on linear sequences of catecholamine units linked through biphenyl-type bonds, and the "eumelanin-polyindole" model, which envisaged a 5,6-dihydroxyindole (DHI) polymer arising by cyclization of dopaminequinone (Scheme 2.1.2).[60,95] However, neither of these models were founded on solid experimental evidence, nor were these models related to specific polydopamine properties and functions.

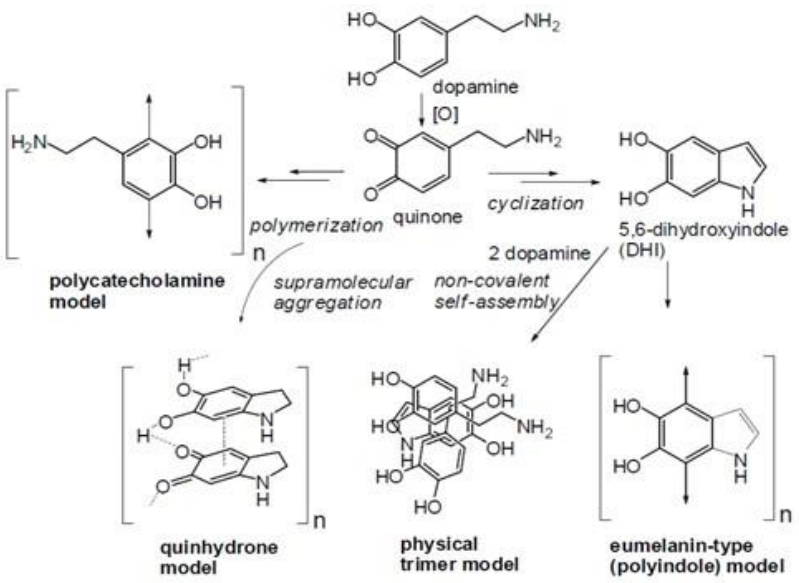

Scheme 2.1.2. Overall view of the possible oxidative pathways to PDA.

Since 2012, several groups have begun to address in detail the chemical nature of PDA, its basic scaffolds, and functional groups. Some structural models have been proposed including:

a) a supramolecular aggregate consisting primarily of 5,6-dihydroxyindoline and dopaminochrome held together through a combination of charge transfer, π-π stacking, and hydrogen-bonding interactions;[96]

b) a physical trimer of $(dopamine)_2$/DHI, derived from a self-assembly mechanism;[97]

c) a three-component structure of polydopamine, comprising uncyclized (catecholamine) and cyclized (indole) units, as well as pyrrolecarboxylic acid moieties, with partial incorporation of tris(hydroxymethyl)-aminomethane (Tris buffer);[98,99]

d) mixtures of different oligomers containing indole units with various degrees of (un)saturation and open-chain dopamine units;[100]

e) dopamine and C=N-containing tautomers of quinone and indole species in growing films deposited on gold surfaces over an interval of time from 2 to 60 min;[101]

f) a $(DHI)_2$/PCA (pyrrolecarboxylic acid) trimer complex (m/z 402) as primary component to build up the supramolecular structure of PDA.[102]

The picture emerging from these studies was still confusing and partly based on theoretical models not adequately supported by experimental evidence. Yet, intense research activity into PDA film deposition over the past few years has contributed to delineate an improved picture of the underlying structural factors and features of the process, including kinetic profiles, concentration dependence, role of oxidants and amine-based additives.

2.1.1 The role of diamines in the film formation properties of catechol systems

The central role of amine groups in the adhesion and cohesion processes underlying PDA film deposition and growth is supported by various lines of evidence. One of them reported that replacing the amine group of dopamine with a hydroxyl group, as in 2-(3,4-dihydroxyphenyl)ethanol (hydroxytyrosol), results in the formation of polymeric materials completely devoid of adhesion and film forming properties.[98]

In a seminal study Chen *et al.* (2014) first reported that copolymerization of gallic acid and hexamethylenediamine (HMDA), a long aliphatic chain diamine, leads to films that can be deposited on various surfaces.[69] Addition of HMDA during PDA deposition was also proposed as a means of obtaining films rich in amine groups, with a high cross-linking degree and resistance to hydrolysis and swelling.[103] Moreover it was found that in the presence of HMDA the oxidation of caffeic acid, which itself has no adhesive properties despite apparent polymerization and darkening of the mixture, produces an adhesive greenish-blue material with high stability and biocompatibility (Figure 2.1.1.1).[70] This was not observed using monoamines of any length or short chain diamines.

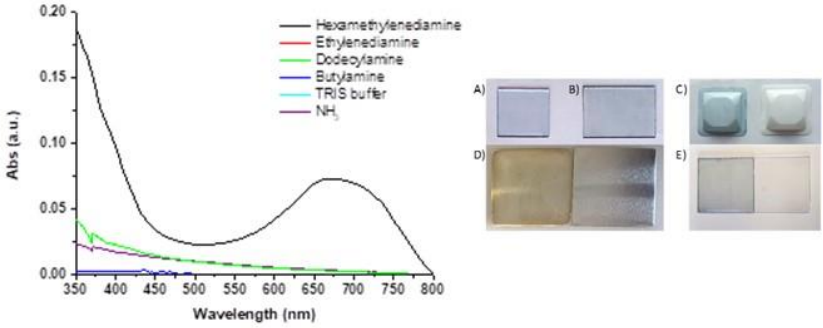

Figure 2.1.1.1. UV-vis spectra of cover glasses dipped into 1 mM solution of caffeic acid in the presence of equimolar amounts of various amines (left); (right) picture of coated substrates: A) quartz; B) borosilicate glass; C) polystyrene; D) aluminum; E) polyethylene and their uncoated control on the right.

Chemically stable functional biocompatible thin films were obtained also by a cross-linking reaction between pyrocatechol and HDMA under oxidizing condition.[73] In all these studies, it was generally suggested or assumed that HMDA gives rise to intermolecular amine-quinone condensation processes leading to highly cross-linked oligomer structures. In other study Lyu *et al.* (2017) demonstrated that the copolymerization of varied catechol(amine)s and functional

nucleophilic additives gave rise to nano-coatings on various surfaces including plastic, metal, glass and polymers with tailored chemical and physical properties, opening new opportunities for the development of novel and versatile functional biomimetic materials for a range of applications.[104]

So far, the detailed mechanism by which HMDA is able to mediate catechol deposition under low concentration conditions and the exact nature of the adhesive components underlying film deposition, has remained elusive. Intense research activity into PDA film deposition over the past few years has contributed to delineate an improved picture of the underlying structural factors and features of the process, including kinetic profiles, concentration dependence, role of oxidants and amine-based additives.[57,102,105,106]

On this basis, in this chapter, the attention will be focused on some crucial mechanistic issues concerning in particular the structural factors affecting PDA film formation and the species involved. To this aim, the investigation was directed to assess: 1) the temporal profile of PDA film formation by autoxidation of dopamine at pH 9.0; 2) the role of the DHI units in the adhesion properties of PDA; 3) the effects of dopamine concentration and oxidants (*e.g.* sodium periodate) on film structure and deposition kinetic; 4) the effect of amine groups on the film forming properties of PDA films.

In this chapter, the results of proof-of-concept investigations are presented demonstrating that film deposition: a) requires high dopamine concentrations (>1 mM); b) is due to species produced in the early stages of dopamine autoxidation; c) cyclized DHI units are not involved as primary determinants of film formation; d) is accelerated by equimolar amounts of periodate causing fast conversion to the *o*-quinone, e) is enhanced by the addition of hexamethylenediamine (HMDA) and

other long chain aliphatic amines even at low dopamine concentrations (<1 mM). In addition, it was shown that soluble monomers/oligomers can be physically adsorbed on the primer coating leading to the UV-vis detectable growth of pre-formed films.

2.2 PDA preparation and kinetics of film formation

In an initial set of experiments the evolution of the film-forming properties of PDA was investigated from 10 mM dopamine. The currently used dip-coating methodology was adopted in which a substrate is immersed into an aqueous solution of the monomer at pH 8.5-9.0 in air to allow the formation of the polymer by autoxidation. To this aim two approaches where pursued in which quartz substrates were dipped in the dopamine solution undergoing autoxidation in carbonate buffer (pH 9.0) and kept for a limited interval of time (between 1 and 24 h from the start of the reaction) or dipped for 1 h in the dopamine solution at different times *after* oxidation had started (Figure 2.2.1). In all the experiments the final absorbance on quartz was taken as a rough index of the degree of coating deposition. UV-vis analysis showed that the final absorbance of the films in the initial hours is considerably less intense compared with the levels observed at 24 h (Figure 2.2.1, panel A) and that the formation of the coating species is highest in the early hours and becomes negligible after 23 h (Figure 2.2.1, panel B), indicating that film formation properties are specifically associated with early intermediates in dopamine autoxidation and are virtually quenched at the end of the process when extensive aggregate precipitate occurs.

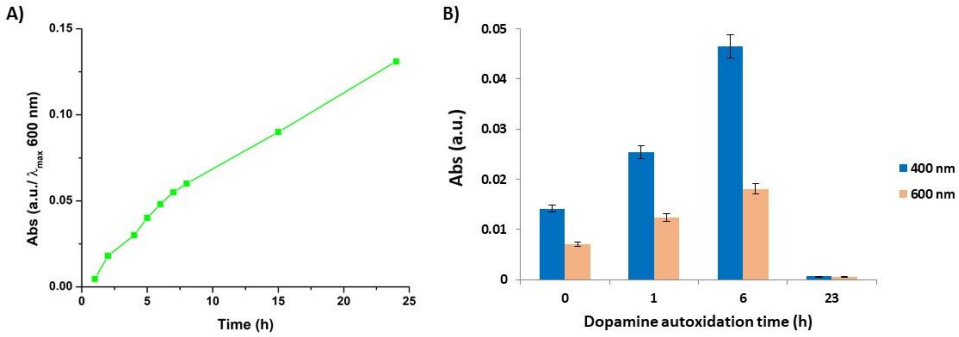

Figure 2.2.1. Kinetics of polydopamine (PDA) film formation. (a) Time course of the absorption at 600 nm of quartz substrates dipped into the reaction mixture up to 24h (b) Absorbance of the films at two selected wavelengths of quartz substrates dipped for 1 h at different reaction time. Data are shown as mean ± standard deviation (SD) of three independent experiments.

2.3 PDA film formation: the role of 5,6-dihydroxyindole-based structure

Though PDA is often referred to as a synonymous of eumelanin because it complies to the definition[46] of "nitrogenous biopolymer produced by oxidative polymerization of a tyrosine-derived indole precursor" and shows similar physicochemical properties, it differs from typical natural or synthetic eumelanins because of the lack of carboxylated indole units (5,6-dihydroxyindole-2-carboxylic acid, DHICA). Nonetheless, PDA may contain DHI units[46] or mixtures of partially degraded indole units. Thus, in another set of experiments, the film forming properties of melanin polymers from DHI and dopamine were compared to assess whether PDA films consist of intact or partially degraded DHI oligomers, and if such components arise from polymerization of preformed DHI or from the

late cyclization of linear dopamine oligomers.

UV-vis analysis clearly indicated that film deposition from DHI or its 2,7′-dimer, under the aerobic conditions at pH 9.0 used for PDA coatings, was null or below detection despite massive precipitation of eumelanin-type polymer (DHI melanin) (Figure 2.3.1).

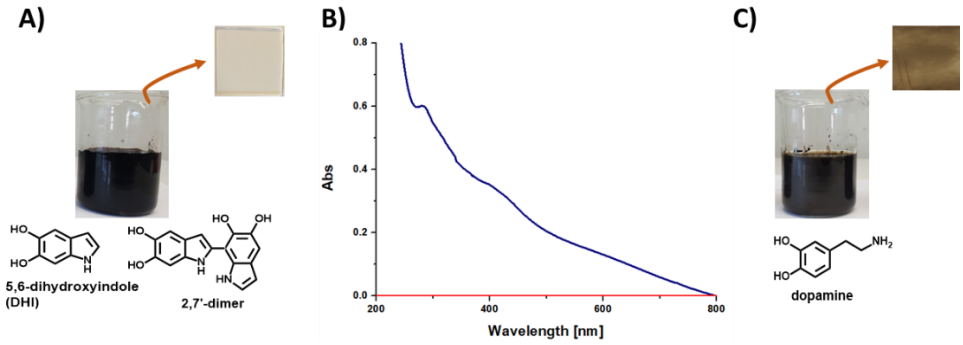

Figure 2.3.1. Quartz substrates immersed in the autoxidation mixture for dip-coating experiments comparing DHI and its dimer melanin (panel A) and PDA (panel C). Panel B, UV-visible absorption spectra of quartz substrates subjected to dip-coating with dopamine (blue curve), DHI and its 2,7'-dimer (red curve).

Morphological characterization. To gain additional insight into PDA films and to definitely rule out film deposition from DHI polymerization, the quartz substrates immersed into PDA and DHI oxidation mixtures were investigated by a combined Atomic Force Microscopy (AFM) and micro-Raman analysis (spectra were run at the Department of Physics, University of Naples Federico II in the frame of a collaborative work with Prof. P. Maddalena and co-workers). The analysis performed onto the DHI sample confirmed the absence of any material attached to the substrate (Figure S2.7.1). Data for PDA film (Figure 2.3.2)

indicated, instead, a mean thickness of 70 nm and dispersed submicron sized grains, a typical topography observed also onto the films of PDA-Tris used as a reference sample and confirming a complete overlap of the topographical and chemical features of the PDA-carbonate with the PDA-Tris films. In the Raman spectrum (Figure 2.3.2) main bands, compatible with the presence of aromatic rings, were detected at 1583, 1416, 1347 and 1242 cm^{-1}, while the broadband around 2900 cm^{-1} was attributable to strongly hydrogen-bonded OH and NH stretching vibrations. Notably and in line with previous Raman spectroscopy studies[107,108] no intense carbonyl band in the 1650-1700 cm^{-1} range was detected.

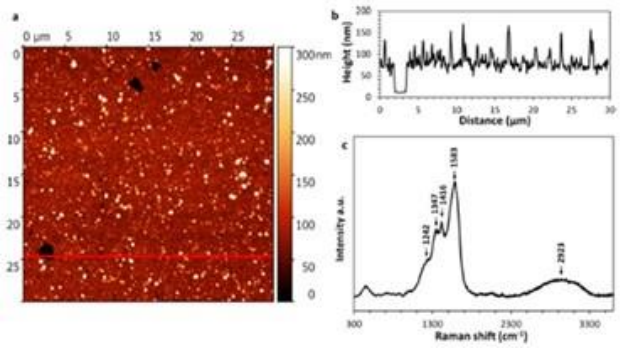

Figure 2.3.2. (a) AFM image of a representative region of the PDA film sample; (b) AFM height profile measured along the red line in panel; (c) Micro-Raman spectrum resulting from the average of 625 spectra collected with a spatial resolution of 2 µm in the sample scanning over an area of 50 × 50 μm^2.

Structural characterization. The data, reported above, suggested that PDA does not contain species compatible with DHI-based oligomers as primary building blocks. To support this conclusion, in separate experiments different PDA films that adhered to the walls of reaction beakers and to immersed glass substrates were carefully washed with water, solubilized and analyzed by MALDI-MS in

comparison with the bulk precipitate from the same mixtures and with DHI melanin (Table 2.3.1). Comparative inspection of traces a and b in Figure 2.3.3 confirmed for both the film and the precipitate the intense peak at m/z 402, reported previously,[102] as the main detectable component. Neither the peak at m/z 402 nor the other minor peaks detected in PDA precipitate could be detected in the spectra of DHI melanin samples (trace c).

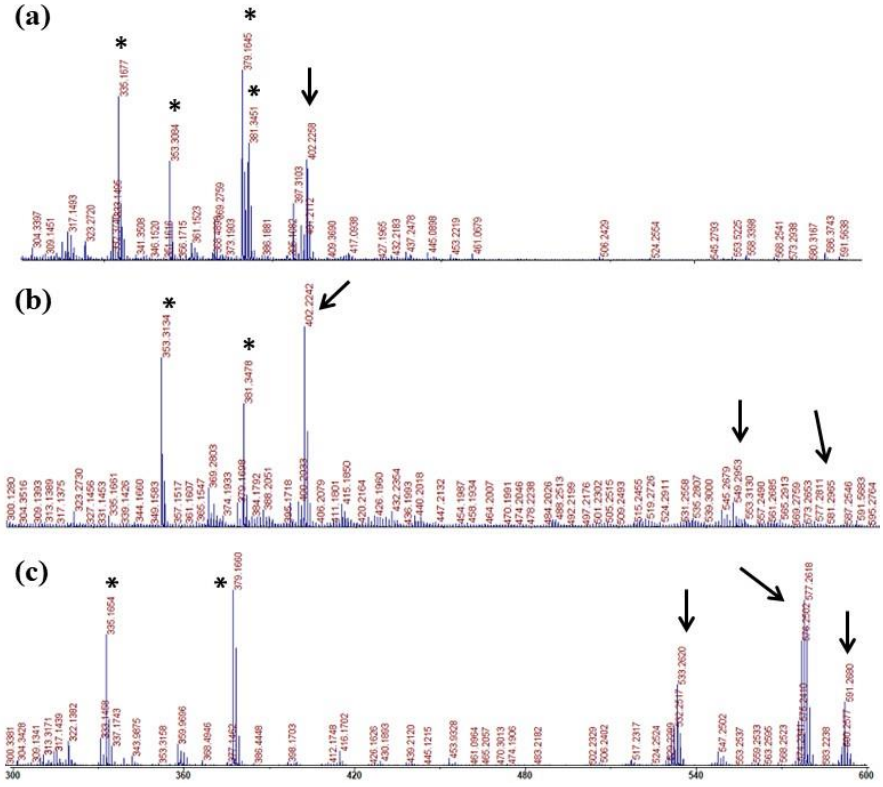

Figure 2.3.3. Segmental spectra of MALDI-ToF (m/z: 300-600 Da) characterizations of (a) PDA film, (b) PDA precipitate in carbonate buffer at pH=9.0, and (c) DHI melanin in carbonate buffer at pH=9.0, respectively. Arrows indicate specific peaks of PDA or DHI melanin, whereas asterisks indicate signals due to matrix or impurities.

Recent studies[109] based on MALDI-MS showed that folic acid (FA), a templating agent, influences the morphology and nanostructure of PDA favoring formation of species giving a cluster of peaks at 585-589 Da that were fitted to a porphyrin-type building blocks derived from oxidative cyclization of DHI tetramers built via 2,7'-bondings.[110] On this basis another related issue was to verify the possible role of porphyrin-like tetramers in PDA film formation. Interestingly, in others experiments it was demonstrated that PDA synthesized in the presence of folic acid (FA) (Table 2.3.1) leads to a peak pattern similar to that observed in the carbonate reaction, but with the presence of additional minor species (m/z 563, 581) the last of which could in principle be compatible with a cyclic tetramer at the 8-electron oxidation level (Figure S2.7.2). However, formation of this species was independent of the presence of FA (Figure S2.7.3), was not observed under the usual reaction conditions in carbonate buffer and was not detected in DHI melanin. To explore further conditions under which the postulated porphyrin tetramer could be obtained, in subsequent experiments the 2,7'-dimer of DHI was oxidized and the resulting black eumelanin-type precipitate was subjected to MALDI-MS analysis. The spectrum showed two small peaks at m/z 551 and 591 (Figure S2.7.4), suggesting a tetramer and a degradation product thereof, but no peak compatible with the postulated porphyrin structures.

Table 2.3.1. Main MALDI-MS peaks considered for structural investigation of PDA and melanins from DHI and its 2,7'-dimer.

n-mer	Dopamine oligomer calcd.[1] (*m/z*)	PDA[2] (*m/z*)	PDA film[3] (*m/z*)	PDA+ FA[4] (*m/z*)	DHI oligomer calcd.[1] (*m/z*)	DHI melanin[2] (*m/z*)	Melanin from 2,7'-dimer[5] (*m/z*)
3	456 (478, 494)	402	402	402	444 (466, 482)	416, 430	
4	607 (629, 645)	549		549, 563, 581	591 (613, 629)	533,577, 591, 621	551, 591

[1]M+H (M+Na, M+K). [2]Precipitate from the reaction in carbonate. [3]Solubilized in MeOH/DMSO. [4]Precipitate obtained in the presence of FA according to Fan *et al.*[109] [5]2,5-dihydroxybenzoic acid as the matrix.

The origin of the species responsible for the main peak of PDA at m/z 402, previously attributed to a physical trimer of two DHI units and a pyrrolecarboxylic acid, was addressed as illustrated in Scheme 2.3.1. Its odd mass (giving an even pseudomolecular ion peak) was compatible with a set of alternative structures containing either 1 or 3 nitrogen atoms. In the Scheme 2.3.1 path A involves a sequence of oxidative condensation, two chain breakdown and deamination processes, leading to 7-(3,4-dihydroxyphenethyl)pyrano[3,4,5-kl]acridine-6,9,10(7H)-trione, which is representative of the one-nitrogen option. Path B involves sequential condensation of intact dopamine units favored however in acids but not under basic conditions, while path C is entirely derived from DHI coupling and oxidative quinone breakdown but it's not compatible with the fact that no peak at m/z 402 could be detected in the DHI melanin spectrum. Assuming path A the sole working hypothesis, the peak at m/z 549 in PDA polymer could arise by coupling of the species at m/z 402 with a cyclized DHI-type unit (+ 147 mass units), while the peak at m/z 581 observed in the presence of FA could arise

by muconic-type oxidative ring cleavage of an *o*-quinone from the species at m/z 549.

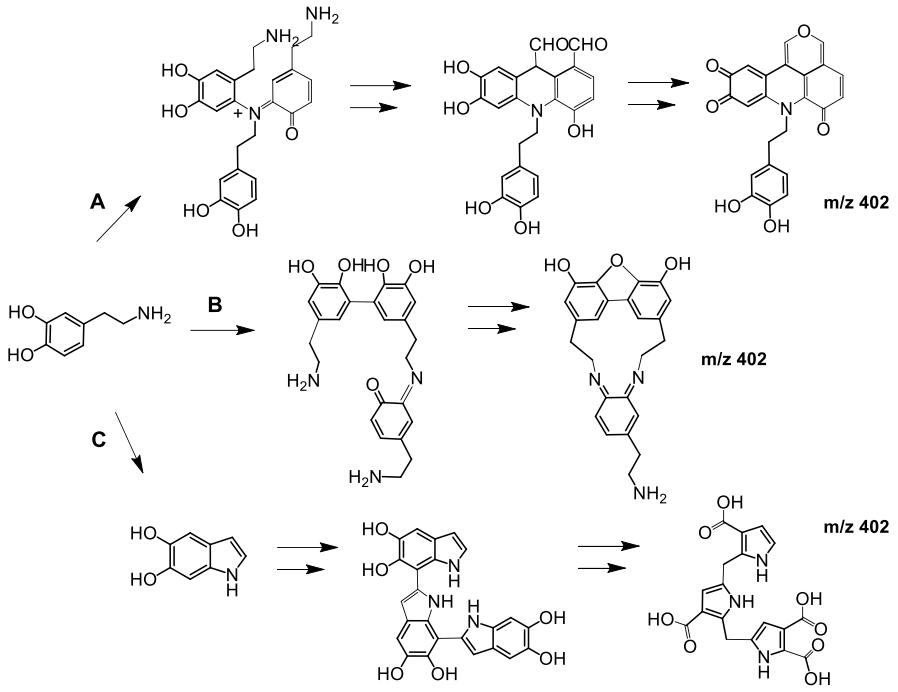

Scheme 2.3.1 Mechanism-based identification of possible structures accounting for the main peak at m/z 402 in PDA films and bulk polymer.

A detailed DFT investigation of the postulated pyranoacridinetrione structure was carried out (by Prof. O. Crescenzi at the Department of Chemistry, University of Naples Federico II) to identify diagnostic signals in UV−vis, Raman and ^{15}N NMR spectra that may be revealing its presence in PDA films. Interestingly, the data obtained supported the structural hypothesis reported above.

2.4 The role of dopamine quinone in film formation

Previous work[92] was directed to provide useful means of controlling PDA properties by a proper selection of the oxidation conditions and the nature of the oxidant. The use of oxidants stronger than dissolved O_2 and higher pHs (up to pH=9.0) allows for faster deposition of PDA films but no detailed information is available on the effects of oxidants on the structure and chemical composition of the films. To assess the role of dopamine quinone in film formation, in subsequent experiments film deposition from 10 mM dopamine at pH 9.0 was investigated using 10 mM periodate to induce fast quinone formation. The data reported in Figure 2.4.1 showed that, compared to autoxidation, the PDA film deposition proceeds at much faster rate in the presence of periodate only in the first hour. Notably, however, the final absorbance of the film at 24 h proved to be considerably less intense than that of the autoxidation process. Use of periodate ensures that all dopamine is rapidly converted to the quinone, favoring cross-linking reactions. However, while a minor amount of the material adheres to the substrate to form the primer layers, the remainder of the dopamine and other monomers would be rapidly converted to large insoluble aggregates, which would no longer contribute to the subsequent growth of the film, as observed in the slow autoxidation process.

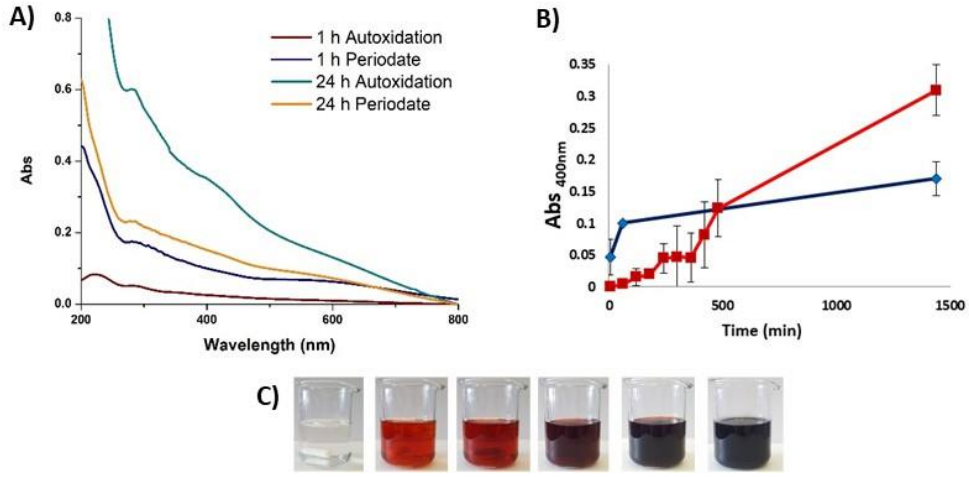

Figure 2.4.1. (a) Evolution of the UV-vis spectra of PDA film formed by dopamine autoxidation or periodate-induced oxidation. (b) Time course of 400 nm absorption development for PDA film formed by dopamine autoxidation (red line) *vs* periodate induced oxidation (blue line). Data are shown as mean ± SD of three independent experiments. (c) Digital pictures of dopamine oxidation in the presence of 1 molar equivalents of periodate.

Morphological characterization To gain additional insight into PDA films, the morphology and thickness of the films obtained in the presence and in the absence of periodate at 1 (Figure S2.7.5) or 24 h (Figure 2.4.2) oxidation time was investigated by means of AFM and Raman analysis (Figure S2.7.6) (spectra were recorded by professor P. Maddalena and co-workers at the Department of Physics, University of Naples Federico II).

Raman spectra did not reveal significant structural differences among the various samples and showed bands compatible with the presence of aromatic rings and a broad band, attributable to strongly hydrogen-bonded OH and NH stretching vibrations, as already described in the paragraph 2.3 (Figure S2.7.6). AFM

analysis showed smoother and more homogeneous films by the periodate reaction. The mean estimated thickness was 55 nm, and the surface was characterized by grains of dispersed sizes and thread-like structures made of the same material as that of the flat sample area. Autoxidation of dopamine led to smoother films as apparent from optical, AFM and Raman images at 24 h with dispersed grains size from 70 to 350 nm by means of AFM. This observation is consistent with previous work showing that increasing the oxygen concentration of the solution[106] or use of oxidants[111] leads to higher film uniformity and lesser roughness compared to autoxidation conditions with ambient oxygenation. This difference can be attributed to the rapid conversion to quinone and generation of homogenous and more regular structures followed by deposition of PDA nanoparticles.

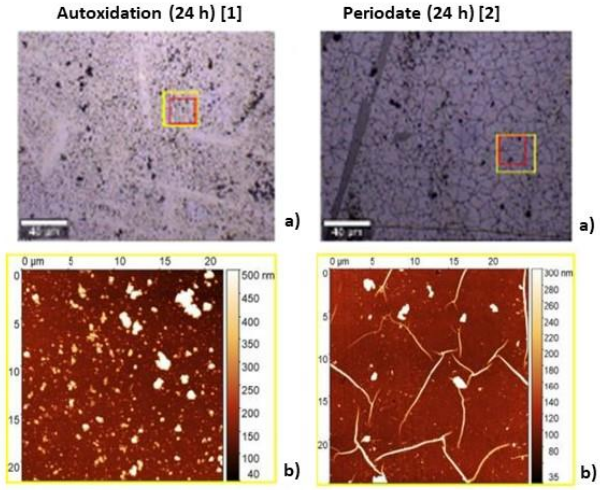

Figure 2.4.2. AFM analysis of PDA films deposited at 24 h following autoxidation (1) and periodate oxidation (2). (a) Bright-field images of the investigated sample region collected by 20 X microscope objective. (b) AFM images of the area indicated by the yellow square in the optical image. Average grain size: 200 nm (1), 150 nm (2). Film thickness: 100 ± 30 nm (1), 55 ± 15 nm (2).

Structural characterization. Insight into the structure of the PDA samples produced by periodate oxidation *versus* autoxidation was then obtained by solid state ^{13}C and ^{15}N NMR (Figure 2.4.3 and S2.7.7) analysis carried out by Drs. Roberto Avolio and Maria Emanuela Errico, IPCB, CNR, Pozzuoli. ^{13}C spectra of the sample obtained by autoxidation and by periodate-induced oxidation showed the same main resonances (Figure 2.4.3). Nevertheless, some differences in the shape of aromatic, aliphatic, and carbonyl/carboxyl peaks can be evidenced. In particular, in the spectrum of periodate-oxidation sample a decrease of the intensity of the band at 145 ppm (OH- bearing carbon of catechol) with respect to the signal at 130 ppm (quaternary carbons) can be related to a lower content of reduced catechol moieties. This conclusion was further supported by the increased intensity of the carbonyl/carboxyl peak at ~170 ppm, indicating a higher conversion of catechol to oxidized quinone groups and to some extent their oxidative fission leading to carboxyl groups in the presence of periodate.[98] Finally, the relative intensity of the aliphatic resonances was slightly higher in the periodate-oxidation sample as expected for a lower content of cyclized, indole-type units.

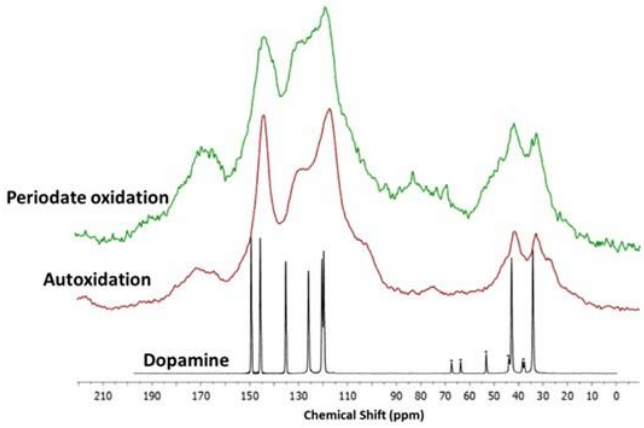

Figure 2.4.3. ^{13}C solid-state NMR spectra of the PDA samples produced by periodate oxidation (green trace) and autoxidation (red trace) of dopamine. The spectrum of dopamine (black trace) is reported as a reference (marked signals are due to spinning side bands).

2.4.1 Mechanisms of film growth

Previous and current data concur to indicate that film formation depends on two distinct and interrelated processes, a deposition phase controlled by adhesion mechanisms, and a growth phase involving progressive thickening of the deposited layer with alteration of its morphology. In another series of experiments the mechanisms of film growth following initial deposition of PDA coating was investigated based on changes in UV-vis absorbance. PDA films obtained by periodate oxidation of 10 mM dopamine for 1 h (namely *primer*) were extensively washed, dried and immersed into solutions of 0.1 mM or 1 mM dopamine at pH 9.0. The results showed a detectable increase in the film absorbance over 6 h at a low dopamine concentration (< 10 mM) which does not lead to detectable coatings

in the absence of the primer film (Figure 2.4.1.1). This observation suggests that as soon as film deposition begins, dopamine and/or other residual components, including cyclized species that are present in solution, may slowly adhere to the primer layers thus contributing to film growth by adsorption and further oxidation on the surface.

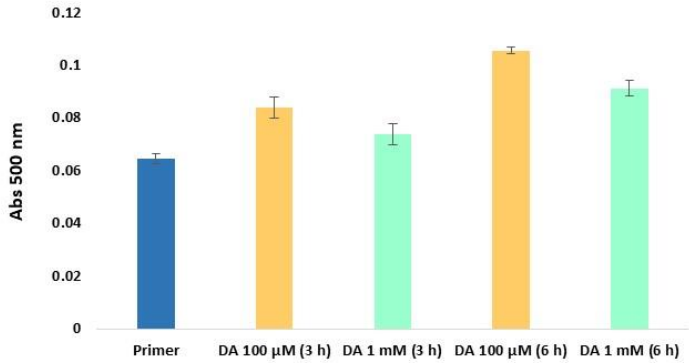

Figure 2.4.1.1. Absorbance of the films at a selected wavelength (500 nm) of *primer* substrates dipped for 3 h or 6 h in dopamine solution, 100 µM or 1 mM respectively.

2.5 Concentration dependence of film growth and the effect of amines

Early studies[89,102] showed that dopamine concentration markedly affects film thickness and the rate of film deposition. Increasing dopamine concentration increases the maximal thickness, which in turn is correlated with greater root-mean-square (RMS) roughness. Notably, no coating formation was reported at low dopamine concentrations (< 0.1 g/L) (Figure 2.5.1) or when the substrate was immersed after the process of PDA formation was completed (*e.g.*, after 24 h autoxidation).

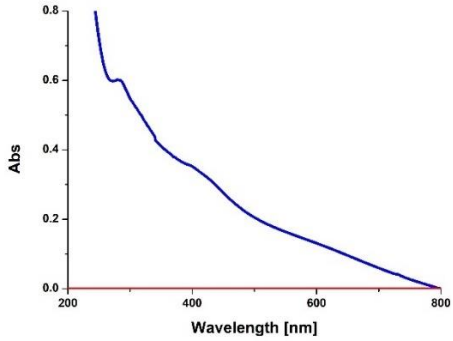

Figure 2.5.1. UV-vis absorption spectra of quartz substrates subjected to dip-coating with 10 mM (blue curve) or 1 mM dopamine (red curve).

The observed concentration dependence of film formation can be explained by considering the evolution of dopamine quinone as a key branching point in the PDA pathway[98] and Michael-type and Schiff-base amine-quinone reactions.[103] In particular, at high dopamine concentration, the quinone may be engaged with sequential bimolecular coupling process toward oligomers featuring uncyclized amine groups and giving rise to adhesive cross-linked structures. Conversely, at relatively low dopamine concentrations the unimolecular cyclization pathway of the quinone would prevail to give DHI, which polymerizes to give insoluble eumelanin-type oligomers with a strong tendency to aggregate and null adhesion properties (see Scheme 2.1.2).

Notably, however, when HMDA or other amines were added to 1 mM dopamine at pH 9.0, variable levels of coating formation were observed. Data in Figure 2.5.2 show that a long aliphatic chain and two amine groups are important structural determinants for film deposition, and the longer the chain, the higher is the effect. Consistent with this conclusion a short chain monoamine (butylamine) proved not

effective at inducing film deposition, whereas the highest extent of coating was induced by 1,12-diaminododecane, based on UV–vis absorption.

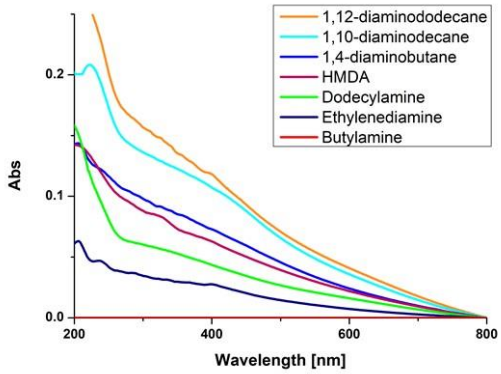

Figure 2.5.2. UV–vis spectra of quartz substrates dipped into 1 mM solution of dopamine in 50 mM carbonate buffer (pH 9.0) in the presence of equimolar amounts of various amines over 24 h.

The effect of long-chain diamines in promoting film formation at low dopamine concentrations can thus be attributed to coupling with the quinone, via *e.g.*, addition or Schiff-base formation. Inclusion of long and flexible aliphatic chains into the main structural components of PDA via amine groups would account for: (a) the provision of a hydrophobic component, which is critical for underwater adhesion; (b) the inhibition of intramolecular cyclization by occupying critical positions or *via* Schiff-base formation; and (c) the inhibition of aggregate formation which is important for adhesion.

However, the detailed mechanism by which HMDA is able to mediate PDA deposition under low concentration conditions has remained so far unknown. On this basis, to gain deeper insights into the structural factors underlying PDA adhesion, in another set of experiments the effects of structural modifications and

experimental protocol variations on HMDA mediated PDA film deposition were investigated under the selected conditions of 1 mM dopamine concentration in carbonate buffer at pH 9.0. In particular, no detectable PDA deposition was observed when the diacetyl derivative of HMDA was allowed to react at equimolar concentration with 1 mM dopamine confirming the importance of the free amine groups for HMDA mediated adhesion. Further experiments were aimed at determining the temporal dependence of the diamine-mediated effects, a parameter that is related to the evolution of reaction intermediates with the progress of oxidation. UV-vis analysis (Figure S2.7.8) showed that formation of the coating species, in the presence of HMDA, is negligible in the first hours, becomes detectable after 6 h and reaches the highest value in absorbance after 24 h. Addition of 1 mM HMDA, 30 min after the dopamine autoxidation had started, resulted in films displaying lower absorbance at 24 h compared to the standard conditions (T = 0). A much more pronounced decrease in film absorbance was determined when HMDA was added after 2 h, supporting the view that the main target species for HMDA amine groups are generated in the early stages of the autoxidation process and that, when the oxidation proceeds further, precipitation of the polymer makes HMDA ineffective in inducing adhesion (Figure 2.5.3).

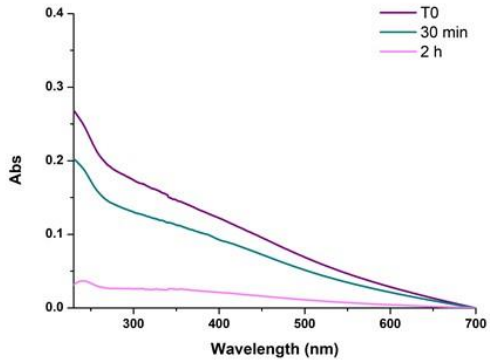

Figure 2.5.3. UV-vis spectra of PDA/HMDA films with diamine added at different times after the beginning of dopamine autoxidation. Each curve refers to a separate experiment in which HMDA was added at the stated time. T0 refers to the reference experiment in which HMDA was added at the beginning of the reaction.

In subsequent experiments since quinones are the most reasonable target for HMDA in film deposition, the effect of fast and efficient quinone formation on film deposition was investigated by oxidizing an equimolar mixture of HMDA and dopamine at pH 9.0 in carbonate buffer with 1 mM sodium periodate. The data reported in Figure 2.5.4 confirmed the role of HMDA as enhancer of film deposition: a marked acceleration of the deposition kinetics was, in fact, observed with respect to the autoxidative process in the first 3 h. Although slower, film deposition was also observed in the presence of HMDA when the reaction is carried out in acetate buffer at pH 5.0, under conditions of substantial amine protonation (Figure S2.7.9).

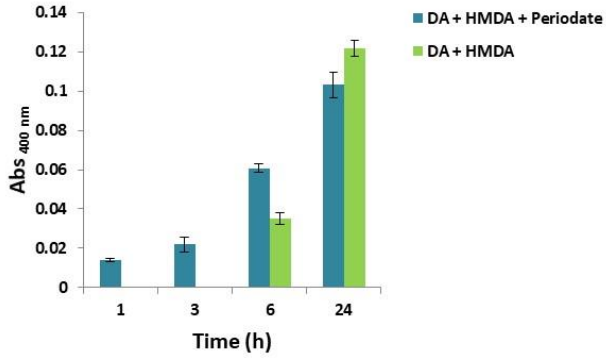

Figure 2.5.4. Kinetics of PDA/HMDA film formation: absorbance of the films obtained in the absence or in the presence of periodate in 0.05 M carbonate buffer pH 9.0 at a selected wavelength (400 nm). No detectable absorption was measured in the autoxidation experiments in the absence of HMDA.

Morphological and structural characterization. To gain further insight into PDA films, the morphology and thickness of the films obtained was investigated by means of AFM (spectra were recorded by Dr. P. Maddalena and co-workers at the Department of Physics, University of Naples Federico II). As apparent from the optical and AFM images (Figure 2.5.5), more uniform films and better grain distribution and dispersion was achieved for the film obtained in the presence of HMDA. In Table S2.7.1 is reported the average film thickness of the substrates prepared in the presence of amines, as determined by AFM.

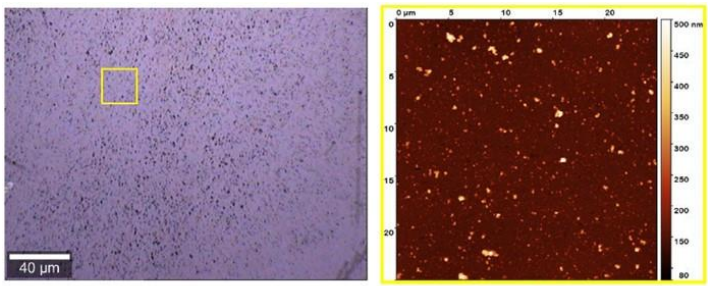

Figure 2.5.5. Atomic force microscopy (AFM) analysis of the polydopamine (PDA) film obtained in the presence of hexamethylenediamine (HMDA). (a) Bright-field image of the investigated sample region collected by 20× microscope objective. (b) AFM image of the area indicated by the yellow square in the optical image. Film thickness: 40 ± 15 nm.

Insight into the structure of the PDA melanin samples produced in the presence and in the absence of HMDA was then obtained by solid state ^{13}C and ^{15}N NMR analysis of the bulk materials that precipitated from the reaction mixtures (carried out by Drs. Roberto Avolio and Maria Emanuela Errico, IPCB, CNR, Pozzuoli.). As reported in Figure 2.5.6 the PDA sample, obtained in the presence of HMDA, showed a change in intensity and a position of the main aliphatic resonances centered at around δ = 27, 32 and 41 ppm, while no shifts were observed in the aromatic region. The ^{15}N NMR spectrum consistently indicated a modest enhancement in the aliphatic amine component relative to the aromatic component in the presence of HMDA.

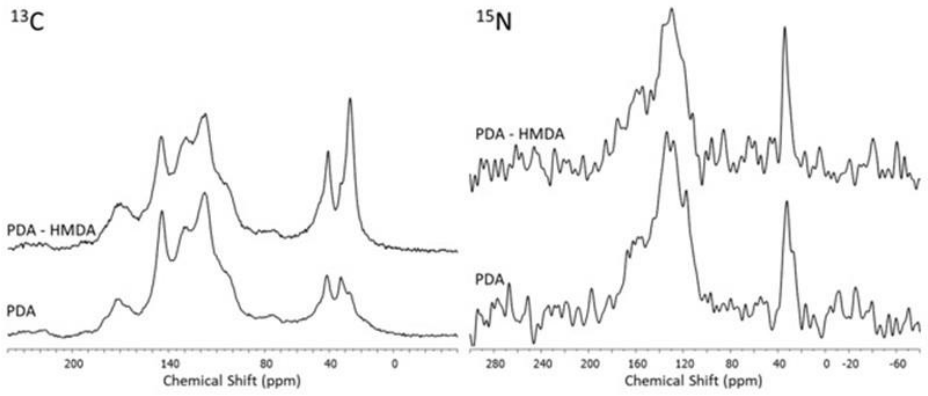

Figure 2.5.6. ^{13}C and ^{15}N NMR spectra of PDA obtained in the presence and in the absence of the diamine.

In separate experiments the bulk precipitates of the 1 mM dopamine oxidation mixture in the presence and in the absence of HMDA were centrifuged, washed with water (7000 rpm, 4 ^{o}C for 15 min), lyophilized and subjected to MS analysis in the MALDI-ToF mode. Interestingly the spectrum of the PDA/HMDA melanin (Figure 2.5.7, panel A) showed an intense peak at $[M+H]^+$ =m/z 501 ($+Na^+$, $+K^+$) which was missing in the control PDA sample (Figure 2.5.7, panel B). This peak was suggestive of two catecholamine units and two HMDA moieties linked *via* loss of two oxygen atoms, suggesting dominant condensation of the amine groups with the carbonyl moieties in dopamine quinone rather than addition at conjugated positions. A tentative structure compatible with a pseudomolecular ion peak at m/z 501 is shown in Figure 2.5.8.

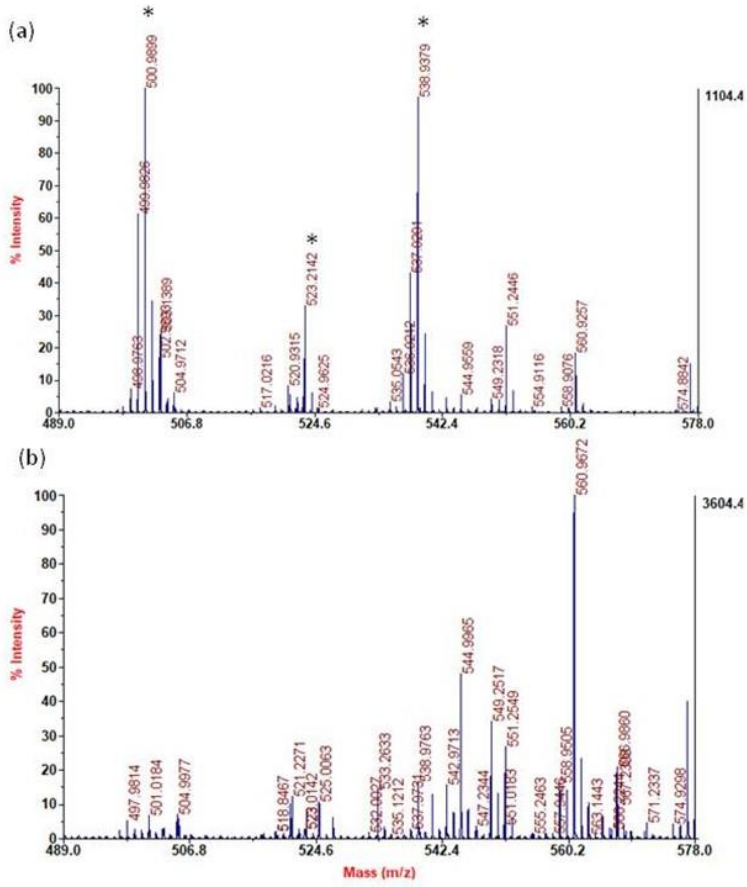

Figure 2.5.7. Segmental spectra of MALDI-MS spectra of the solid separated from PDA/HMDA (a) and PDA (b) mixture after centrifugation. Asterisks indicate specific peaks of PDA/HMDA.

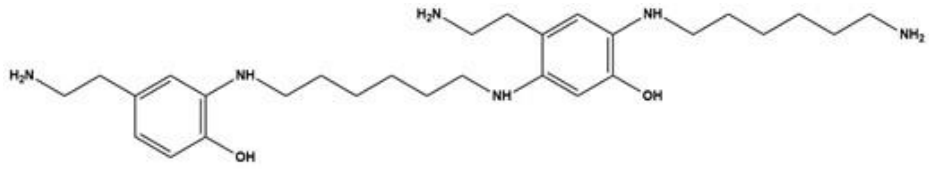

Figure 2.5.8. Tentative structure representative of the possible species responsible for the peak at m/z 501 in the PDA/HMDA mixture.

2.6 Conclusion

The results reported in this chapter may contribute to provide an improved description of the basic chemical mechanisms underlying PDA film deposition and growth. Briefly film deposition: a) requires high dopamine concentrations (>1 mM); b) is due to species produced in the early stages of dopamine autoxidation; c) is not attributable to cyclized 5,6-dihydroxyindole (DHI) intermediates produced by dopamine autoxidation, as DHI melanin does not display appreciable adhesion; d) is accelerated by equimolar amounts of periodate causing fast conversion to the *o*-quinone. In addition, it was shown that soluble monomers/oligomers can be physically adsorbed on the primer coating leading to a UV-vis detectable growth of pre-existing films. A most relevant finding was that hexamethylenediamine (HMDA) and other long chain aliphatic (di)amines enable deposition of PDA films under low dopamine concentration conditions (<1 mM) where no UV detectable coating is normally observed. This observation was of considerable interest for two main reasons: (a) it suggested that long chain flexible cross-linking systems play an important role in adhesion mechanisms evidently compensating the drop in bimolecular coupling processes at low dopamine concentrations; (b) proper selection of diamine additives can substantially widen the scope of PDA based surface functionalization technologies and can pave the way for more versatile coating methodologies based on mixtures of cross-linking and functionalizing additives.

2.7 Experimental section

Materials and methods

Dopamine hydrochloride, hexamethylenediamine (HMDA), ethylenediamine, 1,4-diaminobutane, 1,10-diaminodecane, 1,12-diaminododecane, butylamine, dodecylamine, pyridine, potassium ferricyanide, sodium bicarbonate, sodium dithionite, acetic anhydride, 3,4-dihydroxy-L-phenylalanine, 2,5-dihydroxybenzoic acid and α-Cyano-4-hydroxycinnamic acid (CHCA, 98% purity) have been purchased from Sigma-Aldrich. Sodium periodate has been purchased from AnalytiCals Carlo Erba. DHI was prepared according to Edge *et al.* (2006).[112] Quartz substrates were cleaned by soaking in piranha solution (96% H_2SO_4/30% H_2O_2 5:1 v/v) overnight, rinsed with distilled water and dried under vacuum. The **UV-vis** spectra were recorded on a JascoV-730 Spectrophotometer.

Synthesis of PDA and DHI melanin and general procedure for coating experiments. Polydopamine (PDA)[32] or DHI melanin were prepared as previously reported by autoxidation of dopamine hydrochloride (100 mg, 0.5 mmol) or DHI (100 mg, 0.7 mmol) in 0.05 M carbonate buffer (pH 9.0) (final concentration 1 mM or 10 mM), under vigorous stirring. Quartz substrates were dipped in the autoxidation mixtures after complete dissolution of the catechol for the appropriate time range (between 1 and 24 h). The substrates were then rinsed with distilled water, sonicated in methanol/water solution 1:1 v/v, and air-dried. The coated substrates thus obtained were analyzed by UV-vis spectrometry. When required, after 24 h the reaction mixture was acidified to pH 2.0 with 4 M HCl, centrifuged at 7000 rpm at 4 °C for 15 min and the precipitate washed three times with water and lyophilized to collect the dark pigment (45% and 79 % w/w yields for PDA and DHI melanin respectively).

In separate experiments, dopamine or DHI (0.3 mg/mL) in the absence or in the presence of FA (0.15 mg/mL) was first dissolved in deionized water and stirred for one day at 60 °C in the dark; then NaOH aqueous solution (0.1 M) was used to adjust the pH value (pH *ca.* 8.5) and the mixture was stirred for 3 h at 60 °C in the dark.[109] In the case of DHI, the phase of preincubation with FA was performed by sealing the reaction mixture under argon to prevent the indole oxidation. Then, the dark suspension was centrifuged at 10.000 rpm for 30 min to collect the precipitate. The sediment was washed several times with water and then dried by lyophilization.

PDA film deposition induced by periodate. Dopamine hydrochloride (100 mg, 0.5 mmol) was dissolved in 0.05 M carbonate buffer (pH 9.0) (final concentration 10 mM) followed by sodium periodate addition in a 1:1 molar ratio. The reaction mixture was left under vigorous stirring for 24 h. The quartz substrates were dipped in the solution for the appropriate amount of time according to the experiment (between 5 min and 24 h). They were then rinsed with distilled water, sonicated, dried and analyzed as above. After 24 h the reaction mixture was acidified to pH 2 with 4 M HCl and the dark pigment was collected by centrifugation at 7000 rpm at 4 °C, washed three times with water, and lyophilized (90% w/w yield). PDA-periodate films obtained by periodate oxidation of 10 mM dopamine for 1 h were immersed into solutions of 0.1 or 1 mM dopamine in 0.05 M carbonate buffer at pH 9.0 for 3-6 h. The substrates were rinsed and analyzed as usual.

Amine-promoted film formation from dopamine. To a 1 mM solution of the appropriate amine (HMDA, ethylenediamine, 1,10-diaminodecane, 1,12-diaminododecane, 1,4-diaminobutane, butylamine or dodecylamine) in 0.05 M carbonate buffer (pH 9.0), dopamine hydrochloride was added under vigorous

stirring in a 1:1 molar ratio. Quartz substrates were dipped into the reaction mixture and left under stirring for the appropriate time interval, then rinsed with distilled water, sonicated, dried and analyzed as above.

In other experiments, 30 mg of HMDA were acetylated with 500 µL of acetic anhydride and 50 µL of pyridine at room temperature overnight. The product thus obtained was added to a 1 mM dopamine solution in 0.05 M carbonate buffer, pH = 9.0 and left under stirring for 24 h. A quartz substrate was also dipped in the reaction mixture and then analyzed as above. In further experiments PDA synthesis and deposition was investigated by adding periodate to an equimolar (1 mM) mixture of HMDA and dopamine at pH 9.0 in carbonate buffer or at pH 5.0 in acetate buffer.

Atomic Force Microscopy and Micro-Raman Analysis. The combined atomic force microscopy (AFM) and micro-Raman analysis were conducted with the integrated apparatus Alpha300 RS (WITec, Ulm, Germany). The samples topographies were studied by AFM in intermittent contact (AC) mode using a cantilever with 75 kHz resonant frequency. For the micro-Raman analysis, a laser beam at $\lambda = 488$ nm was used as excitation light source. The samples analysis was conducted in the microregions marked by the colored squares in the optical images of the films. The AFM images correspond to an area of 25×25 µm^2 (yellow square). For the micro-Raman imaging, the samples were scanned over the area of 18×18 µm^2 indicated by the red squares. The Raman spectra results from 500 ms acquisition time, while the Raman images of the analyzed regions were reconstructed integrating for each scanned position the Raman signal in a spectral window of 140 cm^{-1} in width, centered at the 1584 cm^{-1} peak.

Solid State Nuclear Magnetic Resonance. Solid state nuclear magnetic resonance (NMR) spectra were recorded on a Bruker Avance II 400 spectrometer (Bruker Corporation, Billerica, MA, USA) operating at a static field of 9.4 T, equipped with a Bruker 4 mm magic angle spinning (MAS) probe. Samples were packed into Bruker 4 mm zirconia rotors sealed with Bruker Kel-F caps. The spinning speed was set at 10 and 6 kHz for ^{13}C and ^{15}N NMR experiments, respectively. Cross polarization (CP) spectra were recorded with a variable spin-lock sequence (ramp CP-MAS), and a relaxation delay of 4 s; a ^{1}H $\pi/2$ pulse width of 3.0 μs was employed and high-power proton decoupling was applied during acquisition. For ^{13}C spectra, the contact time was set to 2 ms and 20,000 scans were recorded per each sample. Spectra were referenced to external adamantane (CH_2 signal 38.48 ppm downfield of tetramethylsilane (TMS), set at 0 ppm). For ^{15}N spectra, the contact time was set to 1.5 ms and 80,000 scans were recorded. Spectra were referenced to external glycine (amine signal 32.6 ppm downfield of ammonia, set at 0 ppm).

Sample preparation for MALDI-MS Analysis. The solution of matrix CHCA (10 mg/mL) was prepared in acetonitrile/water (1:1 v/v) containing 0.1% TFA. One mL of the analyte, solubilized in dimethylsulfoxide and homogenized with a glass/glass potter (when requests), was premixed with 1 mL of the matrix (2,5-dihydroxybenzoic acid and/or α-cyano-4-hydroxycinnamic acid) in a centrifuge tube, and then 2 μL of the resulting mixture were pipetted on the MALDI target plate and air-dried for MALDI-ToF MS analysis. MALDI spectra were recorded on a Sciex 4800 MALDI ToF/ToF instrument. The laser was operated at 3.700 Hz in the positive reflectron mode. The mass spectrometer parameters were set as recommended by the manufacturer and adjusted for optimal acquisition performance. The laser spot size was set at medium focus

(B50mm laser spot diameter). The mass spectra data were acquired over a mass range of m/z 100-4.000, and each mass spectrum was collected from the accumulation of 1.000 laser shots. Raw data were analyzed using the computer software provided by the manufacturer and reported as monoisotopic masses.

Supplementary materials

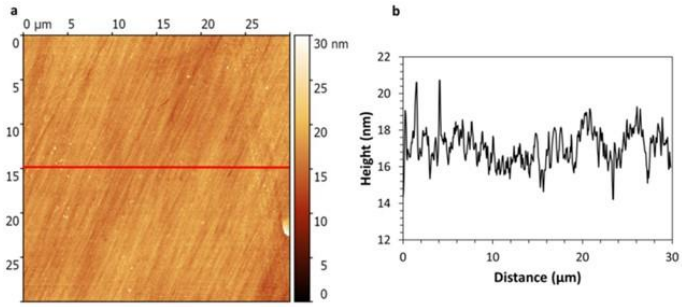

Figure S2.7.1. (a) AFM image of a region of the DHI sample in which no remarkable topography can be distinguished. (b) AFM height profile measured along the red line, compatible with the roughness of the quartz substrate.

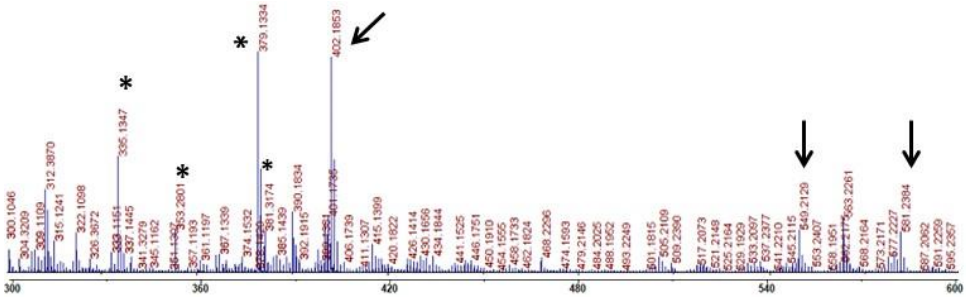

Figure S2.7.2. Segmental spectrum of MALDI-ToF (m/z: 300-600 Da) characterizations of PDA synthesized in the presence of FA (dopamine dissolved in water for over 24 h in the dark at 60°C + NaOH 0.1M to adjust the pH value to ~ 8). Asterisks indicate signals due to matrix or impurities.

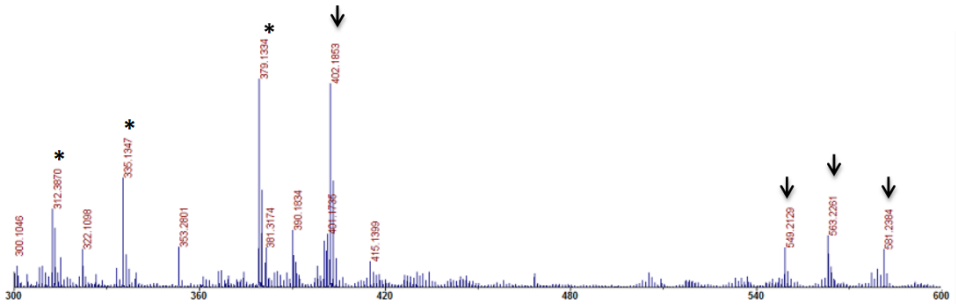

Figure S2.7.3. Segmental spectrum of MALDI-ToF (m/z: 300-600 Da) characterizations of PDA produced under the conditions previously reported for the folic acid templating experiments but without folic acid. Asterisks indicate signals due to matrix or impurities.

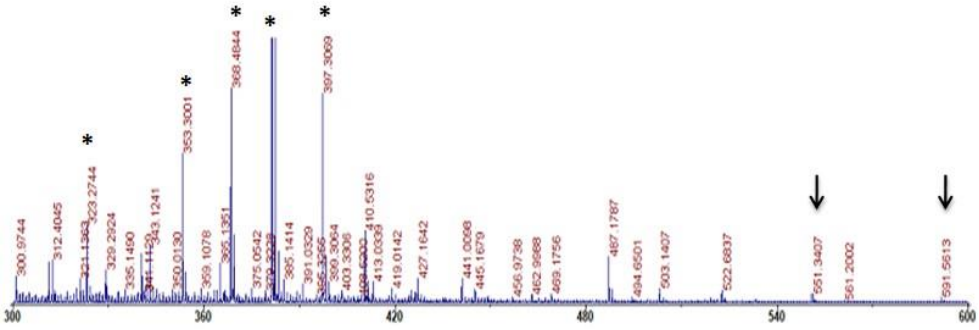

Figure S2.7.4. Segmental spectrum of MALDI-ToF (m/z: 300-600 Da) characterizations of melanin from 2,7'-dimer of DHI from the reaction in carbonate and obtained in 2,5-dihydroxybenzoic acid as the matrix. Asterisks indicate signals due to matrix or impurities.

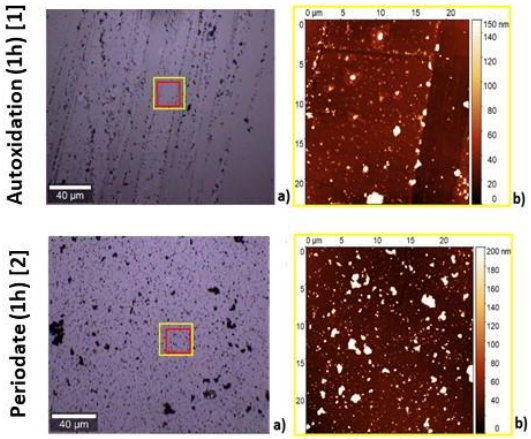

Figure S2.7.5. AFM analysis of PDA films obtained in the presence and in the absence of periodate at 1 h oxidation time. (a) Bright-field image of the investigated sample region collected by 20 × microscope objective. (b) AFM image of the area indicated by the yellow square in the optical image. Average grain size: 60 nm (1), 100 nm (2). Film thickness: 17 ± 7 nm (1), 70 ± 15 nm (2).

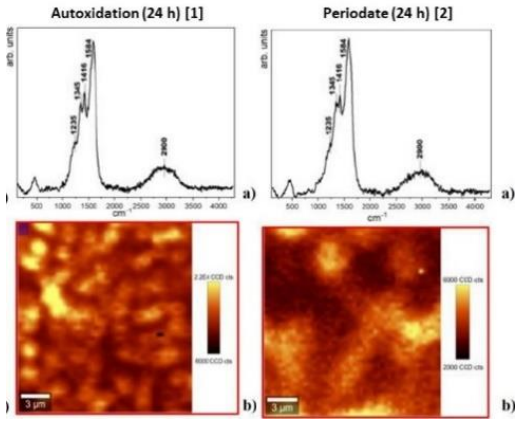

Figure S2.7.6. Micro-Raman analysis of polydopamine films deposited at 24 h following autoxidation (1) and periodate oxidation (2). (a) Raman spectrum and (b) micro-Raman image relative to the red sample region in the optical image (Figure 2.3.2).

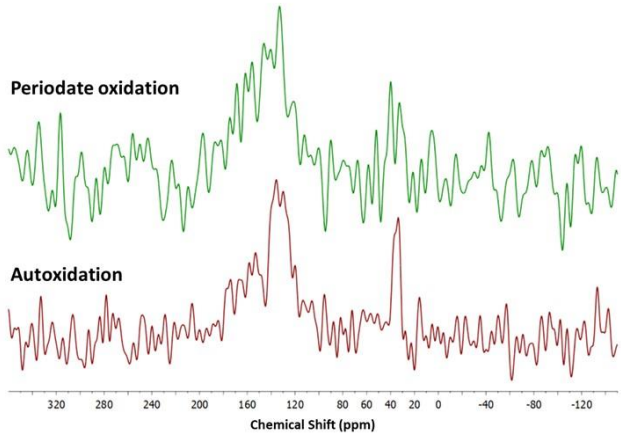

Figure 2.7.7. ^{15}N spectra of samples produced by periodate oxidation (green spectrum) and autoxidation (red spectrum).

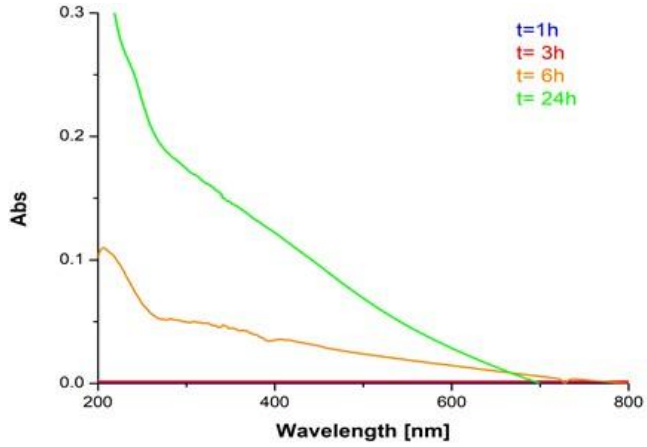

Figure S2.7.8. Evolution of the UV-vis spectra of PDA/HMDA film formation.

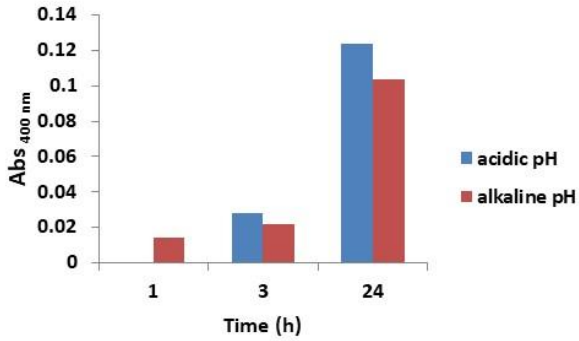

Figure S2.7.9. Evolution of the UV-vis spectra of PDA/HMDA films in the presence of periodate in 0.05 M acetate buffer pH 5.0 or 0.05 M carbonate buffer pH 9.0 at a selected wavelength (400 nm).

Table S2.7.1. Average film thickness of quartz substrates prepared in the presence of amines as determined by AFM.

	1,12-diaminododecane	1,10-diaminodecane	1,4-diaminobutane	Dodecylamine	Ethylenediamine
Thickness (nm)	61 ± 30	53 ± 15	45 ± 20	12 ± 6	5 ±3

Chapter 3

Catechol-based fluorescence turn-on system for sensing and coating

3.1 Introduction

Selective labelling of biomolecules greatly facilitates the understanding of their dynamic roles under physiological and pathological conditions helping the identification of specific biomarkers and the development of therapeutic agents against human diseases.[113] A two-step approach for chemoselective labelling is commonly employed: in the first step a properly functionalized substrate is introduced into the biomolecule of interest by a genetic or chemical method; in the second step an external chemical probe, most frequently fluorescent, is introduced and reacts with the incorporated chemical functionality in a selective and specific manner. In most cases, an excess of the secondary reagent is employed to guarantee an adequate labeling efficiency but, this implies washing steps to remove the unreacted fluorescent reagent and thus eliminate the background fluorescence. On these bases, such florescent reagents cannot be applied to those cases in which a washing step is not applicable, *e.g.* as real-time monitoring of dynamic processes and *in vivo* labeling.[114]

Recent studies have been directed to the design of systems for fluorescence-based imaging and sensing[115,116] based on robust and versatile chromophores responding to specific stimuli with a strong emission (the "turn-on" mode). Compared to the turn-off approach, which usually requires quenching or switching of a preformed

fluorophore, fluorescence turn-on needs low-concentration, reduces the effects of false positive signals, increases both sensitivity and specificity and is achieved mostly by use of preformed emitting systems, *e.g.* perylene or fluorescein derivatives, *via* removal of specific quenchers. Reactivity-based turn-on systems usually exploit cleavage reactions,[117] click chemistry cyclizations,[114,118] organic couplings,[119] metal–ligand substitution,[120] and tandem cascades unmasking fluorogenic scaffolds.[115,121]

A growing interest is directed to the development of novel efficient fluorophore-generating processes that can be triggered in response to specific stimuli and that can be applied for thin film deposition or for inclusion in hydrogels and biomatrices without significant loss of properties. Fluorescent thin films and coatings may provide, in fact, useful tools for a variety of biomedical, environmental and technological applications with special reference to specific and sensing materials operating both in vapor phase (*e.g.* volatile amines, illicit drugs, nitrotoluenes)[122,123] and in solution (*e.g.* Hg^{+}, F^{-}, Au^{3+}),[124] real time monitoring of cell growth and metabolic changes, specific input-responsive packaging and damage detection in cultural heritage.

A still little explored source of inspiration for novel strategies in the field of functional materials and systems is offered by natural products and biologically relevant systems. Catechol systems, especially, are the focus of intense research because of their peculiar redox reactivity, which allows for efficient cross-linking reactions, oxidative polymerization, strong metal chelating properties and for their ability to interact with a variety of functional groups and surfaces. In the 1990s, it was found that resorcin and derivatives, such as phloroglucinol, can efficiently react with enzymatically or chemically-generated quinones from the amino acid DOPA and the neurotransmitter dopamine (DA) to give a highly fluorescent

product featuring a 4,9-dihydroxy-3,4-dihydro-1H-4,11a-methanobenzofuro[2,3-d]azocin-5(2H)-one scaffold (Scheme 3.1.1).[125]

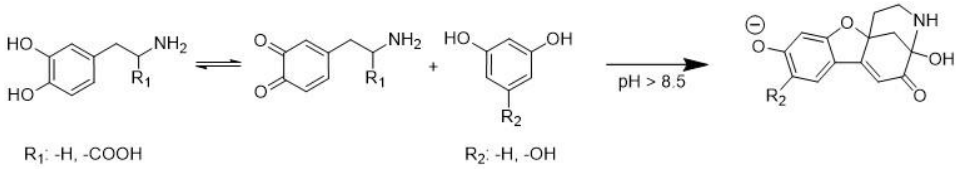

Scheme 3.1.1. Oxidative coupling of catecholamine compounds with resorcinol leading to fluorescent methanobenzofuroazocinone products.

As shown in the Scheme 3.1.2 the reaction involves a nucleophilic attack of resorcin onto the electrophilic transient *o*-quinone produced by oxidation of the catecholamine. A further oxidation step generates then the furan ring *via* intramolecular attack by the OH group to an *o*-quinone intermediate. Finally, intramolecular attack by the ethylamine side chain leads to ring closure of the azocine system and development of fluorescence.[125]

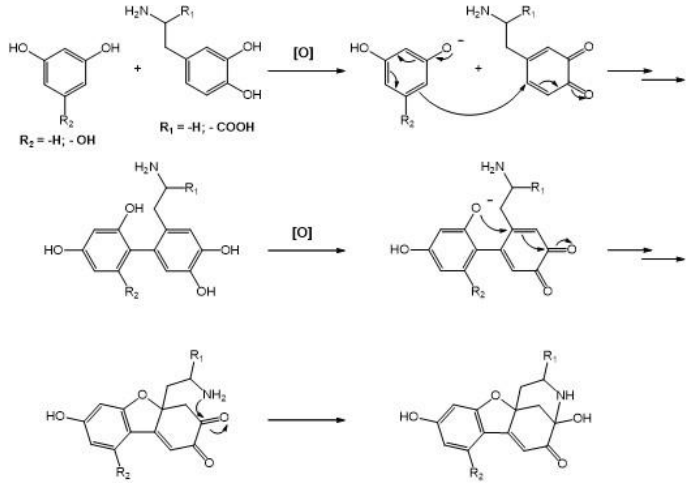

Scheme 3.1.2. Proposed mechanism of the reaction of catecholamine with resorcinol or phloroglucinol to give fluorescent methanobenzofuroazocinone coupling products.

The resulting methanobenzofuroazocinone scaffold is akin to that of monardine in matlaline, the yellow fluorescent product produced in lignum nephriticum by oxidation of Pterocarpus indicus and Eysenhardtia polystachya C- and O-β-glycosylhydroxydihydrochalcones.[126] The unusual four-ring structure of the natural fluorophore was confirmed in 2009 by Acuña *et al.* by isolation from the wood of Eysenhardtia polystachya of two possible bio-synthetic precursors of the fluorophore: coatline A and coatline B, only one of which, in the anion form, proved responsible for the strong blue emission (Figure 3.1.1).[127,128]

Figure 3.1.1. Structure of Coatline B isolated from E. polystachya and its fluorescent oxidation product Matlaline.[126]

The high emission quantum yield in water, pH-dependent switching between bright and dark states, and full compatibility with aqueous solvents suggested the potential of this fluorogenic reaction for turn-on sensing of catecholamines or conditions causing increase in pH. However, a predictable practical limitation of the catecholamine-resorcinol coupling for sensing and other applications is represented by its bimolecular character, which may weaken the fluorescence response under high dilution conditions or in the presence of interfering species in hydrogels and complex matrices.

In attempt to exploit the fluorescence turn-on oxidative coupling of catecholamines with resorcinols to access to novel oxygen and alkali-sensing antioxidants with fluorescence read out,[129-131] new resorcinol-based couplers for

dopamine were designed and their synthesis and characterization will be presented in this chapter.

Specifically, the study was directed to:

a. elucidate the dopamine-resorcinol coupling reaction for fluorescence turn on systems;
b. probe the performance of the system in bio-based hydrogels, as a step toward implementation of amine-sensing devices and smart packaging components;
c. develop fluorescent surface functionalization and coating methodologies based on the rational design of resorcinol-based cross-linking compounds.

3.2 Design of multipurpose fluorescence turn-on system by a dopamine-resorcinol conjugate

In a first series of experiments, to exploit the fluorescence turn-on oxidative coupling of catecholamines with resorcinols, a methylene-bridged dopamine-resorcinol conjugate (4-(2-((2,4-dihydroxybenzyl)amino)ethyl)benzene-1,2-diol (**1**)) was synthesized by condensation of dopamine with 2,4-dihydroxybenzaldehyde followed by a mild reduction step (Scheme 3.2.1).

Quite unexpectedly, under slightly alkaline aerobic conditions (0.05 M carbonate buffer, pH 9.0), **1** was converted into a strongly emitting yellow species (Scheme 3.2.1) which displayed absorption and emission spectrum very close to the methanobenzofuroazocinone fluorescent product derived from the oxidative coupling of dopamine with resorcinol (Figure 3.2.1).

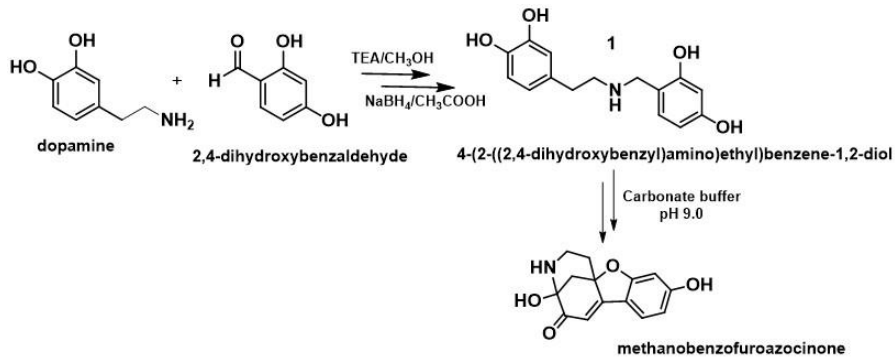

Scheme 3.2.1. Synthesis of the dopamine resorcinol conjugate and its oxidative conversion into the methanobenzofuroazocinone system.

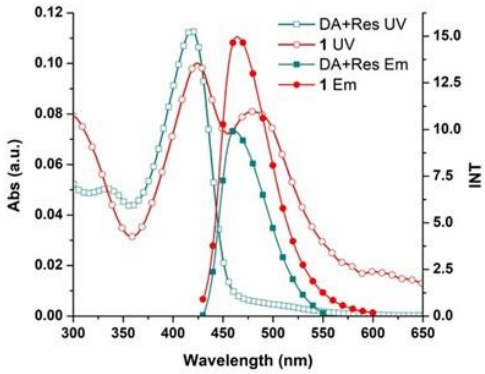

Figure 3.2.1. UV-vis and fluorescence spectra of the reaction mixture from the dopamine resorcinol conjugate compared to the oxidation reaction of dopamine with equimolar resorcinol at 1 h.

LC-MS (ESI^+) analysis of the oxidation mixture, when fluorescence development attained a plateau, confirmed the presence, besides the starting compound (pseudomolecular ion peak at m/z 276), of a main species with a pseudomolecular ion peak at m/z 260 and an elution time identical to that of the coupling product of dopamine with resorcinol (Figure 3.2.2).

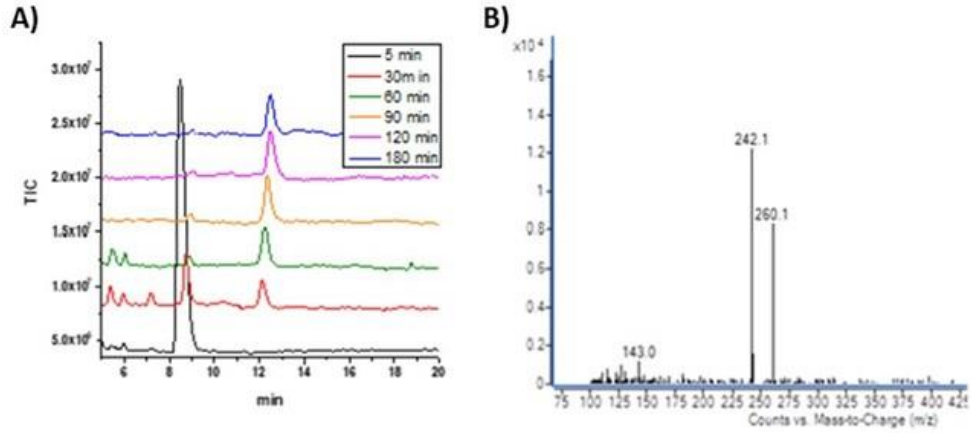

Figure 3.2.2. (a) LC-MS (ESI^+) analysis of the oxidation mixtures of **1** (1 mM) at different reaction times. For analysis, aliquots were withdrawn and diluted up to 0.05 mg/mL in 0.1% formic acid-methanol (1:1 v/v). (b) ESI^+-MS spectrum of the species eluted at 12.2 min. The base peak at m/z 242 is probably due to loss of water.

To confirm the identity of the product, the mixture from the autoxidation of **1** was chromatographed on a Sephadex® G-10 gel filtration column and a more retained yellow band was collected which displayed a distinct maximum at 420 nm shifting hypsochromically to 390 nm with loss of fluorescence upon acidification. LDI-MS analysis of the band gave a pseudomolecular ion peak at m/z 282 $[M+Na]^+$, while the ^1H NMR spectrum definitively validated its identity with the coupling product of dopamine with resorcinol following comparison with an authentic sample (Figure S3.5.1).[125] In another series of experiments the emission properties of **1** were evaluated following autoxidation at different concentrations in comparison with 1:1 dopamine:resorcinol mixture at the same concentration. The data indicated a marked deviation from linearity in the fluorescence response with increasing concentration, consistent with a unimolecular fluorogenic process (Figure 3.2.3).

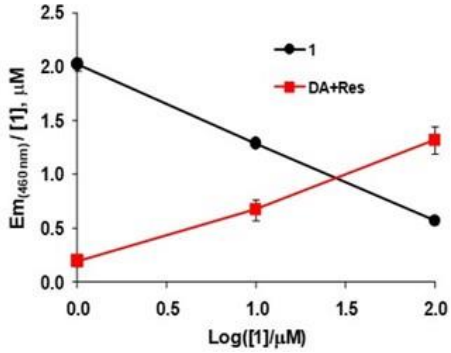

Figure 3.2.3. Emission properties of **1** following autoxidation at different concentrations (λ_{ex}: 420 nm, λ_{anal}: 460 nm, pH 9.0). Visually detectable fluorescence was measurable with **1** above 1 μM concentration.

Mechanistic studies. The mechanisms of the reaction, purportedly involving an oxidative rearrangement with loss of carbon, was investigated by chemical experiments and computational approaches (run at the Department of Chemistry, University of Naples Federico II in the frame of a collaborative work with Prof. O. Crescenzi) (Scheme 3.2.2). The proposed scheme envisaged:

1. the attack of the activated quaternary carbon of the resorcinol moiety onto the *o*-quinone ring to give a spiro intermediate (***I***);
2. furan ring closure (spiro intermediate (***II***)) due to the attack of the phenolic oxygen in the spiro intermediate onto the quinone system;
3. amine-promoted cleavage of the methylene-resorcinol bond driven by re-aromatization of the resorcinol ring yielding ***III***;
4. hydrolytic release of formaldehyde followed by ring closure routes that accounts for the carbon loss accompanying the oxidation reaction.

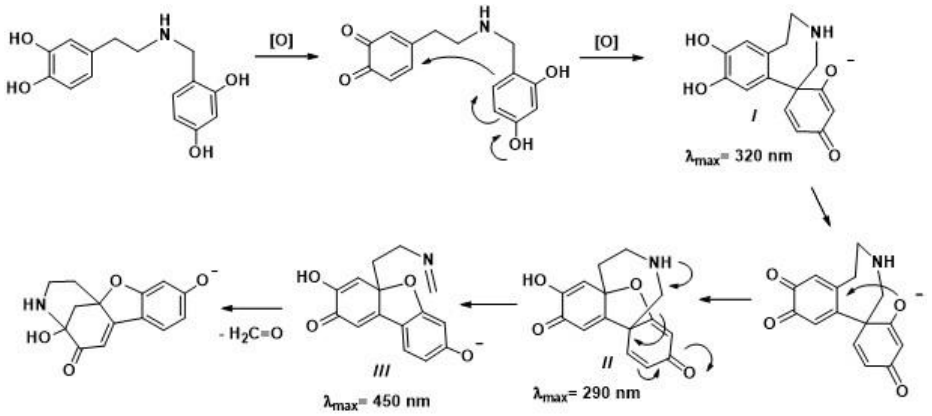

Scheme 3.2.2. Proposed mechanism of conversion of **1** to the methanobenzofuroazocinone product. Predicted absorption maxima (DFT calculations) for the main putative intermediates are reported.

Several efforts were made to get direct evidence for the formation of formaldehyde, including NMR analysis of the reaction mixture over time and search for products arising from trapping of this reactive species by reaction with **1** as observed in previous studies in which the formation of an isoquinoline arising by reaction of dopamine with formaldehyde was observed.[10] Yet, no conclusive result could be obtained and hence the proposed mechanism remains speculative though chemically sound and supported by literature data. In particular monitoring of the reaction course by LC-MS (ESI^+) gave extracted ion chromatograms characterized by a minor species at m/z 274 and another more retained species at m/z 272, compatible with the initial seven-membered spiro intermediate ***I*** (calcd. exact mass m/z 273.10) and the highly constrained species ***II*** preceding the nitrogen-assisted ring opening re-aromatization of the resorcinol moiety (calcd. exact mass at m/z 271.08), respectively (Figure S3.5.2).

Moreover, DFT analysis of the main intermediates in the proposed scheme predicted for the last intermediate ***III*** an absorption maximum at 450 nm compatible with the 480 nm band observed monitoring spectrophotometrically over time the course of the autoxidation of **1** at 10 µM (Figure 3.2.4).

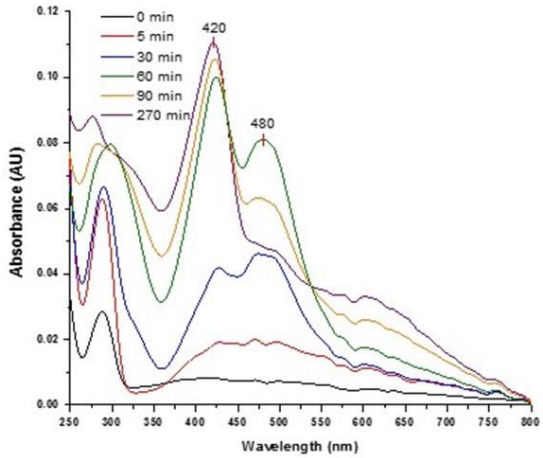

Figure 3.2.4. Spectrophotometric analysis of the autoxidation of 10 µM of **1**.

Persistence of the chromophore at 480 nm during the reaction could then be attributed to the slow hydrolysis of the imine moiety at alkaline pH. This finding, coupled with the markedly different absorption profile calculated for the coupling product prior to furan ring closure, suggested that oxygen attack onto the quinone ring occurs early in the pathway thus favoring the route shown in Scheme 3.2.2.

3.2.1 Sensing applications of the fluorescent methanobenzofuroazocinone formation reaction

In separate experiments the potential use of the development of the fluorophore of **1** in response to the presence of ammonia and volatile amines or oxygen was explored. Detection of basic nitrogenous volatiles is, in fact, an issue of

considerable importance for a variety of applications *e.g.* for assessment of air quality and for food spoilage determination.[132] Initially, the fluorescence response of **1** (0.1 mM) to ammonia or amines was investigated by embedding it in beads of alginate hydrogels exposed to gaseous ammonia in a closed chamber at room temperature. As shown in Figure 3.2.1.1 (panel A), a strong fluorescence was rapidly developed accompanied by a yellow coloration, denoting *in situ* formation of the methanobenzofuroazocinone anion. Complete discoloration with quenching of fluorescence was induced by exposure of the yellow beads to HCl vapours. Since the generation of basic amine-containing volatiles (*e.g.*, NH_3 and NMe_3) is also a primary index of food spoilage due to microbial growth,[133] alginate hydrogel films loaded with **1** were exposed to vapors from decomposing fish fillets for 24 h at room temperature in a closed chamber. A marked fluorescence response was noticed under fish decomposition conditions, but not in the controls that were conducted at -20 °C or at room temperature in absence of fish-fillets, suggesting exploitation of this reaction in smart packaging for expedient monitoring of fish quality (Figure 3.2.1.1, panel B). Compared to colorimetric pH indicators that are commonly used to monitor food microbial spoilage,[134] the reaction based on the formation of **1** would have the advantage of a turn-on of fluorescence with increasing pHs, acting in addition as oxygen sensor. Figure 3.2.1.1 (panel C) shows the potential use of **1** as an oxygen sensor, *e.g.* for package leaking detection. A well detectable emission was, in fact, observed after injection of 1 mL of air *via* syringe into the headspace of a sealed flask containing an alkaline solution of **1** kept under a rigorously oxygen-free atmosphere. To probe the efficiency of the fluorescence turn-on in the presence of a potentially interfering biological matrix, compound **1** (0.1 mM) was added also to raw chicken egg white (CEW, pH ca. 9.0) under vigorous stirring. A rapid oxygen-dependent generation of a strong fluorescence was observed in support of an efficient intramolecular

coupling even in the presence of the biological components of egg white (Figure 3.2.1.1, panel D).

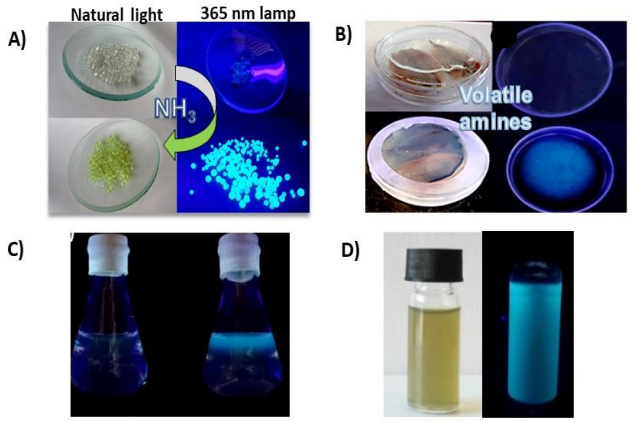

Figure 3.2.1.1. Fluorescence response of **1** (0.1 mM). A) alginate beads following exposure to ammonia vapors, (t = 10 min) *left*, under natural light; *right*, under 365 nm lamp, *top* control in the absence of **1** and *bottom* in the presence of **1.** B) alginate hydrogel films exposed to vapors from decomposing fish fillet, t = 0 h (left under natural light and t =24 h, right, under 365 nm lamp); C) 0.1 mM **1** in 0.05 M carbonate buffer pH 8.5 under an argon atmosphere before (left) and after (right) injection of air (t = 2 h); D) 0.1 mM **1** in CEW after 1 h under natural light (left) and under 365 nm lamp (right).

In others experiments, the ability of **1** to serve as an antioxidant capable of scavenging reactive oxygen species with fluorescence read-out was also explored. To this aim, the autoxidation of 1,2,3-trihydroxybenzene (pyrogallol, PG) at pH 9.0 was selected as an established model reaction for the production of superoxide anion by reduction of molecular oxygen by PG.[135] The ability of **1** to act as scavenger of superoxide anion was measured based on the development of a blue formazan dye by reduction of a tetrazolium compound (Figure S3.5.3). Data in Figure 3.2.1.2 show that **1** can efficiently scavenge superoxide in a dose-

dependent manner and the effect is accompanied by a rapid fluorescence turn-on as a measurable record of antioxidant activity.

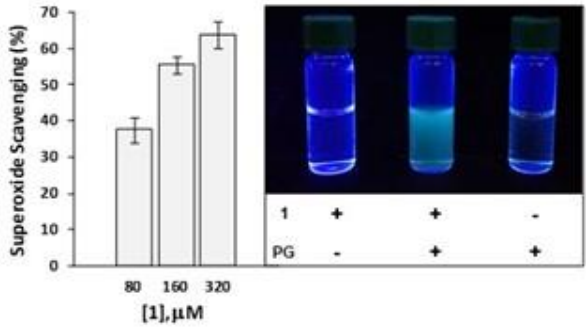

Figure 3.2.1.2. (Left) Dose dependent superoxide scavenging activity of **1** in the presence of 160 μM pyrogallol (PG) as determined by the nitroblue tetrazolium assay (means of three different experiments ± SD). (Right) Digital picture of oxidation mixtures of 160 μM **1** at pH 9.0 under a 365 nm lamp in the absence or in the presence of equimolar PG, after 2 min.

3.3 Development of an adhesive fluorescent coating

Fluorescent thin films and coatings may provide useful tools for a variety of biomedical, environmental, and technological applications, *e.g.* for monitoring pH changes and for sensing metabolic activity in cell cultures.[136-138] Although many examples have been reported of switchable and tunable fluorescent coatings obtained by self-assembled monolayer or sol-gel methodologies,[138-140] only few cases are reported of all-organic films[141] particularly if *in situ* deposition of all-organic, reaction-based fluorescent films and coatings by wet dipping technologies is considered.

On these bases the fluorogenic reaction between resorcinol derivatives with dopamine was investigated with the aim of developing fluorescent thin films for

surface functionalization *via* the dip-coating methodology commonly used for polydopamine.[32] Since no deposition was observed by simply dipping a substrate into a dopamine-resorcinol solution, the attention was then directed to the rational functionalization of the resorcinol coupler to increase hydrophobicity and affinity for glass, polymers and substrates with different surface properties. In this context hexamethylenediamine (HMDA), regarded as a lysine mimic in mussel-inspired adhesive systems,[32] has been shown to enable the deposition of adhesive films from *e.g.* gallic acid,[69] caffeic acid,[70] N-protected DOPA,[104] and other catechol-containing polymers[84,142] and thus provides an entry to the design of a variety of functional films and coatings.

In a first series of experiments a novel symmetrical bis-resorcinol derivative (referred to as Bis-Res) in which the two aromatic rings are held together by a HMDA tether, was synthesized from 2,4-dihydroxybenzaldehyde *via* Schiff base formation and reduction (Scheme 3.3.1).

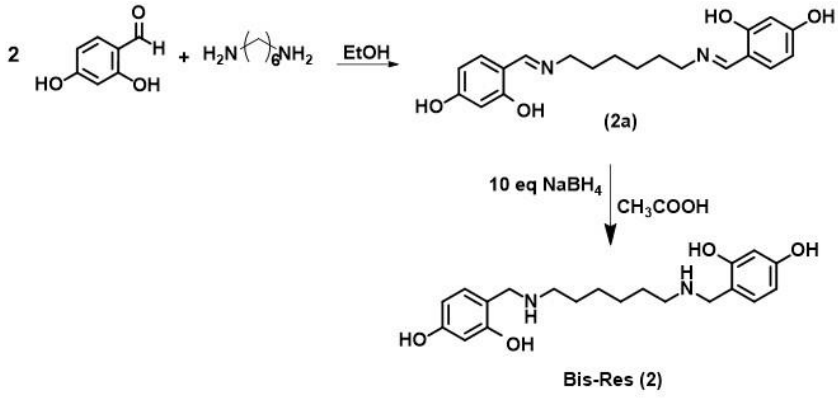

Scheme 3.3.1. Synthetic route to Bis-Res (**2**).

Stirring 1 mM Bis-Res with 2 mM dopamine in carbonate buffer at pH 9.0 (Scheme 3.3.2) led to the gradual development in solution of an intensely emitting

yellow chromophore accompanied by deposition of a fluorescent thin film on a variety of materials immersed in the reaction flask (Figure 3.3.1).

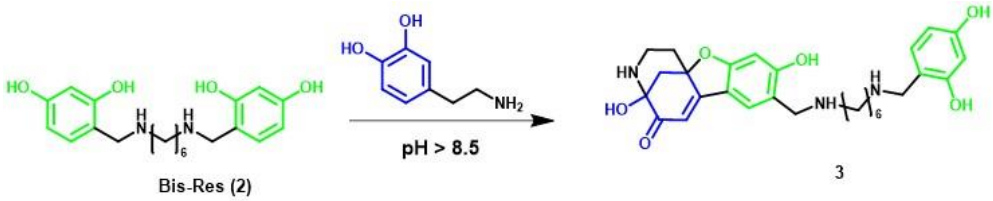

Scheme 3.3.2. Expected structure of the reaction product of Bis-Res with dopamine in 0.05 M carbonate buffer at pH 9.0.

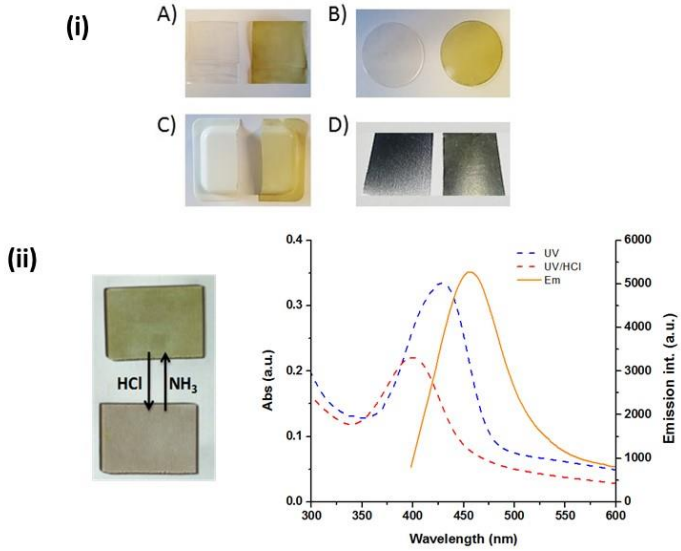

Figure 3.3.1. (i) Bis–Res/DA coatings on various materials: (A) polyethylene, (B) polycarbonate, (C) polystyrene, and (D) aluminum. On the left of each are uncoated materials. (ii) Picture, UV-vis and fluorescence spectra of a Bis-Res-dopamine coated quartz at 6 h reaction time, before and after exposure to HCl vapors.

Spectrophotometric analysis of the coating in the solid state revealed an absorption maximum at 420 nm and an intense fluorescence emission, suggesting

adduct formation of dopamine with Bis-Res, also confirmed by LC-MS analysis of the reaction mixture (Figure S3.5.4) that revealed formation of a main species with m/z = 510 $[M+H]^+$ consistent with the expected coupling product depicted in Scheme 3.3.2.

Profilometry data, reported in Table S3.5.1, indicates a film thickness of 55 ± 2.7 nm, with a roughness of 15 nm. Interestingly, exposure of the coated substrate to HCl vapors caused an apparent discoloration of the film with a consistent hypsochromic shift, a marked quenching of fluorescence, and, most notably, a marked drop of the water contact angle (WCA) of the film from about 50° to values below instrumental limits, indicating conversion into a superhydrophilic material (Figure 3.3.2, left). The HCl-induced absorption shift proved to be completely reversible upon exposure to gaseous ammonia over at least five cycles (Figure 3.3.2, right). This behaviour was attributed to acid-induced protonation of amine residues linked to the methanobenzofuroazocinone scaffold with generation of positively-charged sites increasing the hydrophilic character of the film.

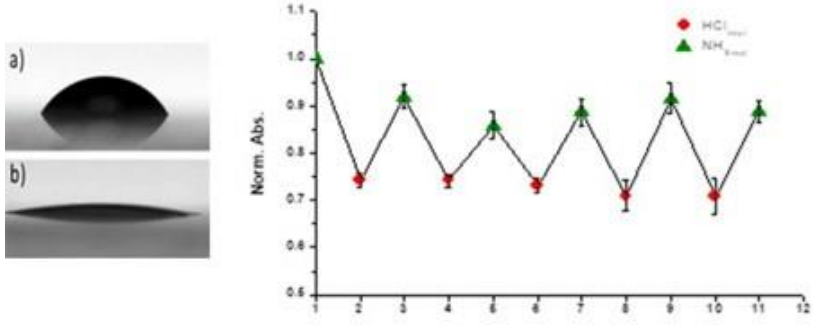

Figure 3.3.2. Left: water droplet on the Bis–Res/dopamine coating before (a) and after (b) exposure to HCl vapors. Right: relative absorbance changes at 420 nm of Bis–Res/dopamine film following repeated sequential exposure to HCl and NH_3 vapors.

The origin of superhydrophilicity following exposure to HCl vapors was then investigated by ATR/FT-IR analysis. Comparison of the spectra of the film deposited on aluminum substrate before and after acid treatment indicated: (1) a detectable shift of the broad N–H and O–H stretching band from *ca.* 3300 cm^{-1} to *ca.* 3100 cm^{-1} and (2) marked changes in the low energy bands, with the development of two weak bands at 1560 cm^{-1} and 1200 cm^{-1} (Figure 3.3.3). Although it is difficult to assign with certainty the spectrum showed also bands, missing in the free base,[143] around 1590 cm^{-1} accounting for protonated secondary amines.

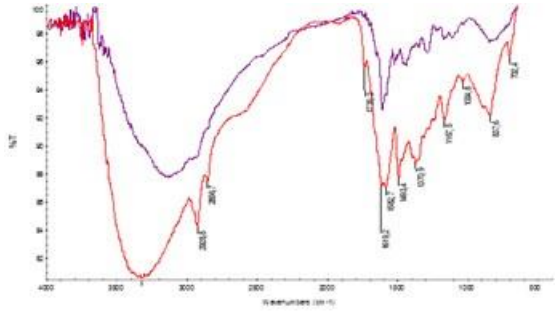

Figure 3.3.3. ATR/FT-IR of the dopamine/Bis–Res coated aluminum slide before (red line) and after (violet line) exposure to HCl vapors.

3.4 Conclusions

In this chapter a remarkable spontaneous conversion of a dopamine-resorcinol conjugate into the strongly emitting methanobenzofuroazocinone scaffold upon exposure to moderately alkaline buffer was disclosed. This unimolecular variant of the dopamine-resorcinol fluorogenic reaction, which can be referred to as *"FluoResCat"*, is efficient, versatile, develops from a cheap and easily available precursor, is endowed with antioxidant properties and operates under mild conditions. It may be useful as oxygen/superoxide scavenger with fluorescence

read-out of activity and can be used in complex biomatrices, or in hydrogels for the sensing of oxygen or volatile amines, *e.g.* for smart packaging applications.

Recently emitting film deposition by fluorescence turn-on processes represents a promising approach to surface functionalization. In this chapter a strategy for the *in situ* development of a highly adhesive and strongly emitting, all-organic film-forming system *via* the autoxidation of dopamine in the presence of a cross-linking, HMDA-resorcinol conjugate referred to as *Bis-Res* was disclosed. The present proof-of-concept investigation demonstrates the potential of this chemistry to produce novel adhesive species that can coat various substrates with acid-tunable emission and surface properties.

3.5 Experimental section

Materials and methods

All solvents and reagents were obtained from commercial sources and used without further purification. Quartz substrates were cleaned by soaking in piranha solution (96 % H_2SO_4/30 % H_2O_2 5:1 v/v) overnight, rinsed with distilled water and dried under vacuum.

UV-vis absorption spectra were registered at room temperature on a V-560 JASCO spectrophotometer.

Steady-state fluorescence emission spectra were recorded with a FP-750 JASCO spectrofluorometer.

^{1}H-NMR and ^{13}C-NMR spectra were recorded in deuterated solvents at 400 MHz on a Bruker DRX 400; δ values are reported in ppm and coupling constants are given in Hz.

Analytical thin layer chromatography (TLC) was performed on 0.25 mm thick pre-coated silica gel plates (60 F_{254}).

HPLC analyses for reaction monitoring were performed on an Agilent 1100 series instrument equipped with a LC-10AD VP pump and a G1314A UV-visible detector using a Sphereclone C18 column (4.6 × 150 mm, 5 µm), 0.1% formic acid – methanol 8:2 was selected as eluting system, at 0.7 mL/min flux. LC-MS analysis was conducted on an ESI-TOF 1260/6230DA Agilent Technologies in positive ion mode using a Zorbax Eclipse Plus C18 column (4.6 × 150 mm, 5 µm), 0.1% formic acid – methanol 8:2 was selected as eluting system at 0.4 mL/min flux.

LDI mass spectrometric analyses were run on a AB Sciex TOF/TOF 4800 instrument loading the samples on the plate at 1 mg/mL in methanol. Spectra represent the sum of 15,000 laser pulses from randomly chosen spots per sample position. Raw data were analyzed using the computer software provided by the manufacturers and are reported as monoisotopic masses.

IR spectra were recorded on Nicolet 5700 FT-IR + Smart performer spectrometer, mounting a Continuum FT-IR Microscope and on Bruker Optics TENSOR 27 FT-IR.

Synthesis of the dopamine-resorcinol conjugate (1). A mixture of dopamine hydrochloride (0.25 g, 1.32 mmol) and 2,4-dihydroxybenzaldehyde (0.18 g, 1.32 mmol) in methanol (31 mL) was stirred at room temperature. After complete dissolution, triethylamine (0.25 mL, 1.72 mmol) was slowly added *via* syringe. The reaction was left overnight under stirring. After removal of the solvent under reduced pressure the desired Schiff base was obtained as a yellow oil in 83% yield. The oil was rinsed in glacial acetic acid at 10 mM and reduced

with $NaBH_4$ (3 molar eqs). When evolution of hydrogen had ceased, the mixture was dried under vacuum, then rinsed in 1 mL of water and 3 M HCl was added to pH 2.0. Desalting of the mixture was carried out on DOWEX resin 50W X 4 using a gradient of HCl from 0.5 M to 3 M as the eluant. Fractions were collected and analyzed by UV-vis spectrophotometry. The desired product eluted in 3 M HCl. Schiff base: R_f = 0.6 ($CHCl_3$-CH_3OH 9:1). UV-vis (CH_3OH): λ_{max}, nm (log ε): 301 (4.47), 370 (4.09). ^1H and ^{13}C NMR see Figure S3.5.5-3.5.6)

4-(2-((2,4-dihydroxybenzyl)amino)ethyl)benzene-1,2-diol (**1**). Off-white amorphous solid (0.28 g, yield = 95 %). Product purity > 90% was assessed by HPLC and proton NMR analysis (Figure S3.5.7-3.5.9), R_T = 15 min, 0.1 % HCOOH - MeOH 8:2; UV-vis CH_3OH: λ_{max}, nm (log ε): 280 nm (3.99); MS(ESI^+) calcd. *m*/*z* $[M+H]^+$: 276.1158. Found: 276.1172.

General procedure for the oxidation of 1. Solutions of **1** in methanol were diluted to the appropriate concentration with 0.05 M Na_2CO_3 buffer pH 9.0, and left under stirring, in air at room temperature until reaction completion as determined spectrophotometrically by monitoring chromophore development. To purify the oxidation mixture after 3 h it was concentrated and fractionated on a Sephadex G10 (10 × 0.1 cm) column using distilled water as the eluant. Product identity was secured by LDI-MS and ^1HNMR spectral characterization (see Figure S3.5.1) (yield: 12 mg, 0.05 mmol, 26%).

Preparation of FluoResCat-alginate hydrogels. Sodium alginate was dissolved in distilled water (20 mL, 2 % w/w), then **1** at 22 mM in methanol (0.09 mL) was added. Beads were prepared by dropping the freshly prepared gel in a 0.1 M solution of $CaCl_2$ allowing alginate reticulation for few minutes and recovery of beads by filtration. Films were fabricated similarly by spreading the gel on a smooth surface followed by dipping in the $CaCl_2$ solution for about 60 s.

Exposure to ammonia (at 28% aqueous solution) or decomposing fish fillets was carried out in sealed glass chambers at room temperature. Control experiments were carried out at -20 °C or at room temperature in the absence of fish fillets.

Superoxide scavenging Assay.[135] **1** (final concentration 80, 160 or 320 μM) was added to 0.05 M ammonium hydrogen carbonate buffer (pH 9.3) containing 0.33 mM EDTA, 10 mM NBT, and 160 μM pyrogallol. The mixture was taken under vigorous stirring, and after 5 min, the absorbance at 596 nm was measured. Results were expressed as percentage of the ratio of the absorbance at 596 nm of a given mixture with respect to that of the control mixture run in the absence of sample. Experiments were run in triplicate.

Synthesis of Bis-Res (2). A mixture of hexamethylenediamine (400 mg, 1.81 mmol) and 2,4-dihydroxybenzaldehyde (950 mg, 3.62 mmol) in absolute ethanol (35 mL) was stirred at room temperature for 1 h. The yellow solid that separated was centrifuged three times at 5000 rpm and washed with cold ethanol, then dried in vacuo to give the Schiff base (2a, 90% yield). The latter was then rinsed in glacial acetic acid (10 mM, 160 mL) and reduced by $NaBH_4$ (605 mg, 16 mmol). When hydrogen evolution ceased, 3 M HCl was added until the pH was 5.0. The mixture was dried under vacuum, then rinsed in 1 mL of water before desalting on Sephadex G-10 resin, using HCl 0.05 M as the eluant. Ten fractions of 8 mL each were collected and analyzed by UV-vis spectrometry. After removal of the acid under reduced pressure, compound **2** was obtained as di-hydrochloride salt in the form of a brownish orange solid (yield= 75 %).

(**2a**) R_f = 0.27 ($CHCl_3$-MeOH 9:1); UV-vis: λ_{max} (MeOH) = 301 nm (ε= 33410 $L \bullet mol^{-1} \bullet cm^{-1}$) and 371 nm (ε = 15879 $L \bullet mol^{-1} \bullet cm^{-1}$); m/z = 357.18 $[M+H]^+$; ATR-FT/IR (cm^{-1}) = 1227 (phenolic C–O stretch), 1358 (phenolic C–O bend), 1637 (C=N stretch), 2932 (aliphatic C-H bend and stretch), 3065 (aromatic C–H

stretches), and 3509–3638 (phenolic O–H stretches). ^{1}H and ^{13}C NMR see Figure S3.5.10-3.5.11.

(**2**) UV-vis: λ_{max} (MeOH) = 279 nm (ε= 4944 L•mol^{-1}•cm^{-1}); m/z: 361.21 $[M+H]^{+}$; ATR-FT/IR (cm^{-1}) = 1172 (C–N stretch), 1593 (N–H bend), 2796–2935 (aliphatic C–H bend and stretch), 3041 (aromatic C–H stretches), 3235–3292 (N–H stretch), and 3531–3622 (phenolic O–H stretches). ^{1}H, ^{13}C and 2D NMR spectra see Figure S3.5.12-3.5.16.

General procedure for the oxidative coupling of compound 2 with dopamine. The reaction was carried out using compound **2** dihydrochloride at 1 mM and dopamine at 2 mM in 0.05 M sodium carbonate buffer (50 mL), pH 9.0, under stirring in air. After complete dissolution of the reagents in the buffer, a neat substrate (glass or quartz coverslips rinsed with piranha mixture H_2SO_4:H_2O_2 5:1, polyethylene or polystyrene cuts, polycarbonate slides, or aluminum foils) was immersed in the reaction mixture for 6 h. The development of a blue fluorescence was rapidly observed, followed by deposition of a thin layer of organic material on the substrate and concomitant separation of a brownish-green solid. The quartz substrates after coating were subjected to repeated ultrasound-assisted washing in water before spectrophotometric/fluorimetric analysis. All other substrates were repeatedly washed with deionized water and dried in air.

Supporting materials

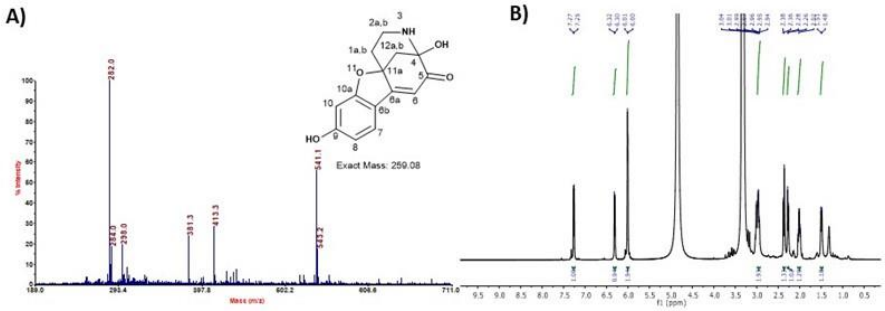

Figure S3.5.1. (a) LDI-MS (base peak 282.0 = $[M+Na]^+$) and (b) ^1H NMR (500 MHz, methanol $-d_4$) spectrum of the fluoroscent product from fractionation of the oxidation mixture of **1**.

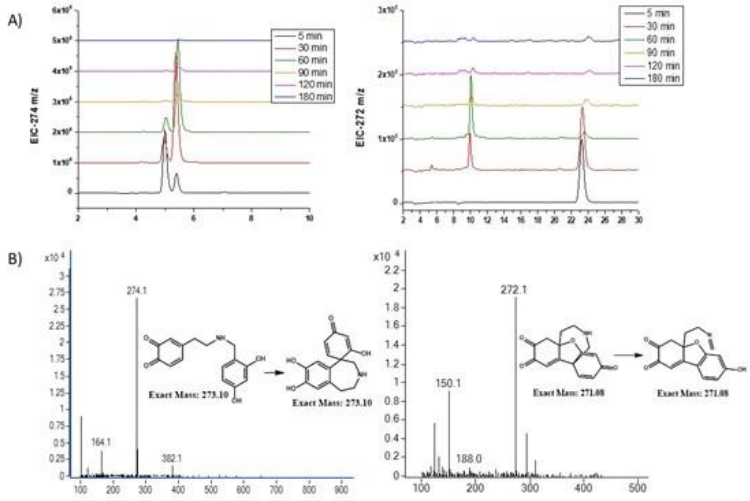

Figure S3.5.2. (a) Extracted Ion Chromatograms at different reaction times *m/z* 274 (left) and *m/z* 272 (right). (b) ESI^+-MS spectra of the species eluting at R_T = 5.0 or 5.25 min (left) and R_T = 10 or 23 min (right) and representative mass spectra of the peak.

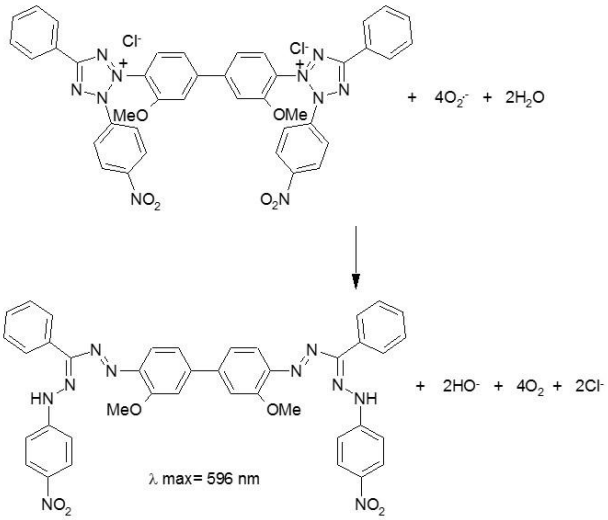

Figure S3.5.3. Reduction of nitro blue tetrazolium chloride to formazan dye absorbing at 596 nm by superoxide generated by oxidation of pyrogallol in air under alkaline conditions.

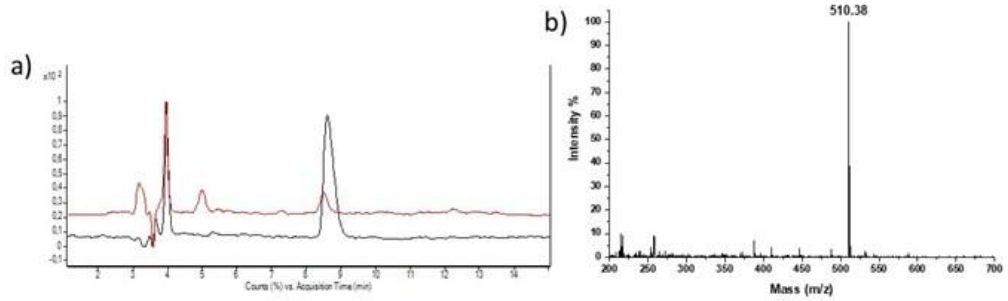

Figure S3.5.4. LC-MS analysis of the reaction mixture of Bis–Res (R_t = 8.9 min) and dopamine (R_t = 4 min). (a) Total ion current chromatogram after 0 min (black) and 150 min (red). (b) Mass spectrum of the peak eluting at 5.1 min, base peak $[M+H]^+$ = m/z 510.4, eluting system = 0.1 % HCOOH-MeOH 8:2.

Table S3.5.1. Profilometry data of the Bis–Res/dopamine (DA) coating on glass before and after $HCl_{(vap)}$ exposure.

Coating	$\lambda_{max/ex}$ (nm)	λ_{em} (nm)	Thickness (nm)	Roughness (nm)	Water Contact Angle (deg)
Bis-Res/DA	420	464	55 ± 2.7	15	52 ± 3.6
Bis-Res/DA-HCl	400	no	48 ± 0.2	16	Not calculable

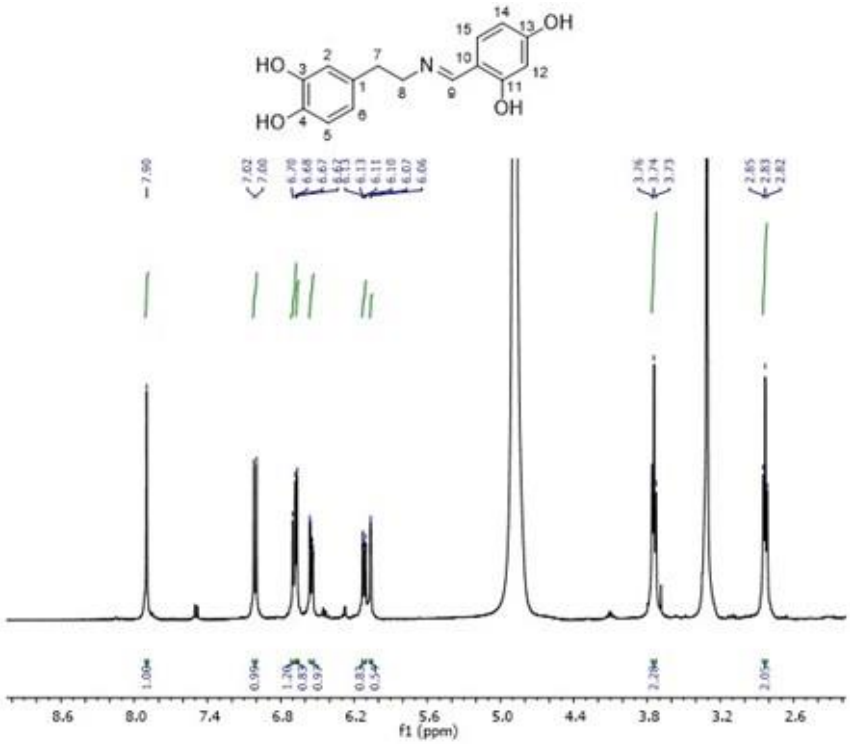

Figure S3.5.5. ^{1}H NMR spectrum of the Schiff base (400 MHz, methanol-d_4): δ 7.90 (s, 1H), 7.01 (d, J = 8.8 Hz, 1H), 6.69 (d, J = 8.3 Hz, 1H), 6.67 (s, d, J = 1.7 Hz, 1H), 6.55 (dd, J = 7.8, 1.7 Hz, 1H), 6.12 (d, J = 8.8 Hz, 1H), 6.06 (s, 1H), 3.74 (t, J = 6.6 Hz, 2H), 2.84 (t, J = 6.6 Hz, 2H).

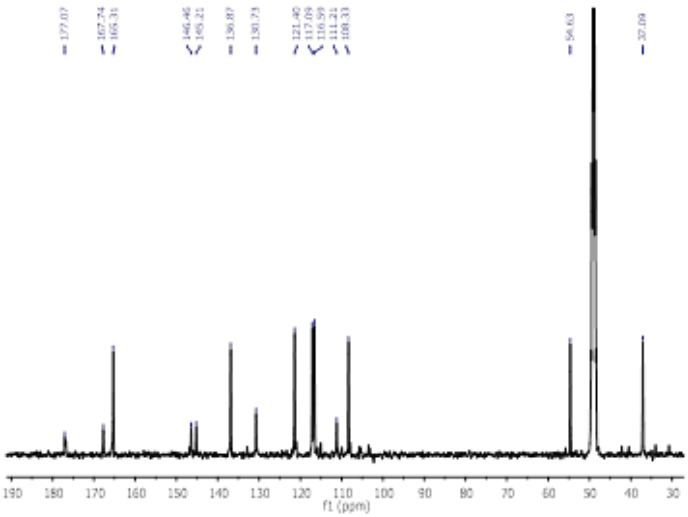

Figure S3.5.6. ^{13}C NMR spectrum of the Schiff base (101 MHz, methanol -d_4): δ 167.7, 165.3, 146.5, 145.2, 136.9, 130.7, 121.4, 117.1, 116.6, 111.2, 108.3, 54.6, 37.1.

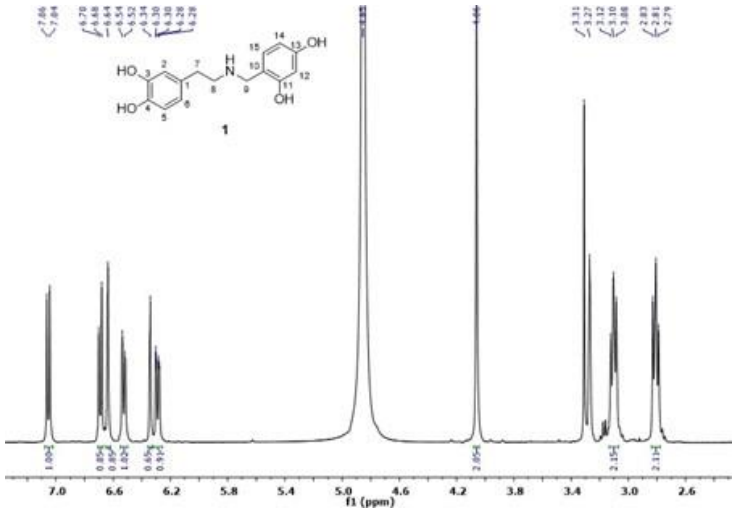

Figure S3.5.7. ^{1}H NMR spectrum of **1** (400 MHz, methanol-d_4): δ 7.05 (d, J = 8.1 Hz, 1H), 6.69 (d, J = 8.1 Hz, 1H), 6.64 (s, H-6, 1H), 6.53 (d, J = 8.1 Hz, 1H), 6.34 (s, 1H), 6.29 (dd, J = 8.3, 1.9 Hz, 1H), 4.06 (s, 2H), 3.10 (t, J = 7.2 Hz, 2H), 2.81 (t, J = 7.2 Hz, 2H).

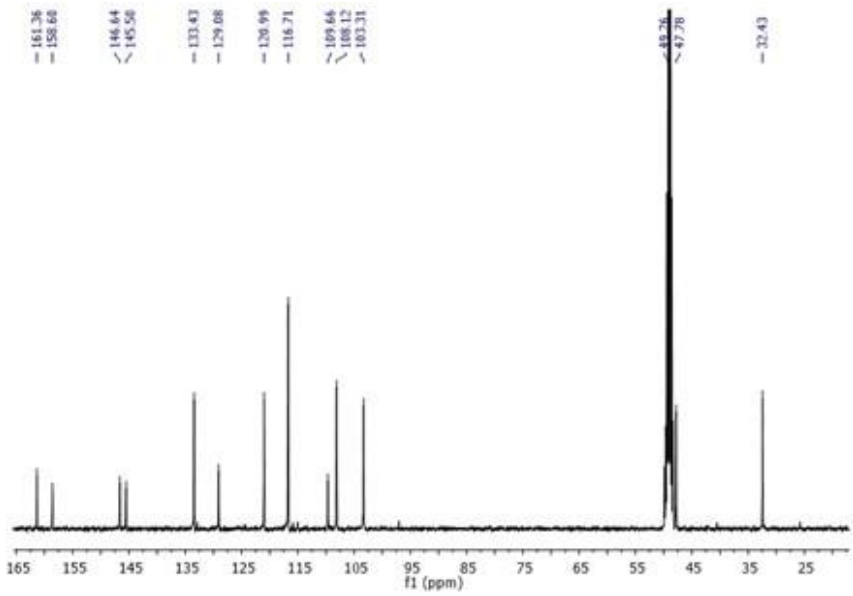

Figure S3.5.8. ^{13}C NMR spectrum of compound **1** (100 MHz, methanol-d_4): δ 161.4, 158.6, 146.6, 145.5, 133.4, 129.1, 121.0, 116.7, 109.7, 108.1, 103.3, 49.3, 47.8, 32.4.

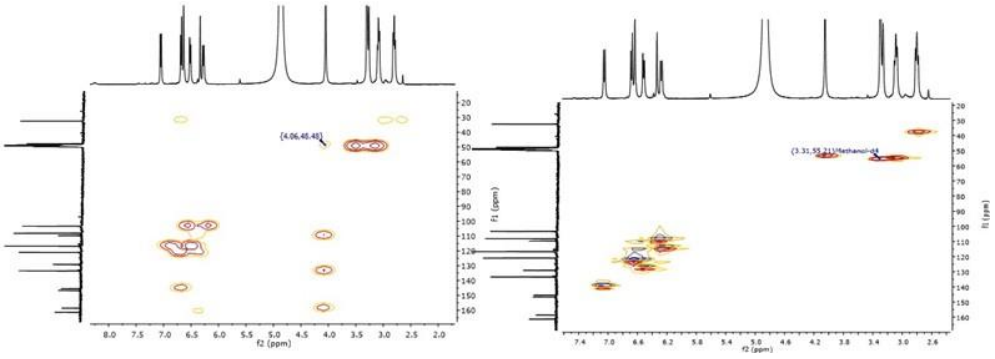

Figure S3.5.9. ^{1}H, ^{13}C HMBC (left) and ^{1}H, ^{13}C HSQC (right) spectra of **1**.

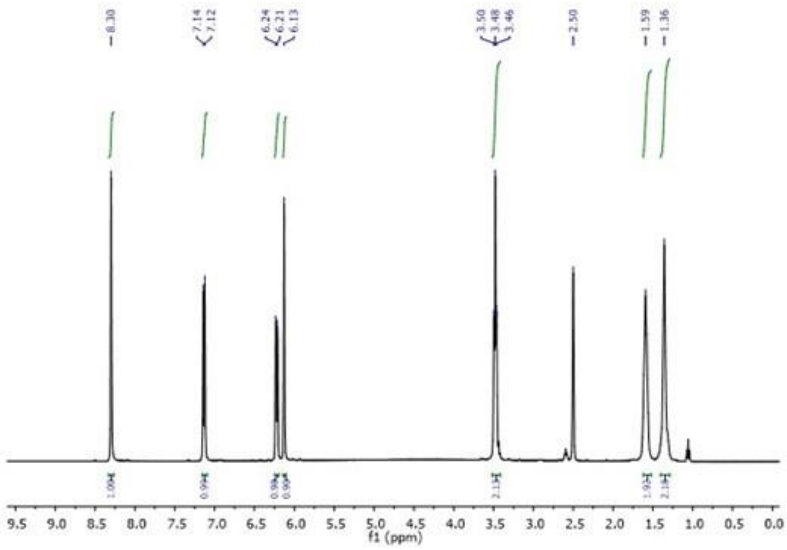

Figure S3.5.10 .[1]H NMR (400 MHz, DMSO-d_6) of the Schiff base (**2a**) δ 8.30 (s, H-7), 7.13 (d, *J* = 8.5 Hz, H-6), 6.22 (d, *J* = 8.4 Hz, H-5), 6.13 (s, H-3), 3.48 (t, *J* = 6.6 Hz, H-8), 1.59 (br. m, H-9), 1.36 (br. m, H-10).

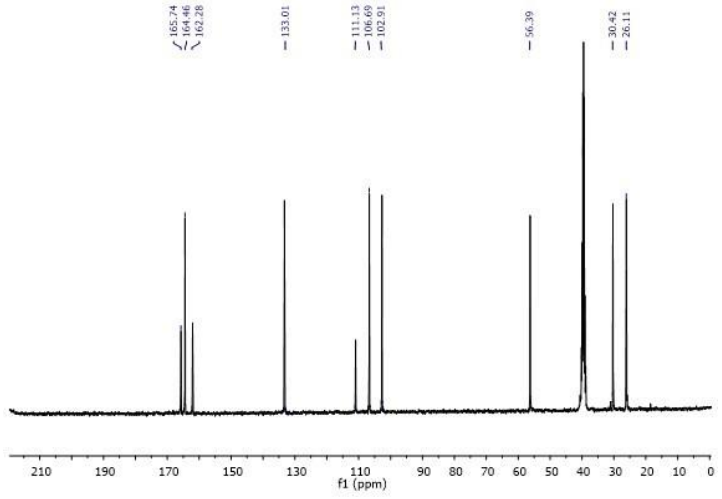

Figure S3.5.11. [13]C NMR (101 MHz, DMSO-d_6) spectrum of the Schiff base (**2a**): δ 165.7, 164.5, 162.3, 133.0, 111.1, 106.7, 102.9, 56.4, 30.4, and 26.1.

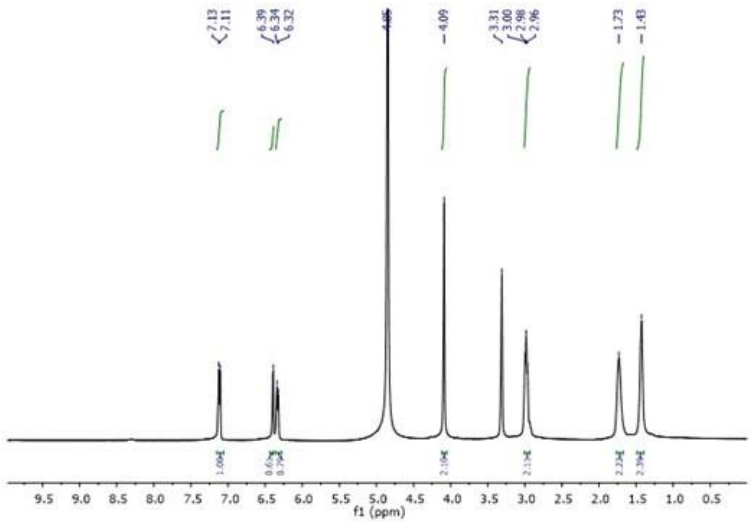

Figure S3.5.12 ^{1}H NMR (400 MHz, MeOH-d_4) of **2** δ 7.12 (d, *J* = 8.2 Hz, H-6), 6.39 (s, H-3), 6.33 (d, *J* = 6.8 Hz, H-5), 4.09 (s, H-7), 3.01 – 2.93 (br. m, H-8), 1.73 (br. m, H-9), 1.43 (br. m, H-10). Resonance assignment follows from analysis of ^{1}H,^{1}H COSY spectrum.

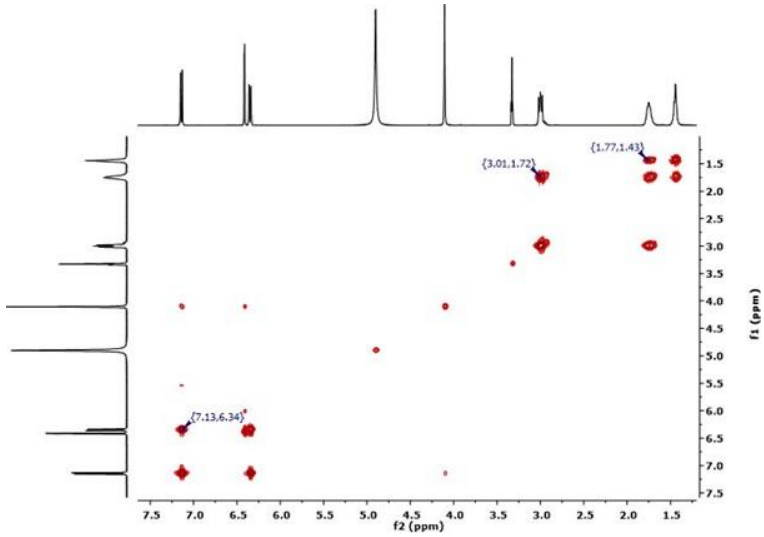

Figure S3.5.13. ^{1}H, ^{1}H COSY spectrum of **2** (400 MHz, MeOH-d_4).

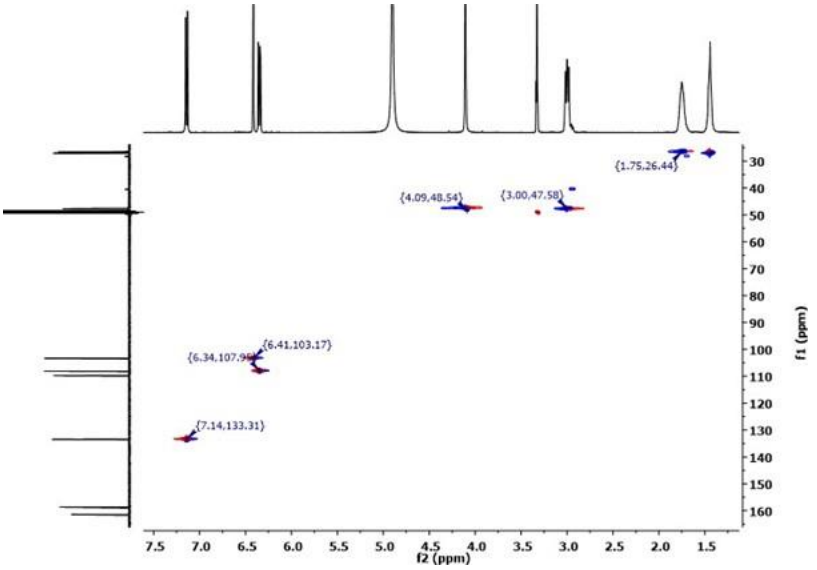

Figure S3.5.14. ^{1}H, ^{13}C HSQC spectrum of **2** (400 MHz, MeOH-d_4)

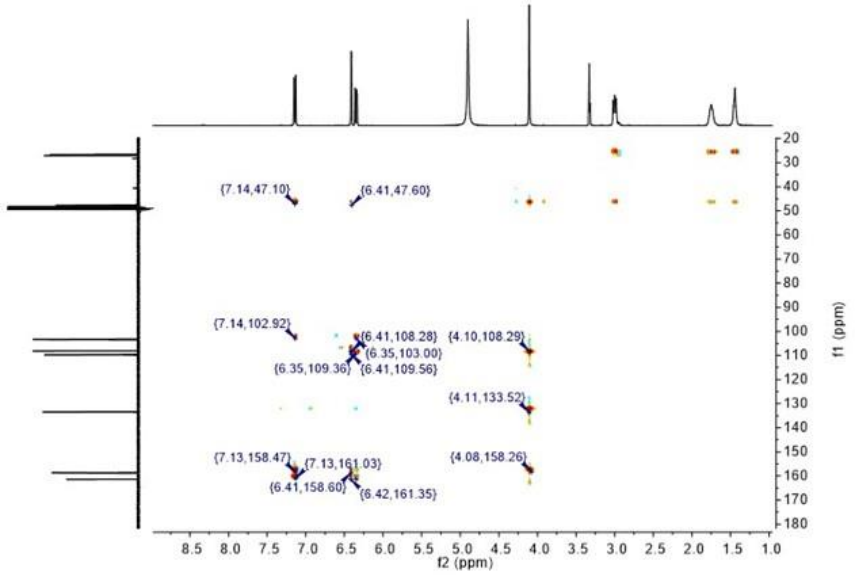

Figure S3.5.15. ^{1}H, ^{13}C HMBC spectrum of **2** (400 MHz, MeOH-d_4).

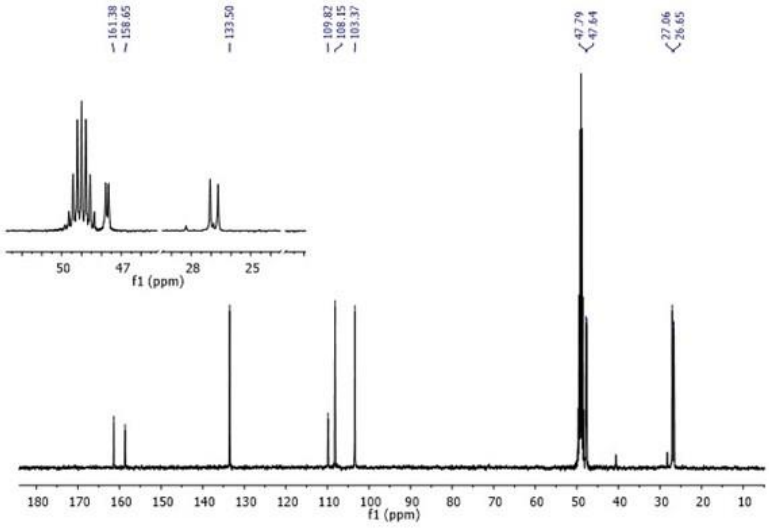

Figure S3.5.16. ^{13}C NMR (101 MHz, MeOD-d4) spectrum of **2** δ 161.4 (C-4), 158.6 (C-2), 133.5 (C-6), 109.8 (C-1), 108.1 (C-5), 103.4 (C-3), 47.8 (C-7), 47.6 (C-8), 27.1 (C-9), 26.6 (C-10).

Chapter 4

Mussel-inspired coating technology by enzymatic oxidation of tyramine

4.1 Introduction

As illustrated in detail in Chapter 2, the multifunctional and universal wet surface dip-coating technology leading to highly adhesive polydopamine (PDA) films has dominated the scene of materials science over the past decade for a broad range of applications including *e.g.* drug delivery, energy storage, molecular detection, bioimaging, catalysis, and nano-interface, to mention only a few.[32,75,88]

Over the past years several attempts have been made to improve coating efficiency by different approaches, *e.g.* use of chemical oxidizing agents (*e.g.*, ammonium persulfate, sodium periodate, copper sulfate), high salt concentrations, acidic pH, UV irradiation, use of additives like hexamethylenediamine (HMDA), and electrochemical oxidation. In all cases, however, improvements in film properties were counterbalanced by a loss in the ease of reaction, including mildness and versatility, *e.g.* for biomedical application.[71,73,92,93,105,144] Although PDA is currently the reference material for surface functionalization and coating, some limitations have prompted intense studies toward novel mussel-inspired surface chemistry beyond PDA-based technology. They are related to: a) the intrinsic toxicity of the precursor dopamine; b) the limited number of functional groups available for post-synthetic modification; c) the use of an alkaline pH, not always compatible with biological systems or alkali-unstable surfaces; d) the need for

high dopamine concentrations (10 mM), with more than 99.9% material lost in the form of black insoluble precipitate; and e) difficulties to control film thickness and properties due to the slow kinetics of autoxidation.[57,89,90] Efficient control of film growth has recently been achieved by using borate buffer, forming stable complexes with the catechol moiety of dopamine,[145] or by adding resorcinol, which traps dopamine quinone preventing polymerization in the presence of HMDA (as illustrated in the Chapters 3 and 5). A possible means of bypassing limitations inherent to the autoxidation protocol relies on the use of enzymes like tyrosinase, a copper containing complex whose structure is highly conserved among different species and widely distributed in the biosphere.

Tyrosinase can catalyzes two different reactions (Scheme 4.1.1):

- hydroxylation of monophenol to *o*-diphenol (cresolasic or monophenolasic activity);
- dehydrogenation of catechol to *o*-quinone (catecholasic or diphenolasic activity).

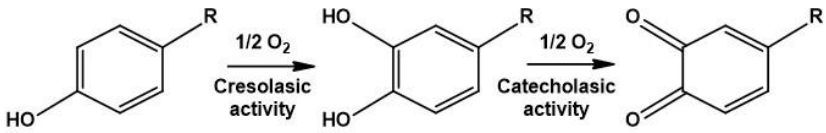

Scheme 4.1.1. Reaction catalyzed by tyrosinase.

In particular tyrosinase can be exploited to modulate catecholamine oxidation at pH values around neutrality,[146] leading to uniform films with diverse functionalities.[146-150] However, despite such a promising set of observations, the great potential of mono-phenolic (*i.e.* non-catecholic) tyrosinase substrates for surface functionalization and coating in view of their expected stability to autoxidation did not receive further attention.

On these bases, in this chapter the deposition of PDA-type films (for which the term of pseudo-PDA or ψ-PDA is proposed) by tyrosinase-catalyzed oxidation of tyramine is disclosed as a practical procedure for surface functionalization and coating at neutral pH and at much lower substrate concentration compared to standard autoxidative PDA coating protocols. Antioxidant properties of the tyramine-derived films were also investigated in comparison with those of PDA obtained under the same conditions. Finally, the possibility of using tyramine together with confined tyrosinase to achieve site-specific polymerization and/or film deposition was assessed against dopamine. The rationale of the experiments was to prevent the uncontrolled autoxidative deposition of black precipitate, a major drawback of PDA coating technology which may interfere with specific applications.

4.2 Thin films by tyrosinase-controlled oxidation of tyramine

In the presence of variable amounts of tyrosinase (20 and 100 U/mL), the oxidation of tyramine (1 mM) at pH 6.8 resulted in the deposition after 24 h of dark films resembling PDA that could be detected by UV-vis spectrophotometry. Data reported in Figure 4.2.1 showed similar UV-vis profiles in the tyrosinase catalyzed reaction for both tyramine and dopamine films (*tyrosinase-PDA*, T-PDA) and indicated significant deposition of PDA films from 1 mM catecholamine concentration. It is noted that in the autoxidation experiments at least 10 mM dopamine is required for film deposition.

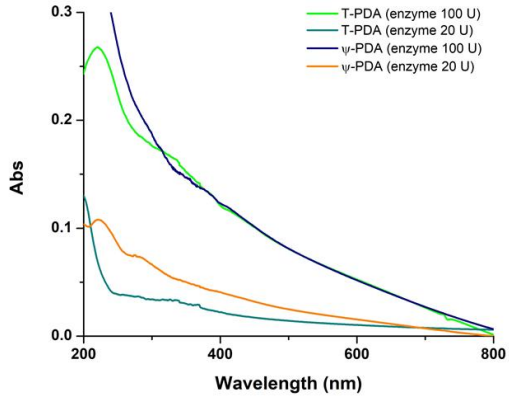

Figure 4.2.1. UV-vis spectra of the films obtained from 1 mM tyramine by varying tyrosinase concentration (20 and 100 U/mL) (ψ-PDA) compared to PDA films obtained by similar enzymatic oxidation of 1 mM dopamine with tyrosinase (*tyrosinase-PDA*, T-PDA).

Efficient tyrosinase-mediated deposition of tyramine films was observed also on quartz and other materials as shown in Figure 4.2.2.

Figure 4.2.2. ψ-PDA coatings on various materials: (A) quartz; (B) polycarbonate and (C) polystyrene. On the left of each are pictures of uncoated materials.

In another set of experiments the evolution of the film-forming properties of ψ-PDA was also investigated from 1 mM tyramine with tyrosinase (100 U/mL). To this aim quartz substrates were dipped in the tyramine solution undergoing oxidation in carbonate buffer (pH 6.8) and kept for 6 and 24 h from the start of the reaction. UV-vis analysis showed that the absorbance of the films in the initial

hours is considerably less intense compared with the levels observed at 24 h (Figure 4.2.3).

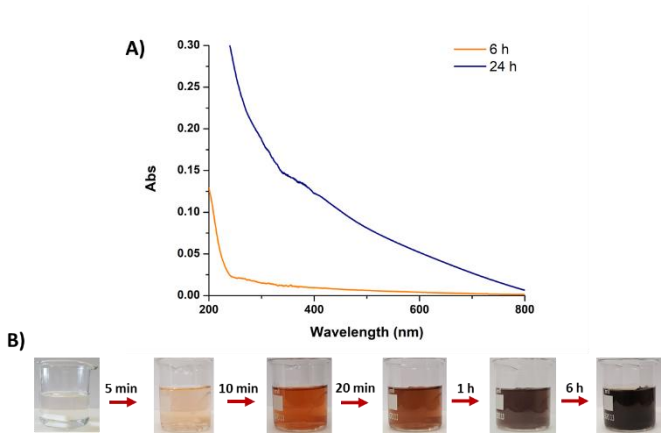

Figure 4.2.3. (a) Evolution of the UV-vis spectra of ψ-PDA film formed by tyrosinase-catalyzed oxidation of tyramine; (b) digital pictures of tyramine oxidation in the presence of 20 U/mL of tyrosinase.

The tyrosinase-catalyzed oxidation kinetics of 1 mM tyramine in carbonate buffer pH 6.8 were also monitored by UV-vis over 24 h compared to enzymatic oxidation of 1 mM dopamine with tyrosinase (Figure S4.4.1). After a few hours a progressive consumption of the starting material was observed, faster in the case of dopamine, together with the usual color change (from colourless to black) and precipitation of black melanin-like materials after 24 h.

The deposition kinetics of the films from tyramine in the presence of variable amounts of tyrosinase (1-100 U/mL) were followed using the Quartz Crystal Microbalance (QCM-D) methodology. When a stable signal was reached ($\Delta f/\nu$ smaller than 1 Hz over a period of 5 min) the tyramine solutions were introduced in the cell and let it flow for about 1 h. As shown in Figure 4.2.4 the deposition kinetics of ψ-PDA are much faster in the presence of 20 or 50 U/mL of enzyme

than with 100 U/mL of tyrosinase, this latter appearing rather smooth over the observed period of time.

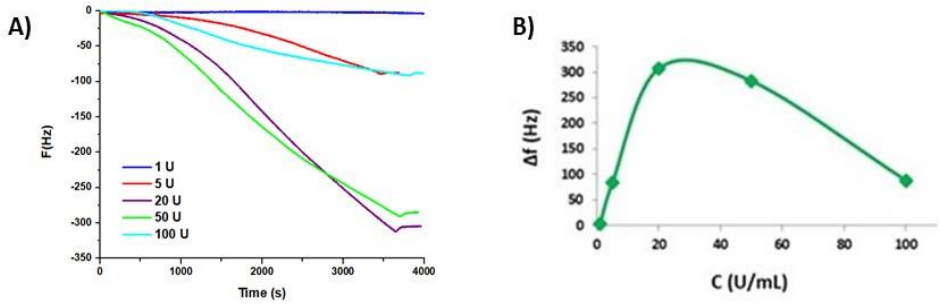

Figure 4.2.4. (a) QCM-D experiment with frequency variations at the 3rd overtone as a function of time during the ψ-PDA deposition in the presence of tyrosinase at different concentrations up to one hour. (b) Evolution of the frequency as a function of the tyrosinase concentration after 1 h of deposition.

For comparative purposes, the same technique and procedure was applied to dopamine enzymatic oxidation mixture, performed under the same conditions adopted in the case of tyramine and in the presence of 20 U/mL of enzyme. In this case the deposition of T-PDA is more significant than that of ψ-PDA in agreement with the notoriously faster reactions of tyrosinase with catechols with respect to monophenols, which often display an induction time (Figure S4.4.2).

The thickness of the films, reported in Table 4.2.1, was calculated using the Sauerbrey equation[151] from the QCM-D data, based on the observation that the frequency change (Δf) of the oscillating quartz could be linearly related to its mass change (Δm) as expressed by

$$\Delta m = -C * \frac{1}{n} * \Delta f$$

where n is the overtone number and C is a constant that depends on the property of the crystal used.

Table 4.2.1. Thickness values for the ψ-PDA and T-PDA films calculated by Sauerbrey equation.

ψ-PDA films	**1 U**	**5 U**	**20 U**	**50 U**	**100 U**	**T-PDA film**	**20 U**
Thickness (nm)	3.5	11.9	42.4	39.5	12.4		46.9

Morphological and structural characterization. In a subsequent series of experiments the morphology and surface properties of the ψ-PDA films, in comparison to that of T-PDA, were investigated. AFM images (recorded by Prof. V. Ball and co-workers at the Faculty of Chirurgie Dentarie, University of Strasbourg, France) in Figure 4.2.5 indicated smooth films with thickness varying with tyrosinase levels within the upper limit of 87 nm (Table 4.2.2). Figure 4.2.5, panel D indicated for the T-PDA film,, higher average roughness compared to the ψ-PDA film obtained under the same conditions.

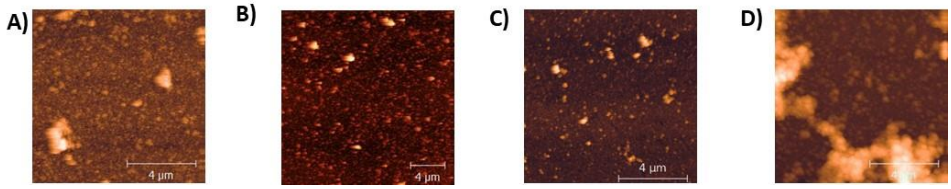

Figure 4.2.5. AFM image of a representative region of the ψ-PDA film sample, after 1 h deposition onto the quartz crystal sensor, in the presence of tyrosinase 20 U/mL (a), 50 U/mL (b) and 100 U/mL (c) respectively or (d) T-PDA film sample in the presence of tyrosinase 20 U/mL. Average grain size: 45.5 ± 3 nm (a), 28.7 ± 5 nm (b), 12.8 ± 0.5 nm (c), 113.5 ± 9 nm. Film thickness: 87 ± 5 nm (a), 63.3 ± 2 nm (b), 58 ± 4 nm (c), 25.3 ± 4 nm.

Water contact angle (WCA) measurements indicated relatively hydrophilic films not exceeding 28°, to be compared with a value of 32° for T-PDA produced under the same conditions (in the presence of 20 U/mL of tyrosinase) (Table 4.2.2).

Table 4.2.2. Characterization of thin films from ψ-PDA and T-PDA on crystal quartz.

Film	Thickness (nm)	Roughness (nm)	Water contact angle (deg)
ψ-PDA 100 U/mL	58 ± 4	12.8	22.3
ψ-PDA 50 U/mL	63.3 ± 2	28.7	17.1
ψ-PDA 20 U/mL	87 ± 5	45.5	28.6
T-PDA 20 U/mL	25.3 ± 4	113.5	32.1

Based on these data, the structural properties of the film produced by tyramine-tyrosinase oxidation were investigated using MALDI-MS in comparison with the PDA film.

Largely overlapped peak patterns were observed in the case of bulk materials, confirming the specific composition of adhesive film components with respect to most of the polymer. However, distinct spectral patterns for the two films were observed, which shared only a few minor peaks in common. Data in Figure 4.2.6 indicate detectable peak clusters at m/z ratios up to just below m/z 800 for PDA but not higher than 700 for tyramine polymer, suggesting for the latter either a lower oxygen content or a different polymerization chemistry. Main peaks, considered for structural analysis and reported in Table 4.2.3, are attributed to

sequences of muconic-type cleavage of *o*-quinones, decarboxylation and hydration/dehydration steps. A plausible structure accounting for the main peak at m/z 657 in ψ-PDA films is shown in Figure 4.2.7 whereas other plausible set of structures are reported in Figure S.4.4.3. Overall these data confirmed a PDA-like composition for ψ-PDA films.

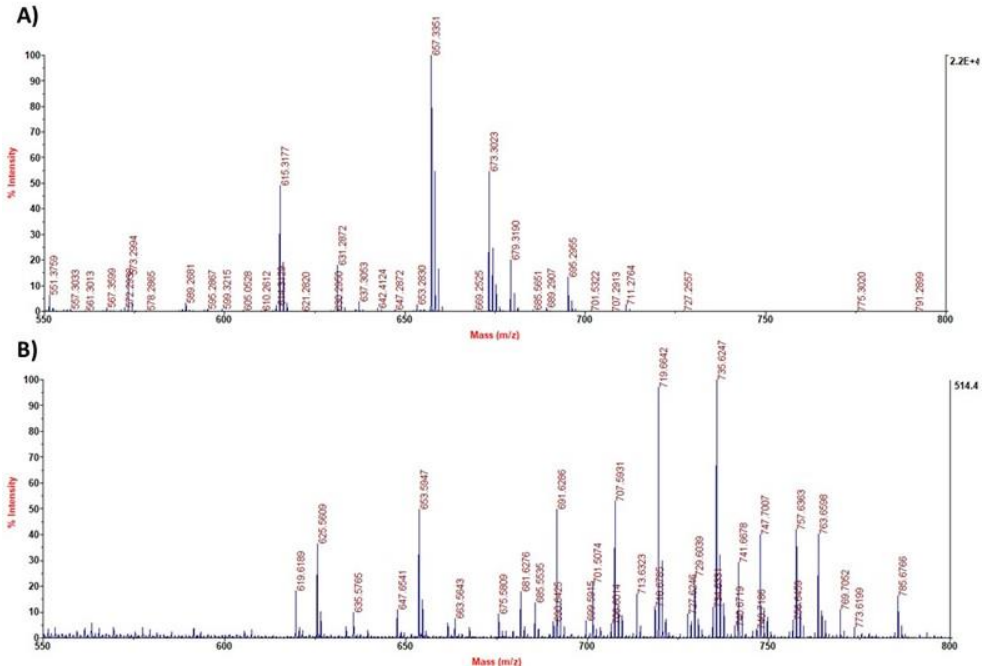

Figure 4.2.6. Segmental spectrum of MALDI-ToF (m/z: 550−800 Da) characterizations of (a) tyramine film in carbonate buffer at pH = 6.8 with 20 U/mL of tyrosinase and (b) PDA film obtained under the same conditions.

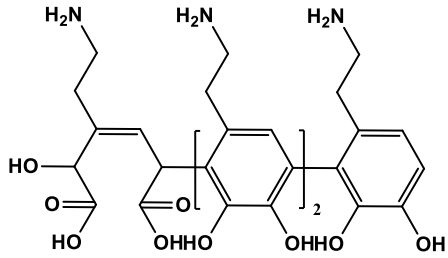

Figure 4.2.7. Tentative structure representative of the possible species responsible for the peak at m/z 657 in the ψ-PDA film.

Tyramine (137 g/mol) polymer		Dopamine (153 g/mol) polymer	
Observed peak clusters	MW	Observed peak clusters	MW
573 (Na^+), 589 (K^+)	550		
615 (Na^+), 631(K^+)	592		
		619 (Na^+), 635 (K^+)	596
		625 (H^+), 647 (Na^+), 663 (K^+)	624
637(Na^+), 653 (K^+)	614		
		653 (H^+), 675 (Na^+) 691 (K^+)	652
657(Na^+), 673 (K^+)	634		
679 (Na^+), 695 (K^+)	656		
/		719 (Na^+), 735 (K^+)	696
/		741 (Na^+), 757 (K^+)	718
/		747 (Na^+), 763 (K^+)	724
/		769 (Na^+), 785 (K^+)	746

Table 4.2.3. Main peaks considered for structural analysis.

Antioxidant activity. In a separate set of experiments the antioxidant properties of ψ-PDA suspensions and films were investigated in comparison with those of T-PDA by two chemical tests, namely 2,2-diphenyl-1-picrylhydrazyl (DPPH),[152] an assay that measures the efficiency of electron transfer processes from the antioxidant and the ferric reducing antioxidant power (FRAP),[153] which measures

the ability of the antioxidant to reduce a Fe^{3+}-tripyridyltriazine complex to a dark blue Fe^{2+} complex with absorption maximum at 593 nm.

Known volumes of a fine methanol suspension (2 mg/mL) of the polymer obtained using a glass/glass homogenizer solution were added to a DPPH solution (200 μM). The mixtures were kept under vigorous magnetic stirring at room temperature and the course of the reaction was followed spectrophotometrically by measuring the absorbance at 515 nm after 10 minutes. Figure 4.2.8 shows the data obtained from the DPPH assay expressed as the EC_{50} value, *i.e.* the amount of antioxidant capable of reducing the initial DPPH concentration by 50 %. For ψ-PDA pigment an EC_{50} value of 54 ± 0.4 μg/mL was obtained, lower than that of the T-PDA pigment of 91.3 ± 0.3 μg/mL.

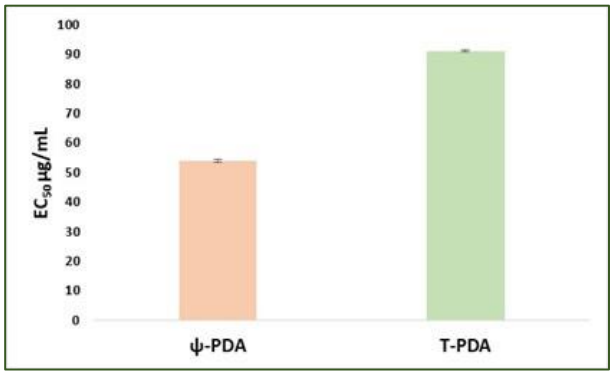

Figure 4.2.8. EC_{50} values obtained from the DPPH assay of the pigments obtained by oxidation of tyramine and dopamine in the presence of 20 U/mL of tyrosinase (2 mg/mL). The average values ± SD obtained from at least three separate experiments are reported.

The antioxidant properties of the films obtained by the oxidation of tyramine or dopamine in the presence of 20 U/mL of tyrosinase were next evaluated. To this aim, glass substrates were coated as described above, and after 24 h were introduced in a beaker containing 15 mL of DPPH (50 μM) in methanol care being

taken to dip all the glass slides up to a fixed level into the solution. The absorption of the DPPH solution was monitored over time. The experiment was repeated on different substrates and showed an acceptable reproducibility. As shown in Figure 4.2.9 the hydrogen donation capacity was well detectable, although it is not possible to evaluate these data on a quantitative basis and establish a comparison with the values obtained for the polymer suspensions. The antioxidant power of the ψ-PDA film proved to be comparable to that of the T-PDA film based on the DPPH consumption at 2 h.

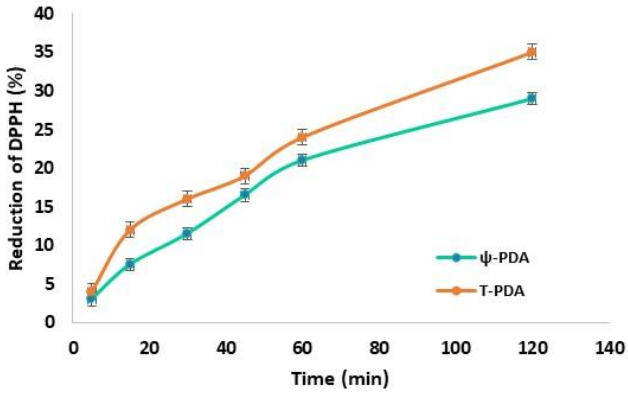

Figure 4.2.9. Reduction of DPPH (50 μM) over time by immersion of glass substrates coated with ψ-PDA or T-PDA.

A similar procedure was followed to evaluate the ferric reducing antioxidant power (FRAP) of the ψ-PDA and T-PDA polymers. A proper amount of a fine methanol suspension (2 mg/mL) of the polymer obtained using a glass/glass homogenizer solution were added to a solution of $FeCl_3$ (20 mM) and 2,4,6-tris (2-pyridyl)-s-triazine (10 mM) in 0.3 M acetate buffer (pH 3.6) at room temperature. After 10 minutes the absorbance at 593 nm was measured. Trolox was used as the reference antioxidant. The results reported in Figure 4.2.10 show

a reducing capacity equal to about 0.15 equivalent of Trolox in the case of ψ-PDA polymer, and higher than that obtained for the T-PDA polymer.

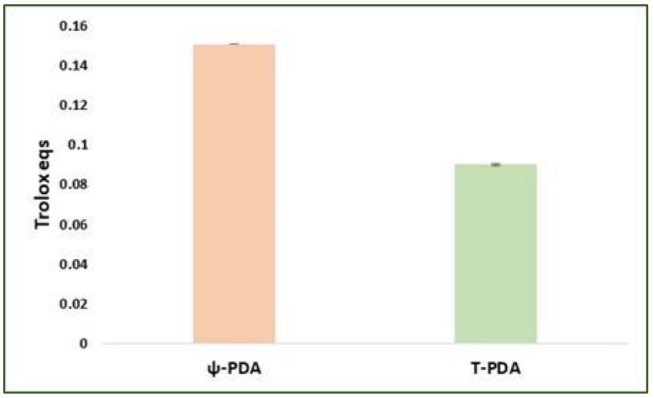

Figure 4.2.10. Trolox equivalents determined in the FRAP assay of the pigments obtained by oxidation of tyramine and dopamine in the presence of 20 U/mL of tyrosinase (2 mg/mL). The average values ± SD obtained from at least three separate experiments are reported.

Also, in this case the antioxidant properties of ψ-PDA film in the FRAP assay were determined in comparison with those of the film obtained with T-PDA. To this aim, the same procedure described before in the DPPH assay was applied. As shown in Figure 4.2.11, also in this case the film from tyrosinase-tyramine exhibited an antioxidant power comparably or slightly worse than that of the tyrosinase-dopamine film.

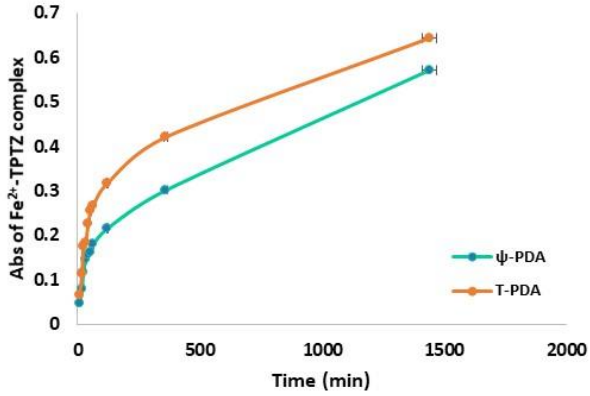

Figure 4.2.11. Kinetics of the development of the absorption of Fe^{2+}-tripyridyl triazine complex obtained by immersion of glass substrates coated with ψ-PDA and T-PDA.

Tyrosinase-loaded alginate. The search for a clean film deposition procedure with no waste of unutilized precursor or massive precipitation of black polymer, was preliminarily assessed. Initially, tyrosinase was incorporated into alginate gel, both spheres and films deposited on glass substrates, and then the gels were exposed to 1 mM tyramine, and for comparison to dopamine, in carbonate buffer at pH 6.8. Figure 4.2.12 shows both the gel spheres and the reaction vessel solutions for both substrates. No precipitate was apparent in the tyramine solution, despite visible darkening of the alginate, in contrast with the case of dopamine, where abundant dark precipitate was produced by autoxidation even at neutral pH. Similar results were obtained on alginate films layered on glass or other surfaces (Figure 4.2.12, panel C). After the reaction is complete, ψ-PDA-gel is removed from the solution and the tyramine-containing solution can be re-used for other reactions for a virtually unlimited number of procedures. This procedure allows to get ψ-PDA nanoparticles or films in a facile, clean and efficient manner with considerable material saving.

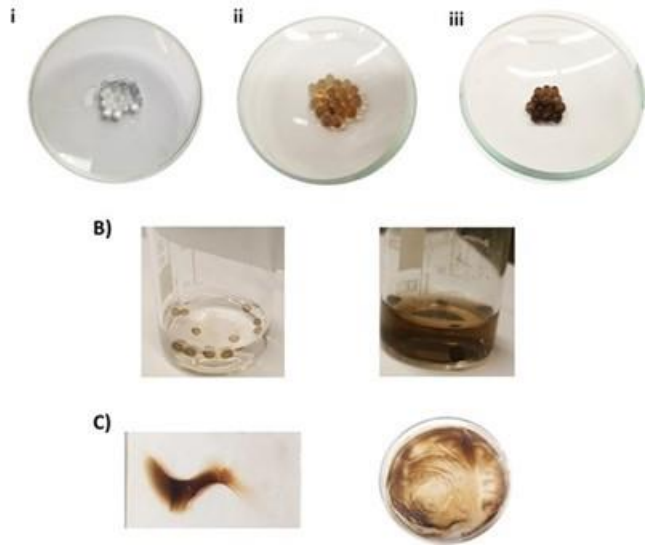

Figure 4.2.12. (a) Calcium alginate hydrogel beads (i) incorporating tyrosinase 0.1% (ii) or 0.5 % (iii) and dipped into tyramine solution; (b) tyrosinase (0.1 %) alginate hydrogel beads incorporating tyrosinase (0.1 %) and dipped in 1 mM tyramine (left) or dopamine solution (right) over 4 h; (c) alginate/tyrosinase hydrogel films after dipping into tyramine solution (1 mM).

4.3 Conclusions

ψ-PDA, produced by tyrosinase catalyzed polymerization of tyramine is disclosed as a valuable alternative to the classical PDA-coating technology with considerable advantages that relate to enzymatic control of film deposition. ψ-PDA films display structural and physicochemical properties similar to those of T-PDA and similar, or even better, antioxidant activity. Confinement or immobilization of tyrosinase at the desired site of functionalization resulted moreover in a highly clean film deposition procedure with complete recovery of unutilized tyramine and no unwanted substrate-consuming autoxidation

processes, which limit cost-effectiveness and may interfere with the film deposition procedure.

4.4 Experimental section

Materials and methods

Tyramine, dopamine hydrochloride, tyrosinase from mushroom (2687 U/mg), 2,2-diphenyl-1-picrylhydrazyl (DPPH), ferric chloride (III) hexahydrate and 2,4,6-tri(2-pyridyl)-s-triazine (TPTZ) were purchased from Sigma Aldrich and used without further purification. Substrates (quartz and borosilicate glass coverslips) are cleaned by soaking in piranha solution (H_2SO_4/30 % H_2O_2 5:1) overnight, then rinsed with distilled water and dried under vacuum.

General procedure for substrate coating. To a 1 mM solution of tyramine or dopamine in 0.05 M sodium carbonate buffer pH = 6.8, tyrosinase (1-100 U/mL) was added under vigorous stirring. Substrates are dipped into the reaction mixture after complete dissolution of the starting materials and left under stirring up to 24 h, then rinsed with distilled water, sonicated and dried under vacuum. The UV-vis spectra were recorded on a Jasco V-730 Spectrophotometer.

Quartz Crystal Microbalance. The measurements were performed with a quartz crystal microbalance-dissipation (QCM-D) system from Q-Sense (Göteborg, Sweden). Briefly the mass change results from the variation of the resonance frequency ($-\Delta f$) of an oscillating quartz crystal when the material is adsorbed onto its surface from a solution and the dissipation factor (ΔD) provides a measure of the energy loss in the system. The crystal is excited at its fundamental frequency (about 5 MHz), and observations are made at the 3rd, 5th, 7th and 9th overtones (v=3,5, 7 and 9) at 15, 25, 35 and 45 MHz, respectively. For rigid films,

$-\Delta f/\nu$ is independent from the overtone number ν. According to the Sauerbrey relation,[151] $-\Delta f/\nu$ can be related directly to the total mass of the film. This mass includes not only that of the deposited material but also that of the water bound to the layer. The gold-coated sensor crystals consist of a quartz disk and electrodes sputtered on both sides of the quartz disk, consisting of a gold surface layer with a chromium under layer to strengthen the adhesion. The Q-Sense sensor crystals were cleaned used a Plasma Cleaner PDC-32G-2 for 15 min before the use. The tyramine or dopamine solutions were injected into the cell during one hour at a flow rate of 0.25 μL/min using a peristaltic pump.

Water contact angle. Water contact angle analyses were performed using a contact angle goniometer (digidrop-gbx, France) equipped with video capture. 1 μL of distilled water was dropped on the air side surface of the substrate.

MALDI-MS analysis. Positive Reflectron MALDI spectra were recorded on a AB Sciex TOF/TOF 5800 instrument using 2,5-dihydroxybenzoic acid as the matrix. The pigments were applied to the plate from a fine suspension in methanol obtained by homogenization in a glass to glass potter or scratched directly from the substrate surface, premixed with the matrix in a centrifuge tube and then pipetted on the MALDI target plate and air-dried for analysis. Spectrum represents the sum of 15,000 laser pulses from randomly chosen spots per sample position. Raw data are analyzed using the computer software provided by the manufacturers and are reported as monoisotopic masses.

Antioxidant assays:

2,2-diphenyl-1-picrylhydrazyl (DPPH) assay. The assay was performed as described.[152] Briefly, to a 200 μM DPPH solution in methanol, a proper amount of a methanol suspension of each pigment (2 mg/mL) homogenized with a

glass/glass potter was added and rapidly mixed. The reaction was followed by spectrophotometric analysis measuring the decrease of the absorbance at 515 nm after 10 min. Values are expressed as the EC_{50}, that is, the dose of the material at which a 50 % DPPH reduction is observed. The glass substrates were instead immersed in a solution of DPPH 50 μM (15 mL) for 2 hours and the antioxidant power was evaluated by UV-vis recording spectra every 5 minutes.

Ferric reducing/antioxidant power (FRAP) assay. The assay was performed as described.[153] The FRAP reagent was prepared by mixing 0.3 M acetate buffer (pH 3.6), 10 mM 2,4,6-tris(2-pyridyl)-s-triazine in 40 mM HCl, and 20 mM ferric chloride in water, in the ratio 10:1:1, in that order. To a solution of FRAP reagent, a proper amount of a methanol solution of each pigment was added and rapidly mixed. After 10 minutes, the increase of the absorbance at 593 nm was measured. Trolox was used as the standard and results were expressed as Trolox equivalents. The glass substrates were instead immersed for 24 h in 15 mL of a solution containing $FeCl_3$ (20 mM) and 2,4,6-tris (2-pyridyl) -s-triazine (10 mM) in 0.3 M acetate buffer (pH 3.6) in the ratio 10:1:1.

Sodium alginate hydrogel. For preparation of alginate hydrogels, tyrosinase was dissolved in water at 0.1 or 0.5 %, then sodium alginate was added (2 % w/w). As described in Chapter 3, beads were prepared dropping the freshly prepared gel in a 0.1 M solution of $CaCl_2$ allowing alginate reticulation for few minutes followed by beads filtration. Films were similarly fabricated spreading the gel on a smooth surface followed by dipping in the $CaCl_2$ solution for about 30 s. The beads and films so obtained were washed in distilled water and dipped in tyramine solution (1 mM).

Supporting materials

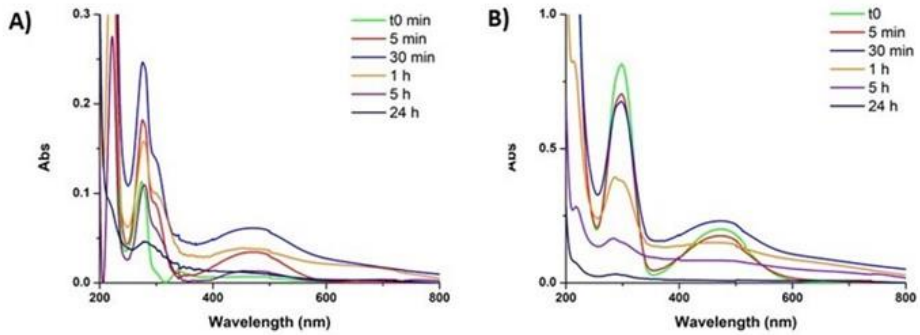

Figure S4.3.1. Evolution of the UV−vis spectra of tyramine solution (1 mM) (a) and dopamine solution (b) during the enzymatic reaction over 24 h but diluted 10-fold before the measurement of the spectra.

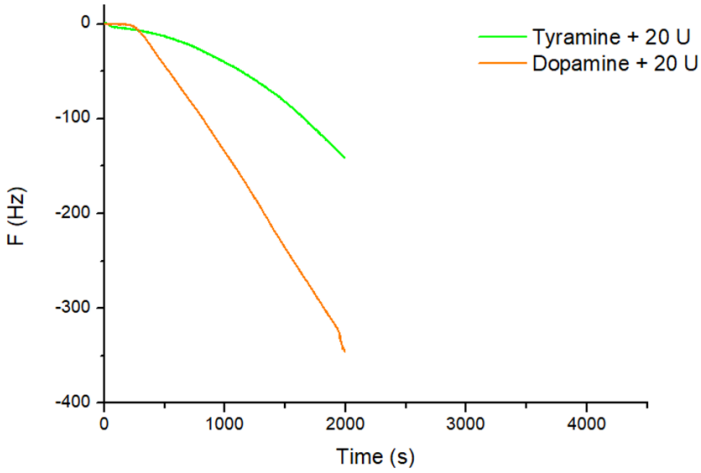

Figure S4.3.2. Kinetics of the deposition of tyramine or dopamine in the presense of 20 U/mL of tyrosinase.

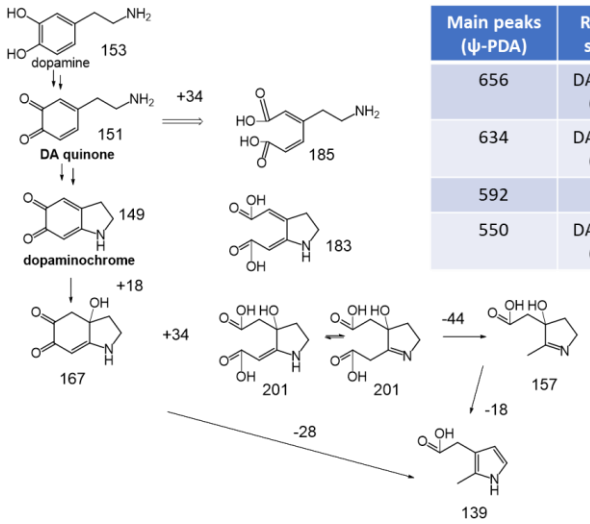

Main peaks (ψ-PDA)	Reference structure	Plausible pathway:
656	DA tetramer 606 m/z	Oxidation/hydration step
634	DA tetramer 606 m/z	Oxidation
592	634	decarboxylation
550	DA tetramer 606 m/z	decarboxylation and dehydration steps

Main peaks (T-PDA)	Reference structure	Plausible pathway:
724	DA tetramer 606 m/z	muconic-type cleavage of o-quinones/hydration steps
696	724	- CO
652	696	decarboxylation
624	652	-28
596	624	-28

Figure S4.3.3. Possible structural features of the species accounting for the main peaks on tyramine- and dopamine-derived films. Main peaks reported in Table are attributed to sequences of muconic-type cleavage of *o*-quinones, decarboxylation and hydration/dehydration steps.

Chapter 5

Eumelanins: from natural pigments to new functional materials

5.1 Introduction

Black and insoluble eumelanin biopolymers are the key determinants for the dark pigmentation of hair, skin and eyes in humans and other mammals. Biological roles of eumelanins include photoprotection and free radical scavenging in the skin and eyes, charge transport and detoxification in internal or nonexposed organs, such as inner ear and melanized dopaminergic neurons of the substantia nigra.[29] Most of the biological roles and functions of eumelanins are attributed to their unique physicochemical properties, including, to mention only some, a broadband ultraviolet and visible absorption, efficient energy dissipation by nonradiative excited state deactivation,[154,155] free radical, redox and antioxidant activity,[156,157] water dependent ionic-electronic conductivity,[55] a persistent electron paramagnetic resonance (EPR),[45] metal and drug binding.[49] Their peculiar properties make them highly attractive candidates in the perspective of their exploitation as biocompatible functional materials for electronics and bioelectronics, for surface functionalization, skin photoprotection and other cosmetic applications.

In human melanocytes eumelanins derive from tyrosinase-catalyzed oxidation of tyrosine leading to dopaquinone. Further steps of melanogenesis can occur spontaneously, at varying rates depending on pH, presence and concentration of

metal cations (particularly zinc and iron), reducing agents, thiols and oxygen.[158] The oxidation product of tyrosine is highly reactive and, when concentration of sulfhydryl compounds is low, undergoes intramolecular cyclization yielding to cyclodopa (or leucodopachrome). Dopachrome, orange-red in color, is then generated together with dopa by a redox exchange between cyclodopa and dopaquinone. This process therefore gives rise to dopa that is formed during melanogenesis. Intramolecular rearrangement of dopachrome leads to 5,6-dihydroxyindole (DHI) and 5,6-dihydroxyindole-2-carboxylic acid (DHICA), that in turn undergo oxidative polymerization to form eumelanin (see Scheme 2.1.2, Chapter 2).[159]

In vitro and in the absence of enzymatic assistance decarboxylation of dopachrome is favored leading to 5,6-dihydroxyindole whereas in melanocytes the enzyme Dopachrome tautomerase or tyrosinase- related protein 2 (Dct, Tyrp 2) directs the tautomerization process through the non-decarboxylative route with formation of DHICA. This latter is also a major circulating melanogen[156] and represents a substantial portion (around 50%) of the indole units of natural eumelanins.[160] Interestingly, in addition to Dct, also several biorelevant transition metal ions, such as Cu^{2+} and Zn^{2+}, can direct the rearrangement of dopachrome to DHICA at physiological pH.[161] Despite an apparent similarity, DHI and DHICA exhibit quite different chemical properties and biological activities, which are still not entirely clarified and that purportedly hold the key to the actual physiological significance of melanogenesis.

The mechanism of the oxidative conversion of melanogenic indoles to eumelanins have been the subject of intensive research work. Most of the information that is presently available derives from a biomimetic approach in which the oxidation of the indoles is carried out under conditions that are mimicking those occurring in the biological environment. Either indoles are converted to black insoluble

pigments resembling natural eumelanins following exposure to oxidizing enzymes, UV radiation, chemical oxidants, or even on standing in air at neutral physiological pHs, although with a different kinetics.[46]

In particular, DHI melanins confer to the pigments the absorption over the visible region, are the main responsible of the chromophore and hence may ensure the photoprotective action. On the other hand, the marked antioxidant and radical scavenging activity of DHICA melanin (Figure 5.1.1) together with their peculiar chromophore, covering the UVB/UVA region that is generally agreed as one of the most dangerous portion of the solar spectrum would suggest its exploitation as an ingredient in dermocosmetic formulations with photoprotective action playing a protective role toward cellular damages induced by UV light and oxidative stress.[45] Moreover both DHI and DHICA melanin are paramagnetic and display similar g-value in their EPR spectra but the DHICA melanin signal is significantly narrower than the DHI one.[45,49]

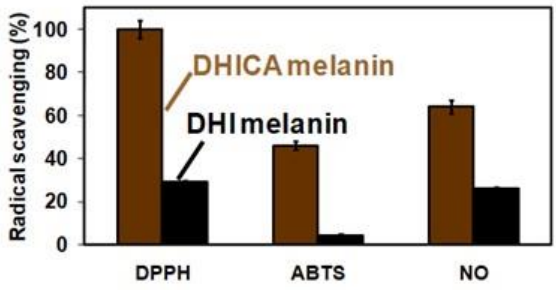

Figure 5.1.1. Free radical scavenging properties of DHICA and DHI melanins.[45]

Limitations to the use of these materials, however, derive from their low solubility in hydroalcoholic or more lipophilic media that are usually employed in cosmetic formulations and the ease to undergo degradation *e.g.,* by photooxidation under UVA as a result of quenching of singlet oxygen with loss of their properties.[162]

To overcome these limits, in a recent study, a model eumelanin obtained from the oxidation of the DHICA methyl ester (MeDHICA) was investigated.[163] This melanin appeared as a regular polymer made of methyl DHICA units by mass spectrometric analysis and exhibited an intense and broad chromophore centred at 330 nm and a fairly good solubility in different water miscible organic solvents like DMSO, in which DHICA melanin proved almost completely insoluble (Figure 5.1.2).

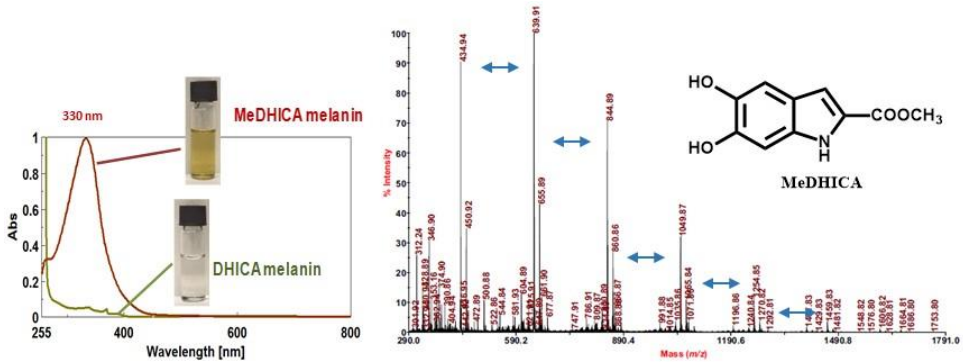

Figure 5.1.2. (Left) Absorption spectra and digital pictures of DHICA and MeDHICA melanins; (Right) MALDI-MS spectrum of the MeDHICA melanin.

Moreover, the antioxidant potential of this melanin was evaluated by use of common tests in comparison with DHICA melanin and their respective monomers. The electron-transfer ability of MeDHICA as determined by the DPPH assay proved higher than that of DHICA with an EC_{50} value very low and almost one half that observed for DHICA melanin, while both monomers were more efficient; in the iron III reduction (FRAP) assay MeDHICA melanin was more active than trolox (1.6 trolox equivalents) and comparable to the monomers (Figure 5.1.3, panel A). In addition, MeDHICA melanin proved fairly stable to air as assessed by evaluating the changes of the ferric reduction activity after

exposure to air in aqueous buffers at neutral pHs as well as to light after 3 h irradiation by a solar simulator (Figure 5.1.3, panel B).

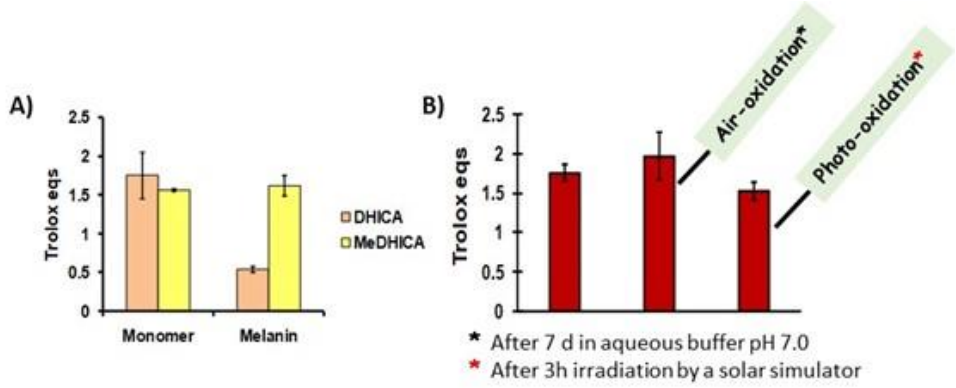

Figure 5.1.3. (a) FRAP assay of DHICA melanin and its methyl ester; (b) Photo-and air-oxidation stability of MeDHICA melanin.

Although polydopamine is currently the reference material for surface functionalization and coating, the possibility to impart film forming ability to natural polymers including eumelanins and polyphenol plant materials endowed with other important biological activity and functional properties has recently represented a focus of intense research.

An attractive approach to this goal may be based on the development of alternative dip-coating methodologies based on separate catechol and amine components allowing access to tailored materials *via* rational combination of precursors. In this view new opportunities in surface chemistry have derived from the discovery, supported by various lines of evidence, that hexamethylenediamine (HMDA) markedly enhances film deposition from the polymerization of dopamine (as reported in Chapter 2) and a variety of catechol substrates.[69,70,103]

On these bases, in this chapter research work is reported that was aimed to:

1. assess whether HMDA can promote film deposition from eumelanin precursors (*e.g.* DHI, DHICA and its methyl esters);
2. investigate the mechanisms by which HMDA can induce film deposition from non-adhesive melanin type polymers by defining structure-property relationships;
3. synthesize novel conjugates of HMDA with DHICA and related compounds and to compare their adhesion and antioxidant properties with diamine-free materials, as a means of developing innovative functional systems.

5.2 Film deposition from oxidation of DHI: the effects of amines

In Chapter 2, it was shown that under the same dip-coating conditions used for PDA, DHI polymerization (both 10 mM and 1 mM) does not produce UV-vis and AFM-detectable films on a quartz surface. In order to assess the effect of HMDA on the mechanisms of film deposition from dopamine at pH 9.0, other experiments were carried out by adding equimolar amounts of HMDA to 1 mM DHI as a later intermediate in PDA film deposition. In particular, as shown in Figure 5.2.1, the addition of 1 mM HMDA led to the deposition, after 24 h, of a dark coating resembling PDA. This finding was remarkable and quite unexpected given the inability of DHI to give films on oxidation.

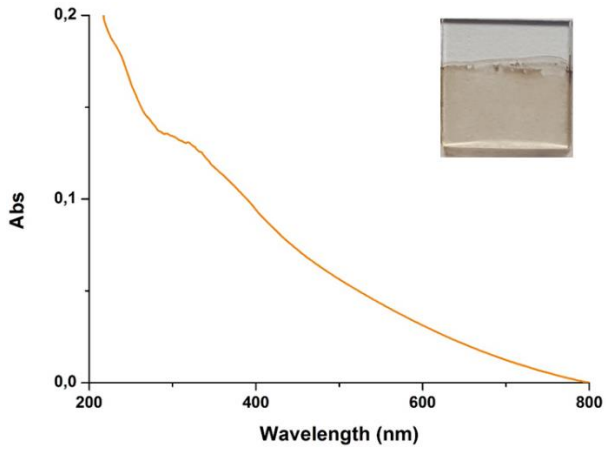

Figure 5.2.1. Picture and UV–vis spectrum of quartz substrate dipped into 1 mM solution of DHI in 0.05 M carbonate buffer (pH 9.0) in the presence of equimolar amount of HMDA over 24 h.

In other experiments the aerobic oxidation of DHI was also performed in the presence of monoamine (butylamine) or one of the following diamines, *i.e.* 1,12-dodecanediamine, 1,10-decanediamine, 1,4-diaminobutane and 1,2-diaminoethane using a 1:1 indole/amines molar ratio. As reported in Figure 5.2.2 amine-dependent coatings were observed under conditions where no film is deposited in the absence of amines. A long aliphatic chain and two amine groups proved again to be important structural determinants to induce film formation. Consistent with this conclusion a short chain monoamine (butylamine) or diamine (1,2-diaminoethane) proved not effective at inducing film deposition.

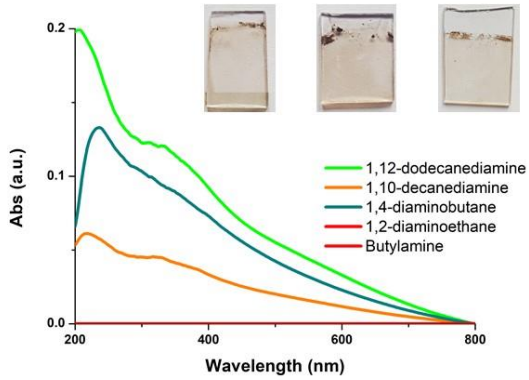

Figure 5.2.2. Pictures, film thickness and UV-vis spectra of quartz substrates dipped into 1 mM solution of DHI in the presence of equimolar amounts of amines. Film thickness: 45 ± 10 nm (1,12-dodecanediamine); 20 ± 7 nm (1,10-decanediamine) and 35 ± 5 nm (1,4-diaminobutane).

Morphological characterization. DHI/HMDA melanin films were then characterized by AFM coupled with micro Raman analysis (spectra were recorded at the Department of Physics, University of Naples Federico II in the frame of a collaborative work with Prof. P. Maddalena and co-workers). Notably, in line with previous Raman spectra of PDA coating reported in the Chapter 2, main bands, compatible with the presence of aromatic rings and attributable to strongly hydrogen-bonded OH and NH stretching vibrations, were detected (Figure 5.2.3). As apparent from the optical and AFM images (Figure 5.2.3), a uniform film with a main estimated thickness of 30 ± 10 nm, grain distribution and dispersion was achieved. The origin of the large roughness of the DHI/HMDA films could be explained by considering both the low solubility of DHI and its oligomers and its fast rate of oxidation leading to fast deposition of aggregates on the growing films.

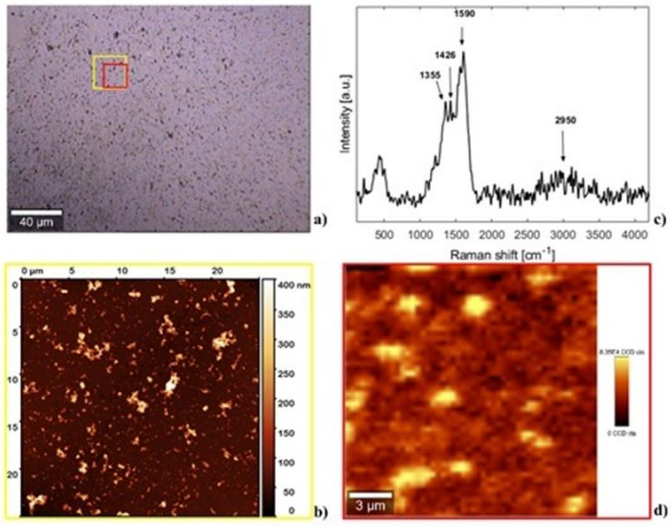

Figure 5.2.3. AFM and micro-Raman analysis of the sample DHI (a) Bright-field image of the investigated sample region collected by 20 X microscope objective. (b) AFM image of the area indicated by the yellow square in the optical image Film thickness: 30±15nm (c) Raman spectrum (d) Raman image relative to the red sample region in the optical image.

Structural characterization. Insight into the structure of the DHI melanins samples produced in the presence and in the absence of HMDA was then obtained by solid state ^{13}C and ^{15}N NMR analysis of the bulk materials that precipitated from the reaction mixtures. A pronounced HMDA-dependent differences were observed in the presence of HMDA, for which distinct aliphatic resonances were appeared in both the ^{13}C and ^{15}N NMR spectra (Figure 5.2.4). An increase in the relative intensity of carbonyl/carboxyl signal was also observed in the amine containing sample according to a certain degree of incorporation of HMDA into the polymer bulk structure, higher to what observed in the case of PDA/HMDA reported in Chapter 2. This observation would suggest that HMDA incorporation is not so important at the dopamine quinone level as it could be at the later

indolequinone stage. It is, in fact, well-documented in literature[164] the covalent coupling of nucleophilic agents with 5,6-indolequinone.

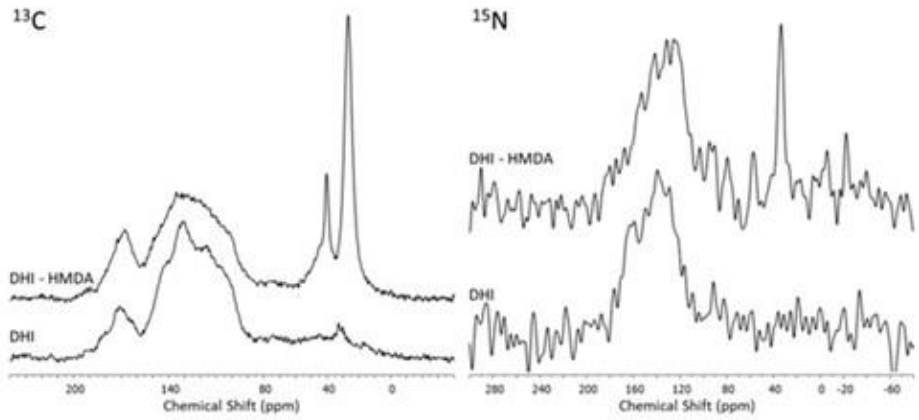

Figure 5.2.4. ^{13}C and ^{15}N NMR spectra (recorded by Drs. R. Avolio and M.E. Errico, IPCB, CNR, Pozzuoli) of the oxidation products of DHI obtained in the presence and in the absence of HMDA.

The bulk precipitates of the 1 mM DHI oxidation mixture in the presence and in the absence of HMDA were also subjected to MS analysis in the MALDI-ToF mode after centrifugation and extensive washings, using 2,5-dihydroxybenzoic acid as the matrix. Interestingly the spectrum of the DHI/HMDA melanin (Figure 5.2.5 panel A) showed an intense peak at $[M+H]^+$ = m/z 425 which was missing in the control DHI sample (Figure 5.2.5, panel B), mainly characterized by peaks attributable to oxidative degradation. This peak, whose tentative structure is shown in Figure 5.2.6, was suggestive of a 5,6-dihydroxyindole unit, a cleaved indolequinone and one HMDA moieties linked *via* loss of an oxygen atoms, suggesting also in this case a dominant condensation of the amine groups with the carbonyl moieties rather than addition at conjugated positions. In support of this

hypothesis, the spectrum shows also an intense peak at $[M+H]^+$ = m/z 329 suggestive of the same indole units without the HMDA chain.

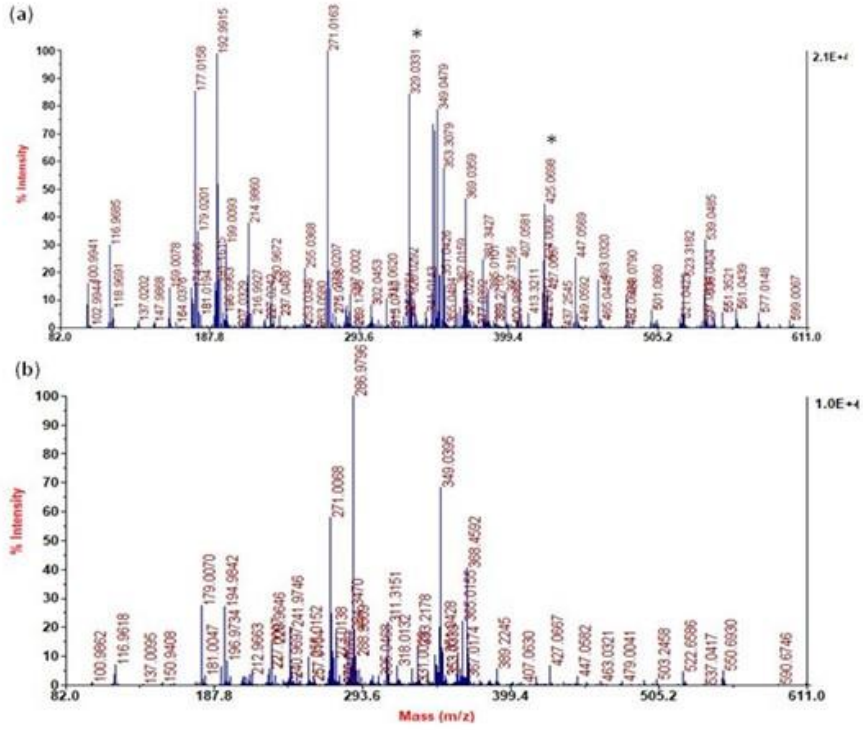

Figure 5.2.5. Segmental spectra of MALDI-MS of the solid separated from DHI/HMDA (a) and DHI melanin mixture after centrifugation (b). Asterisks indicate specific peaks of DHI/HMDA.

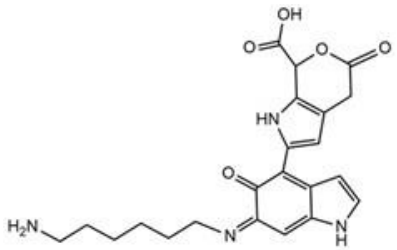

Figure 5.2.6. Tentative structure representative of the possible species responsible for the peak at m/z 425 in the DHI/HMDA mixture.

5.2.1 Effect of resorcinol as dopamine quinone trapping agent

In other experiments, the effect of resorcinol on deposition of PDA or DHI films from 1 mM dopamine or DHI in the presence of HMDA was investigated. Data reported in Figure 5.2.1.1 (panel A) revealed a marked concentration dependent inhibition of PDA film deposition by resorcinol proving that the resorcinol competes with HMDA in the reaction process preventing the generation of adhesive species and blocking the growth of the film *via* addition to dopamine quinone. In support of this conclusion, spectrophotometric analysis of the supernatant from the reaction mixture indicated a yellow chromophoric species with an intense emission at 460 nm compatible with the azamonardine-type adduct described in Chapter 3. A marked, though not complete, inhibition of film deposition was also observed when the reaction was run under the usual dopamine concentration of 10 mM with equimolar inhibitor and in the absence of HMDA, suggesting coupling of resorcinol with quinone intermediates involved in adhesion and cross-linking (Figure 5.2.1.1, panel B). On the other hand, addition of equimolar amounts of resorcinol to a DHI/HMDA solution completely

inhibited DHI melanin deposition on the quartz substrates despite significant polymer precipitation.

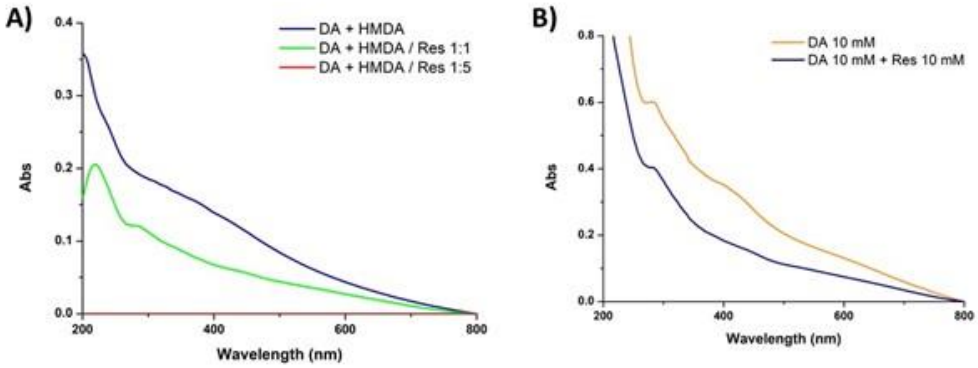

Figure 5.2.1.1. UV-vis spectra of quartz substrates dipped for 24 h into: (a) 1 mM solution of DA with 1 mM HMDA in the absence or in the presence of 1 or 5 mM resorcinol (Res); (b) 10 mM DA in the absence and in the presence of equimolar amounts of Res.

The inhibitory effect of resorcinol on HMDA-induced film deposition with 1mM dopamine reflects the competition between HMDA and resorcinol for nucleophilic attack, but the concentration-dependence of the effect points either to a partial escape of dopamine quinone from trapping by resorcinol and can still undergo coupling with HMDA, intermolecular cross-linking and intramolecular cyclization to give aminochrome and then DHI. According to the well-known instability of 5,6-indolequinone, which cannot be isolated or even identified under standard reaction conditions, the resorcinol is capable of bringing a more efficient nucleophilic attack onto indolequinone intermediates. This effect is a further indirect evidence for the involvement of quinone moieties in PDA film formation and allowed to suggest that DHI/HMDA coatings were made by conjugates of HMDA with DHI and oligomers thereof.

5.3 Film deposition from oxidation of DHICA: the effects of amines

To assess whether HMDA can promote film deposition from other eumelanin precursors besides DHI, in a first series of experiments the aerobic oxidation of DHICA (1 mM) was carried out in 50 mM carbonate buffer at pH 9.0 in the presence of HMDA in a 1:1 indole/diamine molar ratio. The mixture was kept under stirring for 24 h and a quartz substrate was immersed in the reaction mixtures to evaluate the adhesion properties of the pigment. The course of the reaction was followed spectrophotometrically to obtain information on the consumption of the indole compound and the formation of the melanin pigment. As shown in Figure 5.3.1, the absorption peak of the starting product at 320 nm progressively broadens to give rise after 2 h to a more complex peak with a shoulder at about 370 nm. After 24 h only the precipitation of a melanin like material was observed, but without formation of a spectrophotometric detectable film on the quartz support.

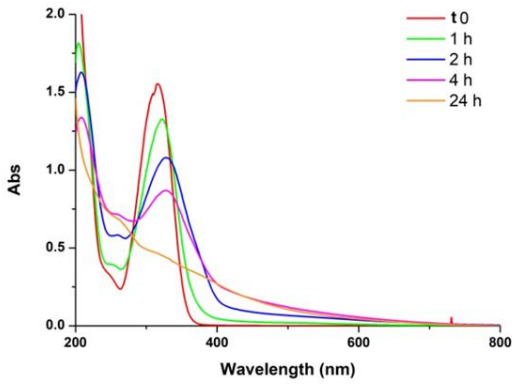

Figure 5.3.1. Spectrophotometric course of the aerobic oxidation mixture of DHICA at 1 mM in 50 mM carbonate buffer (pH = 9.0) in the presence of equimolar HMDA.

A UV-detectable film was instead observed when the reaction was run, under the same conditions described above, but in the presence of 1,12-dodecanediamine (Figure 5.3.2). As already observed in the oxidative polymerization of dopamine or DHI, short chain monoamine (butylamine) proved not effective at inducing film deposition, whereas coating was induced by 1,2-ethylenediamine and 1,10-decanediamine but to a lower extent (Figure S5.6.1). It could be suggested that the film forming properties stemmed from suitable balance of hydrophobicity, aggregation and cross-linking.

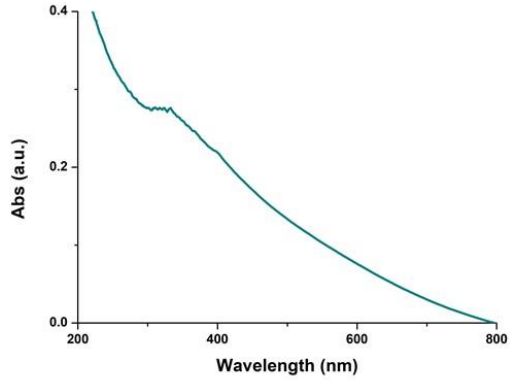

Figure 5.3.2. Picture and UV-vis spectrum of the quartz substrate after 24 h dipping in the DHICA/1,12 dodecanediamine mixture at pH = 9.0.

As apparent from the optical and AFM images shown in Figure 5.3.3, a uniform film with a main estimated thickness of 85 ± 15 nm, grain distribution and dispersion was achieved.

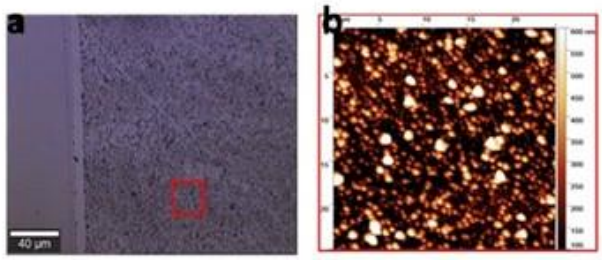

Figure 5.3.3. AFM analysis of the sample DHICA/1,12-dodecanediamine (a) Bright-field image of the investigated sample region collected by 20 X microscope objective. (b) AFM image of the area indicated by the yellow square in the optical image. Film thickness: 85 ± 15 nm.

5.3.1 Coupling DHICA with hexamethylenediamine (HMDA)

To investigate the role of the HMDA moiety in the film forming properties a different approach was also pursued in which the HMDA unit was linked to the DHICA unit through amide bond.

In order to synthesize a new DHICA amide derivative with HMDA a protocol reported in literature for the preparation of amides and esters from caffeic acid and other cinnamic acids was adopted.[165] This procedure involves the use of N-(3-dimethylaminopropyl)-N'-ethylcarbodiimide chlorohydrate (EDC), as a condensing agent in the presence of 1-hydroxybenzotriazole (HOBt) and a base triethylamine (TEA) in anhydrous solvent (dimethylformamide (DMF)), at room temperature and under inert atmosphere. The role of HOBt in the reaction has been examined in several studies and involves its intervention as an efficient nucleophile, on the initial product of addition of the carboxyl group on the imide. The product resulting from this acyl substitution is then attacked by the amine

with favorable evolution of the tetrahedral intermediate resulting from the attack.[166] (Scheme 5.3.1.1).

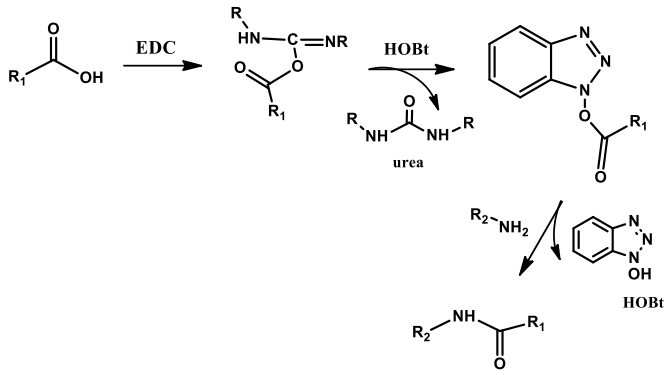

Scheme 5.3.1.1. Mechanism of action of HOBT and EDC for the synthesis of amide derivative.

In the initial experiments the reaction was carried out in anhydrous DMF using a concentration of DHICA 276 mM in the presence of 1.5 molar equivalents of EDC, HOBt and triethylamine (TEA) used as base.[165] The mixture was kept under stirring under an argon atmosphere and after 10 minutes 0.5 equivalents of HMDA were added. The reaction was then transferred to a thermostated bath at about 25 °C for 18 h and then taken to dryness, acetylated with acetic anhydride and pyridine for 24 h and analyzed by HPLC. The chromatographic profile indicated a total consumption of DHICA and the formation of two main components (t_R = 6 and 13 min) in addition to the HOBt (t_R = 4 min) (Figure 5.3.1.1). No significant differences were observed when the reaction was carried out varying the DHICA/HMDA molar ratio.

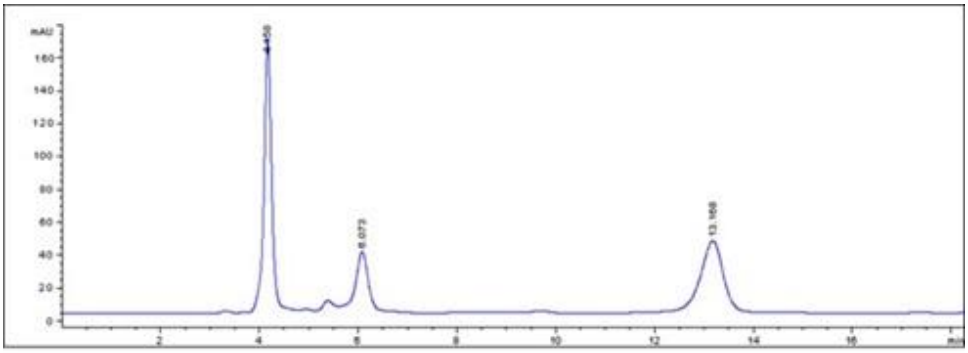

Figure 5.3.1.1. Elutographic profile of the acetylated reaction mixture (λ=300 nm).

To get information on the identity of the reaction products the mixture was analyzed by LC-MS and MALDI-Tof. The component eluted at t_R = 16 min in the Total Ion Current (TIC) shown in Figure 5.3.1.2 exhibited a pseudomolecular ion peak $[M+H]^+$ at m/z 635 ascribable to diamide completely acetylated on the hydroxyl functions (Figure 5.3.1.3) while the less retained component (t_R = 7.5 min) showed a pseudomolecular ion peak $[M+H]^+$ at m/z 418 indicating a monoamidation product with three acetyl groups probably on the hydroxyl functions and the amino function (Figure 5.3.1.3). This result was also confirmed by MALDI-MS analysis. The MALDI spectrum (Figure S5.6.2) exhibited pseudomolecular peaks $[M+K]^+$ at m/z 456 and 673 corresponding to acetylated mono- and diamidation product of DHICA, respectively thus confirming the putative structure.

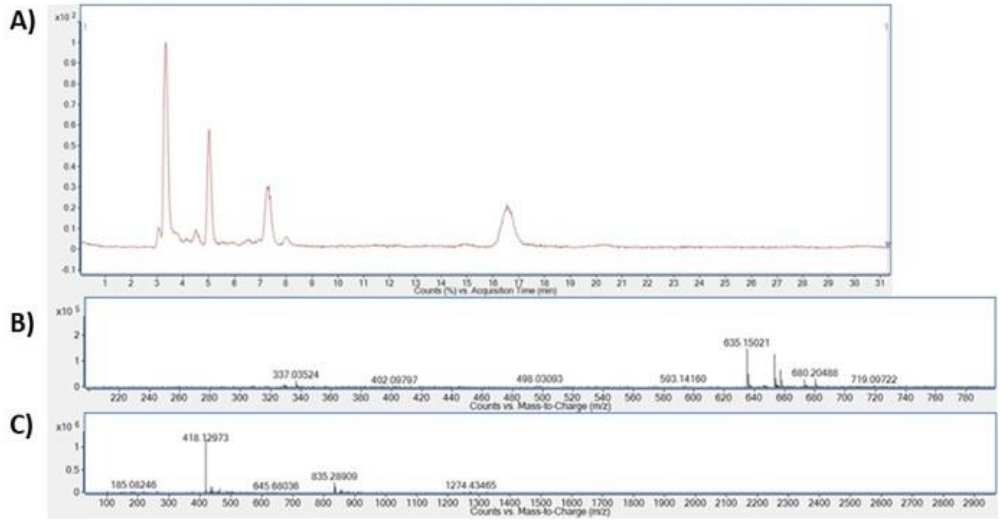

Figure 5.3.1.2. a) Total ion current (TIC) of the acetylated reaction mixture of DHICA; mass spectra of the products at t_R =16 min (b) and at t_R = 7.5 min (c).

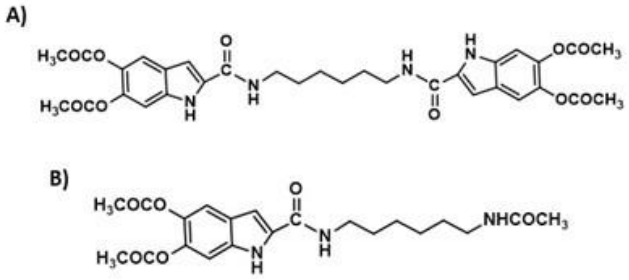

Figure 5.3.1.3. Structure of the expected diamidation $[M+H]^+$ = m/z 635 (a) and monoamidation $[M+H]^+$ = m/z 418 (b) product of DHICA with HMDA.

Treatment of the reaction mixture in DMF with equal volumes of water allowed almost complete removal of HOBt remaining in the supernatants whereas the solid that separated dissolved in DMSO was fractionated by preparative HPLC to get the DHICA/diamide product. However, the isolation yield was very low (*c.a.* 6%) likely due to the oxidation of the catechol compounds during the reaction in a

basic medium. In subsequent experiments, therefore, an alternative procedure was developed for the synthesis of the diamide starting from the *O*-acetyl derivative of DHICA, DAICA, that is much less susceptible to oxidation. The amidation reaction was performed under the same conditions previously described. After removal of HOBt under the conditions described the solid separated from the reaction mixture was recovered by centrifugation and analyzed by HPLC. The chromatographic profile (Figure S5.6.3) revealed the presence of diamide with a satisfactory degree of purity and therefore no further chromatographic purification was performed. The product obtained was subjected to complete spectral characterization and the hypothesized structure, reported in Figure 5.3.1.3, panel A, was confirmed by NMR analysis (Figure S5.6.4-S5.6.8). The ^{1}H NMR spectrum (Figure S5.6.4) shows in the aromatic region the typical proton signals of the DHICA indole ring at 7.12, 7.24 and 7.45 ppm and signals attributable to the amide NH and to the indole NH whereas ^{1}H, ^{1}H-COSY spectrum (Figure S5.6.5) confirmed the presence of signals due to three different sets of CH_2 protons of HMDA.

In subsequent experiments, in order to evaluate the film formation properties of the oxidation product of the diamide, after removal of the acetyl groups by treatment with sodium *t*-butoxide under controlled conditions, the free diamide was oxidized in aqueous buffer in air. A quartz substrate was also dipped in the oxidation mixture and after 24 h precipitation of a dark brown melanin-like pigment was observed (80 % recovery yield), but no adhesion on the quartz substrate was obtained. It can be concluded that only the use of the diamine during the oxidation process may confer film forming capacity to the material whereas the presence of the HMDA unit as in the diamide does not *per se* confer adhesive properties.

5.3.2 Evaluation of the antioxidant properties of the pigments obtained from oxidation of DHICA

In another series of experiments the antioxidant potential of the pigments obtained from oxidation of DHICA with or without HMDA and DHICA/HMDA diamide were comparatively evaluated. Experimentally, known volumes of a fine methanol suspension (1 mg/mL) of the pigment (DHICA/HMDA, DHICA/diamide and DHICA melanins) or the corresponding monomers obtained using a glass/glass homogenizer solution were added to a DPPH solution (200 μM). The mixtures were kept under vigorous magnetic stirring at room temperature and the course of the reaction was followed spectrophotometrically by measuring the absorbance at 515 nm after 10 minutes. As shown in Figure 5.3.2.1 panel A, the melanin from DHICA and DHICA/diamide exhibit similar values (EC_{50} 29.0 ± 0.3 μg/mL and 24.4 ± 0.8 μg/mL, respectively), while addition of HMDA during the aerobic oxidation of DHICA impacts negatively on the antioxidant properties of this latter (EC_{50} 91.9 ± 0.2 μg/mL).

For comparison, the EC_{50} value of the DHICA and diamide monomer were determined as 5.8 ± 0.1 μg/mL and 17.3 ± 0.2 μg/mL, respectively (Figure 5.3.2.1, panel B). As expected, the monomers of DHICA and DHICA/diamide have higher antioxidant power mainly firstly because they are more soluble in methanol and this affects the response of the assay and secondly because they are likely at a lower oxidation status than the polymers.

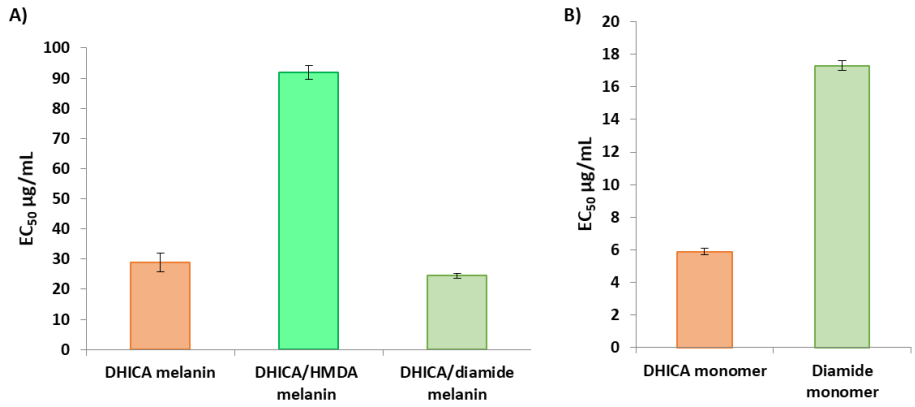

Figure 5.3.2.1. EC_{50} values obtained from the DPPH assay of the melanin pigments obtained by oxidation of DHICA, DHICA/HMDA and the DHICA/diamide (1 mg/mL) or their monomers. The average values ± SD obtained from at least three separate experiments are reported.

The ferric reducing capacity of these pigments was also evaluated in the FRAP assay. The results reported in Figure 5.3.2.2 show a reducing capacity equal to almost 1 equivalent of Trolox in the case of DHICA melanin with respect to a value of about 1.1 equivalent obtained for the DHICA/diamide melanin. It can be concluded that the pigment obtained from DHICA/diamide has a strong antioxidant power as hydrogen donation in the DPPH assay, while the reduction capacity of Fe^{3+} is similar to Trolox.

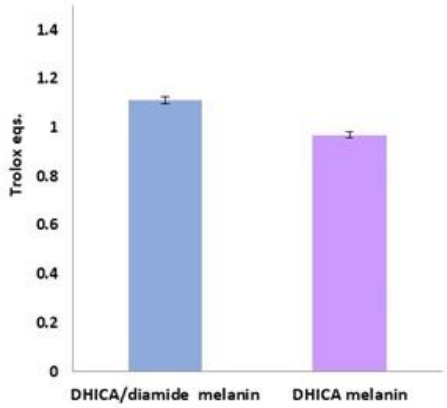

Figure 5.3.2.2. Trolox equivalents determined in the FRAP assay for the melanin pigment obtained from DHICA and DHICA/diamide. The average values ± SD obtained from at least three separate experiments are reported.

5.4 Film deposition from oxidation of MeDHICA: the effects of amines

Considering the remarkable antioxidant properties of the DHICA methyl ester, illustrated in the paragraph 5.1, a full exploitation of this material would greatly expand if the reaction with HMDA confer also adhesive properties.

The MeDHICA oxidation reaction was performed, similarly to what was described for DHICA in the paragraph 5.2, using an indole concentration of 1 mM in 50 mM carbonate buffer at pH 9.0 in the absence and in the presence of HMDA with an indole/diamine molar ratio 1:1.5. A quartz substrate was also dipped in the reaction mixture and the course of the reaction was followed spectrophotometrically to monitor the consumption of the substrate and pigment formation (Figure S5.6.9). After 24 h the formation of an abundant precipitate, which was collected by centrifugation, was observed in both cases whereas only

in the presence of HMDA a well UV-detectable film with an absorption maximum around 340 nm was observed (Figure 5.4.1).

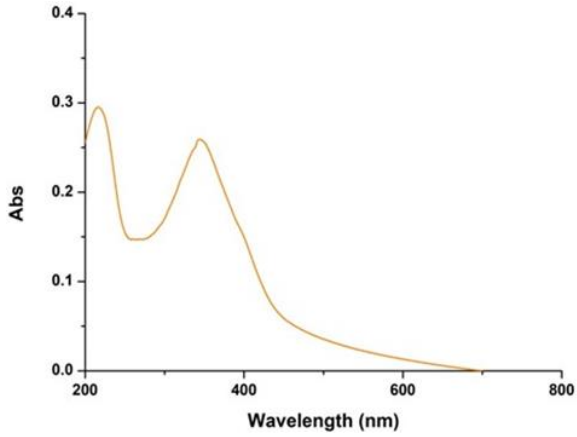

Figure 5.4.1. UV-vis spectrum of the quartz substrate after 24 h dipping in the MeDHICA/HMDA mixture at pH 9.0.

Efficient MeDHICA/HMDA film deposition was observed also on glass surface and other materials as shown in Figure 5.4.2.

Figure 5.4.2. MeDHICA/HMDA coatings on various materials: (A) glass, (B) polyethylene, (C) polycarbonate.

To evaluate the film forming capacity of the MeDHICA pigment, in another series of experiments, the aerobic oxidation of MeDHICA was performed under the same conditions described above, but in the presence of one of the following monoamine (butylamine) or diamines, *i.e.* 1,12-dodecanediamine, 1,4-butanediamine and 1,2-ethylenediamine with a 1:1 or 1:5 indole/amines molar

ratio. A low film deposition was observed only in the presence of 1,4-butanediamine (Figure S5.6.10). It can be concluded that the combination of a long aliphatic chain and two-amine groups is a crucial requisite to confer to catechol polymers a suitable balance of hydrophobicity, aggregation and crosslinking. In fact, neither a monoamine as butylamine nor short chain diamines as 1,2-ethylenediamine are able to lead to film deposition from autoxidizing catechols, whereas in the case of 1,12-dodecanediamine the failure of film deposition is likely due to high hydrophobicity which does not allow amino groups to interact efficaciously with the oxidation products of MeDHICA.

The MeDHICA/HMDA coating was then characterized by AFM (spectra were run at the University of Strasbourg in the frame of a collaborative work with Prof. V. Ball and co-workers). As shown in Figure 5.4.3 (panel A) the film appeared smooth and homogeneous with a main estimated thickness of 37 ± 5 nm. It also exhibits a relatively high Water Contact Angle (WCA) (62.0 ± 0.6), *i.e.* moderate hydrophobicity (Figure 5.4.3, panel B). Interestingly after exposure of MeDHICA/HMDA coating to HCl vapours, the WCA value decreases by 50 % (24.4 ± 0.3), indicating that such a treatment results in a marked increase in the hydrophilicity (Figure 5.4.3, panel C).

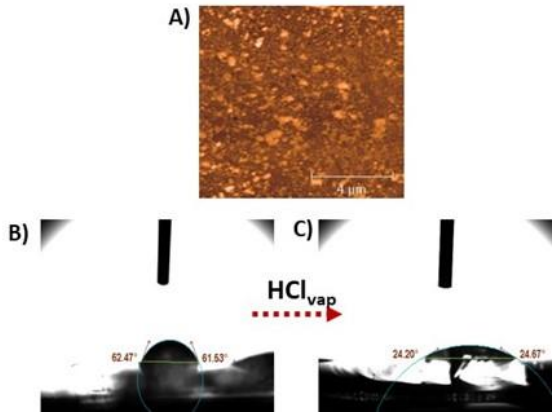

Figure 5.4.3. a) AFM image of MeDHICA/HMDA coating; WCA of the MeDHICA/HMDA coating before (b) and after (c) exposure to HCl vapours.

In further experiments the kinetics of film deposition of MeDHICA/HMDA was followed over 1 h, using the Quartz Crystal Microbalance (QCM-D) methodology. For comparative purposes, the same technique and procedure was applied to PDA/HMDA oxidation mixture, performed under the same conditions adopted in the case of MeDHICA/HMDA.

As shown in Figure 5.4.4, the kinetic deposition of DA/HMDA is higher than that of MeDHICA/HMDA that appears rather smooth over the period observed.

The thickness of the films was also calculated using the Sauerbrey equation from the QCM-D data, illustrated in Chapter 4, and were equal to 8.68 and 15.1 nm for MeDHICA/HMDA and PDA/HMDA respectively.

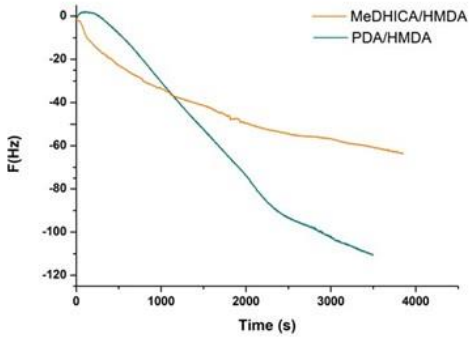

Figure 5.4.4. Kinetics of deposition of MeDHICA/HMDA and PDA/HMDA over 1 h.

From these results, it appears that after one hour the amount of PDA/HMDA film deposited is higher than that of MeDHICA/HMDA. Yet, the data reported in Chapter 2 for PDA/HMDA coating, prepared under the same conditions, at 24 h indicate a value of film thickness of 40 nm, *i.e.* quite similar to 37 nm achieved in the case of MeDHICA/HMDA. This would indicate that after an initial phase (over the first hour) the deposition rate of PDA/HMDA lowers significantly. In addition, WCAs of the crystal quartzes, obtained after deposition of the MeDHICA/HMDA and PDA/HMDA oxidation mixtures over 1 h, showed values for the MeDHICA/HMDA film similar to that determined on the quartz after 24 h dipping and higher than PDA/HMDA as shown in Figure 5.4.5.

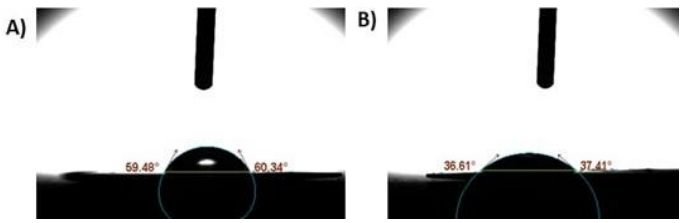

Figure 5.4.5. Water Contact Angle of crystal quartz of: (a) MeDHICA/HMDA (59.9 ± 0.6) and (b) PDA/HMDA (37.0 ± 0.5).

The chemical stability of the MeDHICA/HMDA films was tested under different conditions. Exposure of as prepared films to aqueous solutions containing reducing agents, such as sodium borohydride, does not result in detectable modification of the UV-vis absorption spectra. Interestingly exposure of the films to ammonia vapors cause visible increase in color and a progressive loss of the peculiar absorption maximum up to 48 h (Figure 5.4.6), suggesting further oxidation of the initially deposited products toward melanin like materials.

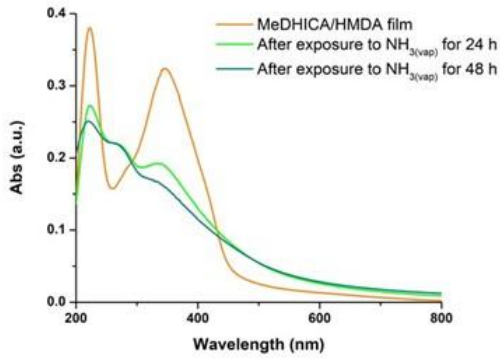

Figure 5.4.6. UV-vis spectra of MeDHICA/HMDA film before and after exposure to ammonia vapours up to 48h.

In preliminary experiments the MeDHICA/HMDA films that adhered to the quartz surface were dissolved in methanol with the aid of an ultrasound treatment and after removal of the solvent the residue was acetylated and analyzed by HPLC. Interestingly the chromatographic profile showed the presence of a main peak due to the MeDHICA monomer and minor peaks attributable to the 4,4'- and 4,7' dimer in comparison with authentic standards (Figure 5.4.7). This result was also confirmed by MS analysis in the MALDI mode. The spectrum exhibited

pseudomolecular peak $[M+K]^+$ at m/z 619 corresponding to a MeDHICA dimer in the acetylated form (Figure S5.6.11).

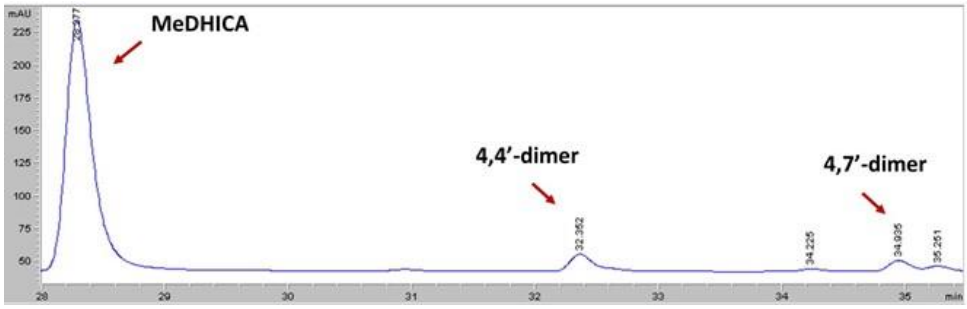

Figure 5.4.7. Elutographic profile of the adhesive material acetylated (Eluent: H_2O/acetonitrile 20-70 %, λ=300 nm).

Notably when the MeDHICA/HMDA substrate was exposed to ammonia vapors over 24h analysis of the methanol washings after acetylation revealed increased consumption of the monomer with concomitant increase of the 4,7'-dimer and higher eluted species likely higher oligomers.

5.4.1. Evaluation of the antioxidant properties of the pigments obtained from oxidation of MeDHICA

In subsequent experiments the antioxidant potential of the yellow-brown pigment obtained from the oxidative polymerization at pH 9.0 of the MeDHICA in the presence of HMDA was evaluated in comparison to that obtained in the absence of the amine. As shown in Figure 5.4.1.1 in the DPPH assay an EC_{50} value of 10.3 ± 0.2 µg/mL was obtained for the MeDHICA/HMDA pigment, lower than that of the MeDHICA pigment of 17.7 ± 0.9 µg/mL and similar to that of the MeDHICA monomer (7.1 ± 0.1 µg/mL).

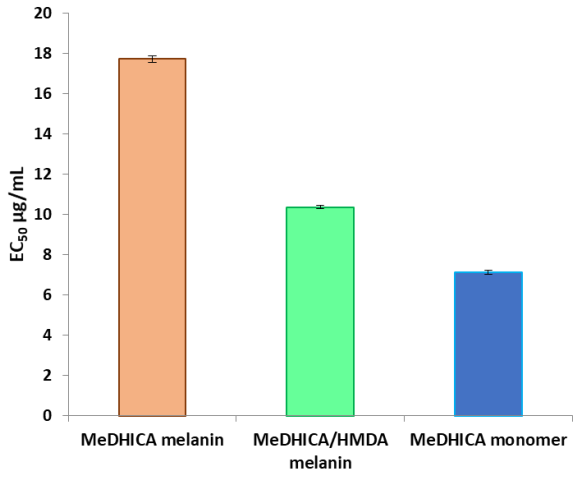

Figure 5.4.1.1. EC_{50} values in the DPPH assay for MeDHICA melanin pigments with and without HMDA and MeDHICA monomer (1 mg/mL). The average values ± SD are reported by at least three separate experiments.

The antioxidant properties of the film obtained by the oxidation of the MeDHICA in the presence of HMDA were then evaluated by dipping the glass substrates in a 50 µM DPPH solution (20 mL). The absorption of the DPPH solution was monitored over time and as shown in Figure 5.4.1.2 the hydrogen donation capacity was well detectable, although it is not possible to evaluate these data on a quantitative basis and establish a comparison with the values obtained for the pigments. After contact with the DPPH solution the colour of the yellow film deepened appreciably (Figure 5.4.1.2).

In order to compare the antioxidant properties of this substrate with reference materials, another film was prepared, as described in Chapter 2, by immersion of a glass substrate in a solution of dopamine and HMDA in equimolar amount (1 mM) in carbonate buffer at pH 9.0 for 24 h and its antioxidant power in the DPPH assay was then evaluated. As shown in Figure 5.4.1.2, the antioxidant power of

the MeDHICA/HMDA film, is comparable or even better than that of the DA/HMDA film based on the DPPH consumption at 30 min.

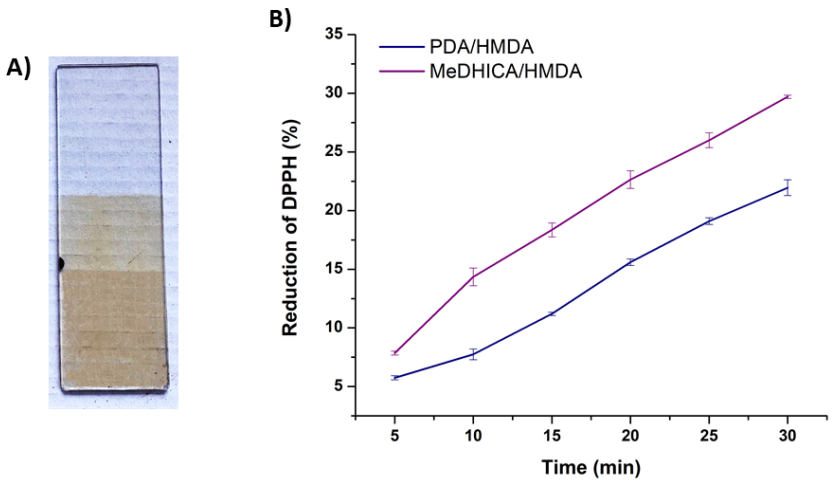

Figure 5.4.1.2. Glass substrates of MeDHICA/HMDA film after immersion in DPPH solution (a) and reduction of DPPH (50 μM) over time by immersion of glass substrates MeDHICA/HMDA and PDA/HMDA (b). The average values ± SD obtained from at least three separate experiments are reported.

In separate experiments the ferric reducing antioxidant power was also evaluated. The results reported in Figure 5.4.1.3 showed a strong reducing capacity in both pigments from MeDHICA and MeDHICA/HMDA.

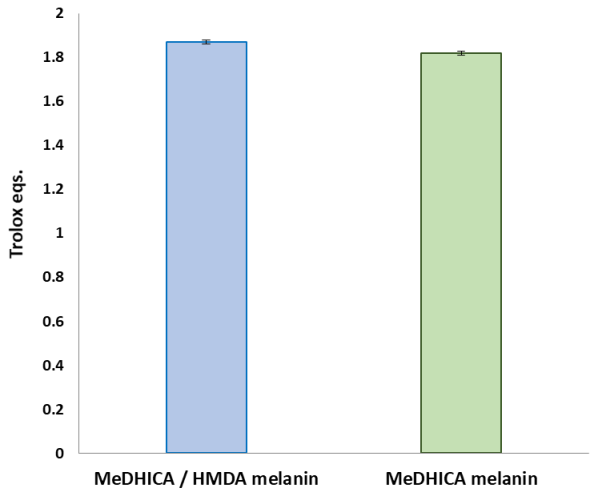

Figure 5.4.1.3. Trolox equivalents determined in the FRAP assay of the melanin pigment obtained from MeDHICA with and without HMDA (1 mg/mL). The average values ± SD obtained from at least three separate experiments are reported.

These results indicated a greater H donation power of the MeDHICA/HMDA pigment with respect to that obtained from the MeDHICA in the absence of the diamine, while such differences are not appreciable in the FRAP assay. This discrepancy is not surprising considering that the antioxidant power measured by the two assays is very different and in particular the FRAP reflects the reduction capacity of Fe^{3+} by electronic donation. It should be noted in any case that the MeDHICA/HMDA pigment has a marked antioxidant activity in both assays.

Also, in this case the antioxidant properties of MeDHICA/HMDA film in the FRAP assay were determined in comparison with the film obtained with PDA/HMDA. To this aim, the same procedure described before for the DPPH assay was applied. As shown in Figure 5.4.1.4, also in this case the film from MeDHICA/HMDA performed comparably or slightly better than the PDA/HMDA film.

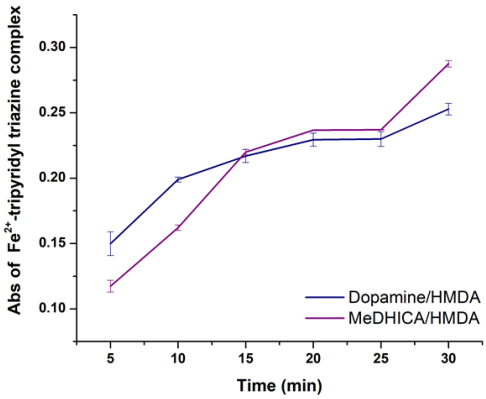

Figure 5.4.1.4. Kinetics of the development of the absorption of Fe^{2+}-tripyridyl triazine complex obtained by immersion of glass substrates MeDHICA/HMDA. The average values ± SD obtained from at least three separate experiments are reported.

5.5 Conclusions

The development of innovative and versatile dip-coating technologies for surface functionalization has been a very active issue over the past decade following the discovery of the extraordinary wet adhesion properties of polydopamine. In this frame it was shown, for the first time, that DHI can form adhesive films under dip-coating conditions in the presence of HMDA or other long chain diamines, a process that is efficiently inhibited by resorcinol. The observation that the inhibitory effect of resorcinol on HMDA-mediated film deposition is much more pronounced in the case of DHI than that of dopamine suggests that DHI-derived quinones are at least as important as dopamine quinone as targets for amine-related crosslinks in film deposition.

Recent studies have provided evidence for the remarkable antioxidant properties of synthetic eumelanins from the other main melanogenic precursor 5,6-

dihydroxyindole-2-carboxylic acid (DHICA) and its methyl ester. On these bases the present chapter was focused at assessing whether HMDA can promote film deposition from other eumelanin precursors besides DHI. Using MeDHICA and HMDA at 1 mM, at 1:1.5 molar ratio, a yellow dark pigment is formed over 24 h exhibiting good film forming properties on different materials. In addition, a significant antioxidant activity, even better than that of MeDHICA melanin was observed for the MeDHICA/HMDA pigment.

5.6 Experimental section

Materials

3,4-dihydroxy-L-phenylalanine (L-DOPA), dopamine hydrocloride, potassium ferricyanide, sodium bicarbonate, sodium dithionite, triethylamine (TEA), dimethylformamide anhydrous (DMF), 1-ethyl 3- (dimethylaminopropyl) carbodiimide (EDC), 1-hydroxybenzotriazole (HOBt), hexamethylenediamine (HMDA), 1,2-ethylenediamine 1,4-butanediamine, 1,12-dodecanediamine, 1,10-decanediamine, butylamine, resorcinol, pyridine, acetic anhydride, 2,2-diphenyl-1-picrylhydrazyl (DPPH), ferric chloride (III) hexahydrate and 2,4,6-tri(2-pyridyl)-s-triazine (TPTZ) were purchased by Sigma-Aldrich.

Methods

UV-vis spectra were run on a V-730 Jasco instrument. Quartz substrates were cleaned by soaking in piranha solution (96% H_2SO_4/30% H_2O_2 5:1 v/v) overnight, rinsed with distilled water and dried under vacuum.

Water contact angle analyses were performed at University of Strasbourg using a contact angle goniometer (digidrop-gbx, France) equipped with video capture. 1 μL of distilled water was dropped on the air side surface of the substrate.

Quartz Crystal Microbalance were performed at University of Strasbourg with a quartz crystal microbalance-dissipation (QCM-D) system from Q-Sense (Göteborg, Sweden). Briefly, in QCM-D the changes in the resonance frequency ($-\Delta f$) of a quartz crystal are measured when material is adsorbed onto it from a solution. The crystal is excited at its fundamental frequency (about 5 MHz), and observations are made at the 3rd, 5th, and 7th overtones ((ν) 3, 5, and 7) at 15, 25, and 35 MHz, respectively. For rigid films, $-\Delta f/\nu$ is independent of the overtone number ν. According to the Sauerbrey relation,[151] $-\Delta f/\nu$ can be related directly to the total mass of the film. Before use the crystal were cleaned with a Plasma Cleaner PDC-32G-2 for 15 min.

^{1}H NMR and ^{13}C NMR spectra were recorded in DMSO-d6 at 400 MHz on a Bruker spectrometer. ^{1}H, ^{1}H COSY, ^{1}H, ^{13}C HSQC, and ^{1}H, ^{13}C HMBC were run at 400 MHz using Bruker standard pulse programs. Chemical shifts are given in ppm.

HPLC analyses were performed on a Agilent 1100 binary pump instrument equipped with and a SPD-10AV VP UV-visible detector using an octadecylsilane-coated column, 250 mm x 4.6 mm, 5 μm particle size (Phenomenex Sphereclone ODS) at 0.7 mL/min. Detection wavelength was set at 300 nm. Eluent system: a) formic acid 0.1% - methanol 50:50 v / v; b) water - methanol 40:60 v / v; c) gradient of water - methanol from T 5 to 45 min from 40 to 70% of methanol; d) gradient of water – acetonitrile from T 5 to 45 min from 40 to 70% of acetonitrile.

Preparative HPLC was carried out on an instrument coupled with a UV detector set at 300 nm using an Econosil C_{18} (10 μm, 22 x 250 mm).

LC-MS analyses were performed on an AGILENT ESI-TOF 1260/6230DA Agilent Technologies in positive ion mode in the following conditions: nebulizer

pressure 35 psig; drying gas (nitrogen) 5 L/min, 325 °C; capillary voltage 3500 V; fragmentor voltage 175 V. A Eclipse Plus C18 column, 150 × 4.6 mm, 5 µm, at a flow rate of 0.4 mL/min was used, with the same mobile phases as above.

TLC were performed on silica gel plates F254 (0.25 mm) using: chloroform / methanol 8:2 and 7:3; chloroform / methanol / acetic acid 8:2:1; butanol / acetic acid / water 6:2:2.

Solid state nuclear magnetic resonance (NMR) spectra were recorded on a Bruker Avance II 400 spectrometer (Bruker Corporation, Billerica, MA, USA) operating at a static field to 9.4T, equipped with a Bruker 4 mm magic angle spinning (MAS) probe. Samples were packed into Bruker 4 mm zirconia rotors sealed with Bruker Kel-F caps. The spinning speed was set at 10 and 6 kHz for ^{13}C and ^{15}N NMR experiments, respectively. ^{13}C and ^{15}N NMR analysis.

The combined AFM and microRaman analysis were conducted with the integrated apparatus Alpha300 RS (WITec, Germany). The system can be switched between AFM and confocal micro-Raman configurations, allowing a combined topographical and spectral characterization of a specified microregion of the sample. The samples topographies were studied by AFM in AC mode. For the micro-Raman analysis, a laser beam at $\lambda = 488$ nm was used as excitation light source.

Positive Reflectron MALDI spectra were recorded on a AB Sciex TOF/TOF 5800 instrument using 2,5-dihydroxybenzoic acid as the matrix. Spectra represents the sum of 15,000 laser pulses from randomly chosen spots per sample position. Raw data are analyzed using the computer software provided by the manufacturers and are reported as monoisotopic masses.

Preparation of DHI, DHICA and DAICA. 1 L of bi-distilled water was degassed under argon flow. After 30 min 2 g of L-DOPA (final concentration 0.01 M), 13.4 g of potassium ferricyanide (4 molar equivalents) and 5 g of $NaHCO_3$, dissolved in 50 mL of distilled water, were added. In the case of DHICA, after 2 minutes 50 mL of 3 M NaOH were added. The mixture was kept under vigorous stirring and under argon flow for about 90 minutes, until the red color due to the dopacrome disappeared. The mixture was then treated with sodium dithionite, acidified to pH 4 with 4 M HCl and extracted three times with ethyl acetate. The combined organic phases were dried with sodium sulfate and dried under vacuum to give a powder (64-70 % yields). The DHICA (700 mg) was then acetylated with acetic anhydride (7 mL) and pyridine (350 µL) for 24 h, followed by hydrolysis with a mixture of water methanol 1:1 at 90 ° C for 2 h. After dried a powder light in color was obtained (DAICA, yield 98%) (Scheme 5.6.1).

UV-vis DHI: λ_{max} in MeOH 280 nm (ε = 6110 $M^{-1}cm^{-1}$ MeOH).

UV-vis DHICA: λ_{max} in MeOH 320 nm (ε = 17700 $M^{-1}cm^{-1}$ MeOH / HCl 1M).

UV-vis DAICA: λ_{max} in MeOH 296 nm (ε= 27829 $M^{-1}cm^{-1}$ MeOH).

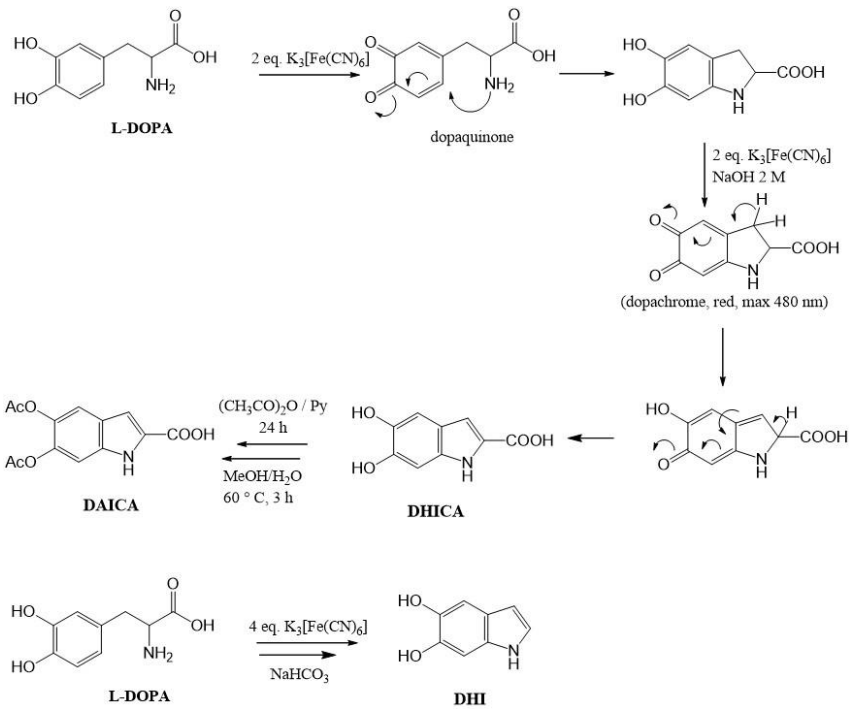

Scheme 5.6.1. Mechanism of the one step synthesis of DHI, DHICA and DAICA.

Preparation of DHICA methyl ester (MeDHICA). DHICA methyl ester was obtained from DOPA methylester prepared by reacting DOPA (2.0 g) in methanol (20 mL) with 96% sulfuric acid (2 mL) under reflux. After 24 h, the mixture was allowed to cool, and sodium bicarbonate was added to neutrality. The solution thus obtained was reacted in water with potassium ferricyanide under the same conditions used for preparation of DHICA, but notably without addition of the NaOH solution, and after 30 min extracted with ethyl acetate to give pure MeDHICA (1.3 g, 65% yield) as a dark yellow-brown solid (Scheme 5.6.2).

UV-vis: λ_{max} (MeOH) 320 nm (ε = 16243 $M^{-1}cm^{-1}$).

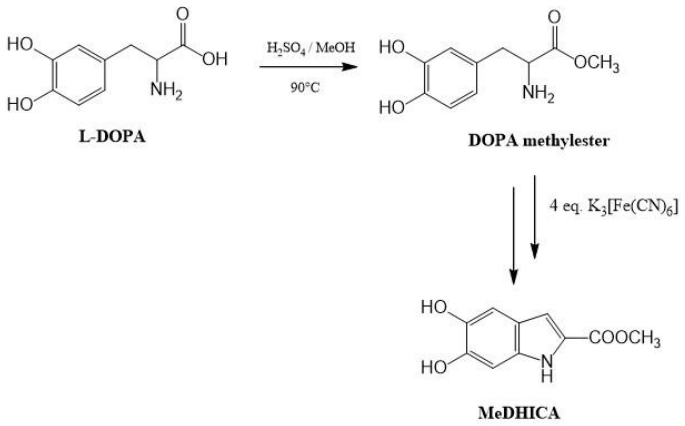

Scheme 5.6.2. Procedure of the synthesis of MeDHICA.

Oxidative polymerization of indole compounds (DHI, DHICA and MeDHICA) in the presence of amines. To a 1 mM solution of the appropriate monoamine (butylamine) or diamine (ethylenediamine, hexamethylenediamine, 1,4-butanediamine, 1,10-diaminodecane and 1,12-dodecanediamine) in 0.05 M carbonate buffer pH = 9.0, DHI and DHICA, in a 1:1 molar ratio, or MeDHICA, in a 1:5 molar ratio, were added under vigorous stirring. Quartz substrates were dipped into the reaction mixture and left under stirring for 24 h, then rinsed with distilled water, sonicated, dried and analysed by UV-vis spectrophotometry. The reaction mixture was acidified to pH 3.0 with 3 M HCl and the pigment was collected by centrifugation at 7000 rpm at 4 °C and lyophilized. In control experiments the reaction was conducted in the absence of diamine.

In another set of experiments, to 1 mM dopamine (50 mg, 0.26 mmol) or DHI solution (50 mg, 0.34 mmol) containing 1 mM HMDA (30mg) in 0.05 M carbonate buffer pH = 9.0, resorcinol (1 or 5 mM), as an inhibitor agent, was added

and the mixture was left under stirring for 24 h. Control reactions with 10 mM dopamine were run in the presence and in absence of resorcinol.

Coupling DHICA with HMDA. A mixture of DHICA (130 mg), EDC (196 mg), HOBt (139 mg) and TEA (143 µL) in anhydrous DMF (2.4 mL) was stirred under an atmosphere of argon for 10 min. HMDA (0.5 equivalents, 69 mg) was added and the mixture was stirred for 18 h at 25°C. After removing the DMF by using a rotary evaporator, the mixture was treated with equal volumes of distilled water. The precipitate obtained was collected by centrifugation (7000 rpm, 4 ° C, 15 min) and washed. The solid obtained was then acetylated with acetic anhydride (500 µL) and pyridine (25 µL) for 24 h at room temperature and purified by preparative HPLC. The fractions containing the desired product were combined and dried to give a yellow solid (6% yield).

Starting from the O-acetylated derivative of DHICA the reaction was initially performed under the same conditions described above. After 18 h the mixture was treated with equal volumes of distilled water and the solid was collected by centrifugation (7000 rpm, 4 ° C, 15 min) and washed (50% yield).

UV-vis: λ_{max} (MeOH / DMSO) 300 nm. ESI $^{+}$ / MS: m / z 418 $[M+H]^{+}$, 635 $[M+H]^{+}$. MALDI-ToF: m/z 456 $[M+K]^{+}$, 673 $[M+K]^{+}$. ^{1}H-NMR δ: 1.38 (4H, m), 1.55 (4H, m), 2.27 (12H, s), 3.34 (4H, m), 7.12 (2H, s), 7.24 (2H, s), 7.45 (2H, s), 8.54 (2H, t) 11.74 (2H, s). ^{13}C-NMR δ: 20.79, 39.92, 26.68, 29.61, 102.83, 106.72, 115.10, 124.92, 133.97, 136.87, 139.47, 161.02, 169.20, 169.41.

27 mL of a 3.6 mM solution of the DHICA/diamide in methanol were treated under an argon atmosphere with sodium tert-butoxide (8 molar equivalents) and after 15 min the pH of the solution was taken to 3 by addition of 6 M HCl and controlled by HPLC. The resulting mixture was added to 70 mL of 50 mM

carbonate buffer (pH 9.0) to reach a final concentration of 1 mM and left under stirring for 24 h. The reaction mixture was then acidified to pH=3 with 3 M HCl, centrifuged at 7000 rpm at 4 °C, and the precipitate washed three times with water and lyophilized to collect the dark pigment (68 % w/w yield).

Antioxidant activity:

2,2-diphenyl-1-picrylhydrazyl (DPPH) assay. The assay was performed as described.[152] Briefly, to a 200 μM DPPH solution in methanol, a proper amount of a methanol suspension of each melanin (1 mg/mL) homogenized with a glass/glass potter was added and rapidly mixed. The reaction was followed by spectrophotometric analysis measuring the absorbance at 515 nm after 10 min. Values are expressed as the EC_{50}, that is, the dose of the material at which a 50% DPPH reduction is observed. The glass substrates were instead immersed in a solution of DPPH 50 μM (20 mL) for 30 minutes and the antioxidant power was evaluated by UV-vis recording spectra every 5 minutes.

Ferric reducing/antioxidant power (FRAP) assay. The assay was performed as described.[153] The FRAP reagent was prepared by mixing 0.3 M acetate buffer (pH 3.6), 10 mM 2,4,6-tris(2-pyridyl)-s-triazine in 40 mM HCl, and 20 mM ferric chloride in water, in the ratio 10:1:1, in that order. To a solution of FRAP reagent, a proper amount of a DMSO solution of each melanin was added and rapidly mixed. After 10 minutes, the absorbance at 593 nm was measured. Trolox was used as the standard and results were expressed as Trolox equivalents. The glass substrates were instead immersed for 30 minutes in 20 mL of a solution containing $FeCl_3$ (20 mM) and 2,4,6-tris (2-pyridyl)-s-triazine (10 mM) in 0.3 M acetate buffer (pH 3.6) in the ratio 10:1:1.

Supporting materials

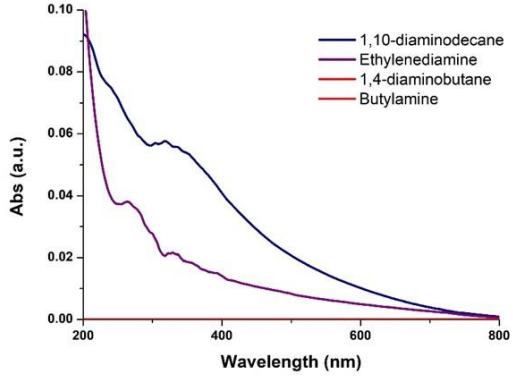

Figure S5.6.1. UV-vis spectra of the quartz substrates after 24 h dipping in the DHICA/diamines mixture.

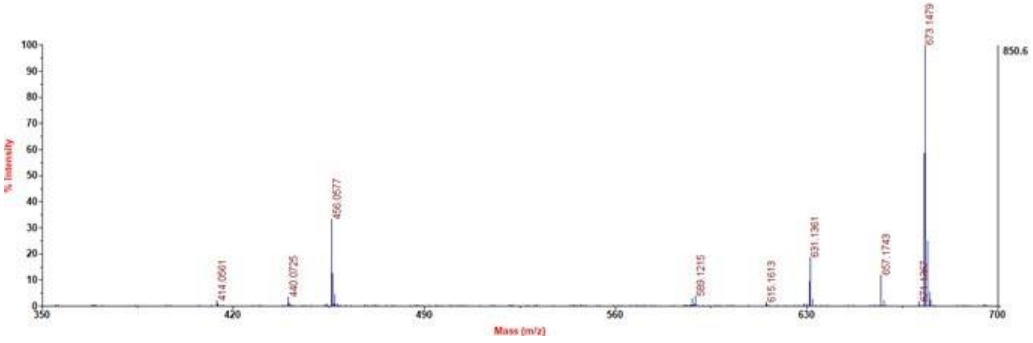

Figure S5.6.2. Mass Spectrum MALDI of the acetylated mixture.

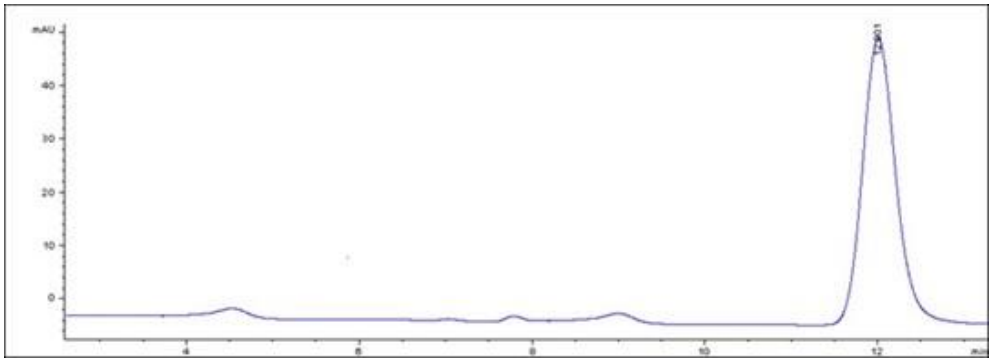

Figure S5.6.3. Elutographic profile of the solid separated after work up of the reaction mixture dissolved in DMSO (λ =300 nm).

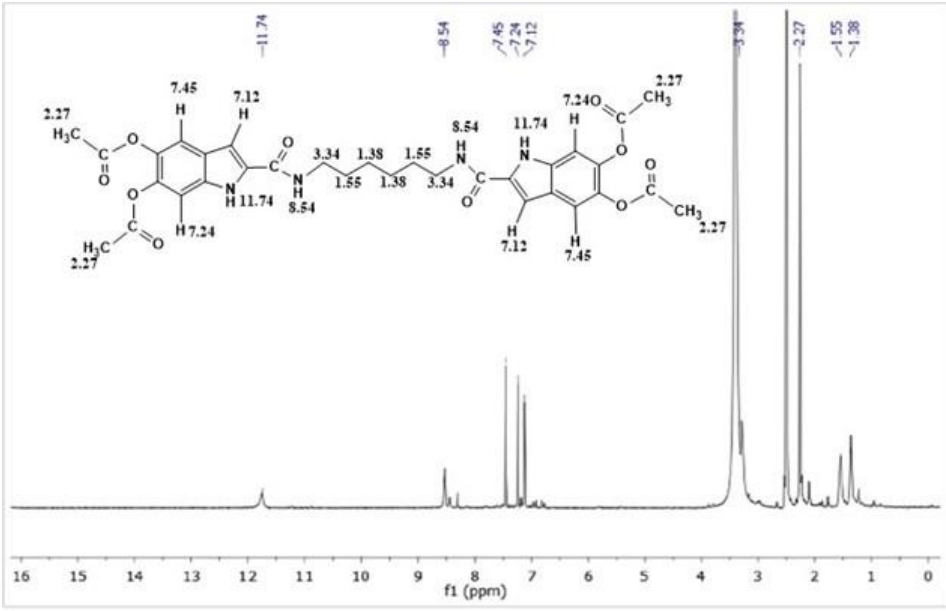

Figure S5.6.4. ^{1}H NMR spectrum of DHICA/diamide product in DMSO-d6.

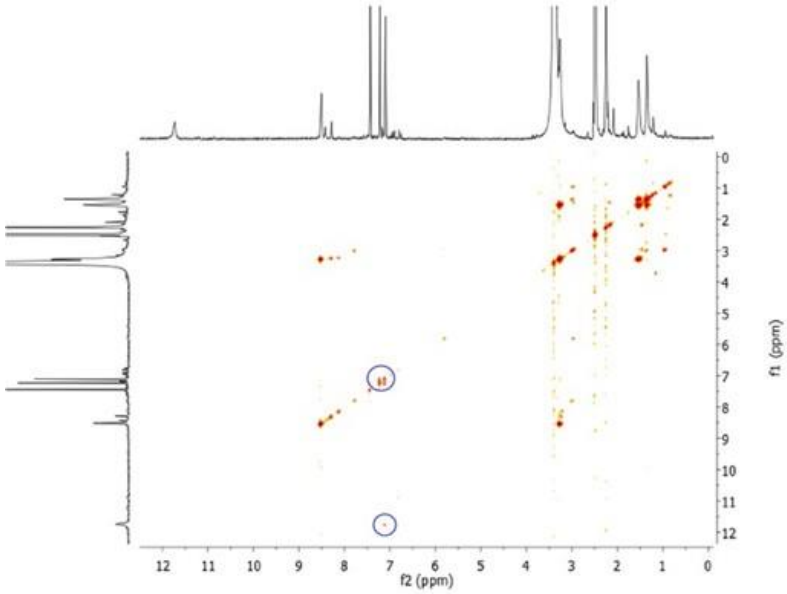

Figure S5.6.5. $^{1}H,^{1}H$-COSY spectrum of DHICA/diamide product in DMSO-d_6.

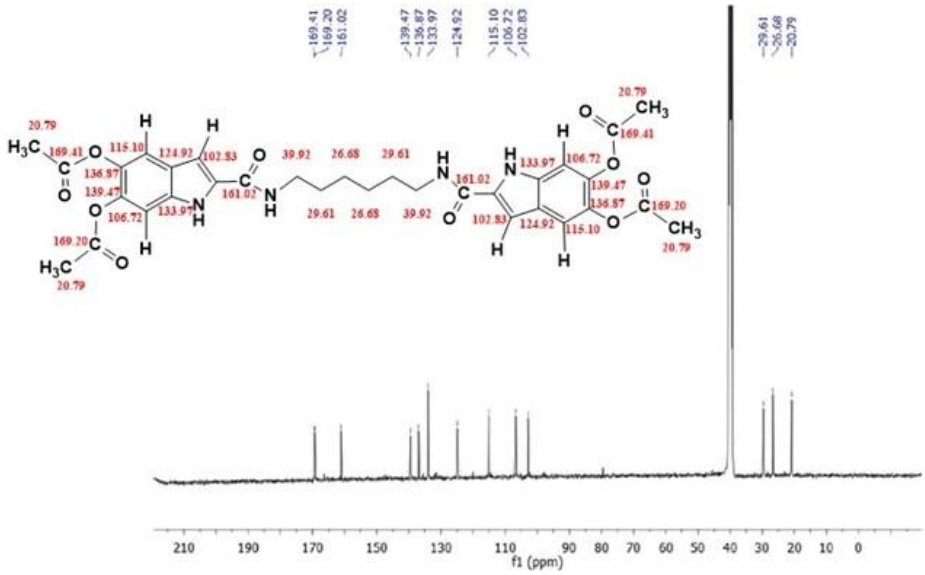

Figure S5.6.6. ^{13}C NMR spectrum of DHICA/diamide product in DMSO-d_6.

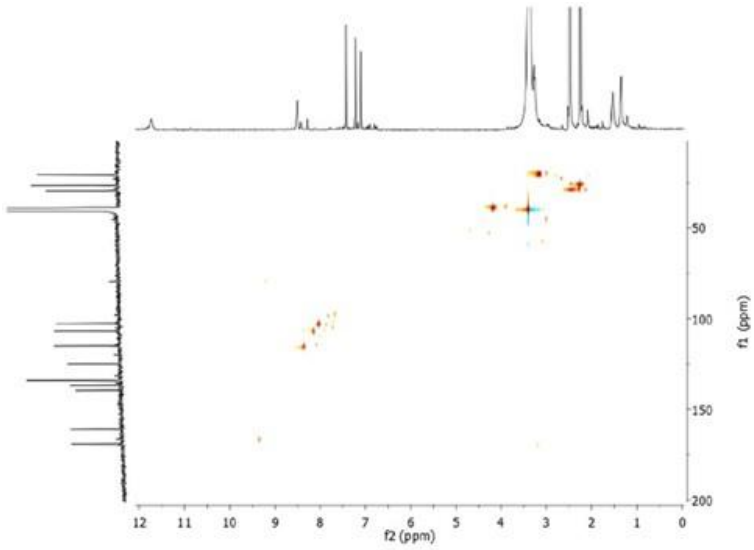

Figure S5.6.7. $^{1}H,^{13}C$-HSQC spectrum of DHICA/diamide product in DMSO-d6.

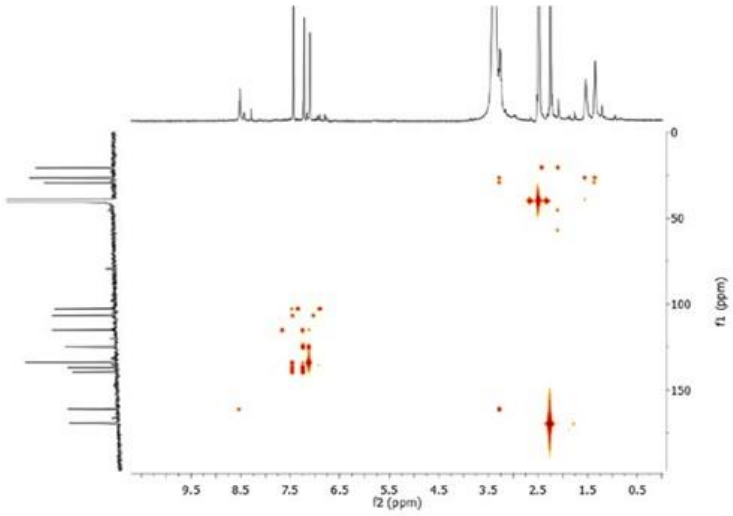

Figure S5.6.8. $^{1}H,^{13}C$-HMBC spectrum of DHICA/diamide product in DMSO-d6.

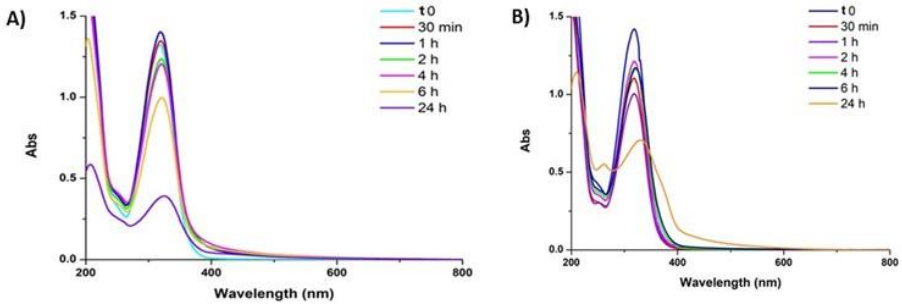

Figure S5.6.9. Spectrophotometric development over 24 h of the aerobic oxidation mixture of MeDHICA 1 mM in 50 mM carbonate buffer (pH = 9.0) in the presence (a) or in the absence (b) of equimolar HMDA.

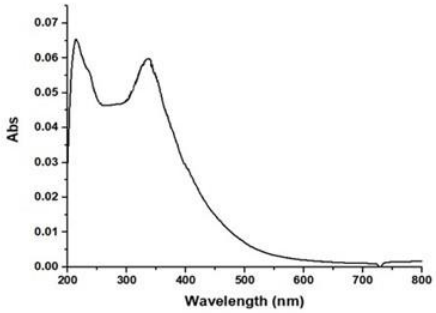

Figure S5.6.10. UV-vis spectrum of the quartz substrate after 24 h of immersion in the MeDHICA/1,4-diaminobutane mixture at pH = 9.0.

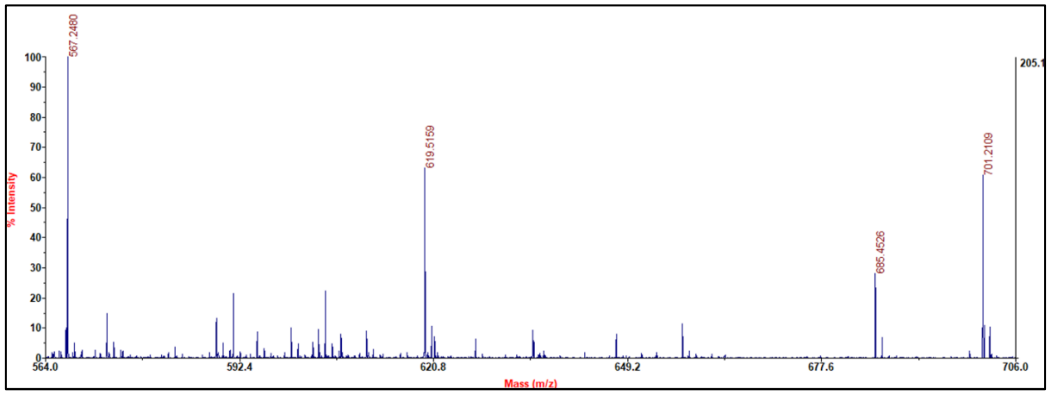

Figure S5.6.11. Mass Spectrum MALDI of the acetylated adhesive material.

Chapter 6

Model eumelanin pigments: synthesis and properties

6.1 Introduction

The structural and supramolecular arrangements of the characteristic broadband absorption spectrum of eumelanins (Figure 6.1.1) accounting for their black or dark colorations have extensively been investigated[30,67,167–169] because of their close relationship to key features of these polymers including the already mentioned photoprotective and antioxidant properties, the UV energy dissipation mechanism, the water dependent ionic-electronic conductivity and the stable paramagnetic state resulting in a signal in the EPR spectroscopy.[45,49,55,154,155,170-172.]

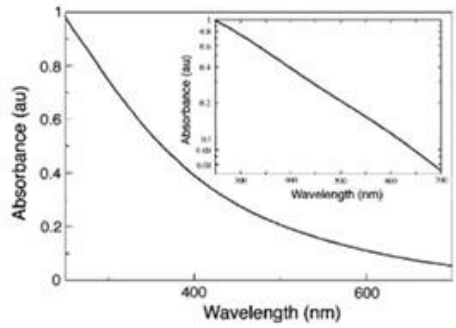

Figure 6.1.1. Broadband UV-visible absorption spectrum of eumelanin (synthetic material derived from the non-enzymatic oxidation of D,L-DOPA).[49]

As already described in Chapter 5, eumelanins are produced within melanosomes by tyrosinase-catalyzed oxidation of tyrosine via oxidative polymerization of 5,6-dihydroxyindole (DHI) and 5,6-dihydroxyindole-2-carboxylic acid (DHICA).

The polymerization processes lead to the generation of extremely complex mixtures of oligomeric species at various levels of oxidation and degrees of polymerization, linked through diverse bonding patterns,[35] accounting for various levels of disorder (Figure 6.1.2).

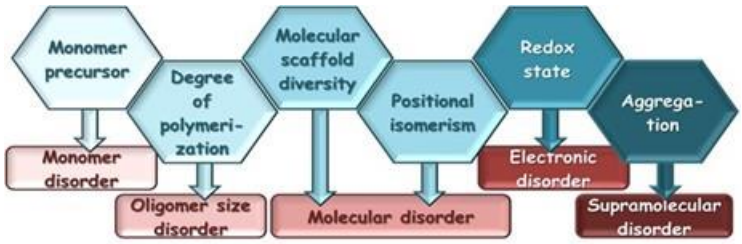

Figure 6.1.2. Main levels of disorder in synthetic eumelanins.

In particular, the first level is the chemical disorder[173] related to the different coupling mode of DHI and DHICA leading to a variety of oligomeric species that can develop complex ensembles of chromophores spanning the entire UV-visible range. The second level of disorder relates to the variety of structures that can arise from a single monomer, due, for example, to molecular weight dispersion with polymerization (oligomers size disorder), molecular scaffold diversity due to positional isomerism, and conformational disorder reflecting atropisomerism, *e.g.*, in DHICA oligomers (molecular disorder). The third level of disorder, electronic disorder, instead, derives from the coexistence of oxidized and reduced moieties that is essential for the broadband visible-light absorption spectrum, as suggested by data from glycated water soluble eumelanin.[53] According with this study, black color would depend not only on the overlap of π-electron conjugated chromophores[174,175] but even on oxidation state- and aggregation-dependent interchromophoric interactions. In this connection, computational studies suggested that the monotonic spectrum of eumelanin is due to delocalization of

excitons over stacked DHI melanin.[174] The current view is that the optical eumelanin properties can be mimicked just by including catechol, semiquinone and quinone building blocks.[176] Finally, the supramolecular disorder, fourth level of disorder, relates to the different modes of aggregation of oligomers as dictated by scaffold-dependent, redox state-controlled conformations and has a major impact on morphology and scattering properties. The recent discovery that poly(vinyl alcohol) (PVA) can prevent precipitation of growing eumelanin polymers, allow to disentangle absorption properties due to chromophore from scattering effects, pointing out that beside the intrinsic chromophore component there is an extrinsic contribute that depend on intermolecular perturbation[177] of π-electron systems.

The mechanism of the oxidative conversion of melanogenic indoles to eumelanins have been the subject of intensive research work and several oligomer intermediates in the oxidation have been isolated and characterized. In particular, oxidation of DHI proceeds rapidly, leading to a series of dimers and trimers, in which the indole units are linked through 2,4'- and 2,7'-bondings.[178-179] Other types of interring bonds, *e.g.* 2,3'-, 4,4'-, and 7,7'- bonds, were found on tetramers generated by oxidative coupling of dimers and thus depending on the starting dimer (Scheme 6.1.1).[48,180-182] For this reason the structural diversity that is generated during eumelanin biosynthesis is high and this would account for the marked heterogeneity of the pigment. On the other hand, DHICA polymerization is conditioned by the presence of the carboxylic acid group at the 2-position, which decreases nucleophilicity on the pyrrole moiety through its electron-withdrawing nature, thereby directing reactivity mainly towards the 4,4'-, 4,7'- and 7,7'-bonding formation, with lower involvement of the 3-position (Scheme 6.1.1).[179,180]

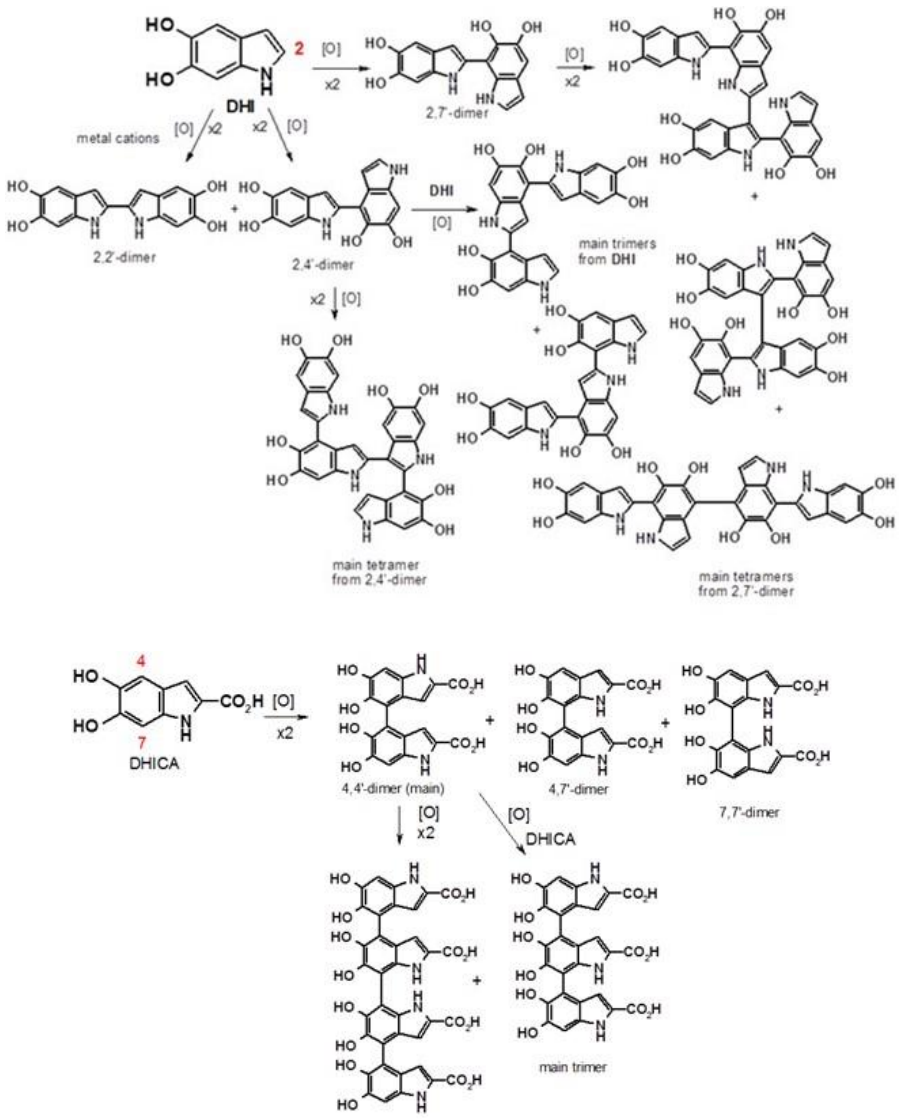

Scheme 6.1.1. Structures of the oligomers isolated by oxidation of DHI (top) or DHICA (bottom).

While DHI oligomers can adopt planar conformations, DHICA polymerizes mainly through biphenyl-type bonds, resulting in the generation of non-planar, partly linear backbones exhibiting hindered rotation (atropisomerism) at the interunit bonds.[48,168] Deviation from coplanarity in DHICA oligomers is supported by the negative charge of the carboxylate groups forcing twisting about the inter-ring bond. The so-formed twisted backbones cannot give rise to π-stacked supramolecular aggregates, at variance with the largely planar oligomeric scaffolds derived from DHI. Therefore, while DHI dimers generate on oxidation largely planar species absorbing strongly in the visible range, DHICA oligomers do not produce significant visible absorption above 400 nm, due to inter-unit dihedral angles of ca. 49° with localized *o*-quinone moieties and significant interruption of inter-unit π-electron delocalization (Figure 6.1.3).[183,184]

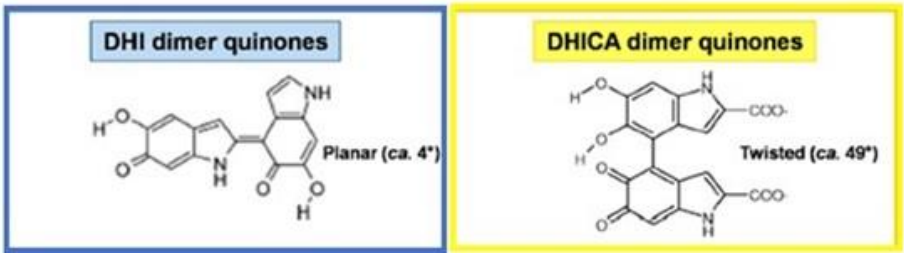

Figure 6.1.3. Predicted structures of DHI and DHICA dimers quinones.

As shown in the spectra of Figure 6.1.4 DHI melanin gives a nearly monotonic profile[185], while the DHICA polymer displays an intense absorption band in the UV region around 320 nm.[45] This latter feature is suggestive of the presence of reduced monomer-like chromophoric components co-existing with quinonoid units and persisting during the polymerization process as a consequence of the hindered inter-unit π-electron delocalization within oligomer/polymer scaffolds. Consistent with this view, treatment of DHICA melanin with a reducing agent

such as $NaBH_4$ did not affect the 320-nm band, but induced a decrease of the absorption in the visible region suggesting the contribution in the latter of reducible quinonoid chromophores.[45,53]

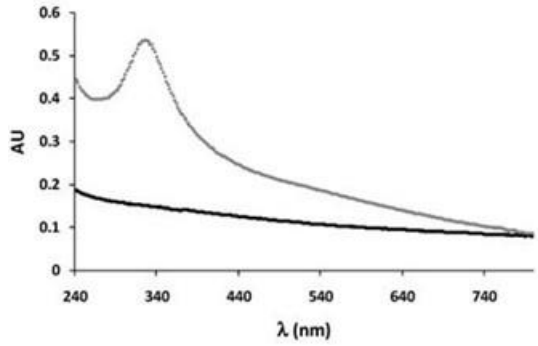

Figure 6.1.4. UV-visible spectra of DHI (black trace) and DHICA melanin (gray trace) at pH 7.5.

Visual inspection of the reaction mixtures from DHICA again revealed the important role of aggregation in color development corresponding to the broadening of the visible absorption maximum. The most noticeable difference of the oxidation of DHICA with respect to DHI oxidation was the lighter coloration of the final melanin (Figure 6.1.5).[186]

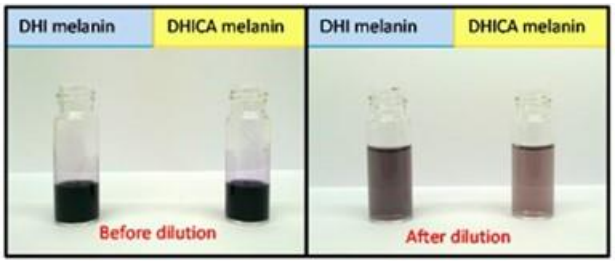

Figure 6.1.5. Melanins from DHI (blue box) and DHICA (yellow box) oxidation before and after diluition.

Consequently, it has been suggested that while the DHI-melanin chromophore is determined for the most part by intrinsic effects relating to efficient π-electron delocalization within the largely planar oligomeric scaffolds, the black chromophore of DHICA melanin derives largely from aggregation-dependent intermolecular perturbations of the π-electron systems, being therefore mainly extrinsic in character.[45,184] These intrinsic and extrinsic contributes (Figure 6.1.6), together with the interaction of geometric order and disorder, would cooperate to generate the absorption spectrum of eumelanin.[56,174,185]

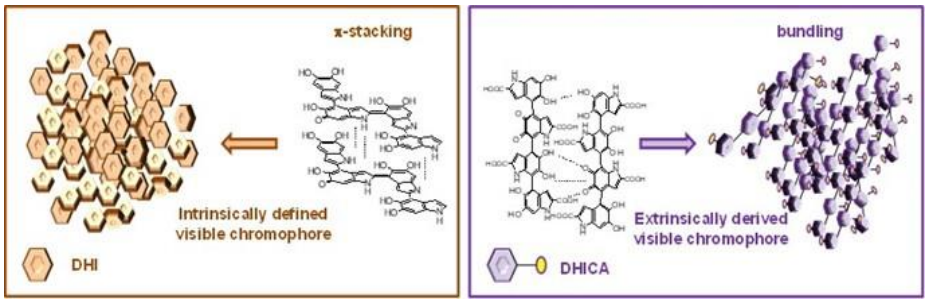

Figure 6.1.6 Intrinsic and extrinsic contributions to eumelanin absorption properties.

All these structural pictures of DHI and DHICA melanins provides a useful interpretative basis also for the different reactivity observed for DHI and DHICA melanins. DHICA-melanin dose-dependently acts as a potent OH radical scavenger in the Fenton reaction, whereas, in the same range of concentrations, DHI-melanin is rather a pro-oxidant capable of generating reactive oxygen species.[187] In addition, DHICA melanin is much more effective as H-donor and NO scavenger with respect to both DHI and DOPA melanin.[45] This difference was ascribed to the de-stabilizing effects of non-planar structures on electron delocalization and aggregation, imparting monomer-like behavior to the polymer.

Formation of weak aggregates would then account for a greater accessibility of free radicals compared to the case of compact π-stacked DHI melanin.

Though this picture allows to satisfactorily interpret the properties of model eumelanin from DHI or DHICA, some issues however remain to be set in particular, whether the properties of the pigment are associated to a specific mode of coupling of the indole units. To address this issue the properties of model pigments at high regioregularity, *e.g.* arising from polymerization of oligomeric species, may be investigated comparatively.

In a recent study,[163] a model eumelanin prepared from the methylester of DHICA (MeDHICA) proved fairly soluble in different water miscible organic solvents and showed an intense and broad chromophore centred at 330 nm with almost no absorption in the visible region differently from DHICA melanin. The pigment exhibited a marked antioxidant potency higher than that of DHICA melanin that persisted also after photoirradiation (Figure 5.1.3). The molecular basis of such differences has not yet been elucidated, but it is clear that the design of model eumelanins with well defined structural features that may exhibit improved properties is an issue of great interest.

On these bases the present chapter was directed to describe the preparation of different model eumelanins in order to have a higher degree of regioregularity and to comparative evaluate their chromophoric and antioxidant properties.

Specific aims of the research work described in this chapter included:

1. the optimization of the synthesis of oligomers from DHICA and MeDHICA *i.e.* the 4,4’ biindolyl and 4,7’ biindolyl dimers;
2. the isolation and characterization of the dimers obtained;

3. the preparation of melanin from these dimers and comparison of the chromophoric and antioxidant properties with relevant melanins.

6.2 Preparation of dimers from DHICA

Previous studies on the oxidative polymerisation of 5,6-dihydroxyindole-2-carboxylic acid (DHICA) had delineated, as illustrated in the paragraph above, a reaction pathway involving mainly repeated coupling of the indole units through the 4 and 7- positions. With the view to investigate the pigment properties associated to specific mode of coupling of the indole units, a re-examination of the DHICA oxidation was considered.

Preliminary, different reaction conditions were investigated and, the course of the reaction was followed by HPLC analysis in order to identify the best conditions to get a substantial consumption of the starting indole associated to formation of the dimers. Carrying out the biomimetic oxidation of DHICA (1 mM) with the enzymatic system peroxidase/H_2O_2 in phosphate buffer at pH 7.4 after one minute a complete conversion of DHICA to melanins without appreciable accumulation of the intermediate dimers was observed, in spite of the very short reaction time. In other experiments when ferricyanide was used as the oxidizing agent, at a 1:1 molar ratio with respect to DHICA, a substantial consumption of the monomer, but a modest accumulation of other components was observed only at lower reaction time (< 3 min) (Figure S6.7.1, panel A). Therefore, a DHICA to oxidant 1:0.5 molar ratio was used, and the reaction time was limited to 10 s. Yet, even under these conditions, a sustained consumption of the monomer was always apparent, but formation of intermediate products was always very low (Figure S6.7.1, panel B).

Aerobic oxidation was then explored using a solution of DHICA at 1 mM in phosphate buffer at pH 7.0 under stirring. The consumption of the starting indole, eluting at t_R = 20.9 min, was slower in this case and still not complete after 6 h (Figure 6.2.1). Formation of other compounds likely the dimers was apparent in the first hours, yet after 3 h also these compounds were consumed without accumulating significantly.

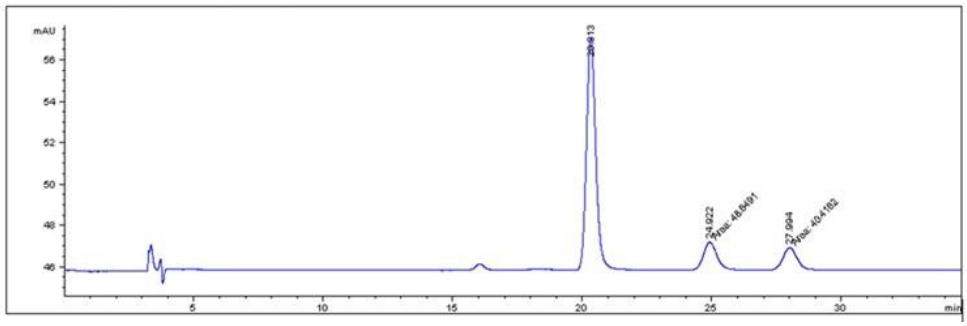

Figure 6.2.1. HPLC profile of the aerobic oxidation mixture of DHICA at 6 h reaction time.

The reaction was carried out in air under vigorous stirring in the presence of copper acetate at 1:1 molar ratio with respect to DHICA using HEPES buffer at pH 7.5 to warrant solubilization of copper ions. Periodical monitoring of the reaction course evidenced a progressive consumption of the starting indole. At 1 min reaction time consumption of the starting compound was too low but at 5 min formation of the dimers was appreciable, with prevalent formation of a species at t_R= 24 min that was subsequently identified as the 4,4' dimer (Figure 6.2.2).

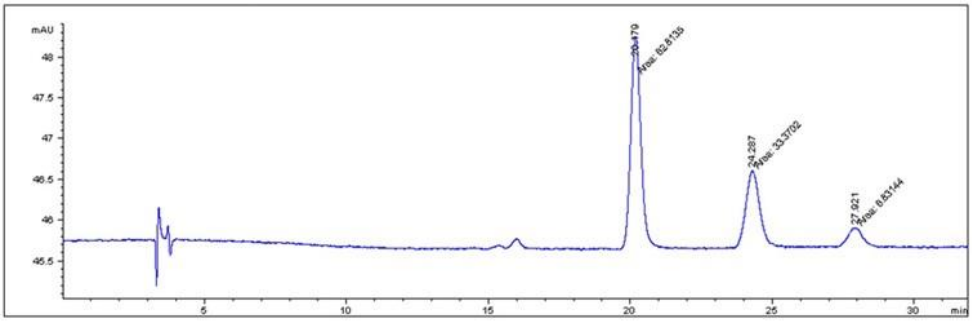

Figure 6.2.2. HPLC profile of the oxidation mixture of DHICA in the presence of 1 eq. copper acetate at 5 min reaction time. Eluent: 1% formic acid-MeOH 90:10 v/v.

In other experiments a solution of DHICA (8 mM) in 0.5 M Tris buffer at pH 7.5 was saturated with oxygen and then treated with copper sulphate under vigorous stirring. After one minute the formation of the 4,4'-dimer was appreciable and almost comparable to the DHICA consumption (Figure 6.2.3).

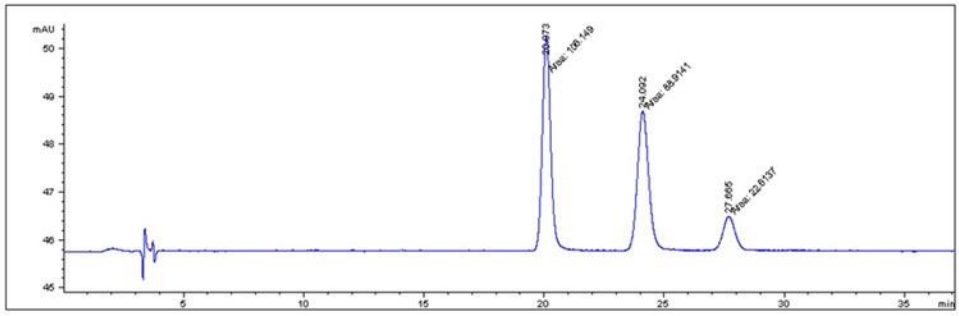

Figure 6.2.3. HPLC profile of the oxidation mixture of DHICA in the presence of copper sulfate at 1 min reaction time. Eluent: 1.5 % formic acid, MeOH 90:10 v/v.

After several experiments metal catalyzed aerial oxidation proved the best condition in terms of DHICA consumption and formation of dimers and, the reaction was carried out in either cases using copper sulfate in 0.5 M Tris buffer pH 7.5. After one minute the reaction was halted by addition of sodium dithionite

followed by acidification to pH 4.0, repeated extracted with ethyl acetate and then the organic layers were taken to dryness. Given the higher stability of DHICA and its oligomers acetylation was not needed and the compounds were analysed in the free OH form, however the elutographic conditions proved critical in this case. Only in the presence of aqueous formic acid at relatively high concentrations (>1.5 %) with methanol narrow symmetrical peaks could be obtained. In addition to DHICA eluting at 20 min, the two components at t_R 24 and 27 min were identified as DHICA dimers based on parallel analysis by LC-MS. Comparison of the eluition with that of authentic standards available allowed to identify the compound at t_R 24 min as the 4,4'-dimer and the less abundant compound at 27 min as the 4,7'-dimer (Figure 6.2.3). Preparative HPLC was selected for oligomer purification as it proved a rapid and straightforward method to get tens to hundreds milligrams amount from similar mixtures. The development of suitable conditions for preparative HPLC fractionation is a necessary step to purify the oxidation mixture. The organic extracts were loaded on preparative HPLC (around 12 mg at each run) and the fractions collected after removal of methanol were extracted with ethyl acetate, the solvent removed and the resulting residue taken under reduced pressure to removal residual formic acid. The identity of the component eluted at 30 min as the 4,4'-dimer was confirmed by ^{1}H NMR analysis.[47] The fractions containing the component eluting at 35 min likely the 4,7'-dimer revealed the presence of a substantial amount of the compound eluting at 30 min (4,4'-dimer) so these fractions were then further purified using a different eluant: formic acid 1% and acetonitrile (90:10 v/v) (Figure S6.7.2). After work up as above the identity of this compound as the 4,7' dimer was confirmed by ^{1}H NMR analysis.[47]

Overall some 1 g of DHICA was subjected to the oxidation under the optimized conditions. Yet, after the fractionation procedure described above the amount of 4,4'-dimer obtained was around 100 mg whereas for the 4,7'-dimer much lower amounts were obtained (around 20 mg). Though this result is not encouraging a scale up of the fractionation procedure may be conceived. An advantage of the procedure so far developed is certainly the possibility to isolate the dimers without protection steps that is in the free form that may be directly subjected to further oxidation for preparation of melanins as described in the subsequent paragraphs.

6.3 Preparation of dimers from MeDHICA

With the aim of isolating substantial amounts of the dimers formed in the early stage of the oxidation of MeDHICA, in further experiments a systematic investigation of different reaction conditions was performed along the directions already explored in the case of DHICA dimers. Following are the most interesting reaction conditions investigated.

Reaction conditions 1. The oxidation in air of MeDHICA dissolved in the minimal amount of methanol was performed using 0.1 M phosphate buffer (pH 8.5) as the medium. HPLC monitoring indicated a relatively slow monomer consumption (peak eluting at around 8 min) whereas dimers formation was well appreciable after 7 h (Figure 6.3.1).

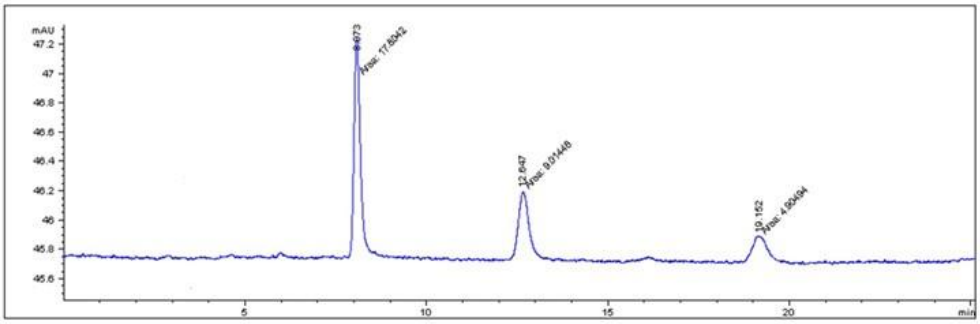

Figure 6.3.1. HPLC profile of the oxidation mixture in air of MeDHICA at 7 h reaction time. Eluent: 1 % formic acid - MeOH 60:40 v/v.

Reaction conditions 2. Aerobic oxidation was repeated in the presence of 1 molar equivalent of cobalt sulphate or copper acetate with the indole at 16 mM in 0.2 M HEPES buffer (pH 7.5). After 3 minutes it appears that while the monomer is decreasing the dimers do not increase significantly (Figure S6.7.3, S6.7.4).

Reaction conditions 3. The oxidation of MeDHICA was carried out in air under the same conditions described above for the DHICA but using an indole concentration of 16 mM. Here again the reaction course was followed in the very early stages as the consumption of the substrate is relatively fast and the dimers accumulate rapidly over the first minutes of the reaction.

Based on these results the best conditions for dimer preparation from MeDHICA appeared aerobic oxidation in the presence of metal salts. The higher accumulation of dimers was observed with copper sulfate. Also, a reaction time of 1 min was chosen to warrant a sufficient consumption of the monomer and accumulation of the dimers. On this basis the reaction was carried out under the selected conditions and halted at 1 min by addition of sodium dithionite. After acidification to pH 4.0, the mixture was extracted with ethyl acetate and the residue obtained after removal of the solvent was analyzed by analytical HPLC to set the optimal conditions for

fractionation. The eluent eventually chosen was 1% formic acid acetonitrile 75:25 (Figure 6.3.2).

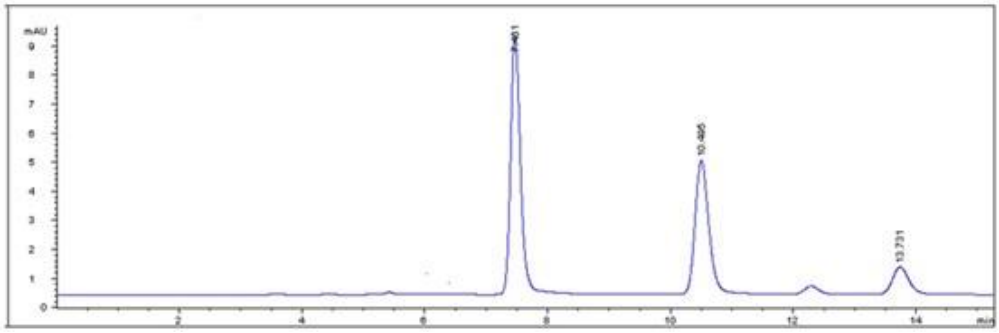

Figure 6.3.2. HPLC profile of the oxidation mixture of MeDHICA with copper acetate at 3 min reaction time. Eluent: 1 % formic acid - acetonitrile 75:25 v/v.

Preparative HPLC was selected for oligomer purification. The organic extracts were loaded on preparative HPLC (around 15 mg at each run) and the fractions corresponding to the peaks eluted at 9 and 11 min after removal of methanol were extracted with ethyl acetate. Overall some 1 g of MeDHICA was subjected to the oxidation under the optimized conditions. Yet, after the fractionation procedure described the amount of t_R 9 min dimer obtained was around 200 mg whereas for the t_R 11 min dimer much lower amounts were obtained (around 50 mg).

The product so obtained was subjected to a complete spectral characterization and the identity of the component eluted at 10 min as the 4,4'-dimer was confirmed also for comparison with the corresponding dimer of DHICA. Peculiar feature of the proton spectrum is the shielded signal at 6.38 ppm due to the H-3 protons belonging to C-4 bonded indole rings (Figure S6.7.5-S6.7.8).

The product at t_R =12 min was identified as the 4,7' dimer based on NMR analysis (Figure S6.7.9-S6.7.13) in comparison with data reported for DHICA dimers.

Peculiar features of ^{1}H NMR spectrum (Figure S6.7.9) are the resonance at 6.38 ppm for the H-3 proton belonging to the C-4 bonded indole ring whereas the H-3 proton belonging to the other C-7 bonded ring resonates at lower fields (6.97 ppm) as in the monomer MeDHICA. Similarly, the two NH protons appear at 11.38 ppm (as in the monomer MeDHICA) and 9.34 ppm, the latter experiencing a shielding effect attributable to the C-7 bonded indole ring.

6.4 Kinetics of the oxidation of dimers

Preliminary the oxidation behaviour of the dimers isolated were investigated in comparison with the respective monomer. Aerobic oxidation at slightly alkaline pHs was used with respect to the enzyme-mediate oxidation as this would avoid contamination and make the scale-up of the reaction for applicative purposes easier. Therefore, a concentration of the indole of 10 mM was chosen and the reaction was carried out in phosphate buffer at pH 8.5 in air under stirring. The course of the oxidation was monitored over by periodical UV-vis and HPLC analysis.

Figure 6.4.1 shows the time profile of the aerobic oxidation of the 4,4' and 4,7' DHICA dimers as determined spectrophotometrically. After 1 h, while the absorption of the indole at 320 nm was completely disappeared, the absorption of the dimers was still present and even after 7 h, especially in the case of 4,4'- dimer, it had not completely disappeared and featured a well-defined shoulder at 378 nm.

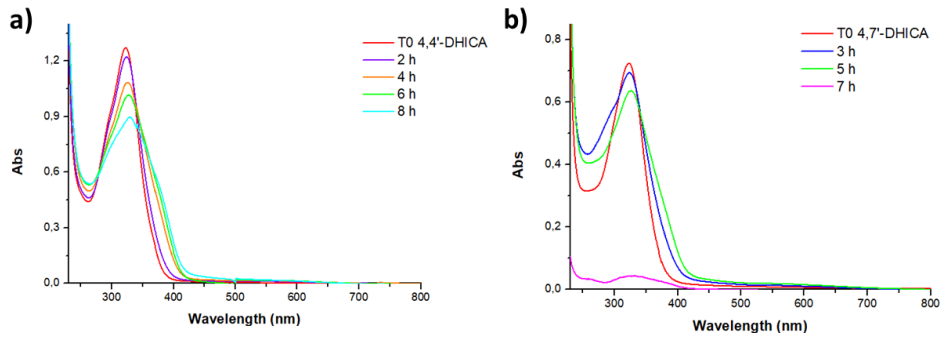

Figure 6.4.1. Spectrophotometric course of the autoxidation mixture of 4,4' (a) or 4,7' (b) DHICA dimer in 0.1 M phosphate buffer, pH 8.5. The mixture was diluted 200-fold before the measurement.

In the case of MeDHICA (Figure S6.7.14) and its dimer (Figure 6.4.2) the autoxidation seemed to be slower, especially for the 4,4' dimer, and after 24 h the absorption maximum at 320 nm was still present. As reported in Figure 6.4.2 panel b the 4,7'-dimer showed a decrease in the absorption maximum after 20 h and a well-detected shoulder at 400 nm.

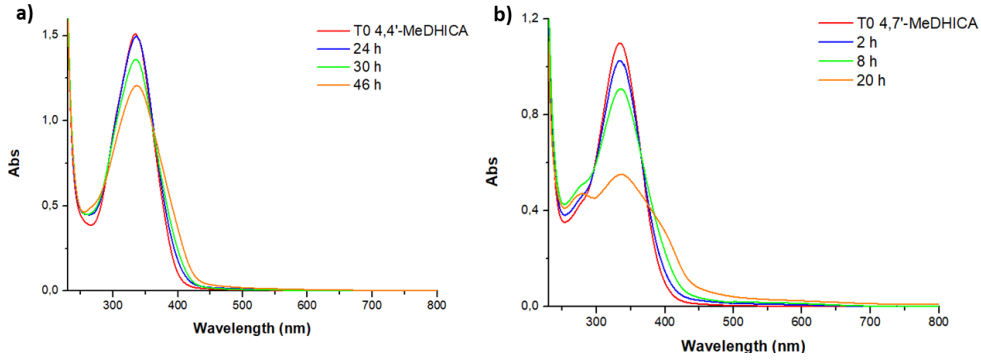

Figure 6.4.2. Spectrophotometric course of the autoxidation mixture of 4,4' (a) or 4,7' (b) MeDHICA dimer in 0.1 M phosphate buffer, pH 8.5. The mixture was diluted 200-fold before the measurement.

Parallel reverse-phase HPLC monitoring of the course of DHICA oxidation confirmed a substantial decay of the indole at 1 h (Figure 6.4.3, panel A). The 4,4'-dimer was substantially consumed within the first hour (*c.a.* 40 %) and then smoothly consumed up to 98 % in 8 h. On the other hand, the 4,7'-dimer was smoothly oxidized in the first hour (21 %) but then substantially consumed after 7 hours (97 %). A plot of the consumption in the first hour of the reaction better highlights such differences (Figure 6.4.3, panel B).

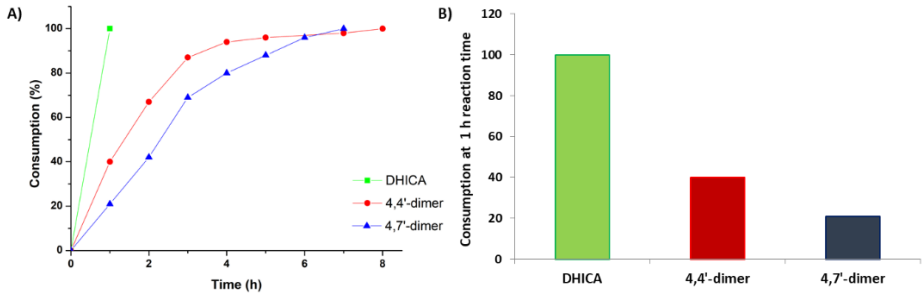

Figure 6.4.3. (a) Kinetics of decay of DHICA and related dimers by oxidation in air; (b) kinetics of consumption at 1 h reaction time.

In the case of MeDHICA and related dimers (Figure 6.4.4, panel A) a similar oxidative behaviour was observed for the monomer and the 4,7'-dimer in the first hours (47 and 42 % respectively after 3 h) reaching an almost complete consumption after 20-24 hr. On the other hand, the 4,4'-dimer is substantially consumed within the first 3 hour (>50 %) and then smoothly consumed up to 98 % in 46 h. This is clearly shown in the plot of Figure 6.4.4 (panel B) at 15 h reaction time.

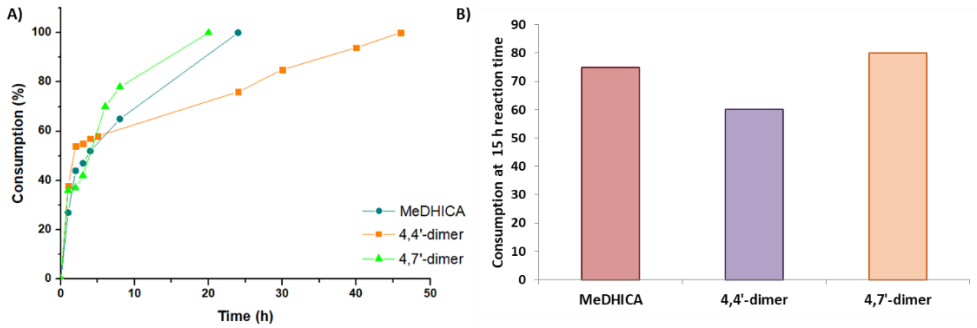

Figure 6.4.4. (a) Kinetics of decay of MeDHICA and related dimers by oxidation in air; (b) kinetics of consumption at 15 h reaction time.

These data indicate that the oxidation rate is very critically affected by the mode of coupling of the indole units, with an appreciable effect also associated to the esterification of the carboxyl group at 2-position.

Based on the information obtained in the preliminary investigation of the oxidation behaviour of the dimers, further experiments were devoted at preparation of melanin pigments from the dimers of both DHICA and MeDHICA. Given the different kinetics of oxidation observed for each dimer the oxidation reaction in air in phosphate buffer at pH 8.5 with the indole at 10 mM was prolonged till complete consumption as evaluated by HPLC analysis. In all cases, the melanin pigment that separated from the oxidation mixture following careful acidification was collected by centrifugation, extensively washed and lyophilized.

The absorption spectra of all model melanins prepared from the dimers were recorded in comparison with the spectra of the relevant dimers, monomers and their melanin (Figure 6.4.5, panel A-C). Either in the case of DHICA (Figure 6.4.5, panel A) or MeDHICA (Figure 6.4.5, panel B), the absorption spectra of the dimers were bathochromically shifted (up to 10 nm) with respect to that of the

monomer. Both MeDHICA and its dimers were shifted bathochromically with respect to DHICA and its dimers, respectively. As to melanin pigments from DHICA, the spectra appear almost featureless particularly in the case of the melanins from dimers that showed a broad absorption in the visible region (Figure 6.4.5, panel C). More defined spectra were obtained in the case of melanin obtained from MeDHICA and its dimers on account primarily of their higher solubility in both DMSO and methanol, the solvent chosen in order to solubilize the pigments. Also, in this case the absorption around 300 nm of the melanins are shifted bathochromically with respect to that of the monomer or the dimers. The MeDHICA melanin exhibit an intense absorption in the 350-450 region that may account for the yellowish brown color of the oxidation mixture and the final pigment. Similarly, the melanin from the 4,7'-dimer features a well-defined shoulder at 420 nm, whereas the melanin from the 4,4'-dimer has an intense chromophore in this region (Figure 6.4.5, panel D).

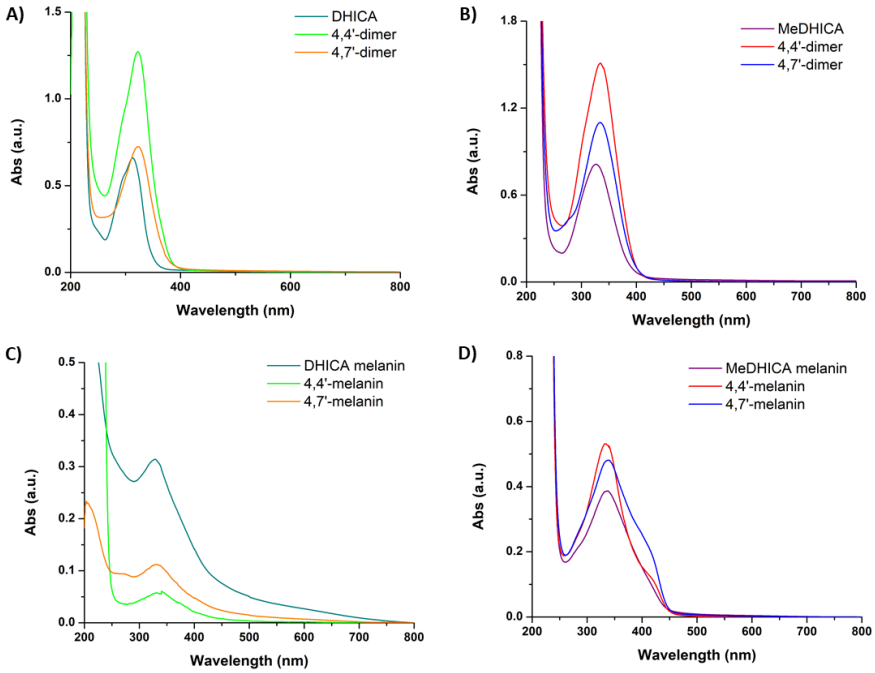

Figure 6.4.5. UV-vis spectra of DHICA, MeDHICA, their 4,4'- and 4,7'- dimers and melanins.

Based on these data it could be concluded that in the case of DHICA the absorption over the visible region of the melanins from either the monomer or its dimers may result from aggregation that is an extrinsic chromophore as previously shown for DHICA melanin. On the other hand, the absorption feature of the pigments from either MeDHICA monomer or its dimers would suggest an intrinsic chromophore that seems to be affected by the mode of coupling of the indole units, with the 4,7'-bonding being favoured for chromophore set up. Expectedly, treating the 4,7'-melanin solution with a reducing agent, *i.e.* sodium borohydride, a decrease of the chromophore intensity in the visible region was observed (Figure 6.4.6).

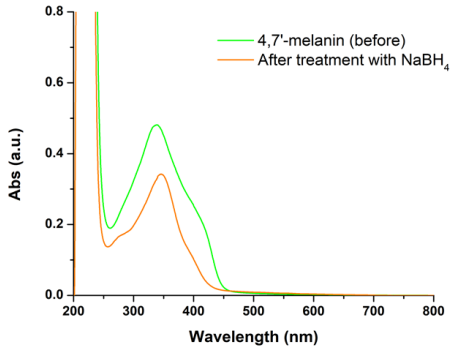

Figure 6.4.6. UV-vis spectra of 4,7'-MeDHICA melanin before and after treatment with a reducing agent.

6.5 Evaluation of the antioxidant properties

In another series of experiments the antioxidant properties of melanins from the dimers prepared from both DHICA and MeDHICA were evaluated, in comparison with the melanins from the monomers, by two chemical tests, the 2,2-diphenyl-1-picrylhydrazy (DPPH),[152] and the ferric reducing antioxidant power (FRAP).[153]

In the case of DPPH, the EC_{50} values for melanins is reported in Figure 6.5.1 (panel A and B) together with those obtained for the corresponding dimers and monomers. Given the different solubilities of the melanins from MeDHICA and its dimers with respect to those from DHICA and its dimers in the solvent used in this assay, that is methanol, it was chosen to run the measurements on aliquots withdrawn from suspensions of the pigments at 1 mg/mL in this solvent after extensive homogenization in a glass to glass potter.

In general, all monomers and dimers exhibit values lower than those of the corresponding melanins. The values obtained for DHICA confirmed higher

activity of the monomer compared to its melanin. Notably the 4,4'-dimer had an activity comparable to that of the monomer. Moreover, the melanin from the 4,4'-dimer showed an antioxidant activity higher than DHICA melanin and 4,7' melanin. In the MeDHICA series, the 4,4'-dimer exhibited an EC_{50} value lower than that obtained for the 4,7'-dimer but both dimers exhibited values higher than the monomer, similarly to what observed for the DHICA series. This trend was maintained also for the melanins, with the highest activity being associated to the MeDHICA melanin followed by the pigment from the 4,4'-dimer, and that from the 4,7'-dimer.

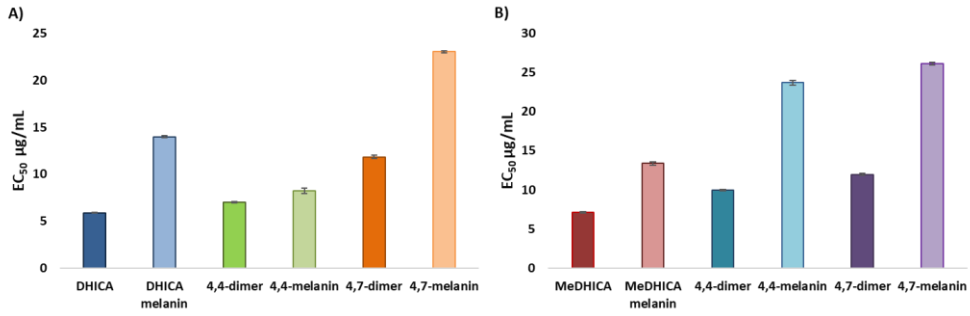

Figure 6.5.1. EC_{50} values from 2,2-diphenyl-1-picrylhydrazyl assay. Data are shown as mean ± SD of three independent experiments.

In the case of FRAP (Figure 6.5.2), results were expressed as trolox equivalents. The DHICA series (Figure 6.5.2, panel A) showed comparable values, and higher than that of Trolox, in the case of the monomer, both 4,4'- and 4,7' dimers and the melanin obtained from the 4,4'-dimer. In the case of MeDHICA (Figure 6.5.2, panel B) the monomer and the dimers exhibited an activity higher than that of Trolox, whereas the melanins obtained from both monomers and dimers were less active.

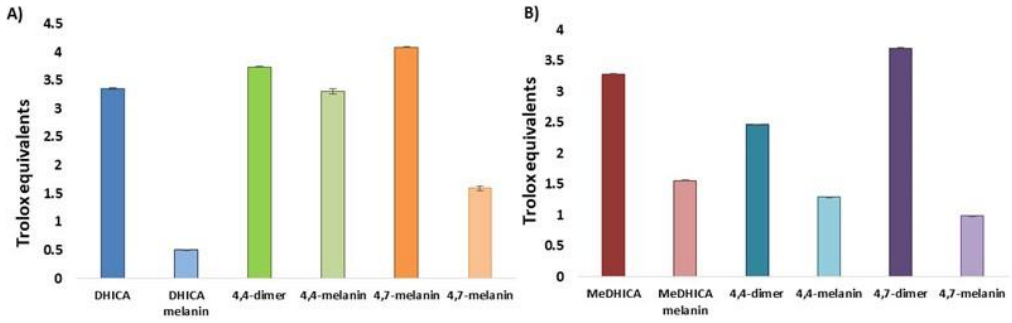

Figure 6.5.2. Ferric reducing antioxidant power expressed as Trolox equivalents. Data are shown as mean ± SD of three independent experiments.

6.6 Conclusions

Synthetic eumelanin pigments prepared from biosynthetic precursors and in particular from 5,6-dihydroxyindole-2-carboxylic acid (DHICA), DHICA melanins, have proved to be of particular interest due to the strong antioxidant properties and the intense absorption in the UVB/UVA region. Based on the consideration of the mode of coupling of DHICA units mainly through 4,4′-, 4,7′-, and 7,7′-bonding patterns, a model has been proposed for this pigment envisaging the presence of biphenyl-type bonds resulting in non-planar, partly linear backbones in which rotation around the interunit bonds is partly hindered. Some issues, however, remain to be set in particular whether the properties of the pigments are associated to a specific mode of coupling of the indole units. On these bases, in this chapter the attention was focused on the properties of melanins at high regioregularity obtained from the two main oligomers intermediates in DHICA melanin formation *i.e.* the 4,4' biindolyl and 4,7' biindolyl dimers.

Procedures reported in the literature for preparation of DHICA dimers were revisited in the perspective of large scale preparation. After several investigation

oxidation conditions were identified that allowed for a substantial formation of the two dimers. Given the interesting properties of MeDHICA melanin, the isolation of the same dimers from oxidation of MeDHICA was also optimized.

Preparative HPLC fractionation allowed to isolate some tens milligrams of each of DHICA and MeDHICA dimers, without need of protection of the catechol functionalities. The kinetics of oxidation of the indole dimers was recorded and compared. Melanin pigments were prepared from each of the dimers, and their absorption features and antioxidant activity as assayed by two chemical assays were compared. Significant differences were observed among the regioregular melanin pigments from dimers compared to the corresponding melanins from the monomers which allow to formulate preliminary conclusions on the contributions of the structural moieties inside melanin pigments and provide hints to preparation of a rationally designed melanin pigment with enhanced properties.

6.7 Experimental section

Materials and methods

3,4-Dihydroxy-L-phenylalanine (L-DOPA), ferricyanide potassium, cobalt sulfate, copper acetate, horseradish peroxidase, hydrogen peroxide, 4-(2-hydroxyethyl)-1-piperazineethanesulfonic acid (HEPES), Tris (hydroxymethyl) aminomethane (Tris), copper sulfate, sodium dithionite, sodium borohydride, 2,2-diphenyl-1-picrylhydrazyl (DPPH) and 6-hydroxy-2,5,7,8-tetramethylchroman-2-carboxylic acid (trolox) were purchased from Sigma-Aldrich. All solvents were HPLC grade.

DHICA and MeDHICA were prepared according to a protocol reported in the Chapter 5 (paragraph 5.6 Experimental section).

UV-vis spectra were recorded on a Jasco V-730 Spectrophotometer.

^{1}H NMR and ^{13}C NMR spectra were recorded in DMSO-d6 at 400 MHz on a Bruker spectrometer. ^{1}H, ^{1}H COSY, ^{1}H, ^{13}C HSQC, and ^{1}H, ^{13}C HMBC were run at 400 MHz using Bruker standard pulse programs. Chemical shifts are given in ppm.

HPLC analyses were performed on a Agilent 1100 binary pump instrument equipped with and a SPD-10AV VP UV-visible detector using an octadecylsilane-coated column, 250 mm x 4.6 mm, 5 µm particle size (Phenomenex Sphereclone ODS) at 0.7 mL/min. Detection wavelength was set at 300 nm. Eluent system: A) gradient of 0.1 % formic acid-methanol from T 0 to 30 min from 10 to 25 % of methanol; B) 0,1 % formic acid-methanol 80:20 v/v; C) 1.5 % formic acid-methanol 80:20 v/v, D) 1.5 % formic acid-methanol 90:10 v/v; E) 1 % formic acid-methanol 60:40 v/v; F) 1 % formic acid-acetonitrile 75:25 v/v; G) 1 % formic acid-acetonitrile 90:10 v/v.

LC-MS analyses were performed on an AGILENT ESI-TOF 1260/6230DA Agilent Technologies in positive ion mode in the following conditions: nebulizer pressure 35 psig; drying gas (nitrogen) 5 L/min, 325 °C; capillary voltage 3500 V; fragmentor voltage 175 V. A Eclipse Plus C_{18} column, 150 × 4.6 mm, 5 µm, at a flow rate of 0.4 mL/min was used, with the same mobile phase as above.

Preparative HPLC was carried out on an instrument coupled with a UV detector set at 300 nm using an Econosil C_{18} (10 µm, 22 x 250 mm). Eluent system: H) 1 % formic acid-methanol 90:10 v/v; I) 1 % formic acid-acetonitrile 90:10 v/v; J) 1 % formic acid-methanol 60:40 v/v; K) 1 % formic acid-acetonitrile 75:25 v/v.

Optimization of the oxidation conditions for preparation of DHICA dimers.

Reaction conditions 1. A solution of DHICA in 0.1 M phosphate buffer pH 7.5 (1 mM) was treated with horseradish peroxidase (42 U/mL) and hydrogen peroxide 30 % v/v. The reaction mixture was taken under vigorous stirring. After 1 min, the oxidation reaction was stopped by addition of sodium dithionite, acidified to pH 4.0 and rapidly extracted with ethyl acetate. The residue obtained following evaporation of the combined organic layers was fractionated by preparative HPLC (eluent A).

Reaction conditions 2. A solution of DHICA (1 mM) in 0.1 M phosphate buffer pH 7.5 was treated with 1 equivalent of potassium ferricyanide reaction and stopped after 10 s - 3 min with dithionite and rapidly extracted with ethyl acetate. The residue obtained following evaporation of the combined organic layers was analyzed by HPLC (eluent B and D).

Reaction conditions 3. A solution of DHICA (1 mM) in 0.1 M phosphate buffer at pH 7.5 buffer was left under vigorous stirring and treated above (eluent system D).

Reaction conditions 4. A solution of DHICA (1 mM) in 0.02 M Hepes buffer pH 7.5 was treated with copper acetate (1 and 0.5 eq. molar), left under vigorous stirring and controlled over time (eluent A, C and D).

Preparation of DHICA dimers. The oxidation mixture containing the two dimers 4,4 'and 4,7' of 5,6-dihydroxyindole-2-carboxylic acid was obtained by reacting a solution of DHICA (500 mg) in 0.5 M Tris buffer (pH 7.5) (300 mL), saturated with oxygen, with copper sulfate (630 mg) under vigorous stirring. After 1 min, the oxidation reaction was halted by addition of sodium dithionite, acidified to pH 4.0 and rapidly extracted with ethyl acetate. The residue obtained following

evaporation of the combined organic layers was fractionated by preparative HPLC (eluent H and I).

4,4'-dimer: ^{1}H-NMR δ: 3.74 (COOMe), 6.31 (1H, H-3), 6.87 (1H, H-7), 11.14 (1H, NH). ^{13}C-NMR δ: 96.0, 108.1, 114.4, 125.2, 120.2, 132.1, 139.0, 146.3, 162.

4,7'-dimer: ^{1}H-NMR δ: 3.74 (COOMe), 6.34 (1H, H-3), 6.90 (1H, H-3'), 6.97 (1H, H-4), 6.87 (1H, H-7), 9.98 (1H, NH), 11.13 (1H, NH). ^{13}C-NMR δ: 96.4, 103.9, 105.2, 107.7, 108.1, 119.2, 125.1, 125.6, 131.5, 132.2, 139.3, 142.4, 142.6, 143.5, 146.2, 162.3, 162.5.

Optimization of the oxidation conditions for preparation of MeDHICA dimers.

Reaction conditions 1. The oxidation in air of MeDHICA (1 mM) dissolved in the minimal amount of methanol was performed using 0.1 M phosphate buffer pH 8.5. The mixture was left under vigorous stirring and controlled over time by HPLC (eluent system E).

Reaction conditions 2. A solution of MeDHICA (16 mM) in 0.2 M HEPES buffer pH 7.5 was treated with cobalt sulfate (1 molar eq.) and left under vigorous stirring and controlled by HPLC over the time interval 1 to 20 min (eluent system E).

Reaction conditions 3. A solution of MeDHICA (16 mM) in 0.2 M HEPES buffer pH 7.5 was treated with 1 molar equivalents of copper acetate and left under vigorous stirring and controlled by HPLC (eluent system).

Preparation of MeDHICA dimers. The oxidation mixture containing the two dimers 4,4' and 4,7' of 5,6-dihydroxyindole-2-carboxylic acid was obtained under the same procedure described above for the DHICA dimers, by reacting a solution of MeDHICA (500 mg) in 0.5 M Tris buffer (pH 7.5) (150 mL) with copper sulfate under vigorous stirring. After 1 min, the oxidation reaction was stopped by

addition of sodium dithionite, acidified to pH 4.0 and rapidly extracted with ethyl acetate. The residue obtained following evaporation of the combined organic layers was fractionated by preparative HPLC (eluent system J or K).

4,4'-dimer: ^{1}H-NMR δ: 3.74 (COOMe), 6.38 (1H, H-3), 6.97 (1H, H-7), 11.32 (1H, NH). ^{13}C-NMR δ: 52.0, 96.2, 109.5, 114.9, 120.9, 124.6, 132.6, 139.9, 146.9, 162.4.

4,7'-dimer: ^{1}H-NMR δ: 3.74 (COOMe), 6.38 (1H, H-3), 6.97 (1H, H-3'), 7.01 (1H, H-4), 6.89 (1H, H-7), 9.34 (1H, NH), 11.32 (1H, NH). ^{13}C-NMR δ: 96.4, 104.1, 105.2, 107.2, 109.9, 112.0, 1206.6, 125.1, 125.6, 131.5, 132.2, 139.3, 142.4, 143.5, 147.6, 162.3, 162.5.

Preparation of melanins. Melanins were obtained by aerobic oxidation in 0.1 M phosphate buffer at pH 8.5 (final concentration 10 mM). The oxidation mixtures were taken at room temperature under vigorous stirring. And were halted at complete monomer or dimer consumption as determined by HPLC analysis after time intervals varying in the range 8-46 h by acidification to pH 2.0. The melanin pigment that separated was collected by centrifugation (7000 rpm, 10 min at 4°C) and was washed three times with 0.01 M hydrochloric acid (15 mL). After lyophilization, the melanins from DHICA, 4,4' and 4,7' were obtained in 90 %, 93 % and 40 % w/w yield respectively, whereas the melanins from MeDHICA, 4,4'dimer and 4,7'dimer were obtained in 65 %, 87 % and 57 % w/w yield, respectively.

2,2-diphenyl-1-picrylhydrazy (DPPH) assay. The assay was performed as previously described.[152] Briefly, to a 200 μM DPPH solution in methanol, a proper amount of a methanolic suspension (1 mg/mL) of each compound homogenized with a glass/glass potter was added and rapidly mixed. The reaction was followed

by spectrophotometric analysis measuring the absorbance at 515 nm after 10 min. Values are expressed as the EC_{50}.

Ferric reducing/antioxidant power (FRAP) assay. The assay was performed as described.[153] To a solution of FRAP reagent, a proper amount of a methanolic suspension (1 mg/mL) of each compound homogenized with a glass/glass potter was added and rapidly mixed. After 10 minutes, the absorbance at 593 nm was measured. Trolox was used as the standard and results were expressed as Trolox equivalents. The FRAP reagent was prepared freshly by mixing 0.3 M acetate buffer (pH 3.6), 10 mM 2,4,6-tris(2-pyridyl)-s-triazine in 40 mM HCl, and 20 mM ferric chloride in water, in the ratio 10:1:1, in that order.

Suporting materials

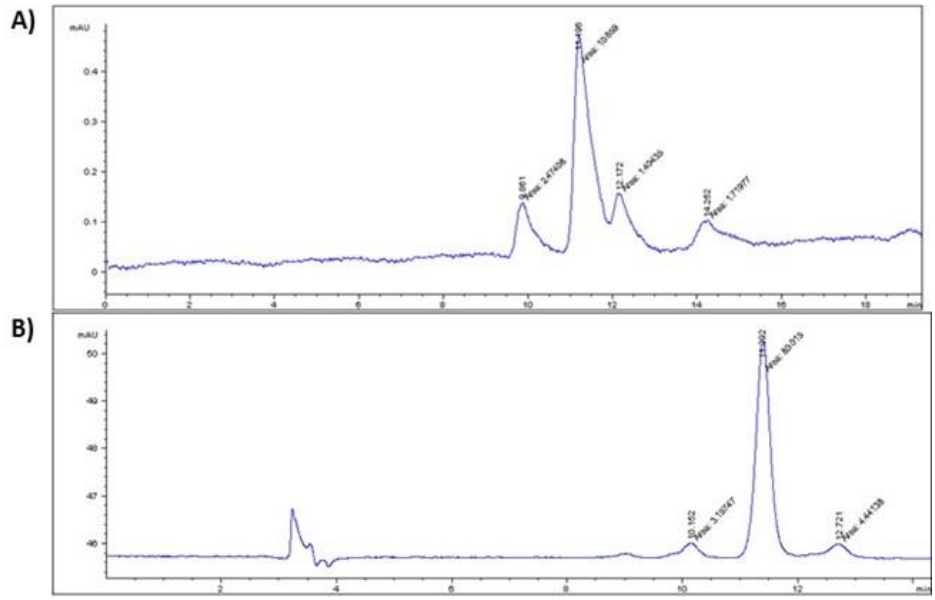

Figure S6.7.1. HPLC profile of the oxidation mixtures of DHICA in the presence of 1 (a) or 0.5 (b) molar equivalents of ferricyanide.

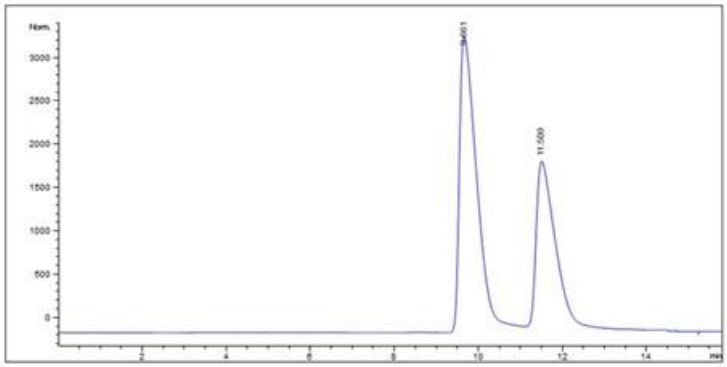

Figure S6.7.2. HPLC profile of the fraction containing the 4,4' (t_R = 9.8 nm) and the 4,7'-dimer (t_R =11.5 nm). Eluent: 1 % formic acid-acetonitrile (90:10 v/v), flow 25 mL/min.

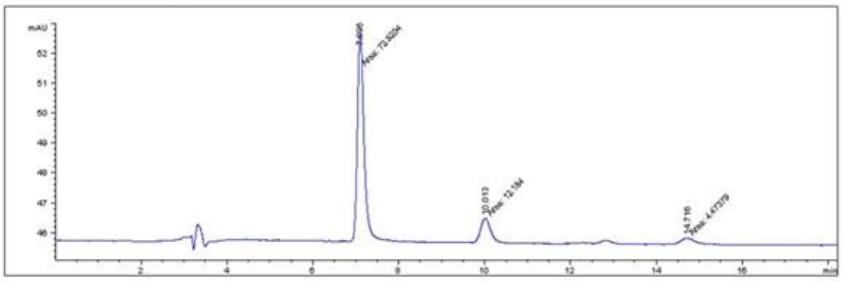

Figure S6.7.3. HPLC profile of the oxidation mixture of MeDHICA with cobalt sulfate at 3 min reaction time. Eluent: 1 % formic acid-MeOH 60:40 v/v.

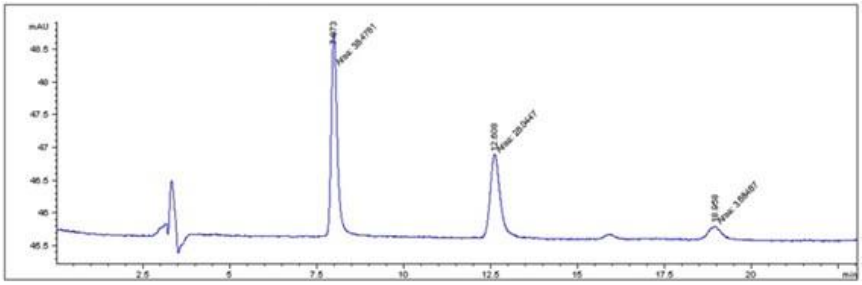

Figure S6.7.4. HPLC profile of the oxidation mixture of MeDHICA with copper acetate at 3 min reaction time. Eluent: 1 % formic acid-MeOH 60:40 v/v.

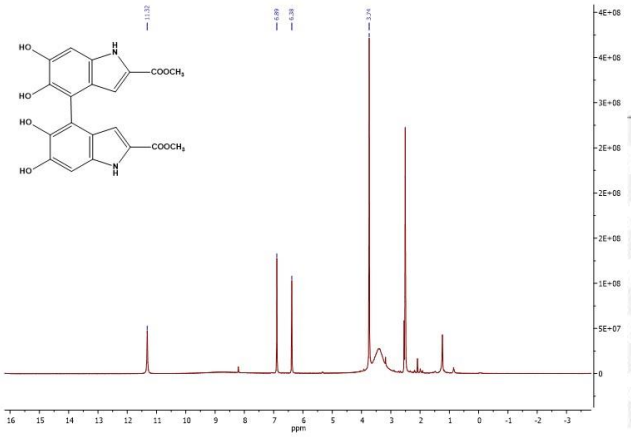

	^{1}H	^{13}C
1/1'	11.32	
2/ 2'		124.6
3/ 3'	6.38	109.5
4/ 4'		114.9
5/ 5'		139.9
6/ 6'		146.9
7/ 7'	6.89	96.2
8/ 8'		132.6
9/ 9'		120.9
$\underline{C}OOCH_3$		162.4
$COO\underline{CH_3}$	3.74	52.0

Figure S6.7.5. ^{1}H NMR spectrum of 4,4'-MeDHICA dimer in DMSO-d6.

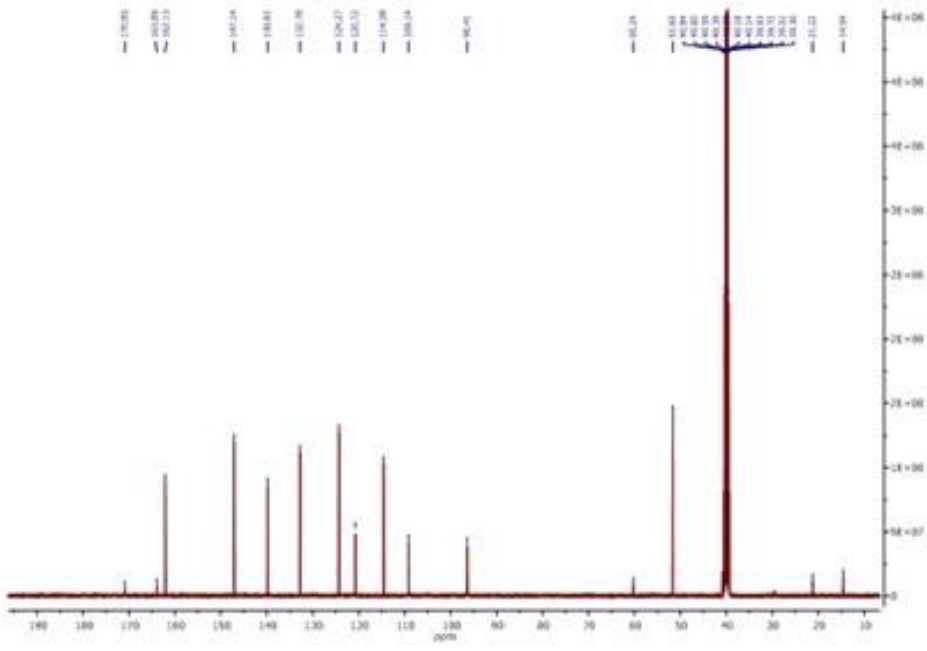

Figure S6.7.6. ^{13}C NMR spectrum of 4,4'-MeDHICA dimer.

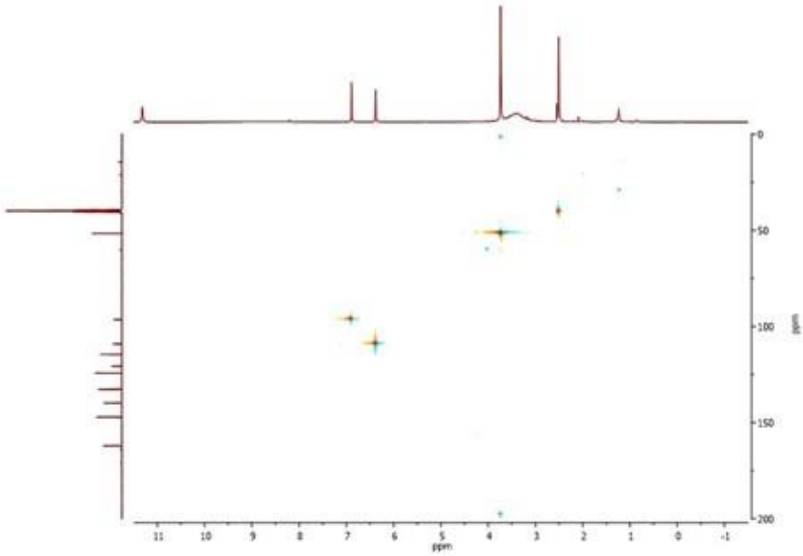

Figure S6.7.7. $^{1}H,^{13}C$ HSQC spectrum of 4,4'-MeDHICA dimer.

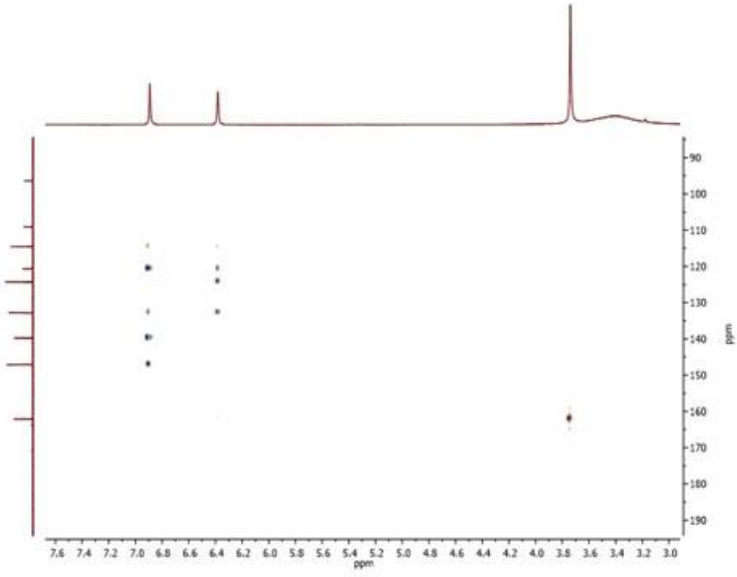

Figure S6.7.8. $^{1}H,^{13}C$ HMBC spectrum of 4,4'-MeDHICA dimer.

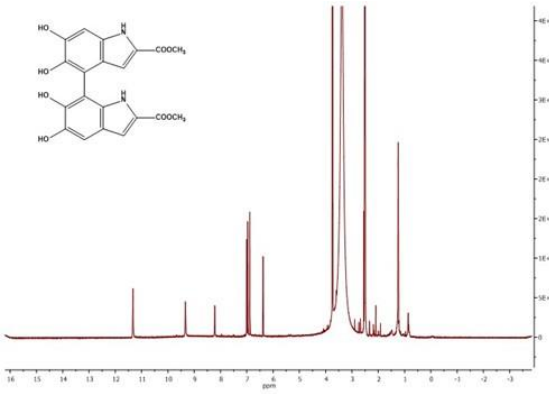

	^{1}H	^{13}C
1/1'	11.32; 9.34	
2/2'		125.1; 125.6
3/3'	6.38; 6.97	107.2; 104.1
4/4'	7.01	112.0;109.9
5/5'		139.3; 142.4
6/6'		147.6; 143.5
7/7'	6.89;	96.4; 105.2
8/8'		131.5;132.1
9/9'		120.6; 139.3
$\underline{C}OOCH_3$		162.3 ;162.5
$COO\underline{C}H_3$	3.74	51.9

Figure S6.7.9. ^{1}H spectrum of 4,7'-MeDHICA dimer in DMSO d6.

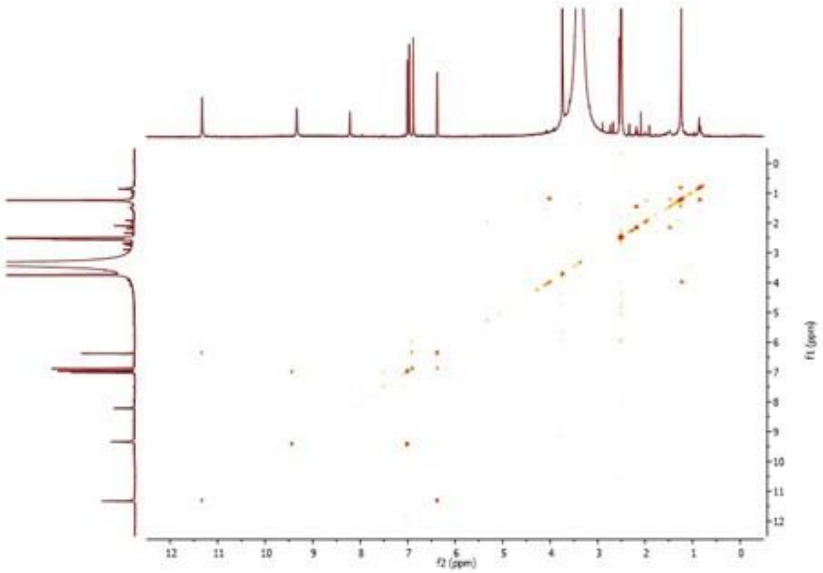

Figure S6.7.10. $^{1}H,^{1}H$ COSY of 4,7'-MeDHICA dimer.

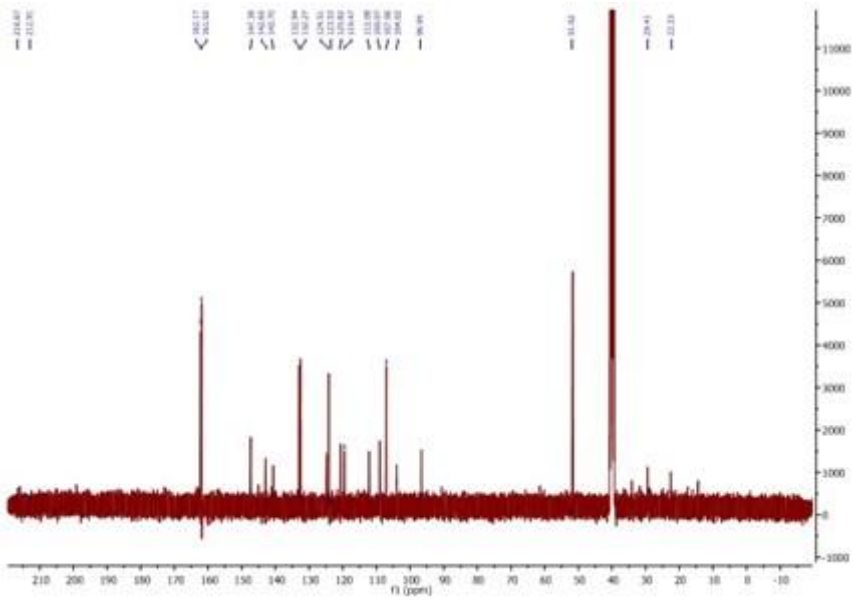

Figure S6.7.11. ^{13}C NMR spectrum of 4,7'-MeDHICA dimer.

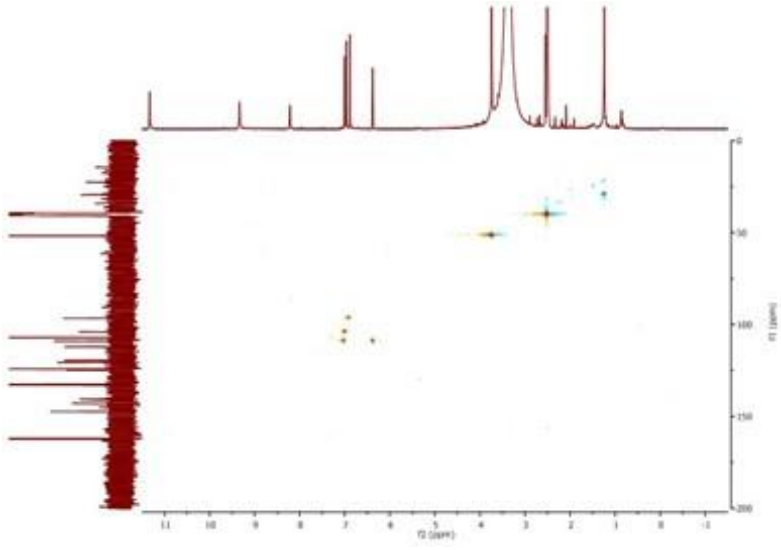

Figure S6.7.12. $^{1}H,^{13}C$ HSQC spectrum of 4,7'-MeDHICA dimer.

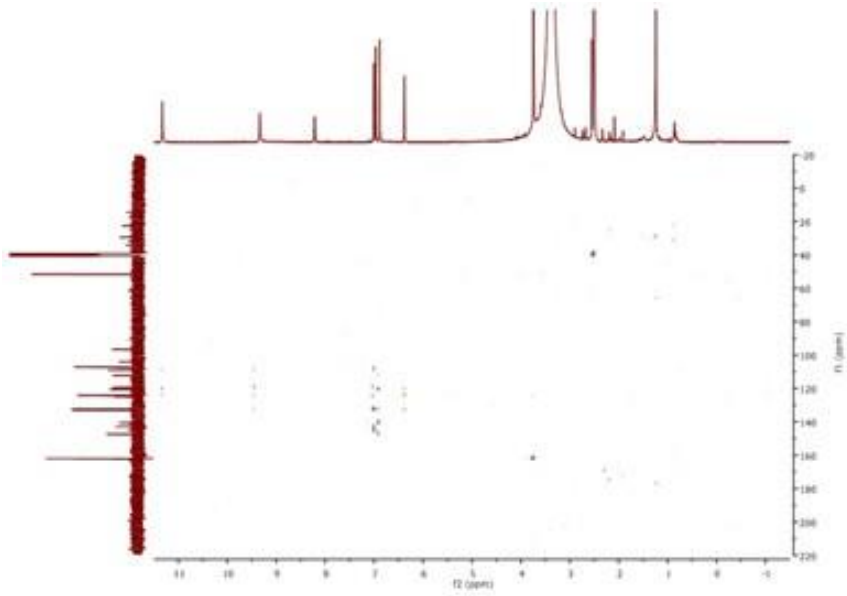

Figure S6.7.13. $^{1}H,^{13}C$ HMBC spectrum of 4,7'-MeDHICA dimer.

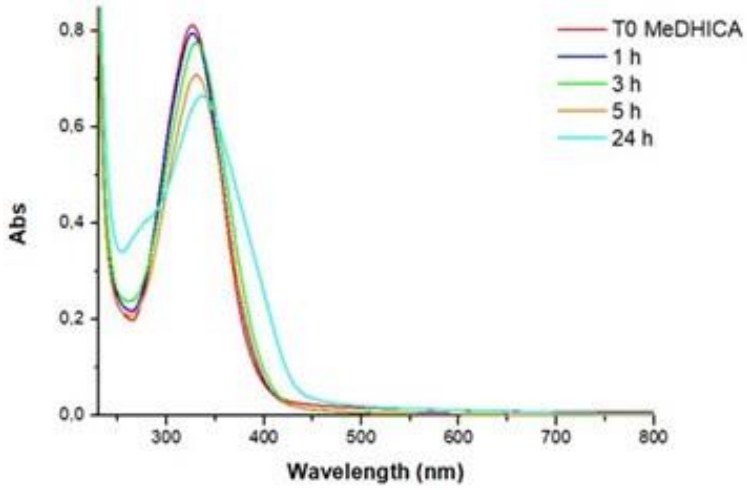

Figure S6.7.14. UV-vis spectra of MeDHICA oxidation over 24 h reaction time in phosphate buffer at pH 8.5.

Chapter 7

Assessment of the potential of gelatin-based hydrogels for the controlled release of melanin-related metabolites

7.1 Introduction

As introduced in the previous chapters two main types of melanin pigments have been identified in the skin: the black eumelanins, typical of darkly pigmented phenotypes, and the sulphur-containing pheomelanins, mainly present in the epidermis of fairskinned subjects. Although eumelanins serve as a filter against UV radiation and possess efficient scavenging properties toward photogenerated free-radical species, several evidences indicated that the entire eumelanogenic pathway is relevant to melanocyte function. However, the precise mechanisms by which the eumelanin-forming pathway would contribute to melanocyte roles in skin homeostasis and (photo)protection remain to be elucidated. While *in vitro* eumelanin synthesis envisages the prevalent spontaneous decarboxylation of dopachrome to DHI[188] *in vivo,* the intervention of the enzyme dopachrome tautomerase (Dct or tyrosinase-related protein Tyrp 2) directs eumelanin synthesis to the formation of DHICA.[185,189,190] As demonstrated in several studies DHICA and its main metabolites, 6-hydroxy-5-methoxyindole-2-carboxylic acid (6H5MICA) and 5-hydroxy-6-methoxyindole-2-carboxylic acid (5H6MICA),[160] have antioxidant properties and play a critical role in melanocyte response to oxidative stress and inflammation.[156,191] In fact, data from DPPH and FRAP assay indicated that both DHICA and 6H5MICA are stronger antioxidant than trolox in

the H-donor capacity and in reducing Fe(III) to Fe(II) ions.[156] Early studies showed that DHICA inhibits lipid peroxidation *in vitro*, is oxidized by nitric oxide and efficiently inhibits H_2O_2-Fe (II)/EDTA (Fenton)-induced oxidation processes.[192-194] DHICA displays an absorption maximum at 313 nm in the UVB erithematogenic region and can act as triplet state quencher.[154] In addition studies on primary cultures of human keratinocytes disclosed its remarkable protective and differentiating effects. At micromolar concentrations, DHICA induced: (a) time- and dose-dependent reduction of cell proliferation without concomitant toxicity; (b) enhanced expression of early and late differentiation markers; (c) increased activities and expression of antioxidant enzymes; and (d) decreased cell damage and apoptosis following UVA exposure.[157] All these data point out that DHICA exerts an antioxidant and protective function *per se* unrelated to pigment synthesis, suggesting that the indole and/or its derivatives could play an important role in preventing and treating inflammatory skin pathologies related to oxidative stress, such as acne, atopic dermatitis and melanoma.[195] Severe limitations in this perspective stem from the ease of this compound to undergo oxidation with consequent loss of its properties. In addition, proper formulation allowing for vehiculation through the skin and a controlled release would greatly add to the beneficial properties prolonging the action and taking the bioavailable concentrations relatively low. In recent years several natural compounds have been tested for the topical treatment of skin disorders by use of a variety of transcutaneous delivery systems including lipophilic nanoparticles like liposomes,[196] solid lipid nanoparticles,[197] nanostructured lipid carriers, monoolein aqueous dispersions,[198] ethosomes[199] and lecithin organogels.[200] Different more hydrophilic delivery systems have also been explored primarily gelatin, the product of collagen hydrolysis, since its chemical nature offers many advantages, including historical safe use in a wide range of medical applications but also

simple fabrication methods, inherent electrostatic binding properties and proteolytic degradability. Gelatin versatility allows the design of different carrier systems, spanning from micro or nanoparticles, to fibers and hydrogels. In particular, hydrogel based bioscaffolds are largely applied in the field of tissue engineering because of their ability to: a) adjust their mechanical features to surrounding tissues in living systems, offering in addition 3D networks for living tissue construction, and b) trap bioactive molecules and/or drugs into the polymer network, thus allowing their controlled release, *e.g.* for pain treatment and wound healing applications.[201,202] However the main limitation in the use of gelatin systems arises from its rapid dissolution in aqueous environments. The possibility to cross-link gelatin with synthetic (metacrylate, glutaraldehyde, polyglutammic acid)[203,204] and natural compounds like dialdehydes (genipin),[205] or biopolymers (chitosan)[206] has additionally greatly expanded the application range of this material allowing to proper tuning the mechanical properties, swelling behavior, thermal properties and other physiochemical properties.[207,208]

In the light of the foregoing in this chapter the ability of gelatin-based hydrogels of incorporating and releasing under controlled conditions DHICA was investigated. The methyl ester of DHICA, MeDHICA, was also tested in view of its higher stability and different solubility profile.

7.2 Loading and release of DHICA and MeDHICA

7.2.1 Gelatin-based system (*Pristine gelatin*)

In the initial experiments, porcine skin gelatin type A, resulting from acid hydrolysis, was dissolved (10 % w/v) in phosphate buffer saline (PBS) at pH 7.4 at 37 °C and DHICA or MeDHICA, previously dissolved in the minimal amout of DMSO, were added under stirring to reach concentration of 10 % w/w with

respect to gelatin (***10% w/w gelatin***). The hydrogels were set for gelation for 12 h at 4 °C and then washed with PBS to remove unreacted indole compounds (Figure 7.2.1.1).[204]

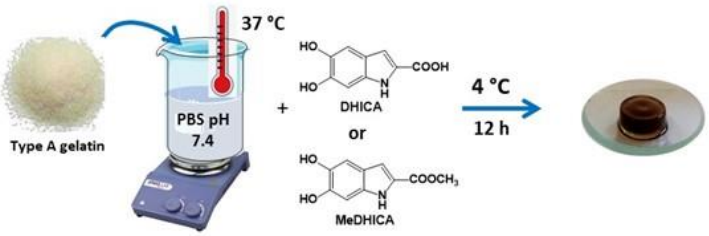

Figure 7.2.1.1. Preparation of gelatin and loading of indole compounds.

UV-vis spectrophotometric analysis of the indoles (λ_{max} 320 nm) in the washings allowed to estimate an extent of incorporation into the gelatins of 62 % in the case of DHICA and even higher up to 80 % for MeDHICA (Figure 7.2.1.2). Lowering the DHICA to gelatin ratio to 5 or 1 % the extent of incorporation proved to be 59 and 48 %, respectively.

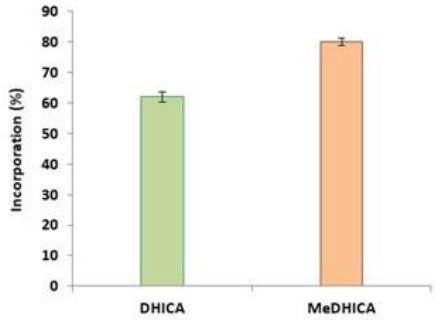

Figure 7.2.1.2. Extent of incorporation of indole compounds (10 % w/w) estimated by UV-vis spectrophotometric analysis. The average values ± SD obtained from at least three separate experiments are reported.

The kinetics of release of the indoles at physiological pH conditions was then evaluated over 72 h, by repeatedly refreshing the medium after the first hour. For either indoles the release was smooth over the observation period reaching values around 30 % of the incorporated indole for the 10 % w/w gelatin (Figure 7.2.1.3, panel A). In the case of DHICA, the release was comparable for the 5 % w/w gelatin and more sustained reaching 60 % (of the incorporated material) after 72 h for the 1 % w/w gelatin (Figure 7.2.1.3, panel B).

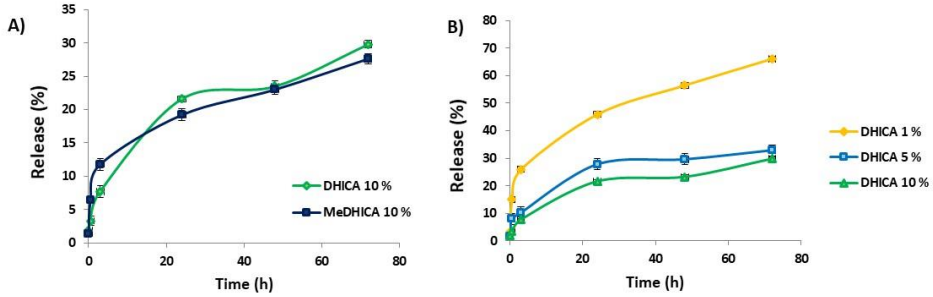

Figure 7.2.1.3. Kinetics of release of the incorporated compound (DHICA or MeDHICA in 10 % w/w gelatin, panel A, and DHICA 1, 5, 10 % w/w gelatin panel B) from gelatin in PBS at pH 7.4 with refreshing of the medium over 72 h. The average values ± SD obtained from at least three separate experiments are reported.

In spite of the favorable release profile that would suggest its potential application for topical uses, this kind gelatin exhibits a poor thermal stability dissolving under physiological temperature conditions which limits its possible applications. Based on this consideration in further experiments the possibility to get a a more hydrolytically stable material that could remain unaltered even after prolonged exposure to physiological temperature or higher was explored by use of cross-linkers.

7.2.2 Cross-linked gelatins

In the frame of a collaboration with Prof. Laura Cipolla and co-workers, at the Univerisity of Milano-Bicocca, two chemically cross-linked gelatins were prepared: a) *CL gelatin 1*, with 4-(4,6-dimethoxy-1,3,5-triazin-2-yl)-4-methylmorpholinium-chloride (DMTMM), a zero-length coupling agent promoting the activation of carboxyl groups for subsequent amide or ester formation and b) *CL gelatin 2*, with the natural polymer chitosan with a 8:1 w/w ratio in the presence of 10 % of DMTMM. Both gelatins proved stable at significantly higher temperature, up to 100 °C. Characterization of the CL gelatins is reported in the supporting material (Figure S7.3.1, S7.3.2).

For the *CL gelatin 1* loaded at 10 % w/w DHICA (***10 % w/w CL gelatin 1***) the uptake into the hydrogel scaffold is around 40 % in the first 30 min with increase up to a complete incorporation within 4 h, while the loading is faster for MeDHICA loaded at 10 % w/w reaching 90% values in the first hour. On the other hand, the *CL gelatin 1* at 5 % w/w loading ratio (***5 % w/w CL gelatin 1***), DHICA incorporation reaches 50 % as the maximum value, but is not appreaciable using lower DHICA or MeDHICA to gelatin ratios (Figure 7.2.2.1).

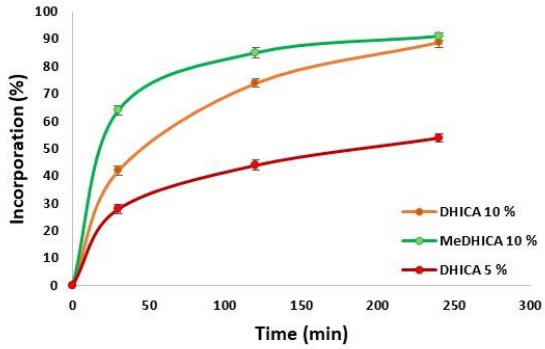

Figure 7.2.2.1. Loading of indole compounds in the *CL gelatin 1* over time. The average values ± SD obtained from at least three separate experiments are reported.

DHICA loading into *CL gelatin 2* starting from a 10 % w/w gelatin proved very fast reaching with a 50% incorporation in the first 30 min up to 80 % in 4 h, whereas for MeDHICA at the same ratio loading is 50 % after 4 hrs (Figure 7.2.2.2).

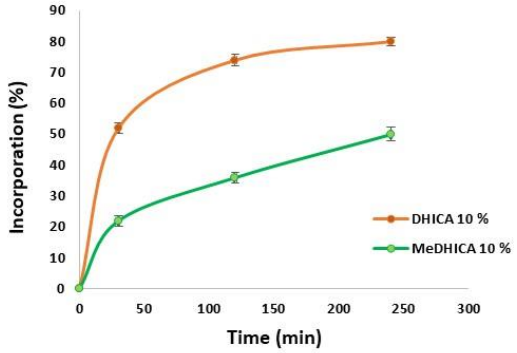

Figure 7.2.2.2. Loading of indole compounds in the *10 % w/w CL gelatin 2* over time. The average values ± SD obtained from at least three separate experiments are reported.

The kinetics of release of indole componds were determined in PBS at 37 °C (Figure 7.2.2.3). In the case of ***10 % w/w CL gelatin 1*** (Figure 7.2.2.3, panel A)

the observed release of DHICA is very smooth with 15 % values at 1 h which increases to 30 % at 6 h after medium refreshing every 1 h, with no significant increase on longer times up to 24 h. The release of DHICA is lower (23 % at 6 hrs) using the ***5 % w/w CL gelatin 1***. MeDHICA in ***10 % w/w CL gelatin 1*** is released rapidly with a 57 % after 1 h, a value that increases to 90 % after 4 h with repeated medium refreshing. Much lower is the release observed for DHICA in the case of ***10 % w/w CL gelatin 2*** with an intial value of 8 % after 1 h which increases to 54 % after 6 h with medium refreshing. On the other hand, MeDHICA is relased to 35 % after 1 h with a steep increase up to 90 % in the first 4 h after repeated medium refreshing (Figure 7.2.2.3, panel B). Based on these results, loading and release values seem to be dictacted mainly by the interactions between the gel and the indoles carboxy groups, and to a lesser extent by the acidic phenolic functionalities. When gelatin carboxy groups are capped by the cross-linking reaction and by the increase of basic amino groups from chitosan, the extent of incorporation of DHICA was higher in the cross-linked gelatins than that in the pristine hydrogel in wich unfavourable interactions of the carboxylate group of DHICA with the carboxylate groups of the acidic aminoacids of gelatin were present. On the contrary, MeDHICA, missing the ionizable and strongly hydrophilic carboxy group does not experience unfavourable interactions with pristine gelatin and *CL gelatin 1*, but has a lower affinity for the highly hydrophilic *CL gelatin 2*, as indicated also by the higher extent of release with respect to DHICA.

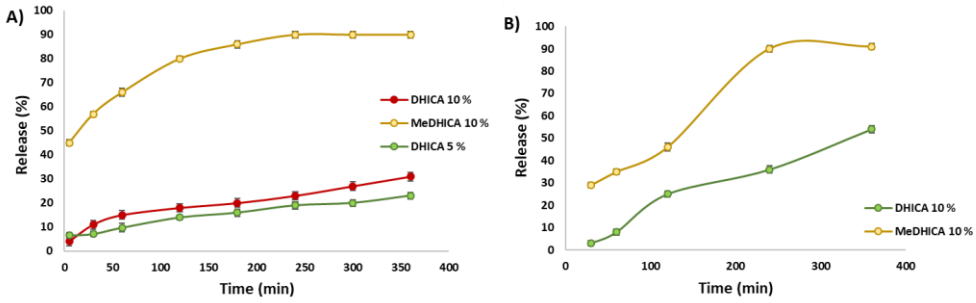

Figure 7.2.2.3. Kinetics of release of the incorporated compound from *CL gelatin 1* (a) or *CL gelatin 2* (b) in PBS with refreshing of the medium at 37 °C. The average values ± SD obtained from at least three separate experiments are reported.

7.2.2.1 Assessment of the stability of indole compounds in the CL gelatins

One of the advantages that should be offered by incorporation of indoles into a biopolymer like gelatin is the increase of its stability to aerial oxidation in aqueous neutral media of physiological relevance.

To evaluate this issue, as an example, the kinetics of decay of free DHICA in PBS at 37 °C was evaluated by HPLC analysis over the time period used for monitoring the release from *CL gelatins* (6 h). ***10 % CL gelatin 1*** incorporating DHICA was immersed in PBS at 37 °C and the release was again monitored over 6 h without medium refreshing leading to a release of 10 % of the incorporated compound. The decay of DHICA free in the PBS solution at the same concentration present in the gelatin based on the estimated incorporation, was monitored by HPLC analysis (Figure 7.2.2.1.1, panel A). Under these latter conditions DHICA is consumed to 70 % over 6 hours leading to dark melanin (Figure 7.2.2.1.1, panel B left picture), whereas the indole entrapped into the gelatin and hence released

slowly into solution is preserved from oxidation to a remarkable extent (panel B right picture).

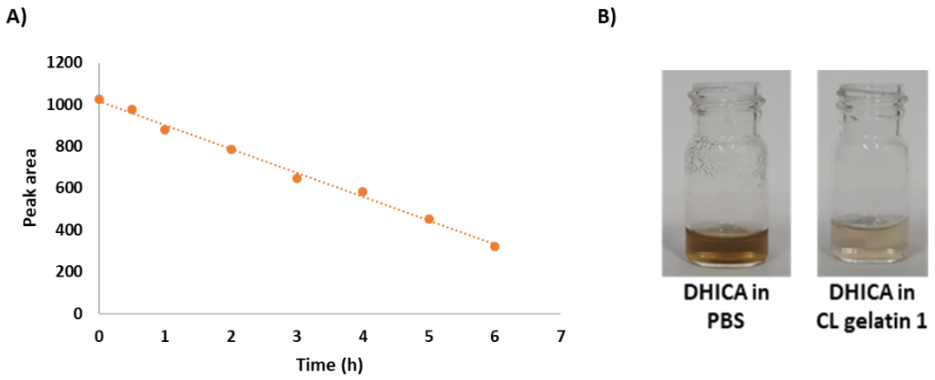

Figure 7.2.2.1.1. Decay of DHICA free in the PBS solution monitored by HPLC analysis (panel A). Digital picture of DHICA free in PBS *vs* ***10 % w/w DHICA CL gelatin 1*** over 6 h (panel B).

7.3 Evaluation of the antioxidant properties

In further experiments, considering the remarkable antioxidant activity of the indole compounds under investigation, the antioxidant properties of the DHICA/MeDHICA released in PBS at 37 °C from the ***10 % CL gelatin 1*** and ***2*** were also evaluated by two chemical assays, DPPH and FRAP. Briefly, aliquots of the medium were withdrawn over time and the DPPH decay after 10 min was evaluated spectrophotometrically (Figure 7.3.1, panel A and B). A similar procedure was followed to evaluate the ferric reducing antioxidant power of the medium containing the 10 % *CL gelatins* (Figure 7.3.1, panel C and D). As expected, the reducing potency increases over time on account of the progressive release of the indoles from the hydrogels further supporting the observed stability of the indole incorporated into the gelatins.

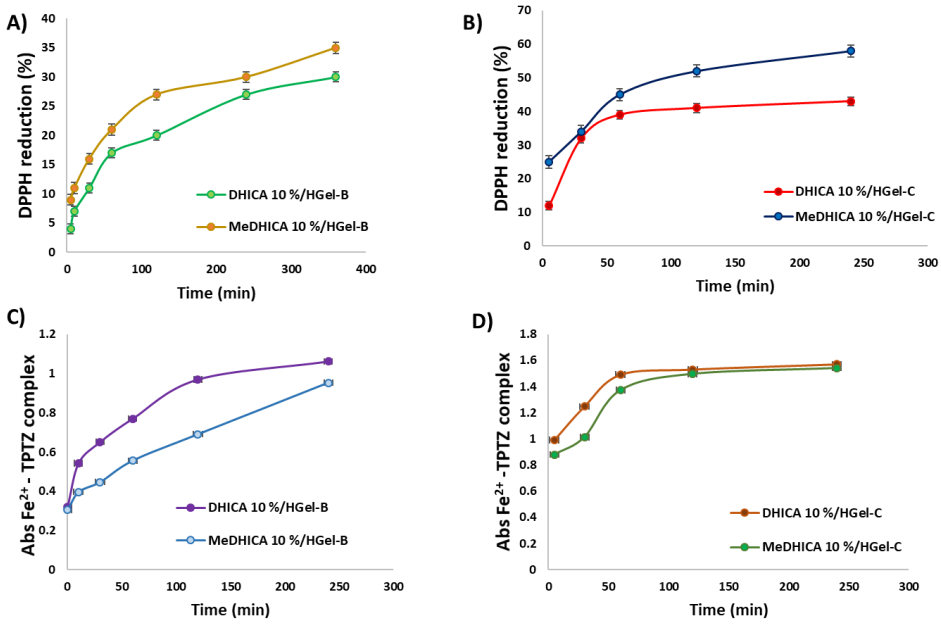

Figure 7.3.1. DPPH reduction of ***DHICA*** or ***MeDHICA 10 % CL gelatin 1*** (panel A) and ***10 % CL gelatin 2*** (panel B) over time; increase of the absorbance at 593 nm due to the Fe^{2+}-TPTZ complex of ***DHICA*** or ***MeDHICA 10 % CL gelatin 1*** (panel C) and ***10 % CL gelatin 2*** (panel D). The average values ± SD obtained from at least three separate experiments are reported.

That the antioxidant potency of the DHICA or MeDHICA incorporated into the gelatin systems (cross-linked or not) persisted even after prolonged gelatin storing (7 days or more) was demonstrated by immersing the DHICA loaded gelatin in the 200 μM DPPH solution at a 0.04 w/V ratio. Figure 7.3.2 shows that the reducing ability of the materials, depending on the extent of incorporation, increased over time reaching an almost complete consumption after 7 days.

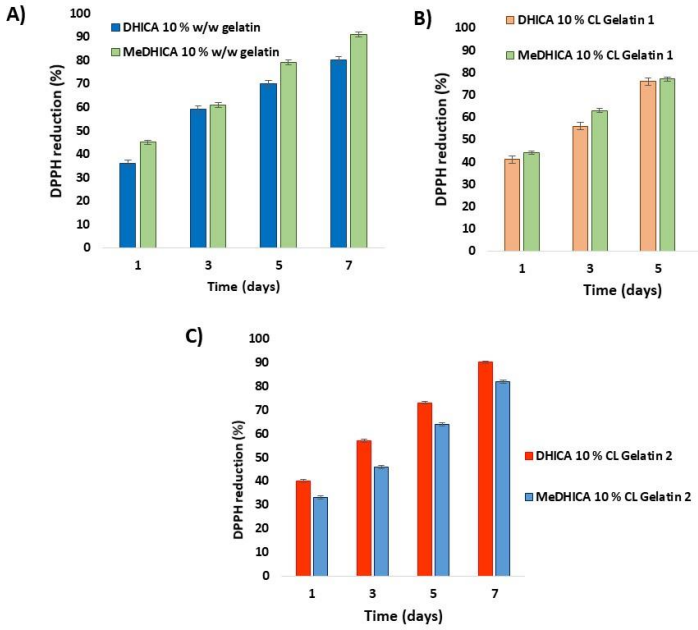

Figure 7.3.2. DHICA or MeDHICA loaded in: (a) *pristine gelatin*, (b) *CL gelatin 1*, (c) *CL gelatin 2* and immersed in DPPH solution (200 µM, 500 mL) up to 7 days.

7.4 Conclusions

The ability of gelatin-based hydrogels of incorporating and releasing under controlled conditions 5,6-dihydroxyindole-2-carboxylic acid (DHICA) and its methyl ester was investigated. In addition to porcine skin type A gelatin, two modified cross-linked gelatins obtained using a bifunctional agent and chitosan were prepared that showed higher mechanical strength at physiological temperatures. The gelatin based hydrogels so obtained could have different potential applications that is for topical uses or as scaffolds for cellular growth. In all cases a satisfactory loading and sustained release at physiological pHs of DHICA and the methyl ester were obtained while chemical assays confirmed the antioxidant power of the indoles incorporated into the gelatin network.

7.5 Experimental section

Material and methods

Gelatin type A from porcine skin, 2,2-diphenyl-1-picrylhydrazyl (DPPH), ferric chloride (III) hexahydrate and 2,4,6-tri(2-pyridyl)-s-triazine (TPTZ), 4-(4,6-dimethoxy-1,3,5-triazin-2-yl)-4-methylmorpholinium-chloride (DMTMM), chitosan, glacial acetic acid, were purchased from Sigma Aldrich. Phosphate buffer saline 10 X was purchased from VWR. DHICA and MeDHICA were prepared according to a procedure previously developed.[46,163]

The UV-vis spectra were recorded on a Jasco V-730 Spectrophotometer.

HPLC analyses were performed on a Agilent 1100 binary pump instrument equipped with and a SPD-10AV VP UV-visible detector using an octadecylsilane-coated column, 250 mm x 4.6 mm, 5 μm particle size (Phenomenex Sphereclone ODS) at 0.7 mL/min. Detection wavelength was set at 300 nm. Eluent system: 1 % formic acid-acetonitrile 85:15 v / v.

Loading of DHICA/MeDHICA into hydrogels and kinetics of release:

Gelatin-based system. For preparation of gelatin hydrogels, a specific amount of gelatin (10 % w/v) was initially dissolved and mixed in phosphate buffered solution (PBS) (pH = 7.4), maintained at 37 °C. After 5 min, DHICA solution (1, 5, 10 % w/w) or MeDHICA (10 % w/w) was added to a final volume of 2 mL and continuously stirred until the solution looks homogeneous. The hydrogels were set for gelation in vials for 12 h at 4 °C and then washed with 5 mL PBS (pH = 7.4) for 30 min to remove unreacted indole compounds. The kinetics of release of the indoles in PBS at pH 7.4 was then evaluated at room temperature by UV-vis analysis over 72 h by repeated refreshing the medium every 1 h.

Cross-linked gelatins. For preparation of *CL gelatin 1*, gelatin (1 g) was initially suspended in 10 mL of PBS, pH = 7.4, at 45 °C with continuous stirring till complete dissolution (1.5 h). DMTMM was then added (44 mg, 0.16 mmol), and the solution was kept under stirring at 45 °C for 30/45 s. Finally, the solution was poured in a 24 multiwell plate (1 mL per well), plugged, and after gelation the gels were kept at 37 °C for 2 h and finally freeze-dried. For preparation of *CL gelatin 2* (gelatin/chitosan 8:1 w/w), gelatin solution (10 % w/v) was poured into the chitosan solution (100 mg in 833 μL of 0.5 M acetic acid) and kept under stirring at 45 °C. After 24 h, DMTMM (18 mg, 0.064 mmol) was added and the solution was poured in cylindric molds and rested till gelations (5-10 min). After that the gels were kept at 37 °C for 2 h and then dried at 4 °C.

The *CL gelatin 1* and *2* were swelled in distilled water for 1 h or 4 h respectively. After that a proper amount of DHICA (5, 10 % w/w) or MeDHICA (10 % w/w) solution in PBS 1 X (pH 7.4) was loaded in the hydrogels. The optimum loading time was determined by UV-vis analysis over time monitoring the remaining indole in the solution. The kinetics of release of indole componds (DHICA 5, 10 % or MeDHICA 10 % from *CL gelatin 1* and DHICA/MeDHICA 10 % from *CL gelatin 2*) were determined in PBS pH 7.4 at 37 °C by UV-vis analysis over time. The medium was repeatedly refreshed after the first hour.

Stability of DHICA

10% CL gelatin 1 incorporating DHICA was immersed in PBS at 37°C and the release was monitored over 6 h without medium refreshing. The decay of DHICA free in the PBS solution at 37 °C at the same concentration estimated based on the incorporation for the DHICA in the system mentioned above was monitored by HPLC analysis.

Antioxidant properties of the DHICA/MeDHICA loaded gelatins:

2,2-diphenyl-1-picrylhydrazyl (DPPH) assay.[152] Briefly, aliquots of the medium of the indoles, released from ***10 % CL gelatin 1*** and ***2*** in PBS at 37 °C, were withdrawn in 200 μM DPPH solution in methanol and rapidly mixed. The reaction was followed by spectrophotometric analysis measuring the absorbance at 515 nm after 10 min. Values are expressed as the DPPH decay over time. The indoles loaded in gelatin systems (cross-linked and not) were instead immersed in 200 μM DPPH solution (500 mL) and the antioxidant power was evaluated by UV-vis recording spectra up to 7 days.

Ferric reducing/antioxidant power (FRAP) assay.[153] The FRAP reagent was prepared by mixing 0.3 M acetate buffer (pH 3.6), 10 mM 2,4,6-tris(2-pyridyl)-s-triazine in 40 mM HCl, and 20 mM ferric chloride in water, in the ratio 10:1:1. To a solution of FRAP reagent, aliquots of the medium of the indoles, released from ***10 % CL gelatin 1*** and ***2*** in PBS at 37 °C, were added and rapidly mixed. After 10 minutes, the absorbance at 593 nm was measured.

Supporting materials

The swelling profile was determined in water at 25 °C and the swollen weight of the hydrogels was recorded at every 10-min interval, after dabbing the hydrogels with a filter paper before weighing. Totally three replicas were run. The degree of swelling (SDi) was calculated as the following:

$$SD_i = [(M_{wi} - M_d) / M_d] \times 100\ \%$$

where M_{wi} is the swollen weight and M_d is the dry weight.

As shown in Figure S7.5.1, in the case of *CL gelatin 1*, the uptake of water is very rapid with respect to what observed for *CL gelatin 2*. For this latter after 6 h the swelling degree was found to be 800 % whereas that of *CL gelatin 1* reached 400 % at 4hrs.

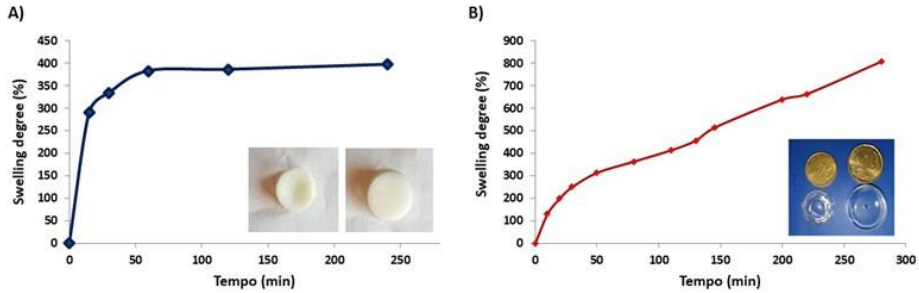

Figure S7.5.1. Digital pictures (before and after swelling in water) and swelling degree over time for *CL gelatin 1* (panel A) and *CL gelatin 2* (panel B).

As shown in Figure S7.5.2 different features were observed for the two hydrogels by means of Scanning Electron Microscopy (SEM). In particular, *CL gelatin 1* had a rough wrinkled surface with some holes while the *CL gelatin 2* exhibited a nonporous, smooth membranous phase consisting of dome shaped orifices and microfibrils.

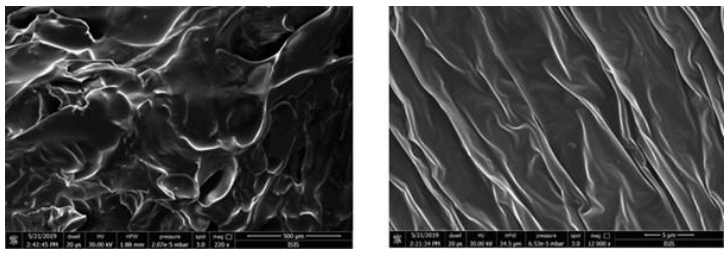

Figure S7.5.2. SEM images of CL gelatin 1 (left) and 2 (right).

Chapter 8

Synthesis and properties of cyanines based on the 1,4-benzothiazine scaffold

8.1 Introduction

The quest of organic chromophores exhibiting tailored electronic features has been extremely active during the last decades for the design and build up of new materials useful in several technological fields. In addition to chemical stability and intense absorption in the visible region, the design of functional dyes is focused on single molecule or polymer systems exhibiting photochromic, solvatochromic properties or any change of the chromophoric properties associated to modification of external parameters or aggregation state. In this connection biological chromophores representing the functional units of light harvesting systems or plant pigments have often been considered as a valuable inspiration or a starting basis in the design of the novel compounds.

An interesting nature-inspired class of compounds are cyanine dyes, a broad class of dyes structurally related to the pigments occurring in fruits and vegetable, the betacyanines, which exhibit red purple chromophores. These dyes feature organic nitrogen centers, one of the imine and the other of the enamine type, which may be included into an heterocyclic system, linked through a variable number of double bonds and some of these, like the indoline cyanines exhibit very high molar extinction coefficients (ranging from 150,000 to 250,000 $M^{-1}cm^{-1}$) and an intense fluorescence emission with potential application as fluorescence reporters and in laser technologies.[209,210] Moreover, cyanines are good candidates for developing

chemosensors because of their excellent photophysical properties, outstanding biocompatibility and low toxicity to living systems.[211,212]

Another class of natural chromophoric systems of potential practical interest is represented by indigoid nitrogenous heterocycles in which the chromophore contains two donor X (S or NH) and two acceptor groups (=O) arranged as shown to form a doubly cross-conjugated push-pull system (Figure 8.1.1)

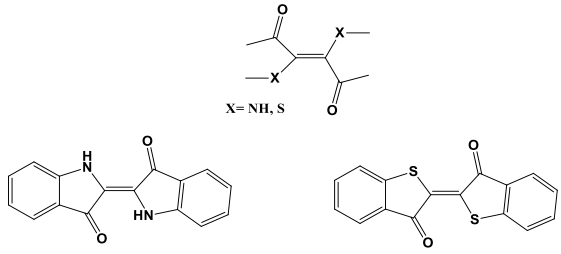

Figure 8.1.1. Indigoid system (top) and indigo chromophores (bottom).

A chromophore closely related to indigo that has been recently re-examined[213-215] is the $\Delta^{2,2'}$-bi-(2H-1,4-benzothiazine) (BBTZ), the core ring system of trichochromes[216] described above. In particular, this system exhibited a significant pH dependence and a marked photochromism under sunlight with reversible conversion in organic solvents of a yellow-orange species with an absoption maximum at 450 nm to a red one (λ_{max} = 470 nm) and a detectable shoulder around 530 nm. In acidic media, a deep violet chromophore was described as a result of a 100-nm bathochromic shift, a consequence of the peculiar disposition of the cross-conjugated push-pull systems which would be highly sensitive to protonation at the imine-type nitrogen(s) with consequent enhancement of the "pull" component. In addition, under strongly acidic conditions the initially-formed violet species, corresponding to the protonated derivative, undergoes

further protonation to give a blue species (λ_{max} 590 nm), identified as the dication (Figure 8.1.2).

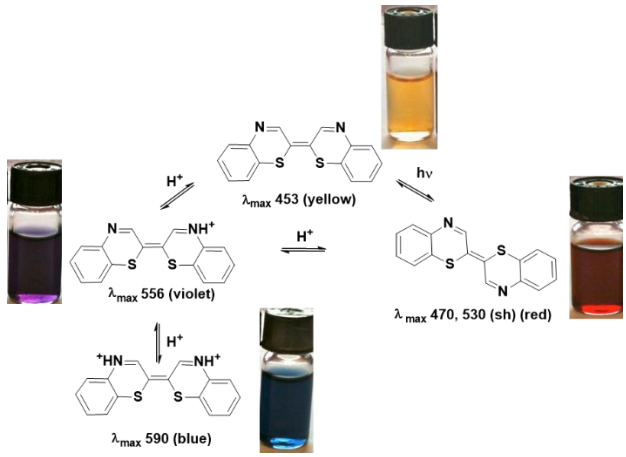

Figure 8.1.2. $\Delta^{2,2'}$-bi-(2H-1,4-benzothiazine) system.

Thus, inspired by the role the $\Delta^{2,2'}$-bi-(2H-1,4-benzothiazine) plays as the photoactive motif of red human hair, several studies were directed to investigate the potential of bibenzothiazine and more generally benzothiazine based dyes for biomedical or technological applications. In particular, further studies were focused on the 3-phenyl-1,4-benzothiazine, a stable benzothiazine obtained from the reaction of *o*-aminothiophenol with phenacyl bromide (Scheme 8.1.1), that differently from the 3-unsubstituted compound can be prepared in relatively large amounts and stored.[217,218]

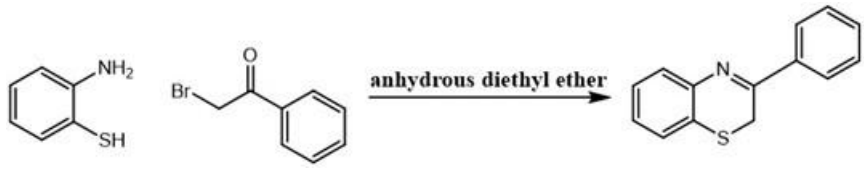

Scheme 8.1.1. Synthesis of 3-phenyl-(2*H*)-1,4-benzothiazine.

In the presence of micromolar peroxides or biometals (Fe(III), Cu(II), V(V) salts), and following a strong acid input, the stable 3-phenyl-(2*H*)-1,4-benzothiazine is efficiently converted to a green-blue $\Delta^{2,2'}$-bi(2H-1,4-benzothiazine) chromophore via dehydrogenative coupling of a 1,4-benzothiazinyl radical and proved to be a mixture of $\Delta^{2,2'}$-bi(3-phenyl-2*H*-1,4-benzothiazine) Z/E isomers (Figure 8.1.3), with potential practical interest for colorimetric detection of micromolar peroxides as well as of redox-active metal ions.[215]

Figure 8.1.3. Scheme of the conversion of the 3-phenyl-(2*H*)-1,4-benzothiazine to the green-blue $\Delta^{2,2'}$-bi(2H-1,4-benzothiazine).

In the search for new benzothiazine based functional dyes, further to the investigation of the $\Delta^{2,2'}$-bi-(2*H*-1,4-benzothiazine) system, another route was explored that may allow access to benzothiazine-based cyanines. These latter show an extension of the conjugated system as =N-C=CH-CH=C-S- compared to those exhibited by $\Delta^{2,2'}$-bi-(2*H*-1,4-benzothiazine), a characteristic that should expectedly result in a larger bathochromic shift in acid. All compounds, as shown in Figure 8.1.4, could be easily prepared in good yields by a facile condensation of 3-phenyl- or 3-methyl-2*H*-1,4-benzothiazines with *N*-dimethyl- or *o*-methoxyhydroxy-substituted benzaldehyde or cinnamaldehyde derivatives. With

all compounds, a significant bathochromic shift (*ca.* 100 nm) was observed upon protonation, which resulted in a marked modification and intensification of the visible color.[219]

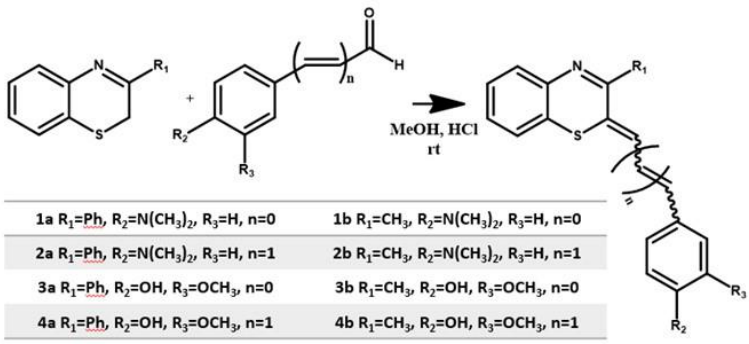

Figure 8.1.4. Synthesis of benzothiazine cyanines.

Overall these data indicate that the new cyanine-type scaffold displays four distinct control points enabling efficient property tailoring and tuning: 1) benzothiazine imine center which provides the primary proton sensitive element allowing for absorption shift and/or for complementary color/emission switch; 2) the 3-substituent on the benzothiazine ring, through which emission can be allowed or blocked; 3) the extension of the π bridge, which finely tunes electronic communication between the push-pull structural elements, and 4) the nature of the electron-donating substituent(s) on the phenyl ring that allows for chromophore tuning at given pH ranges. This versatile dye platform allowed to access to an expandable palette of colors and was used to implement an unprecedented single-use asymmetric molecular cryptography system (Figure 8.1.5).[219]

Figure 8.1.5. Color changes and charge states of trichocyanines under different pH conditions.

On these bases, the research reported in this chapter was focused on:

1) the preparation of new benzothiazine-based systems by reaction of the easily accessible 3-phenyl-(2H)-1,4-benzothiazine with aromatic and heteroaromatic aldehydes and dialdehydes;
2) the structural characterization of the benzothiazine systems obtained and the evaluation of their absorption properties.

8.2 Reaction of 3-phenyl-(2*H*)-1,4-benzothiazine with monoaldehydes

In a first series of experiments the conditions for the reaction between 3-phenyl-(2H)-1,4-benzothiazine and benzothiazole-2-carboxaldehyde or indole-3-carboxaldehyde were optimized starting from those previously developed for the condensation of 3-phenyl-(2H)-1,4-benzothiazine with aldehydes, involving

acetonitrile as the solvent in the presence of HCl. TLC analysis of the reaction mixtures run at different concentrations of the acid showed that concentrations as high as 2.5 M are required to get a satisfactory and rapid consumption of the reagents and to minimize by-products formation. In addition, the reaction proved faster with an almost complete consumption of the starting reagents at 3 h when the temperature was raised from 25 °C to 70 °C. In subsequent experiments, the stoichiometric ratio of the two reagents was varied in the range benzothiazine/aldehyde 1:1, 2:1 and 3:1. A 1:1 molar ratio proved, in both cases, the optimal condition to favour product formation over by-products deriving by dimerization of the benzothiazine as assessed by comparative analysis with a reference $\Delta^{2,2'}$-bi(1,4-2H-benzothiazine) compound.

Based on these observations the reaction was run in the presence of benzothiazole-2-carboxaldehyde, in 12 M HCl/acetonitrile 1:4 v/v, at 70 °C and on preparative scale. After 3 h, acetonitrile was removed under reduced pressure and the mixture red in color was extracted with chloroform. TLC analysis (eluent cyclohexane/ethyl acetate 8:2 v/v) of the residue obtained from the combined organic layers showed the presence of a major yellow product at R_f 0.63, which was purified by column chromatography using cyclohexane/ethyl acetate 98:2 as eluent in 35% yield.

MALDI/MS spectrometry of the pure product indicated a pseudomolecular ion peak $[M+H]^+$ at m/z 371, as expected for the condensation product **1** (Scheme 8.2.1).

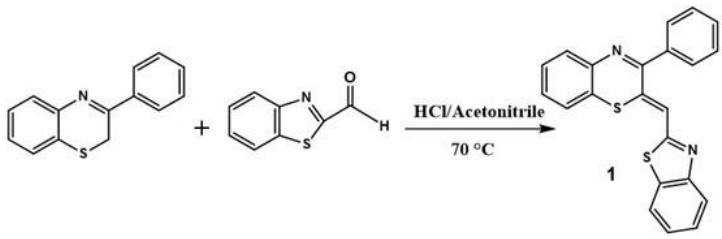

Scheme 8.2.1. Reaction of 3-phenyl-(2H)-1,4-benzothiazine with benzothiazole-2-carboxaldehyde.

The product was then subjected to a complete spectral characterization (Figures S8.6.1-8.6.5) which was consistent with the structure proposed for compound **1**. The complete assignments of ^{1}H and ^{13}C NMR resonances for **1** as deduced by a detailed analysis of the 2D-NMR experiments are reported in Figure 8.2.1.

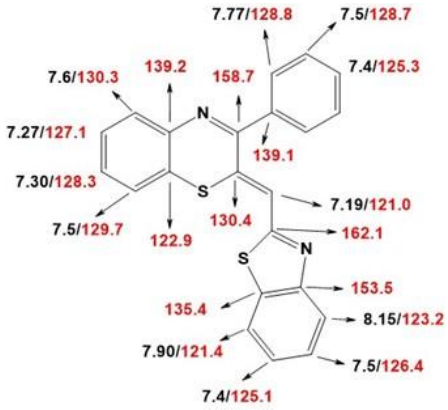

Figure 8.2.1. ^{1}H (black) and ^{13}C (red) NMR resonances of cyanine **1**.

The configuration of the double bond formed in the condensation reaction was assigned as *Z* based on the NOESY spectrum (Figure 8.2.2) showing a cross-peak between the singlet at δ 7.19 and the signal at δ 7.77 due to the phenyl protons at C-2.

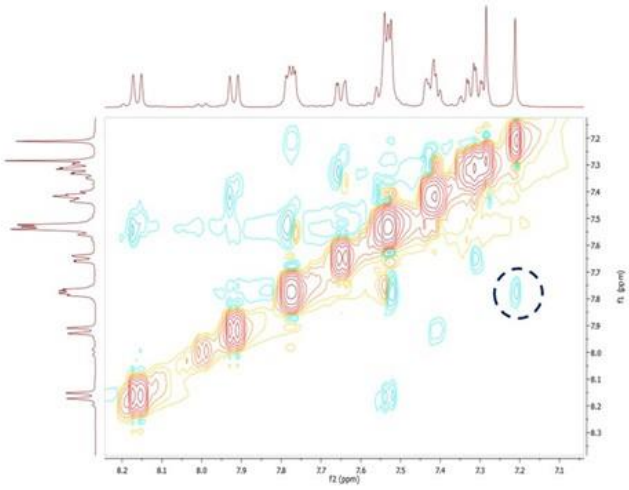

Figure 8.2.2. NOESY spectrum of cyanine **1.**

In subsequent experiments, the reaction was repeated with indole-3-carboxaldehyde using the same conditions described for the synthesis of cyanine **1** that is in 12 M HCl/acetonitrile 1:4 v/v, at 70°C. After 3 h the formation of a main component at R_f 0.42 along with other minor products was observed. However, when the reaction was run on a preparative scale, the organic phases gradually turned from red to purple, and the product at R_f 0.42 also decayed to give more polar compounds, a process that can be likely attributed to the acidity of the chloroform used as the extraction solvent. Accordingly, in subsequent experiments the mixture, after removal of acetonitrile, was extracted with ethyl acetate and the main product was isolated in pure form with moderate yields (*c.a.* 20 %) after purification on preparative TLC.

MALDI mass spectrometry analysis in positive reflectron mode of the pure product indicated a pseudomolecular ion peaks $[M+H]^+$ at m/z 353, as expected for the condensation product **2** (Scheme 8.2.2).

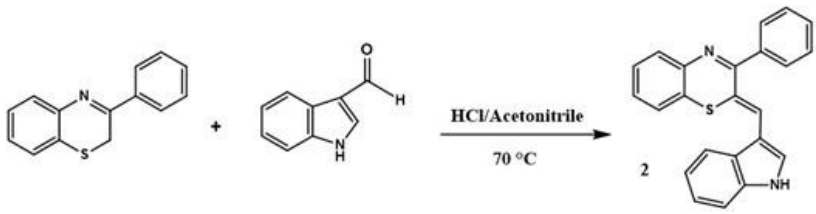

Scheme 8.2.2. Reaction of 3-phenyl-(2H)-1,4-benzothiazine with indole-3-carboxaldehyde.

The product was then subjected to a complete spectral characterization (Figures S8.6.6-8.6.10) which was consistent with the structure proposed for compound **2**. The complete assignments of ^{1}H and ^{13}C NMR resonances for **2** as deduced by a detailed analysis of the 2D-NMR experiments are reported in Figure 8.2.3.

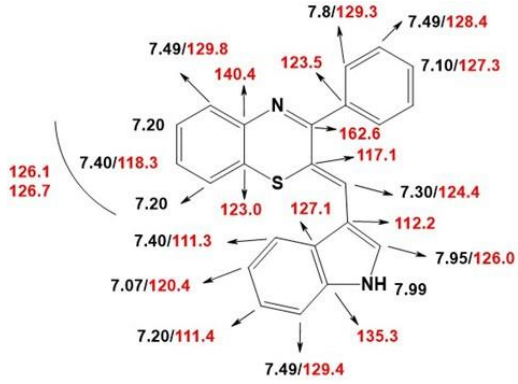

Figure 8.2.3. ^{1}H (black) and ^{13}C (red) NMR resonances of cyanine **2**.

As in the case of **1**, the NOESY spectrum (Figure S8.6.11) allowed to assign the Z configuration to the double bond formed in the condensation reaction (cross-peak between the singlet at δ 7.30 and the signal at δ 7.8 of the phenyl protons at C-2).

8.3 Reaction of 3-phenyl-(2*H*)-1,4-benzothiazine with dialdehydes

The most intuitive strategy to obtain symmetric benzothiazine cyanines from 3-phenyl-(2*H*)-1,4-benzothiazine would imply the build-up of a conjugated bridge between the two units by reaction with suitable dialdehydes such as glyoxal. In preliminary experiments, the reaction was run under the same conditions described for the preparation of **1** and **2**, but in the presence of ten molar equivalents of glyoxal in order to ensure a complete consumption of the starting benzothiazine. After 2 h acetonitrile used as the solvent was removed and the aqueous acid phase was extracted with chloroform. TLC analysis (eluent cyclohexane/ethyl acetate 8:2) showed the presence of a main product (R_f 0.57), red in color, together with traces of other products. The main component of the reaction was isolated in pure form (55 %) by column chromatography fractionation (eluent cyclohexane/ethyl acetate 98:2) and subjected to a complete spectroscopic characterization leading to formulation of the symmetric structure **3** shown in Scheme 8.3.1.

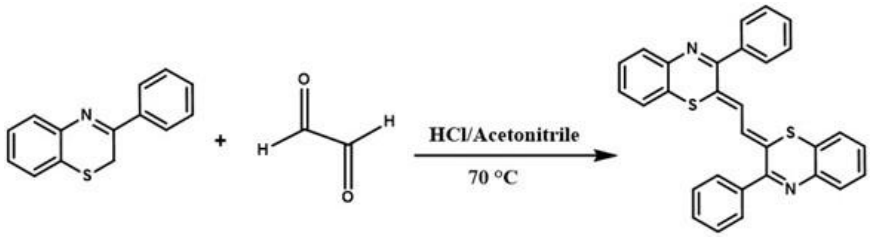

Scheme 8.3.1. Reaction of 3-phenyl-2H-1,4-benzothiazine with glyoxal.

Complete 2D NMR analysis (Figures S8.6.12-8.6.16) led to assign the resonances for compound **3** as reported in Figure 8.3.1.

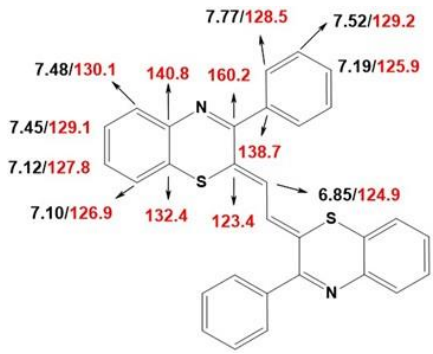

Figure 8.3.1. ^{1}H (black) and ^{13}C (red) NMR resonances of cyanine **3**.

Assignment of the double bond configuration by spectroscopic techniques like ROESY contact was not conclusive. The relative stability of the possible isomers that is the Z,Z isomer in the *s-trans* conformation was evaluated by computational analysis at the DFT level (the analysis was run at the Dept of Chemistry, University of Naples Federico II in the frame of a collaborative work with Prof. O. Crescenzi).

8.4 Characterization of the pH-dependent cyanine chromophores

The chromophoric properties of cyanines **1**-**3** were systematically investigated over the whole pH range in order to characterize a possible acidichromic behavior (Figures S8.6.17-8.6.19). As shown in Figure 8.4.1, cyanine **1** showed two absorption maxima under neutral conditions (λ = 336, 432 nm). Below pH 7.0, the two bands underwent a bathochromic shift (λ = 343, 467 nm) likely due to the formation of a new species that is prevalent in 1 M HCl. Another shift, presumably due to the formation of a further species, was observed at higher concentrations of the acid (λ = 355, 518 nm). The molar extinction coefficient (ε) for the neutral

form was determined at 336 nm (16961 ± 35 $M^{-1}cm^{-1}$) and 432 nm (10979 ± 45 $M^{-1}cm^{-1}$).

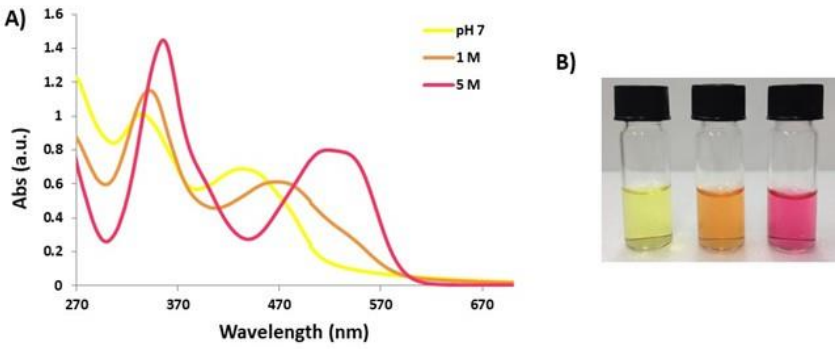

Figure 8.4.1. a) UV-vis absorption spectra of the neutral and acid forms of cyanine **1** (in methanol or methanol HCl), (b) digital pictures of cyanine **1** in methanol, in methanol/0.1 M HCl and methanol/5 M HCl (from left to right).

Considering the structure of cyanine **1** which has two protonation sites, that is the nitrogen of the benzothiazolic system and that of the benzothiazine moiety, identification of the first protonation site is not straightforward. To address this issue the spectrophotometric behaviour of 2-methylbenzothiazole as a model compound was investigated under different pH conditions. Figure 8.4.2 showed a complete bathochromic shift of the absorption maxima of the neutral form 251 nm to 271 nm at pH 1.0, in good agreement with the pKa values reported for other benzothiazoles.[220] On this basis it could be argued that the first protonation site of cyanine **1** is the benzothiazole nitrogen atom.

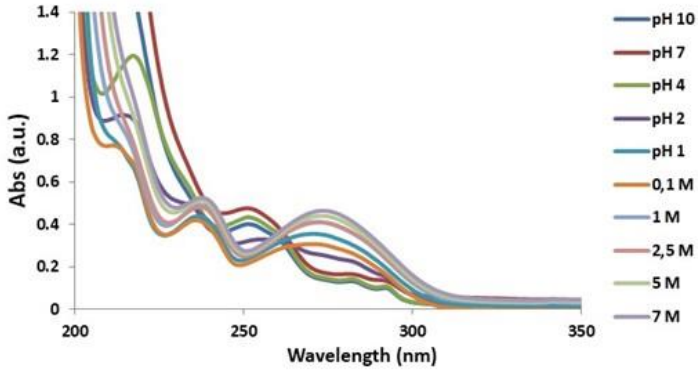

Figure 8.4.2. UV-vis absorption spectra of 2-methylbenzothiazole at different pH values and different HCl concentrations.

Three absorption maxima at λ = 277, 332, 444 nm (as shown in Figure S8.6.18) were observed in the pH range 4-10, whereas at pH 2.0 the band at higher wavelength underwent a large bathochromic shift from 444 to 545 nm, while the other bands shifted from 277 to 281 nm and from 332 to 344 nm (Figure 8.4.3). This shift is likely due to the protonation of the benzothiazine moiety. The higher basicity of this nitrogen with respect to that of cyanine **1** may be interpreted considering the stabilization in the protonated form provided by the indole nitrogen (Figure 8.4.4). The molar extinction coefficients (ε) for the neutral form were found to be 10462 ± 38 $M^{-1}cm^{-1}$ at 332 nm, and 5403 ± 48 $M^{-1}cm^{-1}$ at 444 nm.

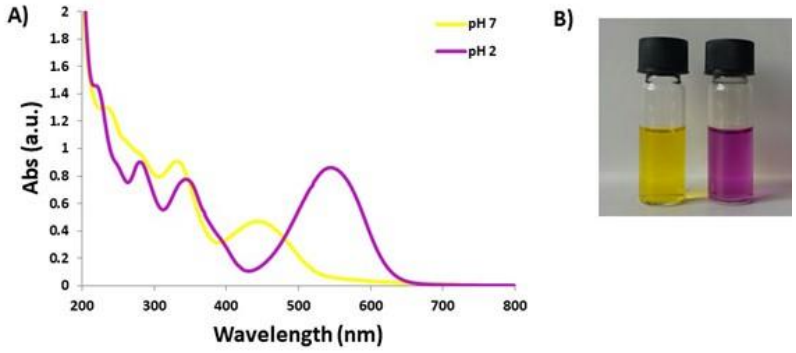

Figure 8.4.3. a) UV-vis absorption spectra of the neutral and protonated form of cyanine **2** (in methanol or methanol HCl), (b) digital pictures of cyanine **2** in methanol (neutral form, left) and in a buffered solution at pH 2.0 (protonated form, right).

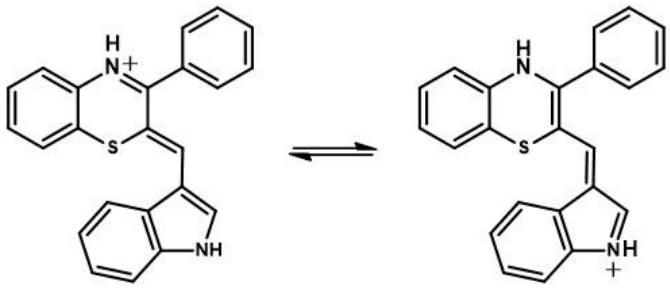

Figure 8.4.4. Structure of protonated cyanine **2**.

In other experiments the UV-vis absorption properties of cyanine **3** were analyzed too under different pH and acid conditions as described above (Figure S8.6.19). As shown in Figure 8.4.5 the cyanine **3** showed an absorption maximum at 474 nm in methanol or at neutral pHs, with a first bathochromic shift to 500 nm in 0.5 M HCl, and a further shift to 643 nm in 2.5 M HCl. These absorption changes may be interpreted in terms of different states of protonation of the two benzothiazine nitrogen corresponding to the neutral, monocation and dication forms. This is in line with the results obtained in a previous study for the $\Delta^{2,2'}$-bibenzothiazine,

although in the case of **3** the bathochromic shift observed on acidification was greater on account of the more extended conjugation of the monocation of the cyanine compared to that of the analog $\Delta^{2,2'}$-bibenzothiazine.[219]

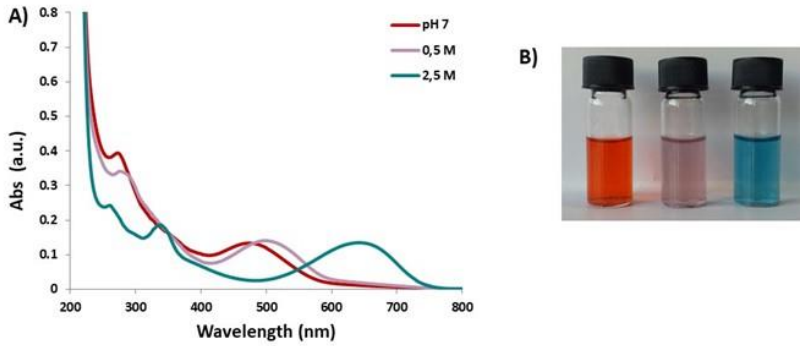

Figure 8.4.5. a) UV-vis absorption spectra of the neutral (ε = 7075 ± 55 $M^{-1}cm^{-1}$) and of acid (ε = 9725 ± 45 $M^{-1}cm^{-1}$) forms of cyanine **3** (in methanol or methanol HCl); b) from left to right: digital pictures of cyanine **3** in methanol (neutral form), in methanol/0.5 M HCl (monocation form) e methanol/2.5 M HCl (dication form).

8.5 Conclusions

In the present chapter the preparation of new 1,4-benzothiazine based cyanine type chromophores has been described starting from 3-substituted 1,4-benzothiazines, namely the 3-phenyl-(2H)-1,4-benzothiazine, pursuing two different approaches: one based on the condensation of the benzothiazine with aromatic aldehydes, in order to obtain a more extended conjugate system between the donor and the acceptor groups, and the other involving reaction with a dialdehyde, glyoxal, that would allow for the build-up of a conjugated bridge between the two benzothiazine units. All the products obtained have been characterized with respect to the chromophoric properties and acidichromic behavior. Notably all the observed shifts proved to be reversible for each cyanine. The ease of the synthetic

procedures and the expected facile scale-up together with the peculiar acidichromic behaviour of these compounds would hint to their exploitation as pH sensors or related applications.

8.6 Experimental section

Materials and methods

Phenacyl bromide, benzothiazole-2-carboxyaldehyde, indole-3-carboxaldehyde, glyoxal, were purchased from Sigma-Aldrich; *o*-aminothiophenol was purchased from Fluka.

UV-vis spectra were recorded with a Jasco V-560 UV-vis spectrophotometer.

^{1}H NMR and ^{13}C NMR spectra were recorded in $CDCl_3$ at 400 and 500 MHz on a Bruker 400 MHz spectrometer. ^{1}H, ^{1}H COSY, ^{1}H, ^{13}C HSQC, and ^{1}H, ^{13}C HMBC were run at 400 MHz using Bruker standard pulse programs.

Positive Reflectron MALDI spectra were recorded on a AB Sciex TOF/TOF 5800 instrument using 2,5-dihydroxybenzoic acid as the matrix. Spectrum represents the sum of 15,000 laser pulses from randomly chosen spots per sample position. Raw data are analyzed using the computer software provided by the manufacturers and are reported as monoisotopic masses.

Analytical and preparative TLC were carried out on silica gel plates (0.25 and 0.50 mm, respectively) from Merck. Cyclohexane/ethyl acetate 8:2 v/v (eluent A); cyclohexane/ethyl acetate 98:2 v/v (eluent B); cyclohexane/ethyl acetate 80:20 v/v (eluent C); dichloromethane/cyclohexane 80:20 (eluent D); cyclohexane/ethyl acetate 85:15 (eluent E).

Synthesis of 3-phenyl-(2H)-1,4-benzothiazine. A solution of *o*-aminothiophenol (1.1 mL) in anhydrous ethyl ether (5 mL) was treated at room temperature with a solution of phenacyl bromide (2.2 g) in anhydrous ethyl ether (25 mL) under magnetic stirring. After 2 h the reaction mixture was filtered, and the yellow solid washed with ethyl ether and dried. On TLC analysis (eluent A, R_f = 0.7) the solid proved to be pure (2.50 g, 82% yield).

ESI^+MS: *m/z* 226 ($[M+H]^+$); UV: λ_{max} (CH_3OH) 323 nm; ^1H NMR ($CDCl_3$) δ (ppm): 4.16 (s, 2H), 7.40-7.45 (m, 3H), 7.48 (m, 1H), 7.68 (t, *J* = 8 Hz, 2H), 7.80 (t, *J* = 8 Hz, 1H) , 8.47 (d, *J* = 8 Hz, 2H); ^{13}C NMR ($CDCl_3$) δ (ppm): 27.86 (CH_2), 125.55 (CH), 125.60 (C), 127.37 (CH), 128.28 (CH), 129.81 (CH × 2), 131.01 (CH), 131.78 (CH × 2), 134.46 (C), 137.31 (CH), 139.39 (C), 164.10 (C).

Reaction of 3-phenyl-(2*H*)-1,4-benzothiazine with benzothiazole-2-carboxaldehyde. 3-phenyl-(2*H*)-1,4-benzothiazine (100 mg, 0.44 mmol) and benzothiazole-2-carboxaldehyde (72.5 mg, 0.44 mmol) were dissolved in acetonitrile (8 mL) and 12 M hydrochloric acid (2 mL). The mixture was taken under stirring at 70 °C for 3 h. TLC analysis (eluent A) showed the presence of a main yellow component (R_f = 0.63) and other by-products. The solution, after removal of acetonitrile, was extracted with water and chloroform, and the organic layers were dried over anhydrous sodium sulphate and taken to dryness. The residue thus obtained was separated by column chromatography (eluent B) to give the pure product 57.6 mg, 35% yield.

UV: λ_{max} (CH_3OH) 336 nm, 432 nm; MALDI+MS: *m/z* 371 ($[M+H]^+$); ^1H NMR ($CDCl_3$) δ (ppm): 7.19 (s, H), 7.28-7.32 (m, 2H), 7.4 (m, 2H), 7.5 (m, 4H), 7.6 (d, *J* = 7.64 Hz, 1H) , 7.7 (m, 2H), 7.90 (d, *J* = 8 Hz, 1H), 8.15 (d, *J* = 8 Hz, 1H); ^{13}C NMR ($CDCl_3$) δ (ppm): 121.5 (CH), 121.9 (CH), 123.4 (C), 123.7 (CH), 125.7 (CH), 125.8 (CH), 126.9 (CH), 127.6 (CH), 128.8 (CH), 129.2 (CH × 2), 129.4

(CH × 2), 130.2 (CH), 130.9 (C), 131.3 (CH), 135.9 (C), 139.6 (C), 139.7 (C), 154.0 (C), 159.2 (C), 162.6 (C).

Reaction of 3-phenyl-(2H)-1,4-benzothiazine with indole-3-carboxaldehyde. 3-phenyl-(2H)-1,4-benzothiazine (50 mg, 0.22 mmol) and indole-3-carboxyaldehyde (25.8 mg, 0.17 mmol), were dissolved in acetonitrile (4 mL) and 12 M hydrochloric acid (1 mL). The mixture was taken under stirring at 70 °C for 3 h. TLC analysis (eluent A) showed the presence of a main yellow product (R_f = 0.42) and other by-products. The solution, after removal of acetonitrile, was extracted with water and ethyl acetate, and the organic layers were dried over anhydrous sodium sulphate and taken to dryness. The products were separated by preparative TLC (eluent C) to give a pure product (15.6 mg, 20% yield).

UV: λ_{max} (CH_3OH) 332 nm, 444 nm; MALDI+MS: *m/z* 353 ([M+H]+); ^{1}H NMR ($CDCl_3$) δ (ppm): 7.07 (m, H), 7.10 (m, H), 7.20 (m, 3H), 7.30 (s, H), 7.40 (m, 2H), 7.49 (d, 3H), 7.8 (m, 2H), 7.95 (s, H), 7.99 (s, H); ^{13}C NMR ($CDCl_3$) δ (ppm): 111.3 (CH), 111.4 (CH), 112.2 (CH), 117.1 (C), 118.3 (CH), 120.4 (CH), 123.0 (C), 123.5 (C), 124.4 (CH), 126.0 (CH), 126.1 (CH), 126.7 (CH), 127.1 (C), 127.3 (CH), 128.4 (CH x 2), 129.3 (CH x 2), 129.4 (CH), 129.8 (CH), 135.3 (C), 140.4 (C), 162.6 (C).

Reaction of 3-phenyl-(2*H*)-1,4-benzothiazine with glyoxal. 3-phenyl-(2*H*)-1,4-benzothiazine (100 mg, 0.44 mmol) dissolved in acetonitrile (8 mL) and 12 M hydrochloric acid (2 mL) was treated with glyoxal (258 mg, 4.44 mmol). The reaction was carried out at 70 °C under stirring. After 2 h TLC analysis (eluent A) showed the presence of a main component (R_f = 0.57) and other by-products. The solution, after removal of acetonitrile, was extracted with water and chloroform, and the organic layers were dried over anhydrous sodium sulphate and taken to

dryness. The residue thus obtained was separated by column chromatography (eluent B) to give the pure product 58 mg, 55% yield.

UV: λ_{max} (CH_3OH) 474 nm; MALDI+MS: *m/z* 473 ($[M+H]^+$); ^1H NMR ($CDCl_3$) δ (ppm): 6.85 (s, 1H), 7.10 (m, 1H), 7.12 (m, 1H), 7.19 (m, 1H), 7.45 (m, 1H), 7.48 (m, 1H), 7.52 (m, 2H), 7.77 (m, 2H); ^{13}C NMR ($CDCl_3$) δ (ppm): 123.4 (C), 124.9 (CH), 125.9 (CH), 126.9 (CH), 127.8 (CH), 128.5 (CH × 2), 129.1 (CH), 129.2 (CH × 2), 130.1 (CH), 132.4 (C), 138.7 (C), 140.8 (C), 160.2 (C).

Supporting materials

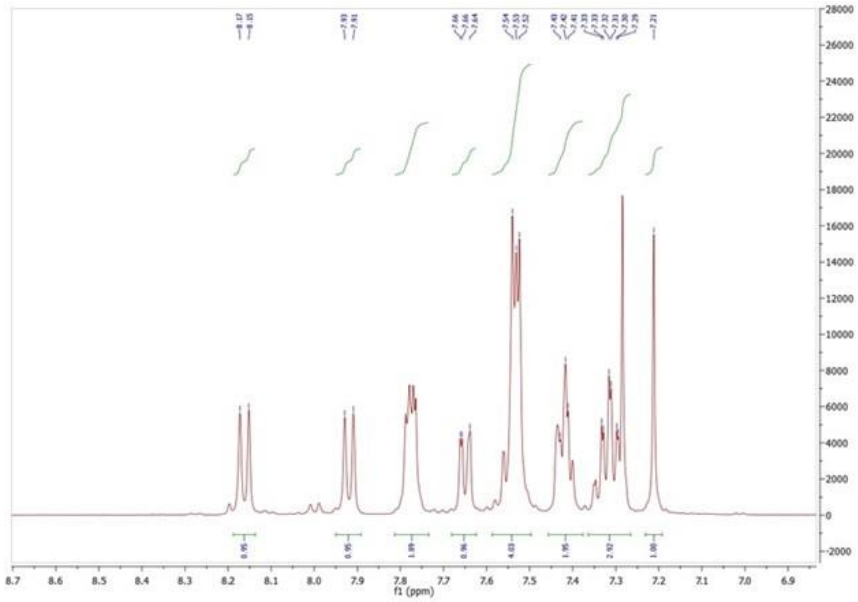

Figure S8.6.1. ^1H NMR spectrum of cyanine **1** in $CDCl_3$.

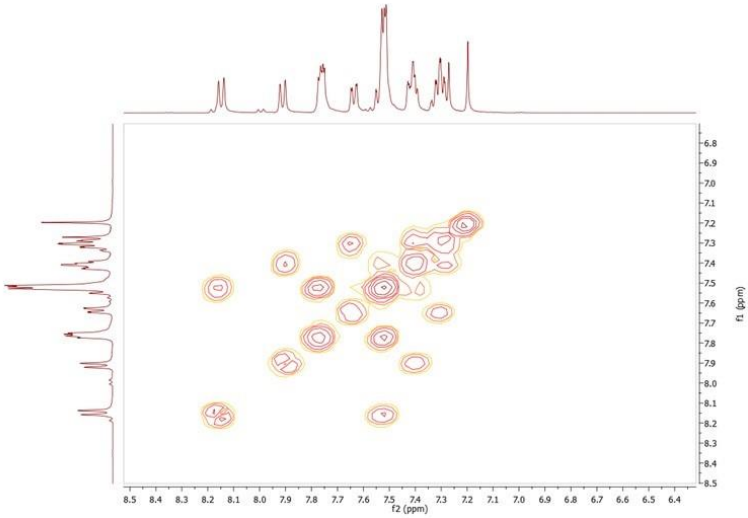

Figure S8.6.2. ^{1}H,^{1}H COSY spectrum of cyanine **1**.

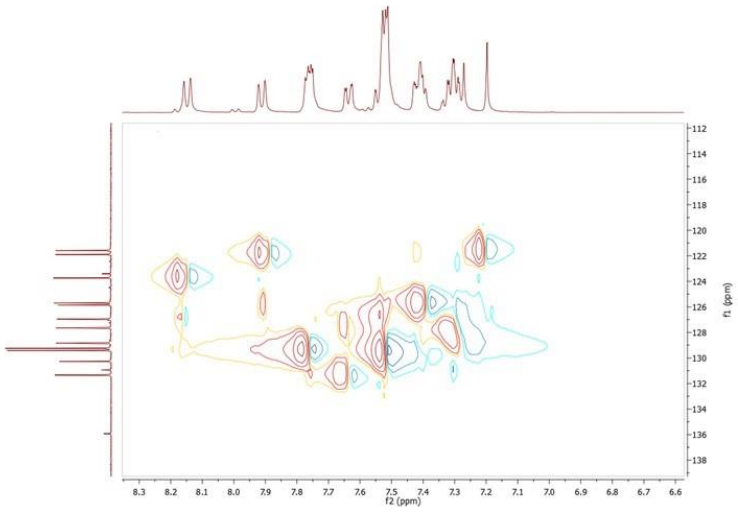

Figure S8.6.3. ^{1}H, ^{13}C HSQC spectrum of cyanine **1**.

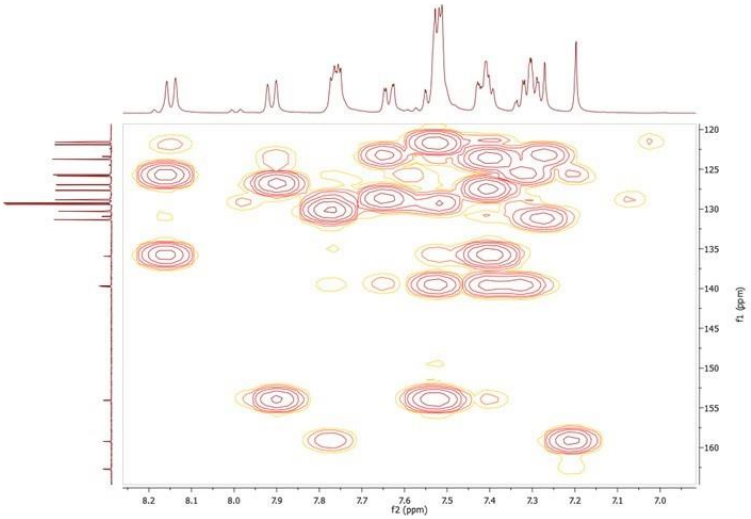

Figure S8.6.4. ^{1}H, ^{13}C HMBC spectrum of cyanine **1**.

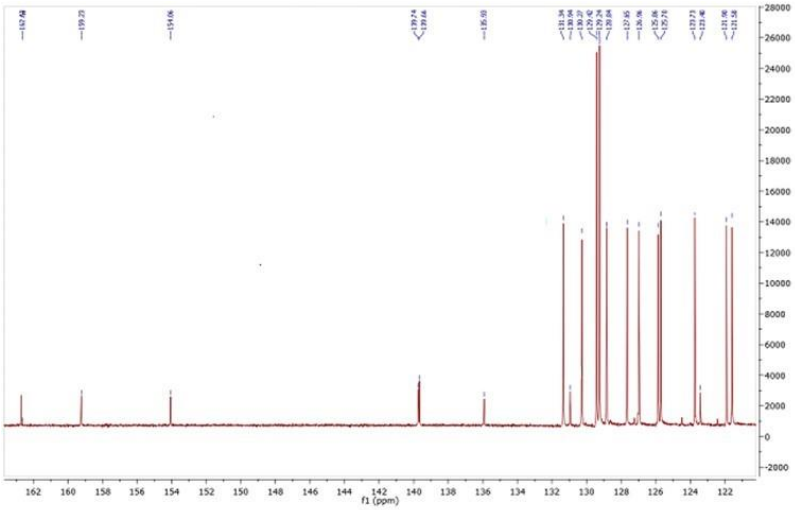

Figure S8.6.5. ^{13}C NMR spectrum of cyanine **1** in $CDCl_3$.

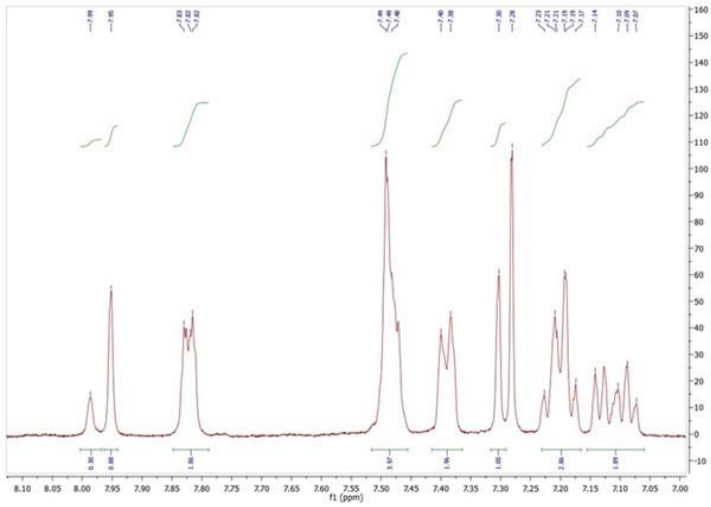

Figure S8.6.6. ^{1}H NMR spectrum of cyanine **2** in $CDCl_3$.

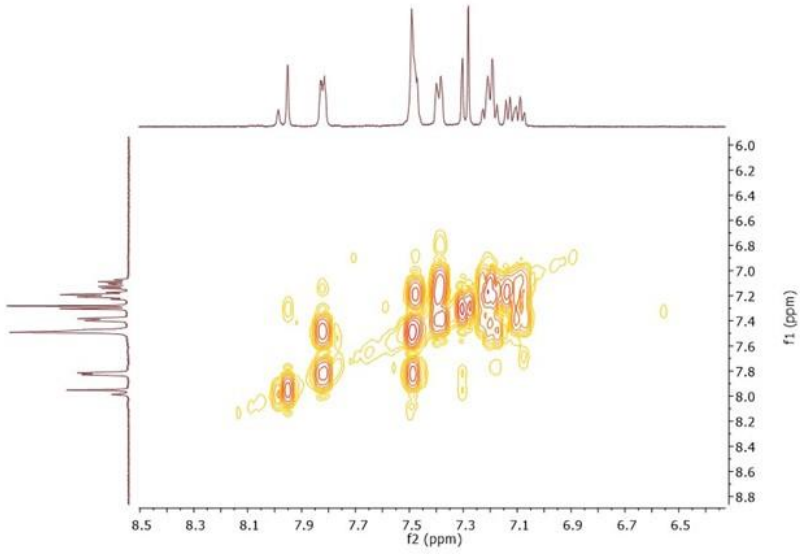

Figure S8.6.7. $^{1}H,^{1}H$ COSY spectrum of cyanine **2**.

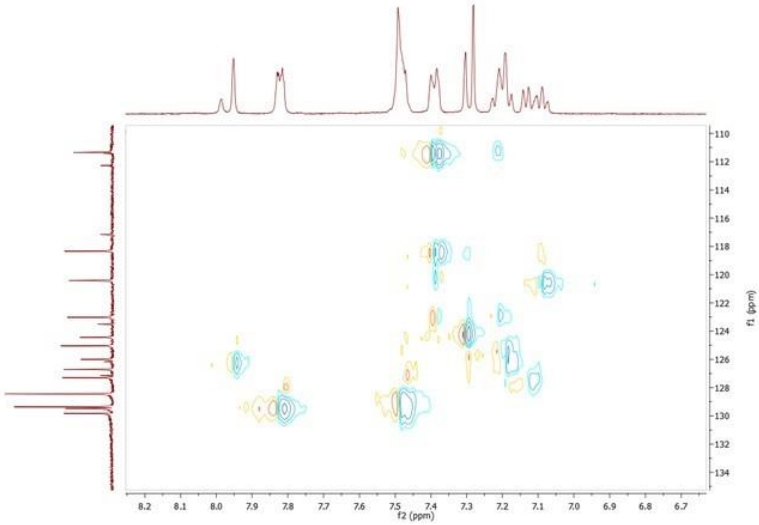

Figure S8.6.8. ^{1}H, ^{13}C HSQC spectrum of cyanine **2**.

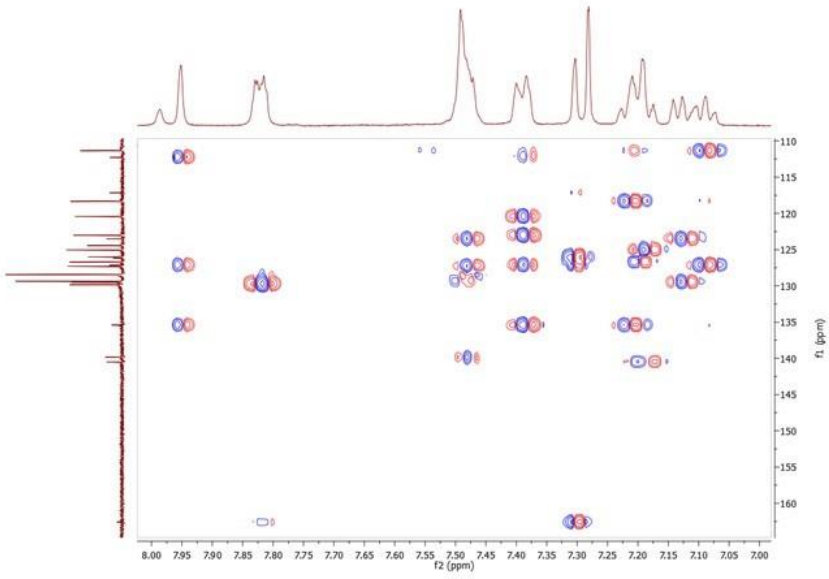

Figure S8.6.9. ^{1}H, ^{13}C HMBC spectrum of cyanine **2**.

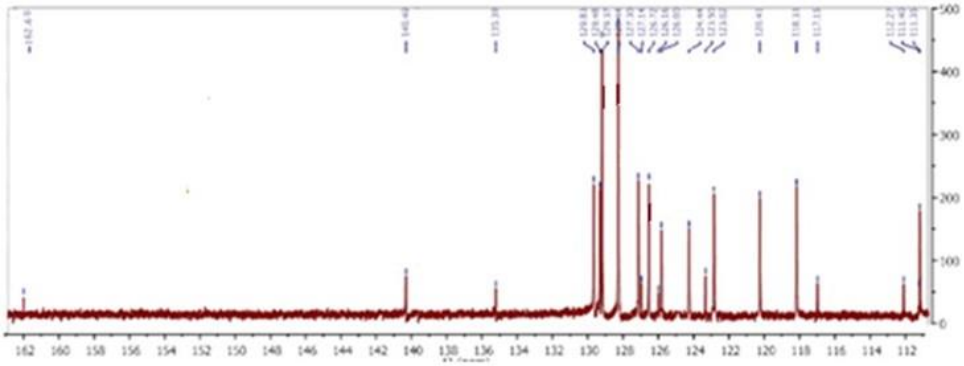

Figure S8.6.10. ^{13}C NMR spectrum of cyanine **2** in $CDCl_3$.

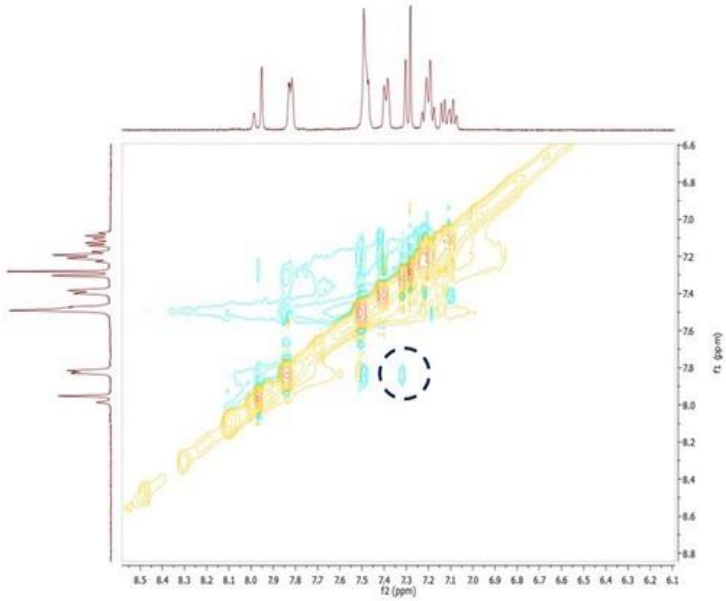

Figure S8.6.11. NOESY spectrum of cyanine **2**.

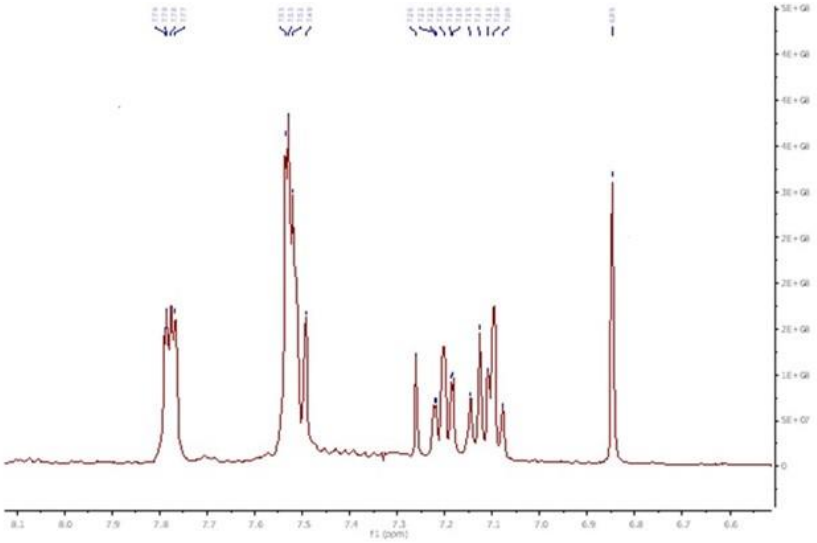

Figure S8.6.12. ^{1}H NMR spectrum of cyanine **3** in $CDCl_3$.

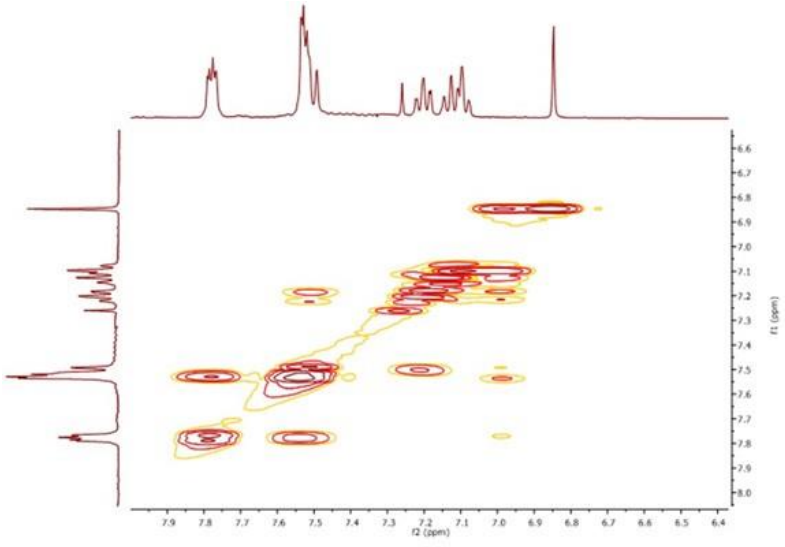

Figure S8.6.13. $^{1}H,^{1}H$ COSY spectrum of cyanine **3**.

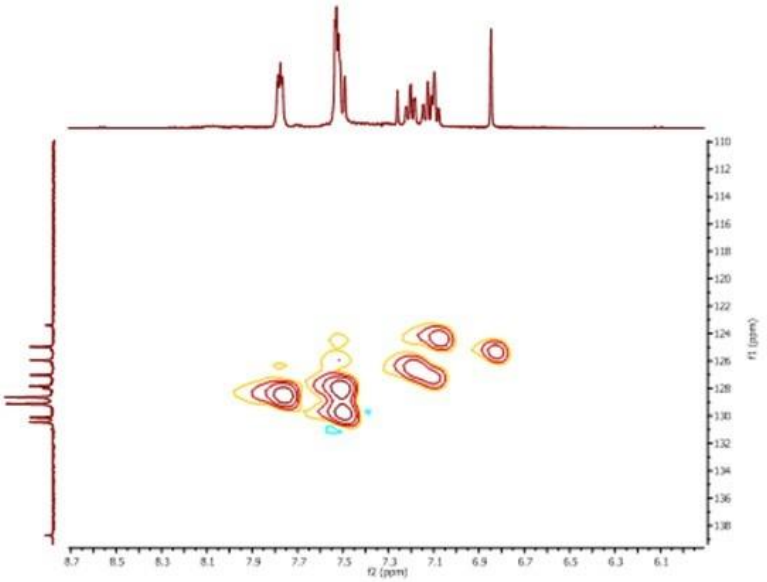

Figure S8.6.14. ^{1}H, ^{13}C HSQC spectrum of cyanine **3**.

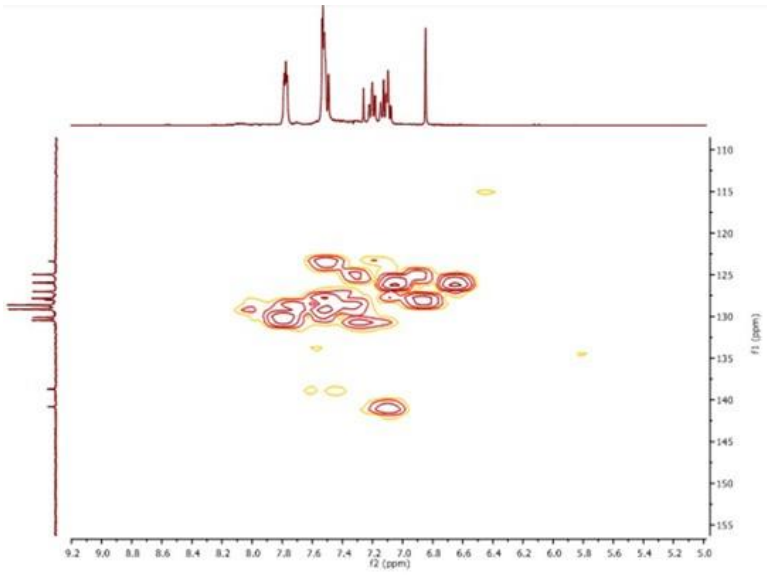

Figure S8.6.15. ^{1}H, ^{13}C HMBC spectrum of cyanine **3**.

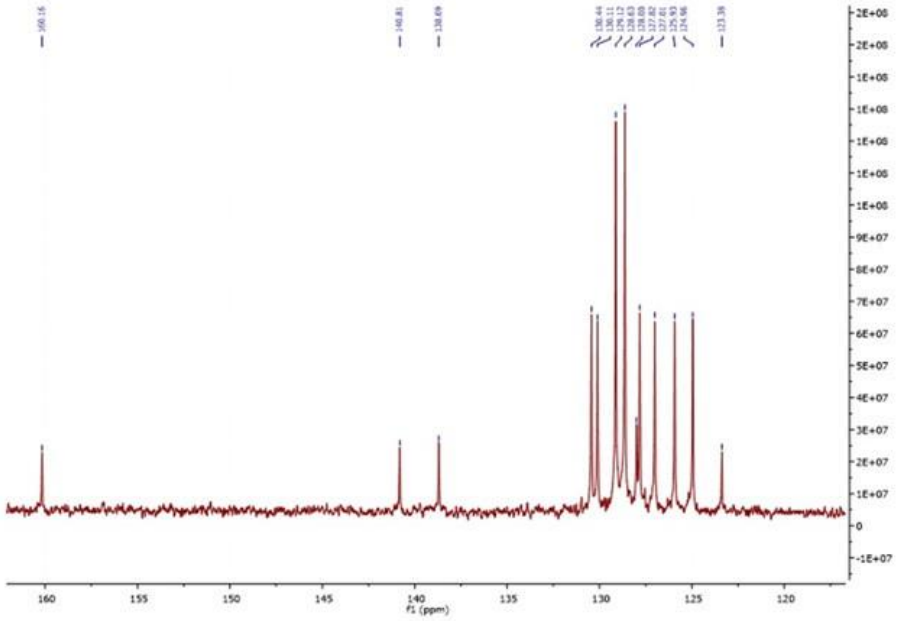

Figure S8.6.16. ^{13}C NMR spectrum of cyanine **3** in $CDCl_3$.

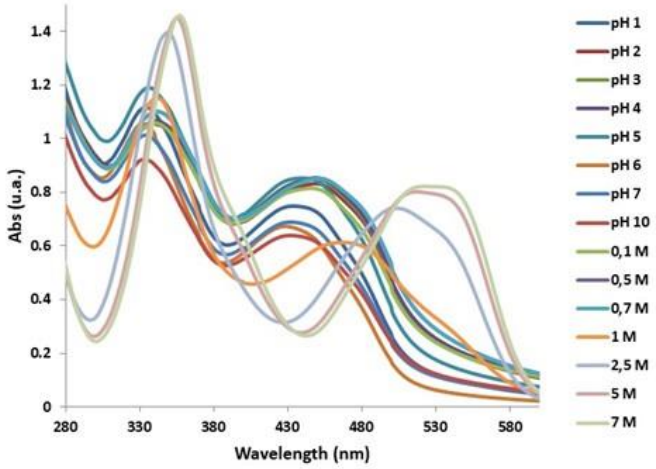

Figure S8.6.17. UV-vis absorption spectra of cyanine **1** at different pHs and different HCl concentrations.

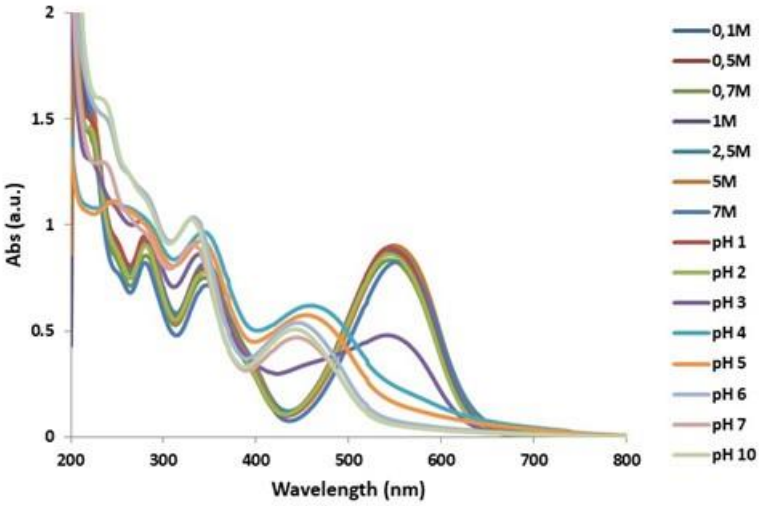

Figure S8.6.18. UV-vis absorption spectra of cyanine **2** at different pHs and different HCl concentrations.

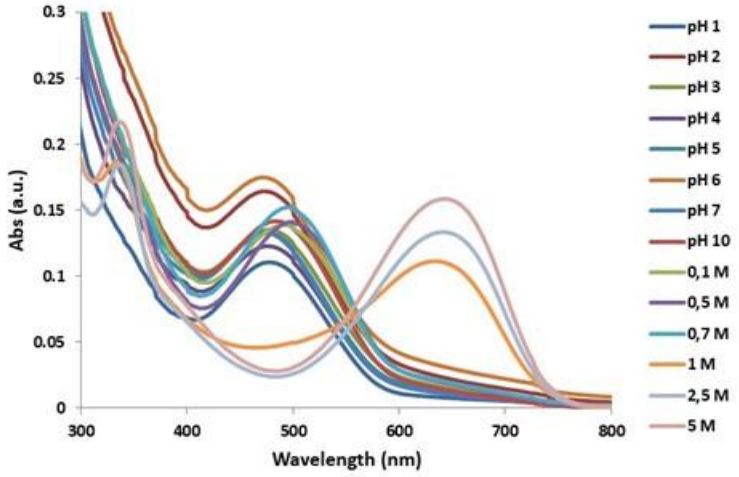

Figure S8.6.19. UV-vis absorption spectra of cyanine **3** at different pHs and different HCl concentrations.

Chapter 9

Redox activity of natural and synthetic melanins

As introduced in the previous chapters, melanins are classified into the black-brown eumelanin or the reddish pheomelanin. Either pigments are biosynthesized by tyrosinase catalyzed oxidation of the amino acid L-tyrosine leading to dopaquinone (Scheme 9.1). As illustrated in Chapter 5, when concentration of sulfhydryl compounds is low, the oxidation of dopaquinone proceeds with intramolecular cyclization leading to 5,6-dihydroxyindole (DHI) and 5,6-dihydroxyindole-2-carboxylic acid (DHICA), that in turn undergo oxidative polymerization to form eumelanin.[159] When L-cysteine is present in melanosomes at sufficient levels, it undergoes a non-enzymatic conjugation with dopaquinone forming the isomers 5-S- and 2-S-cysteinyldopa (5SCD and 2SCD) at a 5:1 ratio.[221] As a result, the intramolecular cyclization pathway of 5,6-dihydroxyindole formation leading to eumelanin polymers is completely or partially inhibited, and an alternate 1,4-benzothiazine route to pheomelanins becomes dominant.

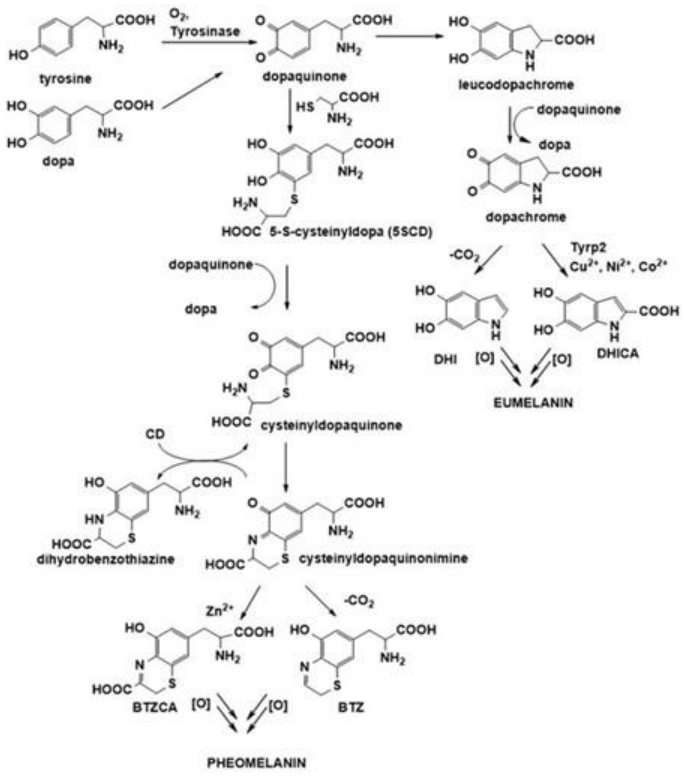

Scheme 9.1. Biosynthetic pathways leading to eumelanins and pheomelanins.

Synthetic melanins can react with both oxidizing and reducing species because the hydroquinone and quinone subunits allow them to act both as electron donor and acceptor. It is generally accepted that eumelanin exhibits UV-protection function[222] whereas pheomelanin has been implicated in the enhanced melanoma susceptibility of people with red hair and fair skin[223] due to the capacity of this pigment to act as a potent photosensitizer leading to intense production of reactive oxygen species (ROS, *e.g.* hydrogen peroxide and superoxide anions) in response to UV-visible light irradiation.[224,225] In addition, chemical studies indicated that natural and synthetic pheomelanins, derived from the oxidation of 5-S-

cysteinyldopa (5SCD), can sustain autoxidation of cellular antioxidants (*e.g.*, glutathione and NADH) in the presence of oxygen with concomitant production of ROS.[43,226] Recent data from EPR experiments suggested that pheomelanin can promote GSH and NADH autoxidation via direct H-atom exchange. The subsequent re-oxidation of reduced pheomelanin by oxygen may generate ROS and restore the free-radical population and thus sustaining a redox cycle.[226]

Despite melanins have spurred much interest through the years, for their biological role but also for their potential as soft and biocompatible functional organic materials, the limited solubility of these pigments in most organic solvents has rendered challenging the understanding of its physicochemical properties, including the electrochemical ones. These latter methodologies have been largely employed in the past years to evaluate the antioxidant activities of food phenolics,[227,228] mimic oxidative drug metabolism,[229] and correlate the biological activities of bioreductive antitumor drugs to their redox potentials.[230]

In recent studies pheomelanins and eumelanins pigments isolated from human hair as well model synthetic pigments prepared by enzymatic oxidation of dihydroxyphenylalanine (DOPA) or 5SCD, have been analysed for the redox behavior by use of an electrochemically-based reverse engineering methodology that allows to characterize the functionality of complex technological and biological systems.[231] The reverse engineering approach requires that the sample is exposed in the solid state to controlled redox perturbations and the output response is then analyzed. Specific features of this technique are the following (summarized also in Figure 9.1):

a. the insoluble melanin sample is entrapped in a thin, non-conducting permeable hydrogel film (*e.g.* aminopolysaccharide chitosan) and is localized near an electrode surface;
b. soluble mediators (*e.g.* $Ru(NH_3)_6Cl_3$ (Ru^{3+})) can shuttle electrons between the sample and the underlying electrode, thus providing redox connectivity between the melanin sample and the electrode and this overcomes the major limitation of electrochemical analysis of insoluble samples;[232]
c. input voltages are applied to the underlying electrode and the potentials are transmitted to the samples through the soluble mediators;
d. the output currents are measured and analyzed to assess the redox activites of the entrapped melanin.

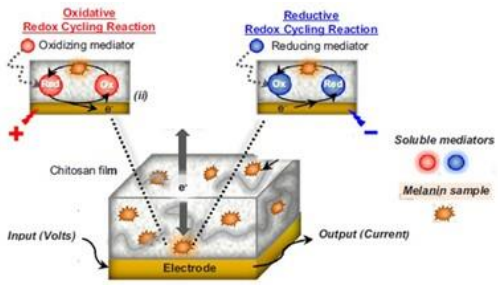

Figure 9.1. Schematic overview of the reverse engineering electrochemical methodology applied to melanin.[233]

A brown, insoluble, melanin-like pigment, the neuromelanin, occurs in the catecholaminergic neurons of the *Substantia Nigra* of human and primates. In recent years, research on neuromelanin has attracted much attention because of its possible role in the pathogenesis of Parkinson's disease, a neurodegenerative disorder associated with the oxidative stress and the selective death of melanin-containing neurons of the *Substantia Nigra*. Currently, it is widely accepted that

the degeneration of dopaminergic neurons, involves mitochondrial dysfunction, the formation of neurotoxic oligomers of alphasynuclein, the dysfunction of protein degradation systems, neuroinflammation, and oxidative and endoplasmic reticulum stress. Epidemiological evidence links exposure to the pesticide paraquat (PQ) to the onset of Parkinson's disease, and this link has been explained by a redox cycling mechanism that induces oxidative stress. On the other hand, insoluble melanin retains redox activity and can accept electrons from reductants and donate electrons to O_2 to generate ROS.[234] Clearly direct investigation of neuromelanin is hampered by the difficulties to access to the material.[235] Yet, based on determination of electrochemical potentials and chemical degradation analyses[171,236] it has been proposed that neuromelanin has a shell-core structure with eumelanin representing the outer layer grown (derived from oxidation of the dopamine) on a pheomelanin highly oxidant nucleus (derived from cysteinyldopamine).[237]

To investigate the redox properties of neuromelanin and whether these features may be critical for the role played by the pigment in the Parkinson's disease by mediating the toxicity of environmental pollutants like paraquat, the electrochemically-based reverse engineering methodology was applied to melanins models of neuromelanin. The results of these experiments run by Professor Payne of the University of Maryland and his research group using model pigments prepared at University of Naples in the frame of the PhD project are reported in the following.

With in mind the core shell model of neuromelanin two model melanins were selected namely:

- a natural melanin from cuttlefish (Sepia melanin) because it is commercially available, it is composed of eumelanin, and it has been used as a model to investigate solute−melanin interactions (*e.g.*, for metal binding);[235,238]
- a synthetic model melanin having a cysteinyldopamine−melanin core and dopamine−melanin shell.[239,240]

Both melanins were firstly entrapped in a nonconducting hydrogel film adjacent to an electrode and then immersed in solutions containing PQ (putative redox cycling reductant) and a redox cycling oxidant (ferrocene dimethanol). To engage reductive and oxidative redox cycling, sequences of input potentials (*i.e.*, voltages) were imposed to the underlying electrode and output sequences of input potentials (*i.e.*, voltages) were imposed to the underlying electrode analyzed. The response characteristics of the PQ−melanin systems to various input potential sequences support the hypothesis that PQ can directly donate electrons to melanin (Figure 9.2).

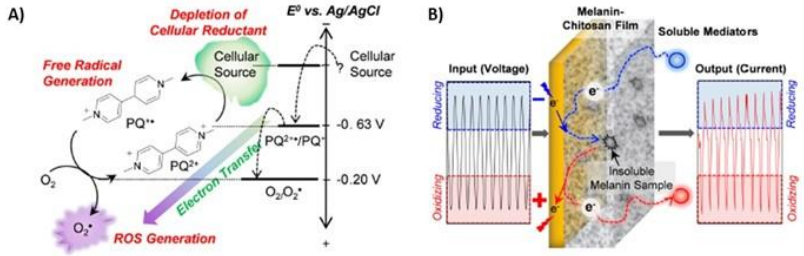

Figure 9.2. (a) Redox-cycling of paraquat (PQ) that contribute to oxidative stress by the depletion of cellular antioxidants or the generation of reactive oxygen species; (b) *in vitro* electrochemistry-based reverse engineering method to evaluate redox-interaction between insoluble melanin and soluble mediators.

Although, these observations of PQ-melanin redox cycling *in vitro* did not prove that such mechanisms were operative *in vivo*, nor did they revealed a role for such a mechanism in disease pathologies, it was possible to demonstrate a redox interaction between two components, PQ and melanin, that have been individually linked to oxidative stress and the etiology of Parkinson's disease.

In the frame of the collaborative work with Professore Payne, further experiments were also directed to demonstrate whether, in addition to toxins, drugs could also undergo redox-cycling with both natural melanin like Sepia melanin and a core−shell model of neuromelanin like synthetic cysteinyldopamine- dopamine. For instance, two drugs acetaminophen (N-acetyl-p-aminophenol, APAP) and clozapine were selected (Figure 9.3).

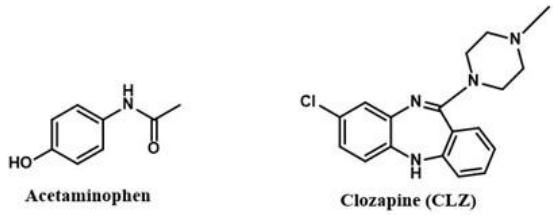

Figure 9.3. Acetaminophen and Clozapine structures.

Several studies have demonstrated that acetaminophen, one of the most largely used drugs,[241] can undergo redox cycling in the liver, a process that is believed to be responsible for the liver damage associated with APAP overdoses whose toxic effects can occur also in the brain.[243] Interestingly, more recent studies have suggested that APAP has also antioxidant properties and at low doses can have protective effect against oxidative stress-induced brain toxicity and neurodegeneration.[243,244]

As to the other drug selected Clozapine (CLZ), this is a second generation antipsychotic with polypharmacological activities.

The results obtained by electrochemistry-based reverse engineering method showed that both drugs could engage the entrapped melanin in oxidative redox-cycling reactions that serve to transfer electrons from melanin to the electrode when an oxidative electrode voltage is imposed. Since the capacity of the melanin to supply electrons is finite and can be depleted by this oxidative redox-cycling, the Ru^{3+} mediator was added and reducing voltages were also imposed that allowed the Ru^{3+} to engage melanin in the reductive redox-cycling mechanism that mediates the transfer of electrons from the electrode to melanin (Figure 9.4). A sequence of voltage inputs was further imposed at the electrode to control these redox-cycling reactions. Specifically, the imposed voltage sequence can be purposefully tailored to probe for specific redox information and the input sequence can be rapidly changed without requiring the addition or deletion of chemical reagents. Finally, the electron transfer reactions at the electrode result in electrochemical currents and these response characteristics were analyzed to detect and characterize the drug-melanin redox-cycling. These *in vitro* observations suggest that the redox activities of drugs may be relevant to their modes of action, and that melanins may interact with drugs in ways that affect their activities, metabolism, and toxicities. Moreover, these results demonstrated that melanins have reversible redox activities, can exchange electrons with various reductants and oxidants, and can quench radicals either by donating or accepting electrons and motivated the use of mediated electrochemical probing for characterizing additional materials whose functions rely on redox properties.

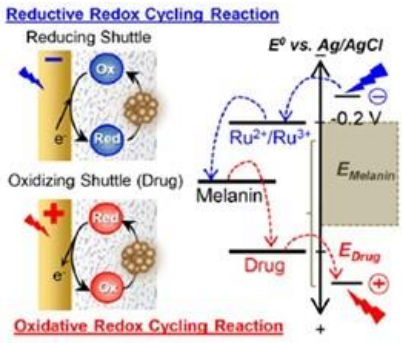

Figure 9.4. Redox-cycling interactions with melanin: reductive redox-cycling with $Ru(NH_3)_6Cl_3$ (Ru^{3+}) transfers electrons from the electrode to melanin and oxidative redox-cycling with either APAP or CLZ transfers electrons from melanin to the electrode.

9.1 Experimental section

Synthetic melanin preparation. 5-S-cysteinyldopamine was prepared on gram scale by adding to 10 mmol dopamine in 2 M H_2SO_4 20 mmol of ceric ammonium nitrate in 100 mL of 2 M H_2SO_4. The resulting orange reaction mixture was poured to a vigorously stirred solution of L-cysteine (5 g) in 50 mL of 2 M H_2SO_4. The resulting mixture was then purified using a Dowex equilibrated with 2 N HCl and the 5-S-cysteinyldopamine was recovered as a pale brown residue in the chlorhydrate form (Scheme 9.1.1). The purity of the product was checked by HPLC, which revealed no contamination by other isomers or unreacted dopamine. Cysteinyldopamine melanin was prepared by peroxidase/H_2O_2 oxidation in 0.1 M phosphate buffer (pH 6.8). The mixture was allowed to stand at room temperature under vigorous stirring for 2 h and then acidified to pH 3.0. The melanin precipitate was collected by centrifugation, washed three times with 1 % acetic acid and lyophilized. The core−shell melanin was prepared by cysteinyldopamine melanin induced oxidation of dopamine (dopamine/cysteinyldopamine melanin 1:1 w/w) as previously described[237] with the exception that the oxidation mixtures were not

acidified for recovery of the melanin pigments but were washed with water three times before drying by lyophilization.

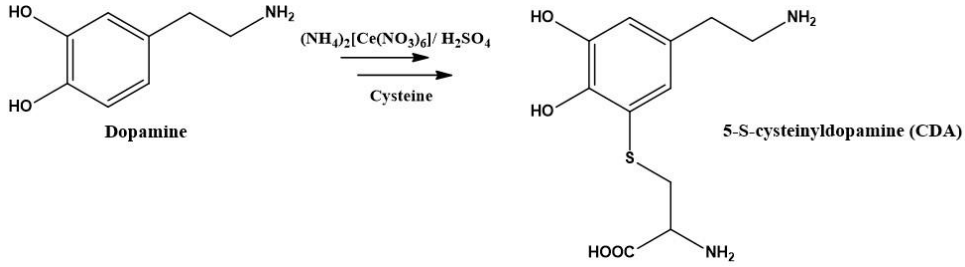

Scheme 9.1.1. Procedure of the synthesis of 5-S-cysteinyldopamine.

Chapter 10

Biomimetic phenolic polymers: evaluation of the structural determinants of the antioxidant activity

10.1 Introduction

Because oxidative stresses cause a number of diseases, including skin deterioration, cardiovascular diseases, carcinogenesis and neurodegeneration, the search of novel antioxidants without severe toxicity has been a very active field. Several evidences have indicated a link between dietary intake of antioxidants and a reducing of the risk of chronic and degenerative diseases.[25,244,245]

In this frame bioinspired phenolic polymers exhibit a wide range of interesting properties, first of all as antioxidants thanks to their distinctive carbogenic diversity and the tunable redox behaviour, and are currently exploited for a variety of applications, including the preparation of resins[246-248] and surface functionalization[249] (*e.g.* for blood-contacting biomaterials and medical device), drug delivery systems[250] or the stabilization of polymers in packaging,[251-253] but also as biomaterial additives to favor cell growth and differentiation.[254-256] Polyphenols are, infact, widely distributed in renewable plant resources such as fruits, leaves, and wood and have recently spurred much interest their substrate-independent adsorption,[257] UV absorption,[258] radical-scavenging,[259] and metal-sequestering properties.[260] Most polyphenols are small organic molecules, not macromolecules, and have both catechol and gallol groups in their chemical structures.

Expected advantages of phenolic polymers with respect to the monomers would include lower volatility (with reduced adverse effects), greater chemical stability under processing conditions, more practical processing, coating and incorporation into polymer blends and lower tendency to be released from the polymer into the contact medium (food, water, etc.).

Despite phenol polymerization can be carried out with a range of chemical oxidants, including typically ferricyanide and persulfate, a most convenient alternative route, to produce biocompatible and stable functional polymers, relies on the ability of peroxidase enzymes to catalyze in a highly efficient manner the oxidative coupling of phenols and substituted phenols under mild and eco-friendly reaction conditions.[251,261] Enzyme-based polymerization processes attract growing interest due to their environmental compatibility associated with the use of catalytic amounts of the enzyme and H_2O_2 as an easily available low-cost oxidant. The reaction on monophenolic substrates proceeds via one-electron oxidation leading to the generation of phenoxyl radicals intermediates, which evolve via sequential oxidative coupling steps. Relevant examples of bioinspired phenolic polymers include poly(caffeic acid methyl ester), poly(pyrogallic acid) and polytyrosol (Figure 10.1.1).[251,252, 261,262]

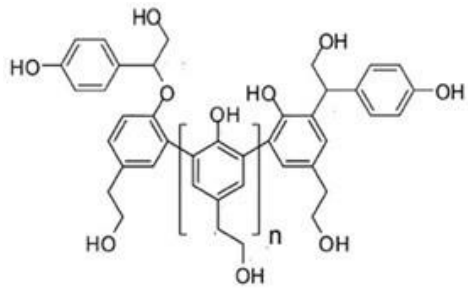

Figure 10.1.1. Proposed representative structures of polytyrosol (OligoTyr).

Although phenolic polymers are highly attractive in terms of biocompatibility, bioavailability, biodegradability and tailorability, actually only little informations about the structure-property-activity relationship are available, in particular as to whether phenolic polymers display structure-dependent patterns of antioxidant reactivity and what structural motifs actually provide the optimal antioxidant power against free radicals and other oxidants.[263] The evaluation of the antioxidant potential could be, in fact, used both for investigative purposes and to guide rational antioxidant design.

On these bases, the research work described in the next paragraph was directed to assess the structural determinants of the antioxidant activity in biomimetic phenolic polymers.

10.2. Structure-antioxidant activity relationships in phenolic polymers

A promising approach to inquire into the structural and chemical basis of the antioxidant activity of phenolic polymers for screening purposes may be represented by EPR spectroscopy. Natural or synthetic phenolic polymers are usually characterized by the presence of intrinsic, EPR-detectable free radical centers, commonly attributed to comproportionation equilibria, *i.e.* the redox equilibrium between fully reduced, fully oxidized, and semi-reduced (semi-oxidized) phenolic units.[49] The antioxidant and radical scavenging activity of phenolic polymers can conceivably be related to the ability of the material to donate electrons or H-atoms at a low energetic cost[25] and to sustain delocalization of resulting unpaired electrons across the aromatic systems. Following recent observations on synthetic melanin polymers from 5,6-dihydroxyindole (DHI) and 5,6-dihydroxyindole-2-carboxylic acid (DHICA), in which was demonstrated that

the highest antioxidant activity, exhibited in the 2,2-diphenyl-1-picrylhydrazyl (DPPH) assay, was associated to a narrow signal in the EPR spectra, it seemed that analysis of EPR spectral features may likely yield useful information on antioxidant properties of phenolic polymers.[45]

In this view a systematic investigation was carried out on a panel of nine biocatalytically-produced phenolic polymers for which a detailed analysis of the EPR spectra was coupled with evaluation of five different antioxidant activity profiles.

Three distinct sets of monomers were thus considered among cheap, non-toxic and easily accessible: monophenols, (tyrosol (TYR), vanillic acid (VA), p-coumaric acid (COUM), and ferulic acid (FER)); diphenols, (catechol (CAT), 4-methylcatechol (MCAT), and caffeic acid (CAF)); triphenols (pyrogallol (PYR) and gallic acid (GA)) (Scheme 10.2.1).

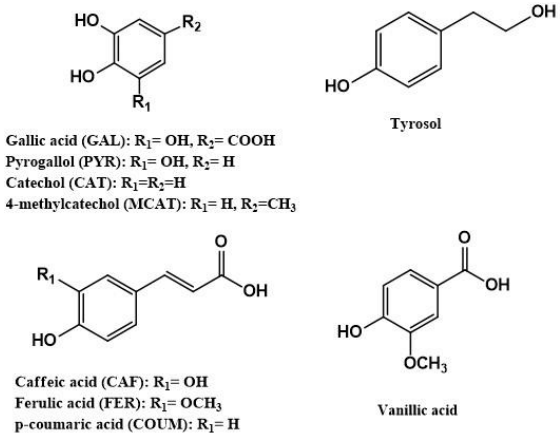

Scheme 10.2.1. Natural phenols used for preparation of the polymers.

The polymers were prepared under biomimetic conditions in phosphate buffer at pH 6.8 using horseradish peroxidase (HRP) and H_2O_2, and were collected in

variable yields (21-93 % w/w), depending on the substrate, by simple centrifugation and washings. As an example, UV-vis spectra of vanillic acid, pyrogallol and catechol polymers, reported in Figure S10.4.1, indicating the good reproducibility of the synthetic procedure obtained from three different preparations. In addition, the VA, CAT and PYR polymers obtained were also investigated by ATR/FT-IR analysis. Comparison of the spectra of the powder before and after polymerization indicated that: 1) in the case of VA: the bands at *ca.* 1660 and 1270 cm^{-1} due to the C=O stretching and O-H bending vibration of the carboxylic group were greatly reduced in the spectrum of the polymer, suggesting extensive decarboxylation of VA during the oxidation process. Polymerization was also responsible for the almost complete disappearance of the C-H bending band at ca. 750 cm^{-1} (Figure S10.4.2); 2) in the case of CAT: a slight decrease and shift to higher frequencies for the O-H stretching band in the region 3500-3000 cm^{-1} and a main band at *ca.* 1250 cm^{-1}, likely due to C–O–C stretching of phenyl ether moieties were observed in the polymer (Figure S10.4.3); in the case of PYR spectral features characteristic of purpurogallin-like moieties were evident for the PYR polymer, *i.e.* two bands at *ca.* 1600 (C=C-C=O stretching) and 1250 cm^{-1} (C−O stretching) (Figure S10.4.4).

For determination of antioxidant activity five assays were selected to measure different specific properties: the DPPH[152] and the ferric reducing antioxidant power (FRAP) assays,[153] which measure the efficiency of electron transfer (ET) processes from the antioxidant, the 2,2'-azobis(2-amidinopropane) dihydrochloride (AAPH)-induced lipid peroxidation inhibition (LP) assay,[264] typically regarded as a hydrogen atom transfer (HAT)-based assay, the NO[265] and superoxide[135] scavenging assays.

Polymers from GAL and PYR, sharing the 1,2,3-triol functionality, and catechol-based polymers proved to be in most cases the most active in all assays compared also to Trolox or quercetin as reference standards (Figure 10.2.1). Indeed, the polymer from MCAT showed a significant DPPH reducing capacity, but poor LP properties. An opposite order of reactivity was determined for the polymers from CAT and CAF in the DPPH and LP assays, whereas partially different activity trends were observed in the superoxide and NO scavenging assays (Figure 10.2.1).

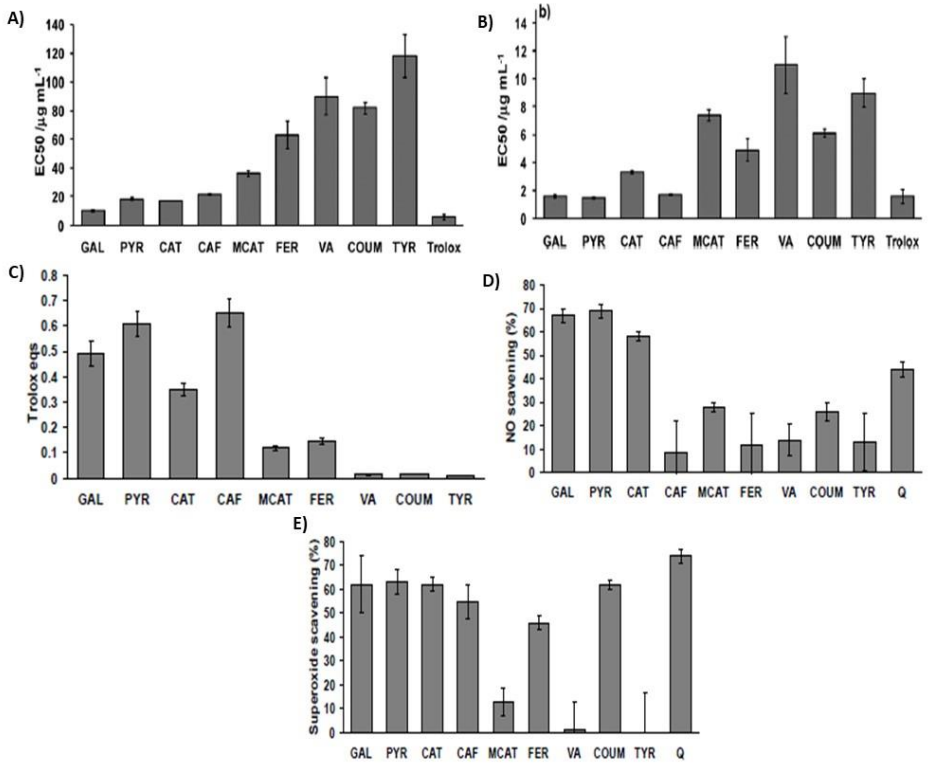

Figure 10.2.1. Antioxidant properties of the phenolic polymers (abbreviations refer to the starting monomer). (a) DPPH assay; (b) LP assay; (c) FRAP assay; NO (d) and superoxide (e) scavenging assay.

Kinetic analysis of the decay of DPPH absorbance at 515 nm in the presence of phenolic polymers or Trolox, reported in Figure 10.2.2, showed a similar trend to that determined based on the EC_{50} values with polymers from tri- and diphenols being most active also. Notably, the polymer from gallic acid proved to be very effective as a DPPH reducing agent, with a rate constant approaching 40% of that determined for the reference antioxidant Trolox.

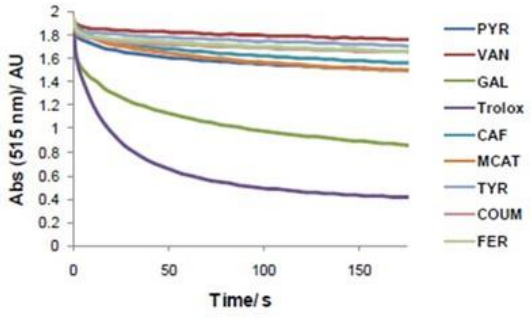

Antioxidant	$k(Lg^{-1}s^{-1})^a$
GAL	5.1 ± 0.4
PYR	1.5 ± 0.1
CAT	1.26 ± 0.09
CAF	1.4 ± 0.1
MCAT	1.34 ± 0.09
FER	0.94 ± 0.07
VA	0.34 ± 0.02
COUM	1.03 ± 0.07
TYR	0.65 ± 0.05
Trolox	12.5 ± 0.9

[a]Rate constant for the fast step (mean ± SD values, n=3).

Figure 10.2.2. Kinetic analysis of DPPH decay.

To gain an insight into the structure-specificity of the antioxidant properties, the π-electron properties of the phenolic polymers were investigated by EPR analysis of the solid polymers (Table 10.2.1).

Table 10.2.1. EPR parameters of the phenolic polymers. Experimental uncertainties are ± 0.0003 on g-factor, ± 10% on spin-density, ±0.2 G on ΔB, ±5% on line shape analysis values.

Monomer precursor	*g*-factor	ΔB (G)	% Lorentzian lineshape	Spin density (spin per g)
GAL	2.0030	3.3	46	1.6×10^{18}
PYR	2.0033	3.8	43	1.3×10^{18}
CAT	2.0033	3.4	41	1.9×10^{18}
CAF	2.0033	3.7	47	7.4×10^{17}
MCAT	2.0033	4.8	40	3.8×10^{16}
FER	2.0033	5.3	11	5.7×10^{17}
VA	2.0028	6.4	3	2.5×10^{16}
COUM	2.0031	6.2	26	6.9×10^{15}
TYR	2.0033	8.8	7	2.4×10^{16}

In all cases a featureless singlet was observed, centered at a g value of ~ 2.0033, indicating mainly carbon-centered free radicals.[55] Polymers from catechols and triphenols displayed relatively narrow signals (low ΔB values) and high spin density values. Remarkable direct linear correlation was found between all antioxidant assay and ΔB values (Figure 10.2.3; Figure S10.4.5). This finding indicated that the ET/HAT capacity of the polymers is determined by specific structural features that affect electron spin properties in such a manner to decrease signal amplitude (ΔB). Considering ΔB values indicative of the extent of aromatic substitution in the phenolic polymers, a low ΔB value is thus expected to correspond to a low number of aromatic H-atoms. This interpretation is supported by the observation that the lowest ΔB value corresponded to the monomer with the lowest number of aromatic H-atoms (GAL), and the highest ΔB value was found for the polymer obtained from a phenol with the highest number of aromatic H-atoms (TYR).

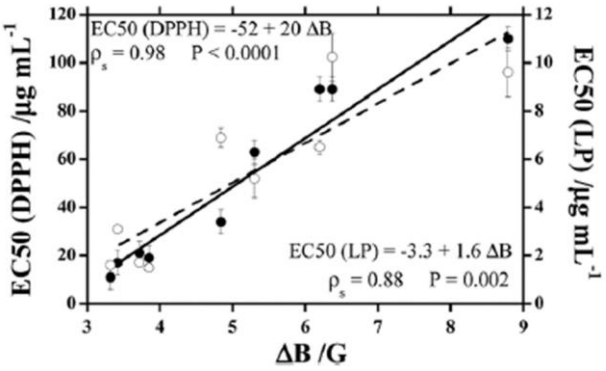

Figure 10.2.3. Correlation between antioxidant activity of the phenolic polymers expressed as the EC_{50} values determined in the DPPH (full symbols) or LP (open symbols) assays and ΔB values.

However, data reported in Table 10.2.1 showed similar ΔB values for the polymers obtained from monomers with a different degree of aromatic substitution indicating that ΔB values are indeed related to the extent of aromatic substitution in the final polymers. Notwithstanding, considering that in the polymerization mechanism a variety of oligomeric species can be produced, the exact structures of the polymers is hardly predictable based on monomer structure. Moreover, as shown in Table 10.2.1, the signals of the polymers with the lower ΔB values were associated to high Lorentzian contribution indicating that the EPR lines were narrowed by exchange interactions along conjugated aromatic moieties, which average to zero the local magnetic fields experienced by the electron spins.[266] Gaussian line shapes were instead observed for polymers with high ΔB values indicating the presence of non-interacting spin systems with no significant exchange interactions and independent narrow absorptions. Thus, the line shape analysis points to π-conjugation as the main factor driving EPR signal narrowing that characterizes polymers with high ET/HAT activity. On these bases

the excellent correlation showed in Figure 10.2.3 and supporting, points to unpaired electrons as sensitive probes of specific structural factors related to extended π-conjugation that would enhance antioxidant efficiency via ET/HAT mechanisms. The homogeneous/heterogeneous distribution of the unpaired electrons has a minor effect on the antioxidant activity of the phenolic polymers as indicated by the power saturation profiles of the EPR signals (Figure S10.4.6).

The polymers with the strongest antioxidant capacity in the DPPH and LP assays usually displayed more intense absorption in the visible region. Since the intensity of absorption in the visible region for soluble samples can be related to the degree of polymerization and π-electron conjugation, it can be argued again that the observed linear correlation between EPR signal properties and ET/HAT capacity can be accounted for by the degree of electron spin delocalization across highly conjugated structural components of the polymer. The higher tendency of catechol and pyrogallol systems to act as electron or H-atom donors can be explained by the intrinsically high oxidation potential of the *o*-diphenol motif stabilized by an intramolecular H-bond between the residual OH(s) and the oxygen radical center. These latter, as produced, would be easily deprotonated due to their relative acidity. On this basis, it could be argued that the relatively high levels of semiquinone anion species that would form even in a neutral H-bonding medium would specifically enhance the electron donor capacity via ET mechanisms, whereas HAT mechanisms would mainly operate at the expenses of the parent (poly)phenols. In addition, ET processes from semiquinone anions to give π-conjugated quinones would trigger comproportionation equilibria with reduced catechol moieties to regenerate semiquinone radicals in a redox cycling process (Scheme 10.2.2).

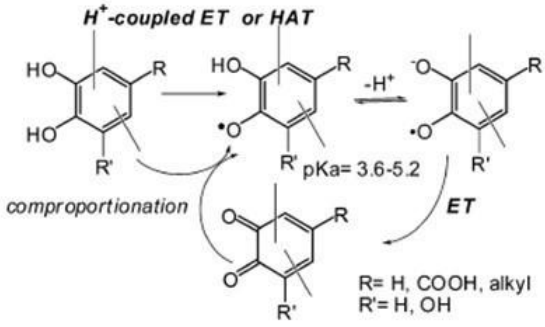

Scheme 10.2.2. Mechanism proposed for the ET/HAT-based antioxidant activity of phenolic polymers.

10.3 Conclusions

Thanks to specific assays coupled with EPR spectroscopy it was possible to disentangle the structure-specific mechanisms of the antioxidant activity of structurally diverse phenolic polymers. The main results: (a) highlighted the superior and multifunctional antioxidant activity of the polymers from triphenolic and catecholic compounds, being in some cases of comparable or even higher efficiency than that exhibited by reference antioxidants; (b) demonstrated that unpaired electrons were sensitive probes of the π-electron make-up of phenolic polymers, pointing to EPR signal amplitude as a reliable parameter to predict and interpret the ET/HAT capacity; (c) suggested π-conjugated semiquinone radical anions as probes of the efficient ET/HAT-based antioxidant activity of *o*-diphenol-containing polymers.

10.4 Experimental section

Materials and methods

Horseradish peroxidase (EC 1.11.1.7) (HRP), hydrogen peroxide (30% v/v water solution), 2,2-diphenyl-1-picrylhydrazyl (DPPH), 6-hydroxy-2,5,7,8-tetramethylchromane-2-carboxylic acid (Trolox®), 2,4,6-tri(2-pyridyl)-s-triazine (TPTZ), ferric chloride hexahydrate, linoleic acid, 2,2'-azobis(2-amidinopropane)dihydrochloride (AAPH), Triton X-100, sodium nitroprusside, N-(1-naphthylethylenediamine)dihydrochloride, sulfanilamide, nitro blue tetrazolium (NBT), ethylenediaminetetraacetic acid (EDTA) and all the phenolic compounds were purchased from Sigma-Aldrich and used as obtained.

UV-vis spectra were recorded on a Hewlett Packard 8453 Agilent spectrophotometer.

Attenuated total reflectance (ATR)/FT-IR spectra were recorded on a Nicolet 5700 Thermo Fisher Scientific instrument.

EPR spectroscopy. is a powerful tool for investigating paramagnetic species, including organic radicals, inorganic radicals, and triplet states. The basic principles behind EPR are very similar to the more ubiquitous NMR spectroscopy (NMR), except that EPR focuses on the interaction of an external magnetic field with the unpaired electron(s) in a molecule, rather than the nuclei of individual atoms. EPR spectroscopy experiments were carried out by means of X-band (9 GHz) Bruker Elexys E-500 spectrometer equipped with a super-high sensitivity probe head. For selected samples, EPR spectra were also acquired using a compact bench-top EPR spectrometer named EMXnano (Bruker Italia is gratefully acknowledged for providing the opportunity to test this instrument). As known, a

molecule or atom has discrete states, each with a corresponding energy. The energy differences (ΔE) between the atomic or molecular states tudied in EPR spectroscopy are predominately due to the interaction of unpaired electrons in the sample with a magnetic field produced by a magnet. From quantum mechanics, the most basic equations of EPR is obtained: $\Delta E = h\nu = g\mu_B B_0$ where g is the g-factor, is a constant of proportionality, whose value is property of the electron in a certain environment, therefore depending on the electronic configuration of the radical or ion. μ_B is the Bohr magneton, which is the natural unit of electronic magnetic moment and B_0 is the magnetic field. Measurement of g-factors provide useful information, about a paramagnetic center's electronic structure. Value of ΔB is obtained experimentally from the EPR spectra, in fact it is the distance, on x axis, between maximum and minimum of signal. Therefore, ΔB gives information about the speed of the relaxation processes and the distance between the paramagnetic centers.

Phenolic polymer preparation. A solution of the proper phenol (10 mM phenol final concentration) in ethanol was added to 0.1 M phosphate buffer, pH 6.8, containing 1% KCl (ethanol/buffer ratio= 1:4 v/v). HRP (2 U/mL final concentration) and hydrogen peroxide (20 mM final concentration) were then added in two portions at 1 h interval, and the mixture was allowed to stand at room temperature under vigorous stirring. After 24 h the mixture was acidified to pH 3 with 3 M HCl and stored at 4 °C for 24 h. The polymer that separated was then collected by centrifugation (7500 rpm, 4 °C, 30 min), washing with 0.1 M HCl and freeze-drying.

2,2-Diphenyl-1-picrylhydrazyl (DPPH) Assay.[152] To 2 mL of a 200 μM DDPH solution in methanol, 200 μL of 3 mg/mL water solution of sulfated

derivatives or 30-360 µL of a 0.33 mg/mL polymer or Trolox solution in DMSO were added.

Ferric Reducing/Antioxidant Power (FRAP) Assay.[153] To a solution made up of 0.3 M acetate buffer (pH 3.6) (3 mL) plus Fe^{3+} solution (300 µL) and TPTZ solution (300 µL), 50, 100 and 150 µL of each sulfated sample or 5-500 µL of a 0.33 mg/mL polymer or Trolox solution in DMSO were added.

AAPH-induced lipid peroxidation inhibition (LP) assay.[264] 30 µL of the linoleic acid solution were added to 2.80 mL of 0.05 M phosphate buffer, pH 7.4, prethermostated at 37 °C. The oxidation reaction was initiated at 37 °C under air by the addition of 150 µL of the AAPH solution. Oxidation was carried out in the presence of different amounts (0-150 µL) of a 0.33 mg/mL polymer or Trolox solution in DMSO and the increase in absorption at 234 nm was periodically determined.

NO scavenging assay.[265] 600 µL of a 0.33 mg/mL polymer or quercetin (Q) solution in DMSO were added to 6 mL of a freshly prepared 10 mM solution of sodium nitroprusside in 0.2 M phosphate buffer (pH 7.4) and the mixture was taken under vigorous stirring at room temperature. After 2 h, 1 mL of the mixture was withdrawn and added to 2 mL of Griess reagent (0.5% sulfanilamide and 0.05% *N*-(1-naphthylethylenediamine) dihydrochloride in 2.5% phosphoric acid) and the absorbance at 540 nm was measured.

Superoxide scavenging assay.[266] To 1.6 mL of a 0.5 mM EDTA solution in 0.05 M ammonium hydrogen carbonate buffer (pH 9.3) 400 µL of a 300 µM NBT solution in the same buffer and 100 µL of a 0.33 mg/mL polymer or quercetin solution in DMSO were added, followed by 400 µL of a 20 mM pyrogallol solution in 0.05 mM HCl. The mixture was taken under vigorous stirring and after 5 min the absorbance at 596 nm was measured.

Supporting materials

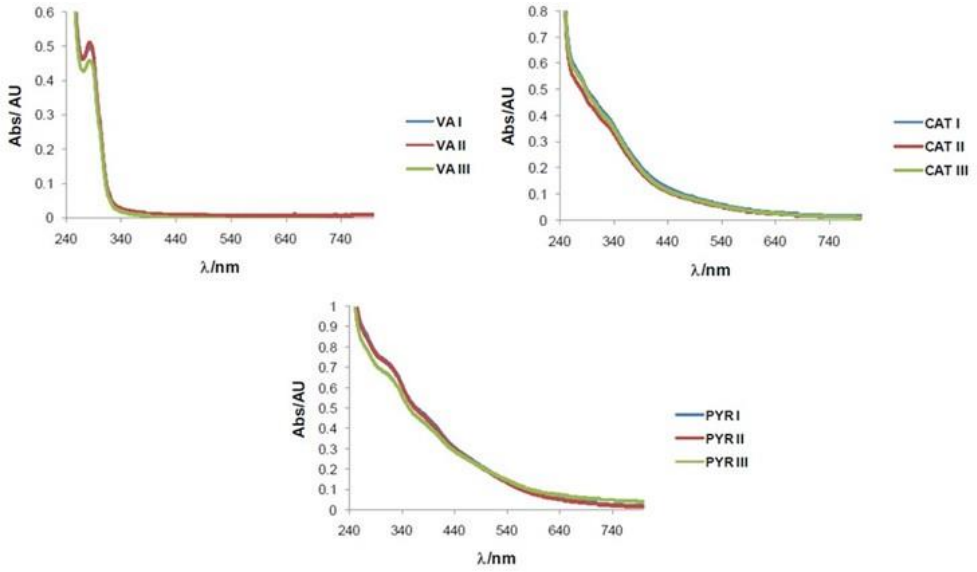

Figure S10.4.1. UV-vis spectra of VA, CAT and PYR polymers obtained from three different preparations.

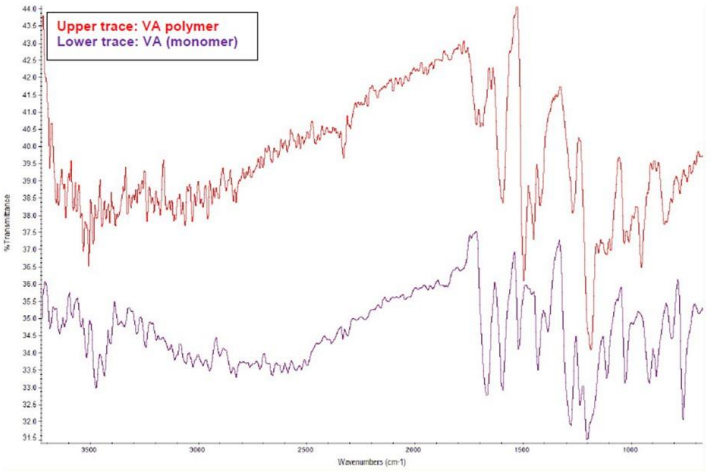

Figure S10.4.2. ATR/FT-IR spectra of VA monomer *vs* polymer.

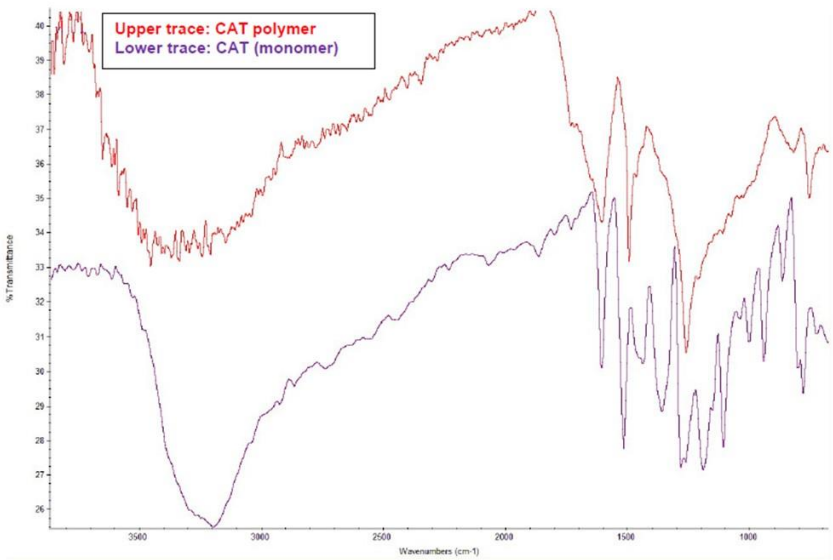

Figure S10.4.3. ATR/FT-IR spectra of CAT monomer *vs* polymer.

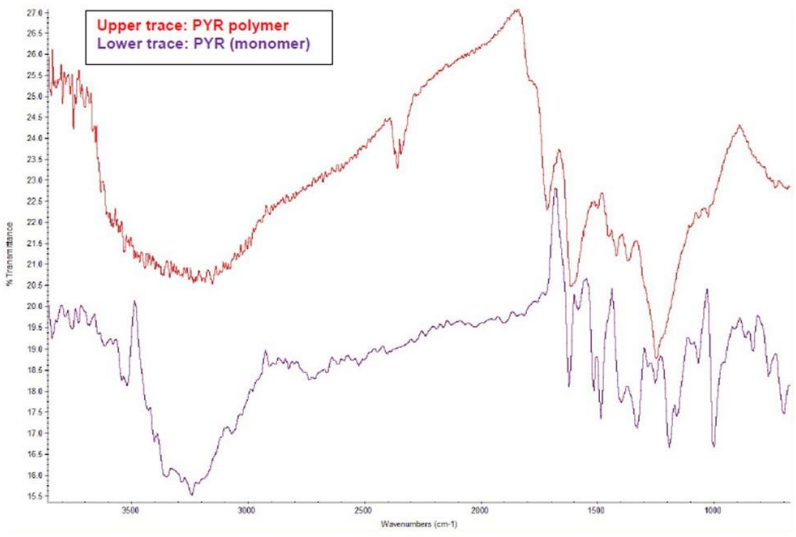

Figure S10.4.4. ATR/FT-IR spectra of PYR monomer *vs* polymer.

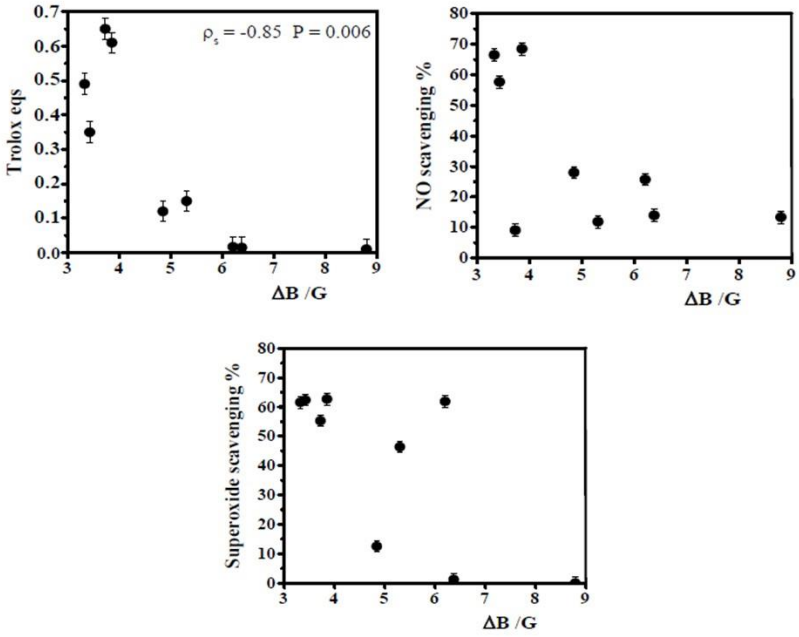

Figure S10.4.5. Correlations between the results of antioxidant assays (FRAP, NO scavenging and superoxide scavenging) and EPR parameters.

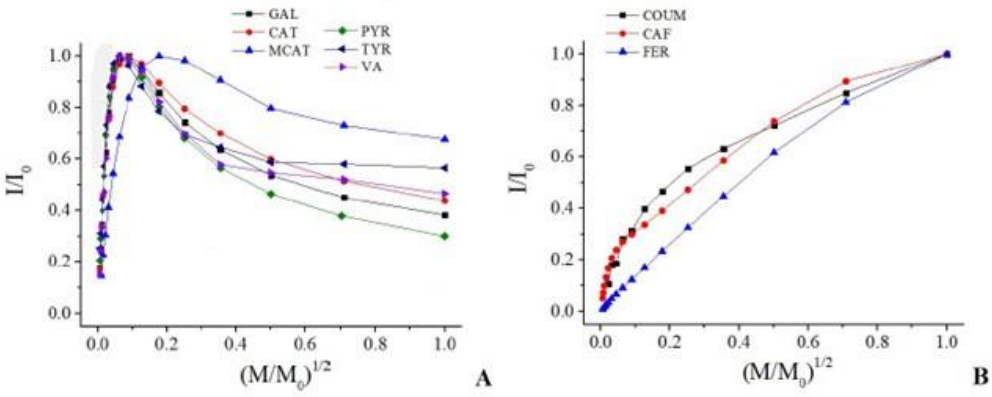

Figure S10.4.6. Power saturation profiles for all investigated phenolic polymers showing a homogeneous trend (panel A) and a heterogeneous trend (panel B).

Chapter 11

Preparation and evaluation of the biological activity of sulphur modified phenols and polyphenol polymers

11.1 Introduction

The Mediterranean diet, in which olive oil is the major fat component, has been associated with a lower incidence of coronary heart disease, brain cognitive deficiencies and certain cancers thanks to olive oil chemical components (*e.g.* oleic acid, tocopherols, sterols, polyphenols) (Figure 11.1.1). Especially 3,4-dihydroxyphenylethanol (hydroxytyrosol) and 2-(4-hydroxyphenyl)ethanol (tyrosol) are the most representative phenolics components of olive fruits and olive oil where they occur as such or in the form of esters of the secoiridoid elenolic acid and are responsible for the cardiovascular, cerebral and metabolic effects of oil.

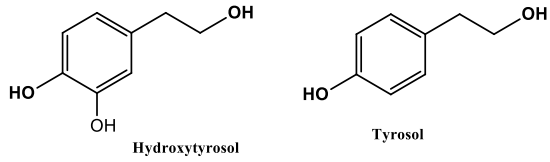

Figure 11.1.1. Phenolic compounds in extra virgin olive oil.

Over the last few years, many *in vitro* and *in vivo* studies have clearly demonstrated that olive oil phenolic alcohols possess potent antioxidant, anti-atherogenic, anti-inflammatory and anti-cancer activities which may be the basis of their positive effects on human health.[267-271]

Tyrosol has been shown to be effective in inhibiting the oxidation of cholesterol in LDL and leukocyte 5-lipooxygenase, preventing the modification of the apoproteic moiety and protecting the Caco-2 intestinal mucosa cells against the cytostatic and cytotoxic effects produced by oxidized LDL. However, due to its lack of ortho-diphenolic structure, the *in vitro* antioxidant activity of tyrosol is weak, in contrast to that of hydrotyrosol (HT). Moreover, hydroxytyrosol proved to be more active as a scavenger of reactive oxygen species also compared to antioxidant vitamins and synthetic antioxidants,[272,273] displayed metal chelating properties,[274,275] was highly protective against the peroxynitrite-dependent nitration of tyrosine and DNA damage caused by peroxynitrite formed by reaction of the superoxide radical -anion ($O_2^{\cdot -}$) and nitric oxide (NO).[276,277] Cytoprotective effects of HT against xenobiotic compounds have been reported, including protection from acrolein-induced DNA damage,[278] acrylamide-induced mithocondrial dysfunction[279] and carbon tetrachloride-induced oxidative stress.[280]

Human red blood cells (RBCs) are a useful model to evaluate the antioxidant properties of natural or synthetic compounds. Being RBCs, the cells most frequently exposed to oxygen, they are more susceptible to oxidative damage than other cells. Invasion of the RBC membrane by peroxides may lead to cell hemolysis. Moreover, the hemoglobin in RBCs is a strong catalyst which may initiate lipid peroxidation. RBCs may also represent an important target of mercury (Hg) toxicity. This metal, indeed, preferentially accumulates in these cells and induces morphological changes which increase their pro-coagulant activity.[281-283] Recent data suggesting a positive correlation between Hg exposure and the origin of cardiovascular diseases. Mercury, indeed, is a highly toxic, redox-active, heavy metal which represents one of the main agents responsible for environmental pollution.[284] Human exposure to mercury occurs primarily via

medical preparations as well as nutritional sources and the consequence for human health can be severe[285,286] and include renal injury,[287] immune-toxicity and neuronal disorders.[288] In this respect, Hg is considered a potential contributing factor to Alzheimer's and Parkinson's disease.[289]

Increased formation of reactive oxygen species (ROS) is generally agreed to be one of the key mechanisms responsible for Hg-induced toxicity.[290,291] Mercury is endowed with high affinity for sulfhydryl groups and it is therefore able to react with low molecular-weight thiols, including glutathione (GSH),[292] that significantly decrease following Hg exposure, with consequent damaging of the antioxidant defense system.[293] On these bases a number of antioxidants,[294,295] including phenolic compounds,[296,297] have been evaluated for their protective action against Hg toxicity. In this connection, recent studies have highlighted the potential of hydroxytyrosol to modulate cytotoxicity and the oxidative stress induced in human RBC by Hg treatment, and the efficacy in inhibiting methylmercury-induced neuronal cell dysfunction as highlighted by the decrease of ROS formation and maintenance of an efficient endogenous defense system, including GSH levels and superoxide dismutase and catalase activities.[298-300] Several efforts have been directed toward the preparation of HT derivatives and analogues with improved solubility properties, particularly enhanced lipophilicity,[301−303] and antioxidant and pharmacological activities. In particular, 5-*S*-lipoylhydroxytyrosol (Lipo-HT), synthesized by conjugation of HT with the biologically relevant thiol dihydrolipoic acid (DHLA) (Scheme 11.1.1), showed increased antioxidant activities compared to HT in several chemical assays and exerted potent protective effects against ROS generation and oxidative cell damage in human hepatocellular carcinoma HepG2 cell line.[304,305] In addition, DHLA features two SH groups onto a short carbon chain ending with a carboxyl

group, thus providing not only the necessary SH functionality for conjugation with HT but also a second SH group as reactive site for secondary functionalization as well as a flexible chain expected to favor interaction with membranes, lipid bilayers, and other hydrophobic environments. Considering the promising results, one of the research topics developed in this chapter concerns the evaluation of the effects of Lipo-HT on oxidative alterations of human erythrocytes.

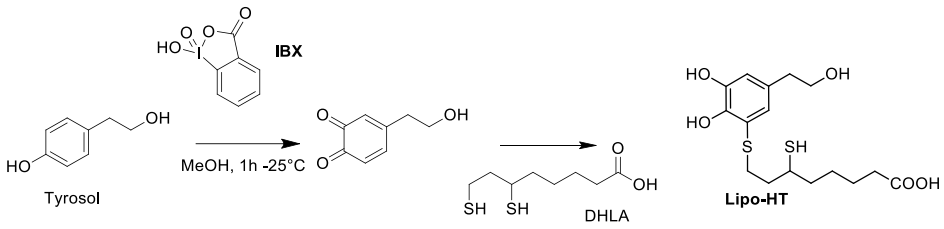

Scheme 11.1.1. Synthetic route to 5-S-lipoylhydroxytyrosol.

Nature uses sulfation of endogenous and exogenous molecules mainly to avoid potential toxicity. Thanks to some important biological activities, such as antiplatelet,[306] antiviral,[307,308] anti-inflammatory,[309,310] immunomodulatory,[311] antitumor,[312,313] and, most importantly, anticoagulant[314] the design and exploitation of highly-sulfated bioactive polyphenols has recently attracted a growing interest. Sulfated polyphenols showed, indeed, effective antithrombotic effects both *in vitro* and *in vivo*, high solubility and stability, and low toxic potential.[315,316] Remarkable examples are the sulfated derivatives of flavonoids, hydroxycinnamic acids and resveratrol. Apart from sulfated small molecules, heparin-mimicking polymers have also been emerging as a valuable alternative strategy for application as anticoagulants.[317,318] Indeed, although heparin and its low (LMWH) and ultralow (ULMWH) molecular weight derivatives are widespread anticoagulant agents, their use suffer from a number of limitations such as enhanced bleeding and thrombocytopenia risk, unpredictable response,

and lack of inhibition of clot-bound thrombin.[319,320] As an example, sulfated polymers obtained by oxidation of hydroxycinnamic acids under biomimetic conditions effectively prolonged activated thromboplastin (APTT) and prothrombin time (PT) with approximately equal potency as low-molecular weight heparin (LMWH).[321,322]

In the light of this background specific aims of the research work described in this chapter are:

1) evaluation of the effects of Lipo-HT on oxidative alterations of human erythrocytes induced by exposure to $HgCl_2$ comparatively to HT;
2) synthesis and evaluation of the antioxidant and anticoagulant activities of sulfated derivatives of polymers from tyrosol.

11.2 5-S-lipoylhydroxytyrosol protecting activity of human erythrocytes against mercury toxicity

The rationale of testing the ability of Lipo-HT to prevent human RBC from the oxidative alterations induced by Hg treatment stems from the possibility of exploiting, in addition to the antioxidant power of the catechol moiety activated by the adjacent thioalkyl group, the free SH group of dihydrolipoic acid capable of effectively chelating Hg.

Preliminary Lipo-HT was prepared from tyrosol and dihydrolipoic acid according to a procedure previously developed.[48] Intact RBC were exposed *in vitro* to 40 μM $HgCl_2$ concentration taken as the optimal dose to study the oxidative stress-mediated cytotoxicity. Cellular lysis, ROS formation, and intracellular GSH levels were evaluated in RBC following 4 h incubation. Data in Figure 11.2.1 (obtained in the frame of a collaborative work with Prof. C. Manna and co-workers,

University of Campania "Luigi Vanvitelli") showed a dramatic increase in the hemolytic process confirming the cytotoxicity resulting from exposure of cells to $HgCl_2$. Both compound HT and especially Lipo-HT were effective in preventing the toxic effect decreasing the hemolysis.

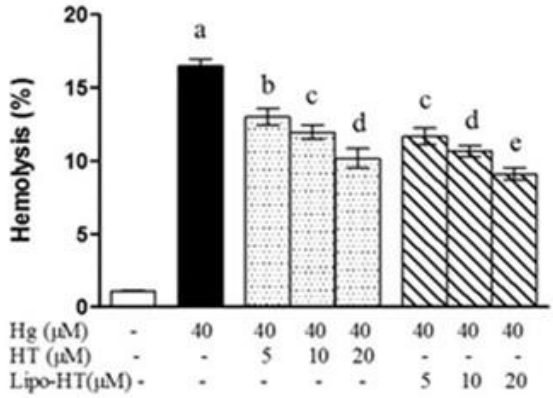

Figure 11.2.1. Effect of HT and Lipo-HT on Hg-induced hemolysis. Cells were treated with $HgCl_2$ at 40 μM for 24 h in the presence of increasing concentrations of the selected compounds. Data are the means ± SE (n=9). Statistical analysis was performed with one-way ANOVA followed by Dunnett's test ($p<0.05$). Means with different letters are significantly different.

Figure 11.2.2 reports ROS production in the presence of Hg^{2+} and varying amounts of Lipo-HT or HT in the concentration range 5-20 μM as determined by DCF fluorescence assay. The Hg-induced ROS generation was dose-dependently prevented in the presence of increasing concentrations of either Lipo-HT or HT. Interestingly, at a 5 μM concentration, Lipo-HT proved more effective producing a 57 % decrease of ROS production with respect to only 34% decrease in the presence of HT (Figure 11.2.2).

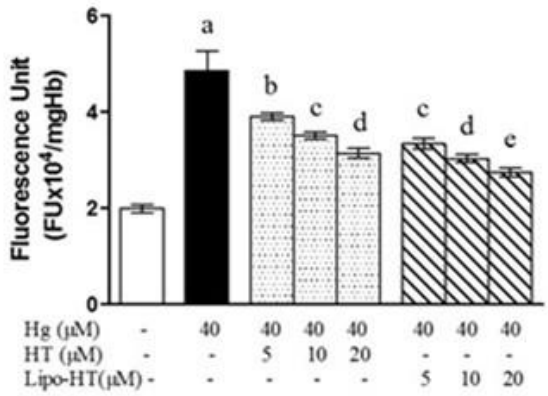

Figure 11.2.2. Effect of HT and Lipo-HT on Hg-induced ROS production in RBC. ROS production was evaluated by means of the fluorescent probe DCF. Data are the means ± SE (n=9). Means with different letters are significantly different.

To confirm the observed markedly protective action of Lipo-HT, its effect on GSH intracellular concentrations was evaluated. Hg^{2+} specifically binds to biological thiols, including GSH, and is able to induce their oxidation with consequent depletion of the intracellular levels. Following cell exposure to Hg^{2+} the GSH level was significantly reduced with respect to the control RBC as determined spectrophotometrically by Ellman's assay (Figure 11.2.3). Also, in this case, co-incubation with Lipo-HT at 5 μM prevents GSH depletion by about 30 %, an effect that is obtained with 10 μM HT and lipoic acid.

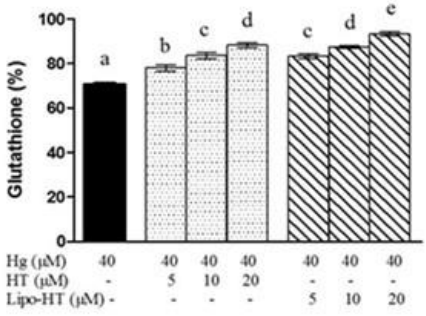

Figure 11.2.3. Effect of HT and Lipo-HT on Hg-induced GSH decrease in RBC. Data are the means ± SE (n=9). Means with different letters are significantly different.

In order to obtain information about the mechanisms responsible for these protective effects, the course of the reaction of Lipo-HT with Hg^{2+} at pH 7.4 was followed by HPLC and LC-MS under conditions mimicking those of the cellular assays. As shown in Figure 11.2.4 (panel A) an almost complete consumption of Lipo-HT was observed after 5 min, with concomitant formation of two major products eluted at *ca.* 22 and 25 min. This latter showed pseudomolecular ion peaks $[M+H]^+$, $[M+Na]^+$ and $[M+K]^+$ at m/z 921, 943 and 959, in that order, suggestive of a 2:1 complex of Lipo-HT with Hg. Consistently with the presence of the seven stable isotopes of Hg (with ^{202}Hg being the most abundant at 29.86 %), these peaks showed a distinct isotopic pattern (Figure 11.2.4, panel B), which provided further evidence for the formation of the complex.[323] Ellman's assay[324] indicated a more than 90 % abatement of sulfhydryl groups in the reaction mixture after 5 min, pointing to the involvement of the thiolate moiety rather than the catechol unit in Hg-complex formation. The MS spectrum of the compound eluted at 22 min was characterized by pseudomolecular ion peaks $[M+Na]^+$ and $[M+K]^+$ at *m/z* 381 and 397, respectively. A $[M-H_2O+H]^+$ at *m/z* 341 together with $[2M+Na]^+$ and $[3M+K]^+$ at *m/z* 739 and 1113, respectively, were also present

(Figure 11.2.4, panel C). HPLC and LC-MS analysis of the mixture at 1 h reaction time revealed that the Lipo-HT/Hg complex had disappeared, and the presence of an oxidation product of Lipo-HT, likely a thioketone, as the only residual product.

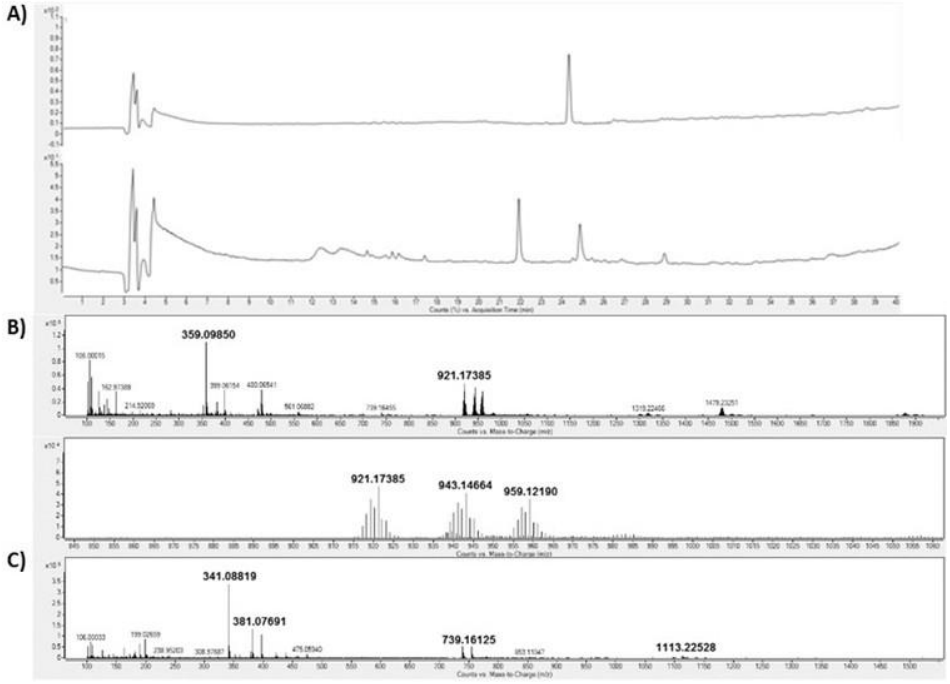

Figure 11.2.4. Analysis of the reaction mixture of Lipo-HT with Hg^{2+} ions at pH 7.4. (A) Total ion current (TIC) chromatograms of the reaction mixture of Lipo-HT (50 µM) with Hg^{2+} (100 µM) at pH 7.4 (top: before addition of Hg^{2+}, bottom: 5 min after addition of Hg^{2+}); (B) Top: MS spectrum of the product eluted at 25 min; bottom: inset showing the Hg isotopic signatures of the complex; (C) MS spectrum of the product eluted at 22 min.

In control experiments run in the absence of Hg, only a 20 % consumption of Lipo-HT was observed after 1 h, and no other product could be detected, apart from traces of thioketone and of the disulfide of Lipo-HT.[305] Moreover, a complete consumption of Lipo-HT, together with the formation of the products eluted at 22

and 25 min, was observed even when the reaction was run under an argon atmosphere, ruling out a possible role of oxygen in the oxidation reaction. Based on all these observations, a mechanism for the reaction of Lipo-HT with Hg^{2+} was proposed as depicted in Figure 11.2.5. This involves the rapid formation of the Lipo-HT/Hg^{2+} complex, followed by oxidation with formation of a thioketone, likely coupled with the reduction of Hg^{2+}. Hence, Lipo-HT would act as both a chelating and reducing agent toward Hg ions, thus limiting their capacity to induce oxidative damage in biological compartments.

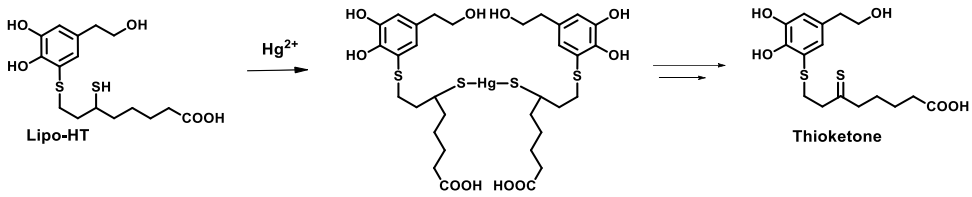

Figure 11.2.5. Mechanism proposed for the reaction of Lipo-HT with Hg^{2+} at pH 7.4.

Notably, under the same reaction conditions, HT underwent about 30 % consumption after 1 h, giving rise to the methanooxocinobenzodioxinone derivatives identified by comparison of the chromatographic behavior and mass spectra with those of authentic samples.[325] UV-vis spectrum and LC-MS analysis of the mixture in the early stages of the reaction revealed the formation of an oxidation product of HT, likely the *o*-quinone in close agreement with that previously reported in literature.[326] No Hg complex formation could be observed, either by UV-vis or LC-MS analysis.

11.3 Sulfated tyrosol polymers

Recently the interest in the design and exploitation of highly-sulfated bioactive polyphenols, that could be a valuable alternative for application as anticoagulants, has increased. In this perspective a sulfated derivative of tyrosol polymer was prepared. A mild sulfation procedure, previously reported for the synthesis of sulphated derivatives of hydroxycinnamic acid oligomers,[321,322,327,328] was developed and optimized firstly on the monomer with a view to modify only the alcoholic OH group leaving underivatized the phenolic OH group essential to the antioxidant activity. In particular, tyrosol (Tyr) was reacted with 5 molar equivalents of SO_3-TEA in anhydrous dimethylformamide (DMF) at 60 °C for 24 h. HPLC analysis indicated the presence of a main compound eluted at 10 min (Figure 11.3.1), which was isolated on a preparative scale following DMF removal and gel filtration.

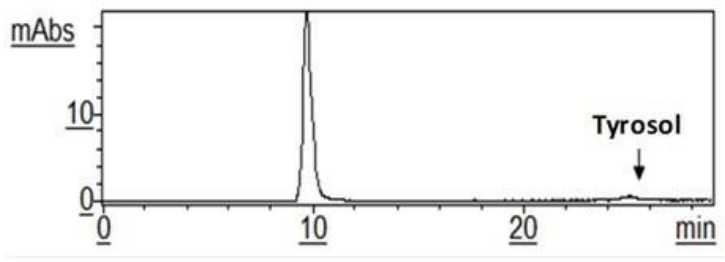

Figure 11.3.1. HPLC profile of the reaction mixture of tyrosol in the presence of 5 molar equivalents of SO_3-TEA after 24 h.

ESI-MS and NMR experiments allowed to formulate the compound as the monosulfated derivative, TyrS (Scheme 11.3.1).

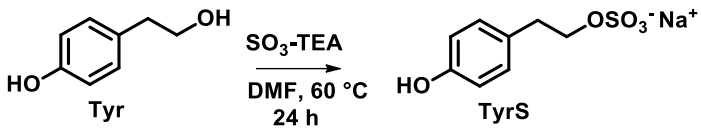

Scheme 11.3.1. Synthesis of a monosulfated tyrosol derivative.

In the ^{1}H NMR spectrum (Figure S11.5.1) particularly diagnostic was the presence of a triplet at δ 4.22 due to the β-protons of the hydroxyethyl chain, significantly shifted toward lower fields compared to Tyr (3.66 ppm) as a consequence of alcoholic OH group sulfation, also confirmed in the ^{13}C NMR spectrum in which the C_{β} is shifted toward higher fields (69.7 ppm) (Figure S11.5.2). No significant differences were indeed observed in the chemical shift values of the signals due to the aromatic ring. The better leaving-group character compared to the alcoholic group could in fact account for the lack of sulfation of the phenolic group in the isolated product.

In further experiments the sulfation protocol was extended to a tyrosol polymer, namely OligoTyr, prepared according to Antenucci *et al.* 2016 by oxidation of tyrosol with the horseradish peroxidase (HRP)-H_2O_2 system.[261] The sulfated polymer (OligoTyrS I) was thus obtained in 69 % w/w after purification by dialysis with cellulose membrane. Both ^{1}H (diagnostic signals at *ca* δ. 4.2 ppm) (Figure S11.5.3) and ^{13}C NMR analysis (69.5 ppm) indicated the presence of significant amounts of hydroxyethyl sulfated chains (Figure S11.5.4). OligoTyr S I was found to consist of a mixture of linear oligomers, as demonstrated in a previous work,[261] in which the 3 and 5 positions of tyrosol were involved in polymerization reaction as suggested from the C-3,C-5 signals around 115 ppm significantly abated while the hydroxyethyl chain (39 ppm) was not involved in the polymerization mode (Figure S11.5.4). In agreement with these observation,

elemental analysis indicated a S/C ratio of 40 % with respect to the monosulfated unit.

The sulfated polymer was also subjected to MS analysis in the MALDI-Tof mode using 2,5-dihydroxybenzoic acid as the matrix. Despite its low volatility MALDI-MS spectra suggested the presence of linear tyrosol units partially (*e.g.* $[M+H]^+$ = m/z 751 (+ Na^+)) or totally sulfated on the alcoholic chains up to examer (*e.g.* $[M+Na]^+$ = m/z 1442) (Figure S11.5.5-11.5.6). A tentative structure compatible with a pseudomolecular ion peak at m/z 1442 is shown in Figure 11.3.2.

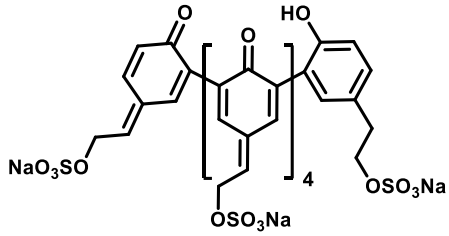

Figure 11.3.2. Tentative structure representative of the possible species responsible for the peak at m/z 1442 in the OligoTyrS I sample.

With the aim of obtaining a fully-sulfated tyrosol polymer, in further experiments TyrS was reacted with HRP-H_2O_2 under the same conditions used for the preparation of OligoTyr to give, after dialysis purification, OligoTyrS II (61% w/w yields). Altough elemental analysis indicated a higher S/C ratio (45 %) with respect to the TyrS, a relatively higher percent of O was determined, suggesting nucleophilic addition of water and/or hydrogen peroxide to the polymer, likely due to the full solubility and hence to the higher reactivity of this latter in the reaction medium, different to what observed for the OligoTyr that as formed immediately separated from the reaction medium. Consistent with this conclusion the low field region of ^1H NMR spectrum appeared to be more complex and ^{13}C

NMR spectrum showed, in addition to the signals around 69.7 ppm indicating the presence of sulfated groups on the hydroxyethyl chains, also intense signals corresponding to the hydroxyethyl chain with some branching point as indicated from the resonances observed at around 48 and 85 ppm (Figure S11.5.7-11.5.8). In agreement with these observation MALDI-MS spectra of OligoTyrS II (Figure S11.5.9) suggested the presence of both oligomers sulfated (*e.g.* $[M+H]^+$ = m/z 954) and not sulfated (*e.g.* $[M+K]^+$ = m/z 721) and also some peaks in common with OligoTyrS I.

In subsequent experiments, the antioxidant properties of OligoTyrS I and II were investigated with respect to TyrS using two chemical tests, the 2,2-diphenyl-1-picrylhydrazy (DPPH) (Figure 11.3.3),[152] and the ferric reducing antioxidant power (FRAP) (Figure 11.3.4).[153] In both assays, OligoTyrS I exhibited significantly improved antioxidant properties compared to the monomer, in agreement with what previously reported in the case of OligoTyr, as a result of the stabilizing effect of the aromatic rings in ortho position to the phenoxyl radical in the oligomeric structures. Notably, the effect of polymerization was weaker or even null, depending on the assay, in the case of OligoTyrS II, in line with the hypothesis based on the structural characterization of the polymer, pointing to the occurrence of reaction pathways, such as water addition, which would interfere with the linear polymerization mode of tyrosol thus disrupting the regular sequence of conjugated aromatic rings.

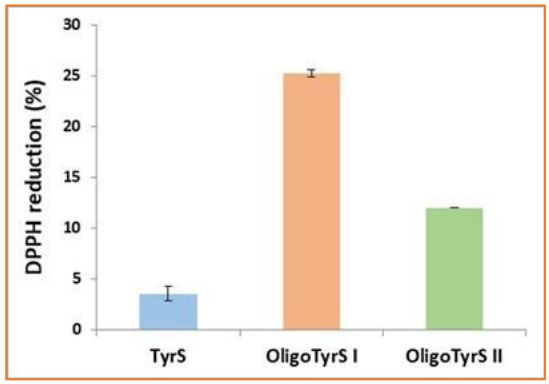

Figure 11.3.3. 2,2-diphenyl-1-picrylhydrazyl assay of TyrS and sulfated polymers (0.3 mg/mL) expressed as DPPH reduction. Data are shown as mean ± SD of three independent experiments.

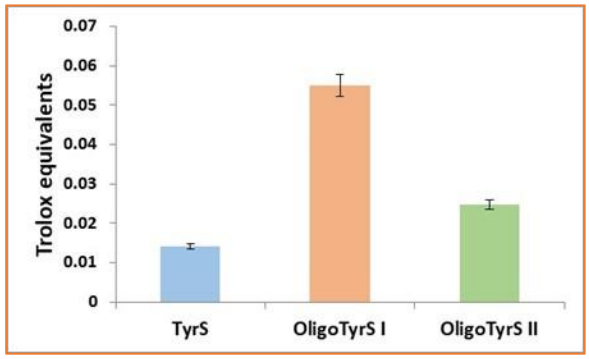

Figure 11.3.4. Trolox equivalents determined in the FRAP assay of the sulfated monomer and polymers (0.3 mg/mL). The average values ± SD obtained from at least three separate experiments are reported.

In the frame of a collaborative work with Prof. M. Correia da Silva and co-workers (MedChem University of Porto, Portugal) the anticoagulant activity of the sulfated molecules was evaluated *in vitro* human plasma by activated partial thromboplastin time (APTT), prothrombin time (PT) and thrombin time (TT)

clotting assays. The three coagulation tests allow to differentiate between effects on the extrinsic or intrinsic pathway or on fibrin formation. Briefly the APPT measures the overall speed at which blood clots and is often used in conjunction with PT that measures the speed of clotting by means of the extrinsic pathway whereas TT measures the time it takes for a clot to form in the plasma of a blood sample containing anticoagulant, after an excess of thrombin has been added. Interestingly OligoTyrS I, respect to OligoTyrS II, showed considerable concentration-dependent prolongation of clotting time in both prothrombin time and activated partial thromboplastin time assay characterized by a rapid increase in the time needed to clot. The anticoagulant activity is typically defined in terms of the concentration of the anticoagulant needed for doubling the normal plasma clotting time. Notably in the presence of OligoTyrS I a significant increase of the APTT and PT was observed with a concentration required to double clotting time of 26.19 ± 3.91 mg/L whereas OligoTyrS II and TyrS performed less efficiently with values of 215.91 ± 31.81 mg/L and > 600 mg/L, respectively (Figure 11.3.5, S11.5.10).

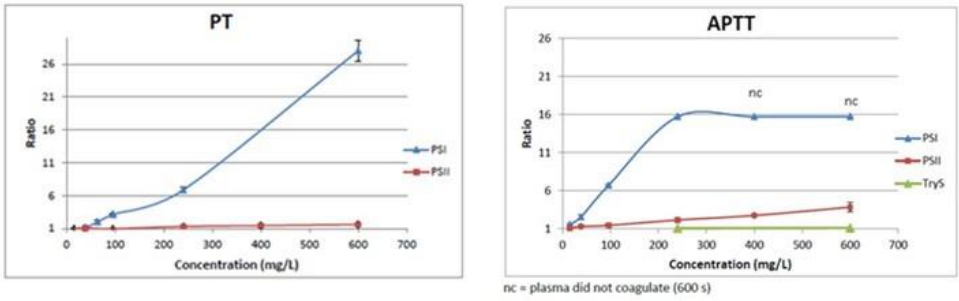

Figure 11.3.5. Prolongation of clotting time as a function of concentration of the sulfated compounds in either prothrombin time assay (left) or the activated partial thromboplastin time assay (right).

The relatively structurally more homogeneity of the OligoTyrS I compared to the OligoTyrS II could account for the better response observed in the *in vitro* test.

In further experiments, to assess the putative efficacy and a predictable anticoagulant response *in vivo* studies in mice were performed on OligoTyrS I, the most active in the *in vitro* tests.

As shown in Figure 11.3.6, the weight of the thrombus induced in mice treated intraperitoneally with OligoTyrS I was lower (55 %) than that formed in control mice. The positive control, enoxaparin, caused a marked decrease in thrombus weight (about 30 %) when compared with that formed in control mice.

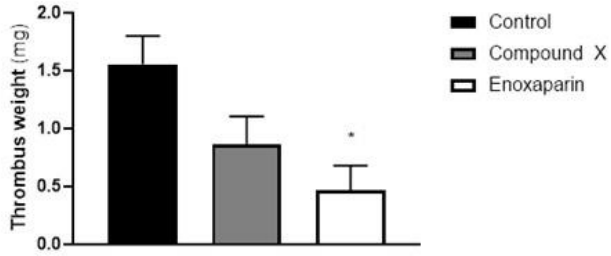

Figure 11.3.6. Thrombus weight (mg) formed in each experimental group (n=5 in each).* $p<0.05$ *vs* control group.

11.4 Conclusions

The use of natural compounds of plant origin with a potential to control the oxidative cellular alterations associated with Hg exposure is a strategy that is gaining increasing interest to counteract the toxicity of this and other heavy metal pollutants. In this connection, the research activity described in this chapter provide a significant contribution showing the potency of a derivative of the olive oil polyphenol HT, which contains the active sulphydryl moiety of dihydrolipoic

acid in the molecular scaffold, in controlling the oxidation events triggered by Hg ions and in protecting the intracellular homeostasis warranted by GSH levels.

Recently the interest in the design and exploitation of highly-sulfated bioactive polyphenols that could be a valuable alternative for application as anticoagulants has increased. In this view sulfated derivatives of OligoTyr polymer, obtained by oxidation of the tyrosol in biomimetic conditons (OligoTyrS I) or by sulfation of the OligoTyr polymer (OligoTyrS II) were prepared. The sulfated polymers thus obtained proved to be more efficient than the corresponding monomer. OligoTyrS I was also able to significantly increase the activated partial thromboplastin time (APTT) and prothrombin time (PT). Finally, *in vivo* studies in mice showed significant antithrombotic effect in the case of OligoTyrS I compared to enoxaparin.

11.5 Experimental section

Materials and methods

2',7'-dichlorodihydrofluorescein diacetate (DCFH-DA), mercuric chloride (HgCl2), tyrosol, lipoic acid, 5,5'-dithiobis(2-nitrobenzoic acid) (DTNB) (Ellman's reagent), HT, sulfur trioxide triethylamine complex, 2,2-diphenyl-1-picrylhydrazyl, horseradish peroxidase (EC 1.11.1.7) (HRP), hydrogen peroxide (30 % v/v water solution), 6-hydroxy-2,5,7,8-tetramethylchromane-2-carboxylic acid (Trolox®), 2,4,6-tri(2-pyridyl)-s-triazine (TPTZ), ferric chloride hexahydrate, linoleic acid, were purchased from Sigma Aldrich.
UV-vis spectra were recorded on a Jasco V-730 spectrophotometer.
^{1}H NMR and ^{13}C NMR spectra were recorded in D_2O at 400 MHz on a Bruker 400 MHz spectrometer.

HPLC analysis was carried out on an Agilent instrument equipped with a UV detector set at 254 nm. The chromatographic separation was achieved on a Phenomenex Sphereclone ODS C18 column (250 mm × 4.6 mm, 5 μm) using binary gradient elution conditions as follows: 0.1% trifluoroacetic acid (solvent A), acetonitrile (solvent B); from 5% to 90% B, 0-45 min or isocratic elution condition 1% formic acid – methanol 95:5 v/v; flow rate 0.7 mL/min.

LC/MS analyses were run on a LC/MS ESI-TOF 1260/6230DA Agilent instrument operating in positive ionization mode in the following conditions: nebulizer pressure 35 psig; drying gas (nitrogen) 8 L/min, 325 °C; capillary voltage 3500 V; fragmentor voltage 175 V. An Eclipse Plus C18 column, 150 × 4.6 mm, 5 μm, at a flow rate of 0.4 mL/min was used, with the same mobile phase as above.

Positive Reflectron MALDI spectra were recorded on a AB Sciex TOF/TOF 5800 instrument using 2,5-dihydroxybenzoic acid as the matrix. Spectrum represents the sum of 15,000 laser pulses from randomly chosen spots per sample position. Raw data are analyzed using the computer software provided by the manufacturers and are reported as monoisotopic masses.

Synthesis of 5-*S*-lipoylhydroxytyrosol (Lipo-HT). The reaction was carried out on tyrosol according to Panzella et al 2005[305] affording Lipo-HT in *ca.* 30% yield. The purity of the compound was evaluated (> 95%) by HPLC and ^{1}H NMR analysis.

Reaction of Lipo-HT or HT with Hg^{2+} ions. 5μL of a 100 mM $HgCl_2$ solution were added to 5 mL of buffer (pH 7.4), followed by 5 μL of a 50 mM DMSO solution of Lipo-HT or HT (100 μM and 50 μM final concentration for $Hg^{2+}$and Lipo-HT or HT, respectively). The reaction mixture was taken under stirring and periodically analyzed by HPLC, LC/MS and UV-vis spectroscopy. When required the reaction mixture was taken to pH 3 with 4 M HCl before analysis. In other

experiments, aliquots (1.5 mL) of the reaction mixture of Lipo-HT were periodically withdrawn, added with 11 μL of a 10 mM Ellman's reagent solution in 0.1 M phosphate buffer (pH 7.4), and after 15 min the absorbance at 412 nm was read. In other experiments the reaction was run: i) in the absence of $HgCl_2$; ii) under an argon atmosphere.

Preparation of RBC and treatment with Hg. The RBC fraction was obtained from whole blood obtained from human healthy volunteers deprived of leucocytes and platelets by filtration on a nylon net, washed twice with isotonic saline solution (0.9 % NaCl) and finally re-suspended with Buffer A (5 mM Tris-HCl containing 0.9 % NaCl, 1 mM $MgCl_2$ and 2.8 mM glucose, pH 7.4) to obtain a 10 % hematocrit. Intact RBC were incubated at 37 °C with 40 μM $HgCl_2$ for 4 h. For the experiments with Lipo-HT or HT stock solutions (100 mM) were prepared in DMSO and diluted to 1 mM before adding to the incubation medium. After 5 min Hg was added.

Determination of the hemolysis. At the end of the incubation, the reaction mixture was centrifuged at 1100 g for 5 min and the hemoglobin (Hb) released was evaluated by measuring the absorption of the supernatant at 540 nm. Packed RBC were hemolyzed with ice-cold distilled water at 40: 1 v/v, the lysate centrifuged at 1500 g for 10 minutes and the absorption of the supernatant (B) measured at 540 nm.

Determination of ROS. Intact RBC were incubated with DCFH-DA at 10 μM final concentration for 15 min at 37 °C. After centrifugation at 1200 g for 5 min, the supernatant was removed, and the hematocrit value was adjusted to 10 % with buffer. RBC were then treated with $HgCl_2$ in the dark. At the end of incubation, 20 μL of RBC were diluted in 2 mL of water and the fluorescence intensity of the oxidized derivative DCF was recorded (λ_{ex}=502 nm; λ_{em}=520 nm). The results were expressed as fluorescent intensity/mg of Hb.

Quantification of intracellular GSH. The samples were centrifuged, the supernatants removed and RBC were lysed by addition of 0.6 mL of ice-cold water. Proteins were precipitated by the addition of 0.6 mL ice-cold metaphosphoric acid solution. After incubation at 4 °C for 5 min, the protein precipitate was removed by centrifugation at 18000 g for 10 min and 0.45 mL of the supernatant was mixed with an equal volume of 0.3 M Na_2HPO_4. 100 μL of DTNB solution was then added to the sample, and after 10 min incubation at room temperature, the absorbance of the sample was read against the blank at 412 nm.[329]

Preparation of sulfated derivatives (TyrS, OligoTyrS I and II). To a solution of tyrosol or OligoTyr (200 mg, 1.44 mmol) in DMF, SO_3-TEA (5 molar equivalent) was added and the mixture was taken under stirring at 60 °C for 24 h. After DMF removal the residue was washed with ethyl acetate and NaOH 3 M was repeatedly added till pH 9.0. The residue was fractionated on a Sephadex G10 column (48 % w/w yield) or, for OligoTyrS I and II, desalted by dialysis against water for 6 h (69 % w/w and 61 % w/w yield respectively).

ESI^+/MS: *m/z* 263 ($[M+Na]^+$). ^1H NMR (D_2O) δ (ppm): 2.91 (t, J= 6.8 Hz), 4.22 (t, J= 6.8 Hz), 6.88 (d, J= 8.4Hz), 7.19 (d, J= 8.4 Hz). ^{13}C NMR (D_2O) δ (ppm): 33.9, 69.7, 115.4, 129.8, 130.3, 154.1.

2,2-diphenyl-1-picrylhydrazyl (DPPH) Assay.[152] To 2 mL of a 200 μM DDPH solution in methanol, 200 μL of 3 mg/mL water solution of sulfated derivatives or Trolox solution in DMSO were added.

Ferric Reducing/Antioxidant Power (FRAP) Assay.[153] To a solution made up of 0.3 M acetate buffer (pH 3.6) (3 mL) plus Fe^{3+} solution (300 μL) and TPTZ solution (300 μL), 50, 100 and 150 μL of each sulfated sample or Trolox solution in DMSO were added.

Supporting materials

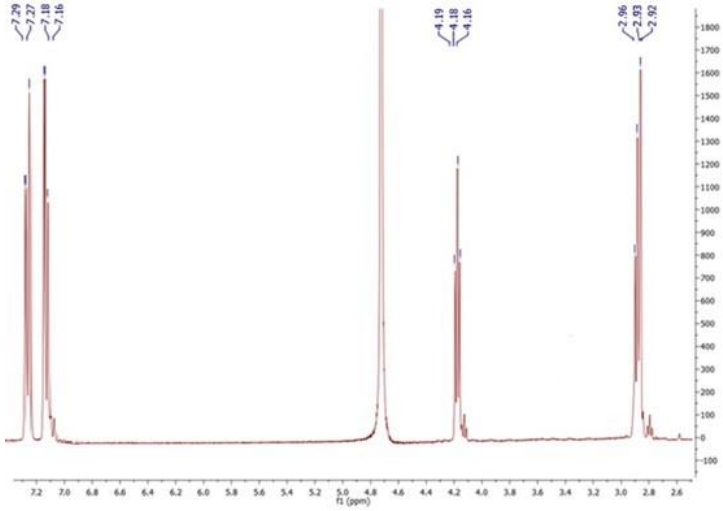

Figure S11.5.1. ^{1}H NMR spectrum of the monosulfated derivative, TyrS (400 MHz in D_2O).

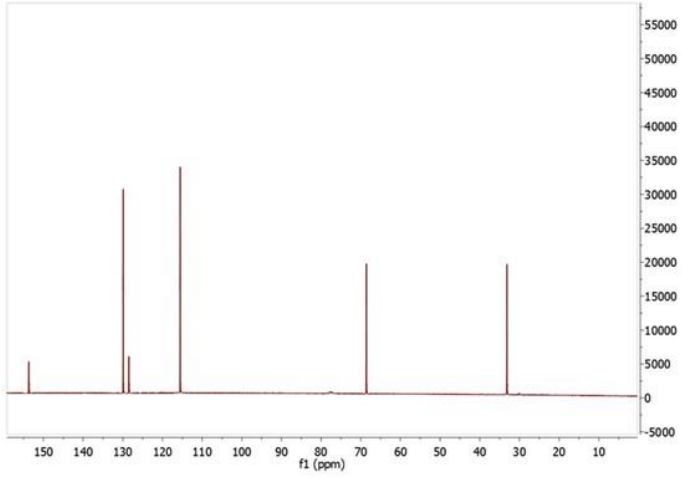

Figure S11.5.2. ^{13}C NMR spectrum of the monosulfated derivative, TyrS (400 MHz in D_2O).

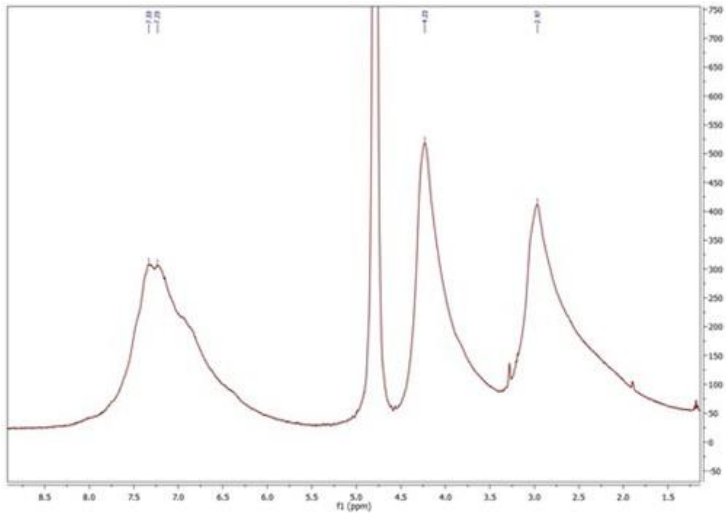

Figure S11.5.3. ^{1}H NMR spectrum of OligoTyrS I (400 MHz in D_2O).

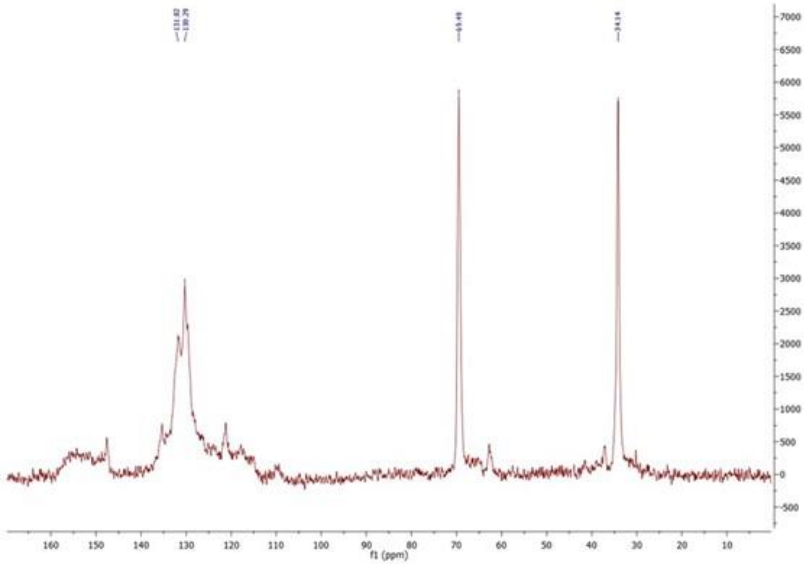

Figure S11.5.4. ^{13}C NMR spectrum of OligoTyrS I, in D_2O.

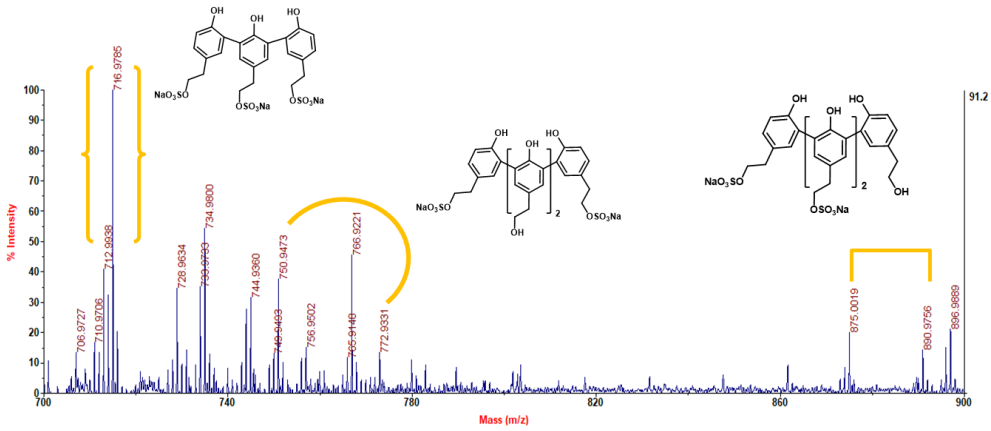

Figure S11.5.5. Segmental spectrum of MALDI-MS spectra of the OligoTyrS I and tentative structures representative of the possible species responsible for the peaks at [M+ Na]$^+$ = m/z 717, [M+ Na]$^+$ = m/z 751 (+ K$^+$), [M+ Na]$^+$ = m/z 875 (+ K$^+$).

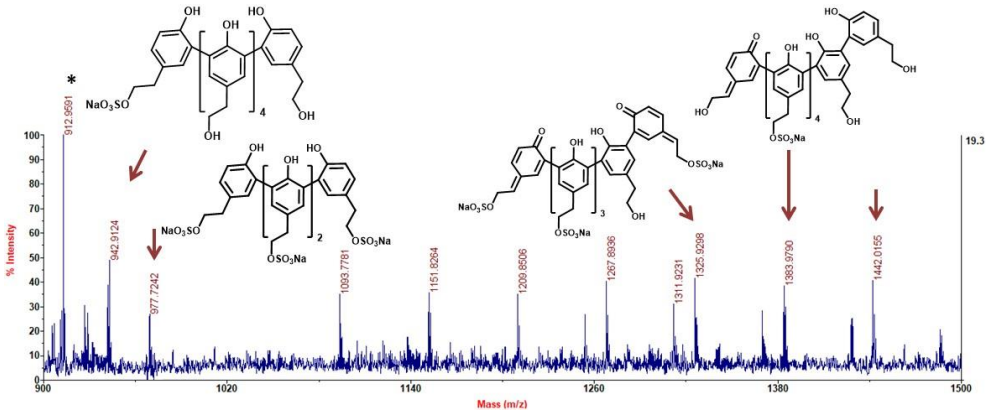

Figure S11.5.6. Segmental spectrum of MALDI-MS spectra of the OligoTyrS I and tentative structures representative of the possible species responsible for the peaks at [M+ Na]$^+$ = m/z 943, [M+ Na]$^+$ = m/z 977, [M+ H]$^+$ = m/z 1326 and [M+ Na]$^+$ = m/z 1383. Asterisk indicate signal due to matrix or impurities.

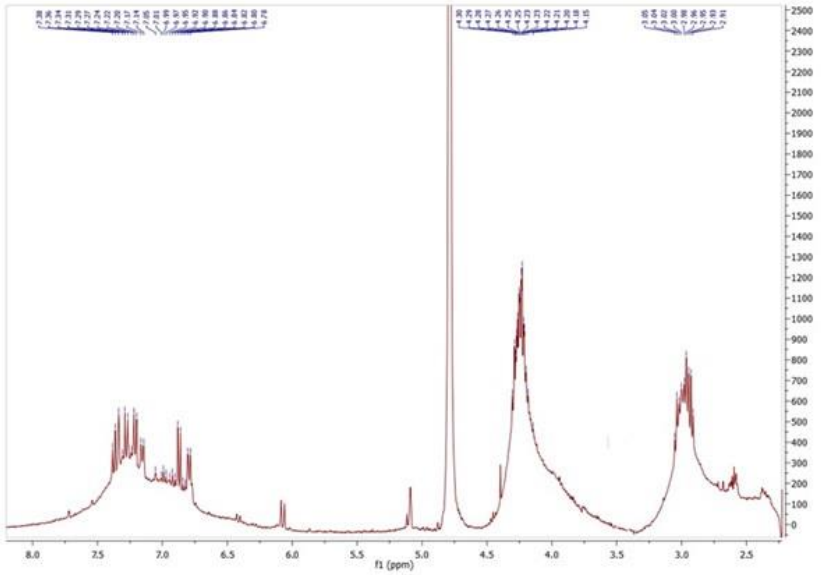

Figure S11.5.7. ^{1}H NMR spectrum of OligoTyrS II (400 MHz in D_2O).

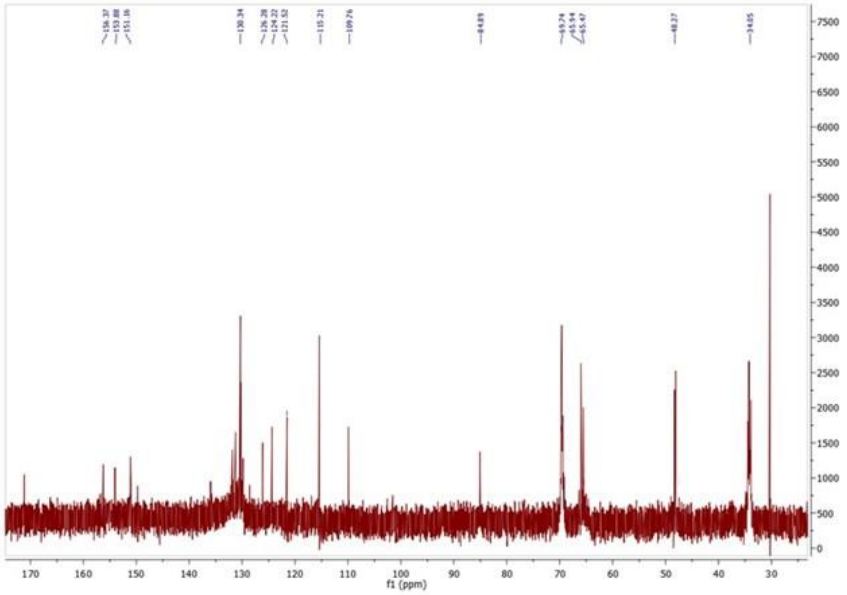

Figure S11.5.8. ^{13}C NMR spectrum of OligoTyrS II, in D_2O.

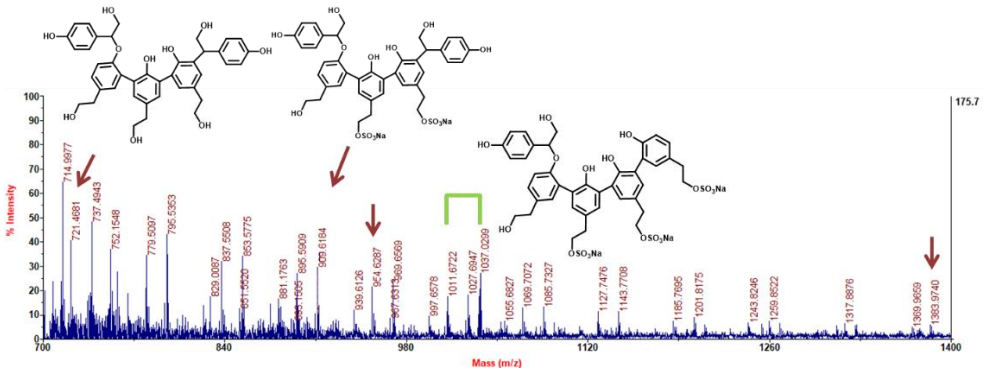

Figure S11.5.9. Segmental spectrum of MALDI-MS spectra of the OligoTyrS I and tentative structures representative of the possible species responsible for the peaks at $[M+ K]^+$ = m/z 721, $[M+ Na]^+$ = m/z 909 and $[M+ Na]^+$ = m/z 1011 (+ K^+).

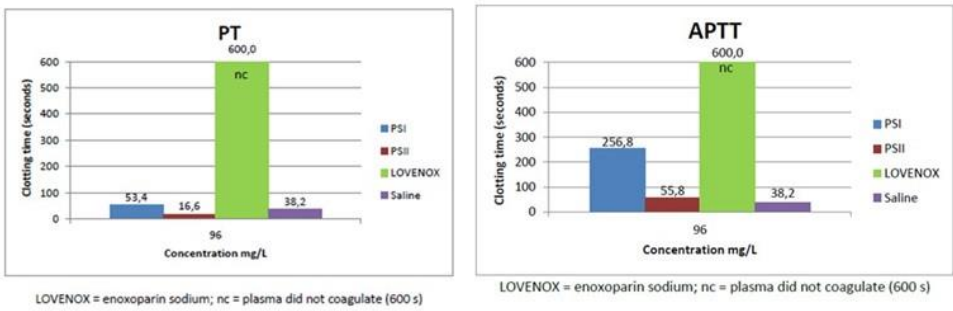

Figure S11.5.10. (Left) prothrombin time assay and (right) activated partial thromboplastin time assay of sulfated derivatives in comparison with a reference compound, Lovenox.

List of abbreviations

AFM. Atomic Force Microscopy

CAF. Caffeic acid

CAT. Catechol

CDA. Cysteinyldopamine

CEW. Chicken egg white

CHCA. α-Cyano-4-hydroxycinnamic acid

COUM. p-coumaric acid

DA. Dopamine

DHI. 5,6-dihydroxyindole

DHICA. 5,6-dihydroxyindole-2-carboxylic acid

DMF. Dimethylformamide

DMTMM. 4-(4,6-dimethoxy-1,3,5-triazin-2-yl)-4-methylmorpholinium-chloride

DPPH. 2,2-diphenyl-1-picrylhydrazy

EDC. N-(3-dimethylaminopropyl)-N'-ethylcarbodiimide chlorohydrate

EPR. electron paramagnetic resonance

FA. Folic acid

FER. Ferulic acid

FRAP. Ferric reducing antioxidant power

GA. Gallic acid

GSH. Glutathione

HEPES. Ferric chloride,4-(2-hydroxyethyl)-1-piperazineethanesulfonic acid

HMDA. Hexamethylenediamine

HOBt. 1-hydroxybenzotriazole

HRP. Horseradish peroxidase

HT. Hydroxytyrosol

L-DOPA. 3,4-dihydroxy-L-phenylalanine

Lipo-HT. 5-S-lipoylhydroxytyrosol

MCAT. 4-methylcatechol

MeDHICA. DHICA methyl ester

NMR. Solid state nuclear magnetic resonance

PDA. Polydopamine

PG. pyrogallol

PQ. Paraquat

QCM-D. Quartz Crystal Microbalance methodology

RBC. Human red blood cells

RES. Resorcinol

SEM. Scanning electron microscopy

TEA. Triethylamine

TPTZ. 2,4,6-tris(2-pyridyl)-s-triazine

Tris. Tris (hydroxymethyl) aminomethane

Trolox. 6-hydroxy-2,5,7,8-tetramethylchroman-2-carboxylic acid

Tyr. Tyrosol

VA. Vanillic acid

WCA. Water Contact Angle

References

1. A.S. Lubbe, T. van Leeuwen, S.J. Wezenberg, B.L. Feringa “Designing dynamic functional molecular systems” Tetrahedron, 73 (2017), 4837-4848.
2. S.J. Rego, A.C. Vale, G.M. Luz, J.F. Mano, N.M. Alves “Adhesive bioactive coatings inspired by sea life” Langmuir, 32 (2016), 560−568.
3. T. Sun, G. Qing, B. Su, L. Jiang “Functional biointerface materials inspired from nature” Chem. Soc. Rev., 40 (2011), 2909-2921.
4. S. Saxer, C. Portmann, S. Tosatti, K. Gademann, S. Zurcher, M. Textor “Surface assembly of catechol-functionalized poly(l-lysine)-graft-poly(ethylene glycol) copolymer on titanium exploiting combined electrostatically driven self-organization and biomimetic strong adhesion” Macromolecules, 43 (2010), 1050–1060.
5. S. Kim, C.B. Park “Mussel-inspired transformation of $CaCO_3$ to bone minerals” Biomaterials, 31 (2010), 6628-6634.
6. S. Pina, J. M. Oliveira, R.L. Reis “Natural-based nanocomposites for bone tissue engineering and regenerative medicine: a review” Adv. Mater., 27 (2015), 1143–1169.
7. H.J. Park, K. Yang, M.J. Kim, J. Jang, M. Lee, D.W. Kim, H. Lee, S.W. Cho “Bio-inspired oligovitronectin-grafted surface for enhanced self-renewal and long-term maintenance of human pluripotent stem cells under feeder-free conditions” Biomaterials, 50 (2015), 127-139.
8. J. Della Rocca, D. Liu, W. Lin “Nanoscale metal-organic frameworks for biomedical imaging and drug delivery” Acc. Chem. Res., 44 (2011), 957-968.
9. F. Khan, M. Tanaka “Designing smart biomaterials for tissue engineering” Int J Mol Sci., 19 (2018), 17.
10. A.I. Neto, A.C. Cibrão, C.R. Correia, R.R. Carvalho, G.M. Luz, G.G. Ferrer, G. Botelho, C. Picart, N.M. Alves, J.F. Mano “Nanostructured polymeric

coatings based on chitosan and dopamine-modified hyaluronic acid for biomedical applications" Small, 10 (2014), 2459–2469.

11. F. Li, Y. Tu, J. Hu, H. Zou, G. Liu, S. Lin, G. Yang, S. Hu, L. Miao, Y. Mo "Fabrication of fluorinated raspberry particles and their use as building blocks for the construction of superhydrophobic films to mimic the wettabilities from lotus leaves to rose petals" Polym. Chem., 6 (2015), 6746–6760.
12. S. Huang, Y. Zhang, J. Shi, W. Huang "Superhydrophobic particles derived from nature-inspired polyphenol chemistry for liquid marble formation and oil spills treatment" ACS Sustain. Chem. Eng., 4 (2016), 676–681.
13. A.G. Dumanli, T. Savin "Recent advances in the biomimicry of structural colours" Chem. Soc. Rev., 4 (2016), 6698-6724.
14. Q. Li, Q. Zeng, L. Shi, X. Zhang, K.-Q. Zhang "Bio-inspired sensors based on photonic structures of Morpho butterfly wings: a review" J. Mater. Chem. C, 4 (2016), 1752–1763.
15. L. Wu, J. He, W. Shang, T. Deng, J. Gu, H. Su, Q. Liu, W. Zhang, D. Zhang "Optical functional materials inspired by biology" Adv. Opt. Mater., 4 (2016), 195–224.
16. H. Wang, Y. Yang, L. Guo "Renewable-biomolecule-based electrochemical energy-storage materials" Adv. Energy Mater., 16 (2017), 17-19.
17. P. Poizot, F. Dolhem "Clean energy new deal for a sustainable world: from non-CO_2 generating energy sources to greener electrochemical storage devices" Energy Environ. Sci., 4 (2011) 2003.
18. K.J. Fallon, N. Wijeyasinghe, N. Yaacobi-Gross, R.S. Ashraf, D.M.E. Freeman, R.G. Palgrave, M. Al-Hashimi, T.J. Marks, I. McCulloch, T.D. Anthopoulos, H. Bronstein "A nature-inspired conjugated polymer for high performance transistors and solar cells" Macromolecules, 48 (2015), 5148–5154.

19. T. Zhuang, S. Sasaki, T. Ikeuchi, J. Kido, X.-F. Wang “Natural-photosynthesis-inspired photovoltaic cells using carotenoid aggregates as electron donors and chlorophyll derivatives as electron acceptors” RSC Adv., 5 (2015), 45755–45759.
20. J. Wang, T. Zhu, G.W. Ho “Nature-inspired design of artificial solar-to-fuel conversion systems based on copper phosphate microflowers” ChemSusChem, 9 (2016), 1575–1578.
21. K.I. Oyama, T. Yamada, D. Ito, T. Kondo, K. Yoshida “Metal complex pigment involved in the blue sepal color development of Hydrangea” J. Agric. Food Chem., 63 (2015), 7630–7635.
22. R. Guitard, J.F. Paul, V. Nardello-Rataj, J.-M. Aubry “Myricetin, rosmarinic and carnosic acids as superior natural antioxidant alternatives to α-tocopherol for the preservation of omega-3 oils” Food Chemistry, 213 (2016), 284-295.
23. A. Umeno, M. Takashima, K. Murotomi, Y. Nakajima, T. Koike, T. Matsuo, Y. Yoshida “Radical-scavenging activity and antioxidative effects of olive leaf components oleuropein and hydroxytyrosol in comparison with homovanillic alcohol” J Oleo Sci., 64 (2015), 793-800.
24. S. Chen, J. Wu, Q. Tang, C. Xu, Y. Huang, D. Huang, F. Luo, Y. Wu, F. Yan, Z. Weng, S. Wang “Nano-micelles based on hydroxyethyl starch-curcumin conjugates for improved stability, antioxidant and anticancer activity of curcumin” Carbohydr Polym., 228 (2020), 115398.
25. S. Quideau, D. Deffieux, C. Douat-Casassus, L. Pouységu “Plant polyphenols: chemical properties, biological activities and synthesis” Angew. Chem. Int. Ed., 50 (2011), 586 – 621.
26. H. Zhu, P. Li, S. Ren, W. Tan, G. Fang “Low-cost Ru/C-catalyzed depolymerization of the polymeric proanthocyanidin-rich fraction from bark to produce oligomeric proanthocyanidins with antioxidant activity” ACS Omega, 4 (2019), 16471–16480.

27. J.M. Landete “Ellagitannins, ellagic acid and their derived metabolites: a review about source, metabolism, functions and health” Food Research International, 44 (2011), 1150–1160.
28. D.A. Kirke, T.J. Smyth, D.K. Rai, O. Kenny, D.B. Stengel “The chemical and antioxidant stability of isolated low molecular weight phlorotannins” Food Chemistry, 221 (2017), 1104–1112.
29. S. Ito, K. Wakamatsu, M. d’Ischia, A. Napolitano, A. Pezzella In Melanins and Melanosomes: Biosynthesis, Biogenesis, Physiological and Pathological Functions (Eds: P.A. Riley, J. Borovansky) Wiley-VCH, Germany, Ch, 6 (2011), 167–185.
30. Y. Liu, J.D. Simon “Isolation and biophysical studies of natural eumelanins: applications of imaging technologies and ultrafast spectroscopy” Pigment Cell Research, 16 (2003), 606–618.
31. J. Saiz-Poseu, J. Sedó, B. García, T. Parella, C. Benaiges, R. Alibés, J. Hernando, F. Busquè and D. Ruiz-Molina “Versatile nanostructured materials via direct reaction of functionalized catechols” Adv. Mater., 25 (2013), 2066–2070.
32. H. Lee, S.M. Dellatore, W.M. Miller, P.B. Messersmith “Mussel-inspired surface chemistry for multifunctional coatings” Science, 318 (2007), 426-430.
33. M. d'Ischia, A. Napolitano, A. Pezzella, P. Meredith,T. Sarna “Chemical and structural diversity in eumelanins: unexplored bio-optoelectronic materials” Angew. Chem. Intl. Ed., 48 (2009), 3914-3921.
34. Y. Liu, K. Ai, L. Lu "Polydopamine and its derivative materials: synthesis and promising applications in energy, environmental, and biomedical fields" Chem Rev, 114 (2014), 5057-5115.
35. M. d'Ischia, K. Wakamatsu, F. Cicoira, E. Di Mauro, J.C. Garcia-Borron, S. Commo, I. Galvan, G. Ghanem, K. Kenzo, P. Meredith, A. Pezzella, C. Santato, T. Sarna, J.D. Simon, L. Zecca, F.A. Zucca, A. Napolitano, S. Ito

"Melanins and melanogenesis: from pigment cells to human health and technological applications" Pigment Cell & Melanoma Research, 28 (2015), 520-544.

36. C.T. Chen, F.J. Martin-Martinez, S. Ling, Z. Qin, M.J. Buehler "Nacre-inspired design of graphene oxide–polydopamine nanocomposites for enhanced mechanical properties and multi-functionalities" Nano Futures, 1 (2017).
37. A.B. Mostert, B.J. Powell, F.L. Pratt, G.R. Hanson, T. Sarna, I.R. Gentle, P. Meredith "Role of semiconductivity and ion transport in the electrical conduction of melanin" Proc Natl Acad Sci U S A, 109 (2012), 8943–8947.
38. M. Schieber, N.S. Chandel "ROS function in redox signaling and oxidative stress" Curr Biol., 24 (2014), R453-462.
39. A.M. Mileo, S. Miccadei "Polyphenols as modulator of oxidative stress in cancer disease: new therapeutic strategies" Oxidative Medicine and Cellular Longevity, 7 (2016), 1-17.
40. D. Trachootham, J. Alexandre, P. Huang "Targeting cancer cells by ROS-mediated mechanisms: a radical therapeutic approach?" Nature Reviews, 8 (2009), 579-591.
41. D. Tanini, L. Panzella, R. Amorati, A. Capperucci, E. Pizzo, A. Napolitano, S. Menichetti, M. d'Ischia "Resveratrol-based benzoselenophenes with an enhanced antioxidant and chain breaking capacity" Org Biomol. Chem., 13 (2015), 5757-5764.
42. C. Gaucher, A. Boudier, J. Bonetti, I. Clarot, P. Leroy, M. Parent "Glutathione: antioxidant properties dedicated to nanotechnologies" Antioxidants, 7 (2018), 62.
43. A. Napolitano, L. Panzella, G. Monfrecola, M. d'Ischia "Pheomelanin-induced oxidative stress: bright and dark chemistry bridging red hair phenotype and melanoma" Pigment Cell & Melanoma Res., 27 (2014), 721-733.

44. R. Micillo, L. Panzella, K. Koike, G. Monfrecola, A. Napolitano, M. d'Ischia ""Fifty shades" of black and red or how carboxyl groups fine tune eumelanin and pheomelanin properties" Int. J. Mol. Sci., 17 (2016), 746.
45. L. Panzella, G. Gentile, G. D' Errico, N.F. Della Vecchia, M. E. Errico, A. Napolitano, C. Carfagna, M. d'Ischia "Atypical structural and π-electron features of a melanin polymer that lead to superior free-radical-scavenging properties" Angew. Chem., Int. Ed., 52 (2013), 12684-12687.
46. M. d'Ischia, K. Wakamatsu, A. Napolitano, S. Briganti, J.C. Garcia-Borron, D. Kovacs, P. Meredith, A. Pezzella, M. Picardo, T. Sarna, J.D. Simon, S. Ito "Melanins and melanogenesis: methods, standards, protocols" Pigment Cell Melanoma Res., 26 (2013), 616–633.
47. A. Pezzella, A. Napolitano, M. d'Ischia, G. Prota, "Oxidative polymerisation of 5,6-dihydroxyindole-2-carboxylic acid to melanin: a new insight" Tetrahedron, 52 (1996), 7913–7920.
48. A. Pezzella, D. Vogna, G. Prota "Atropoisomeric melanin intermediates by oxidation of the melanogenic precursor 5,6-dihydroxyindole-2-carboxylic acid under biomimetic conditions" Tetrahedron, 58 (2002), 3681–3687.
49. P. Meredith, T. Sarna "The physical and chemical properties of eumelanin" Pigment Cell Research, 19 (2006), 572–594.
50. N.R. Martinez Rodriguez, S. Das, Y. Kaufman, J.N. Israelachvili, J.H. Waite "Interfacial pH during mussel adhesive plaque formation" Biofouling, 31 (2015), 221–227.
51. J.H. Waite, M.L. Tanzer "Polyphenolic substance of mytilus edulis: novel adhesive containing L-Dopa and hydroxyproline" Science, 212 (1981), 1038–1040.
52. S.J. Rego, A.C. Vale, G.M. Luz, J.F. Mano, N.M. Alves "Adhesive bioactive coatings inspired by sea life" Langmuir, 32 (2016), 560–568.
53. A. Pezzella, A. Iadonisi, S. Valerio, L. Panzella, A. Napolitano, M. Adinolfi, M. d'Ischia "Disentangling eumelanin "black chromophore": visible

absorption changes as signatures of oxidation state- and aggregation-dependent dynamic interactions in a model water-soluble 5,6-dihydroxyindole polymer" J. Am. Chem. Soc., 131 (2009), 15270–15275.

54. S.B. Rienecker, A.B. Mostert, G. Schenk, G.R. Hanson, P. Meredith "Heavy water as a probe of the free radical nature and electrical conductivity of melanin" J. Phys. Chem. B, 119 (2015), 14994–15000.
55. A.B. Mostert, G.R. Hanson, T. Sarna, I.R. Gentle, B.J. Powell, P. Meredith "Hydration-controlled X-band EPR spectroscopy: a tool for unravelling the complexities of the solid-state free radical in eumelanin" J. Phys. Chem. B, 117 (2013), 4965–4972.
56. L.B. Assis Oliveira, T. L Fonseca, B.J. Costa Cabral, K. Coutinho, S. Canuto "Hydration effects on the electronic properties of eumelanin building blocks" J. Chem. Phys., 145 (2016), 84501.
57. B.P. Lee, P.B. Messersmith, J.N. Israelachvili, J.H. Waite "Mussel-inspired adhesives and coatings" Annu. Rev. Mater. Res., 41 (2011), 99–132.
58. D. Fan, C. Wu, K. Wang, X. Gu, Y. Liu, E. Wang "A polydopamine nanosphere based highly sensitive and selective aptamer cytosensor with enzyme amplification" Chem. Commun., 52 (2016), 406–409.
59. Y. Liu, W.-Z. Qiu, H.-C. Yang, Y.-C. Qian, X.-J. Huang, Z.-K. Xu "Polydopamine-assisted deposition of heparin for selective adsorption of low-density lipoprotein" RSC Adv., 5 (2015), 12922–12930.
60. J.H. Jiang, L.P. Zhu, X.L. Li, Y.Y. Xu, B.K. Zhu "Surface modification of PE porous membranes based on the strong adhesion of polydopamine and covalent immobilization of heparin" J. Memb. Sci., 364 (2010), 194–202.
61. Q. Liu, B. Yu, W. Ye, F. Zhou "Highly selective uptake and release of charged molecules by pH-responsive polydopamine microcapsules" Macromol. Biosci., 11 (2011), 1227–1234.

62. W.X. Mao, X.J. Lin, W. Zhang, Z. X. Chi, R. W. Lyu, A. M. Cao, L. Wan "Core–shell structured TiO2@polydopamine for highly active visible-light photocatalysis" J. Chem. Commun., 52 (2016), 7122–7125.
63. A.R.C. Rodríguez, J. Saiz-Poseu, J. García-Pardo, B. García, J. Lorenzo, I. Ojea-Jiménez, D. Komilis, J. Sedó, F. Busqué, A. Sánchez, D. Ruiz-Molina, X. Font "Biocompatible polydopamine-like particles for the removal of heavy metals at extremely low concentrations" RSC Adv., 6 (2016), 40058–40066.
64. L. Zhou, Y. Zong, Z. Liu, A. Yu "A polydopamine coating ultralight graphene matrix as a highly effective polysulfide absorbent for high-energy LiS batteries" Renew. Energy, 96 (2016), 333–340.
65. P. Manini, V. Criscuolo, L. Ricciotti, A. Pezzella, M. Barra, A. Cassinese, O. Crescenzi, M.G. Maglione, P. Tassini, C. Minarini, V. Barone, M. d'Ischia "Melanin-inspired organic electronics: electroluminescence in asymmetric triazatruxenes" Chempluschem, 80 (2015), 919–927.
66. K.Y. Ju, Y. Lee, S. Lee, S.B. Park, J.K. Lee "Bioinspired polymerization of dopamine to generate melanin-like nanoparticles having an excellent free-radical-scavenging property" Biomacromolecules, 12 (2011), 625–632.
67. M. Arzillo, G. Mangiapia, A. Pezzella, R.K. Heenan, A. Radulescu, L. Paduano, M. d'Ischia "Eumelanin buildup on the nanoscale: aggregate growth/assembly and visible absorption development in biomimetic 5,6-dihydroxyindole polymerization" Biomacromolecules, 13 (2012), 2379–2390.
68. Y. Liu, K. Ai, L. Lu "Polydopamine and its derivative materials: synthesis and promising applications in energy, environmental, and biomedical fields" Chem. Rev., 114 (2014), 5057–5115.
69. S. Chen, X. Li, Z. Yang, S. Zhou, R. Luo, M.F. Maitz, Y. Zhao, J. Wang, K. Xiong, N. Huang "A simple one-step modification of various materials for

introducing effective multi-functional groups" Colloids Surf B Biointerfaces, 113 (2014), 125-133.

70. M. Iacomino, J.I. Paez, R. Avolio, A. Carpentieri, L. Panzella, G. Falco, E. Pizzo, M.E. Errico, A. Napolitano, A. Del Campo, M. d'Ischia "Multifunctional thin films and coatings from caffeic acid and a cross-linking diamine" Langmuir, 33 (2017), 2096-2102.
71. C. Lim, J. Huang, S. Kim, H. Lee, H. Zeng, D.S. Hwang "Nanomechanics of poly(catecholamine) coatings in aqueous solutions" Angew. Chem. Int. Ed., 55 (2016), 3342-3346.
72. W.-Z. Qiu, G.-P. Wu Z.-K. Xu "Robust coatings via catechol–amine codeposition: mechanism, kinetics, and application" ACS Appl. Mater. Interfaces, 10 (2018), 5902–5908.
73. S. Suárez-García, J. Sedó, J. Saiz-Poseu, D. Ruiz-Molina "Copolymerization of a catechol and a diamine as a versatile polydopamine-like platform for surface functionalization: the case of a hydrophobic coating" Biomimetics, 2 (2017), 22.
74. V. Ball "Composite materials and films based on melanins, polydopamine, and other catecholamine-based materials" Biomimetics, 2 (2017), 12.
75. J.H. Ryu, P.B. Messersmith, H. Lee "Polydopamine surface chemistry: a decade of discovery" ACS Applied Mater. Interfaces, 10 (2018), 7523–7540.
76. M.J. Harrington, A. Masic, N. Holten-Andersen, J.H. Waite, P. Fratzl "Iron-clad fibers: a metal-based biological strategy for hard flexible coatings" Science, 328 (2010), 216–220.
77. N. Holten-Andersen, M.J. Harrington, H. Birkedal, B.P. Lee, P.B. Messersmith, K.Y.C. Lee, J.H. Waite "pH-induced metal-ligand cross-links inspired by mussel yield self-healing polymer networks with near-covalent elastic moduli" Proc. Natl. Acad. Sci. U. S. A., 108 (2011), 2651–2655.
78. L. Petrone, A. Kumar, C.N. Sutanto, N.J. Patil, S. Kannan, A. Palaniappan, S. Amini, B. Zappone, C. Verma, A. Miserez "Mussel adhesion is dictated

by time-regulated secretion and molecular conformation of mussel adhesive proteins" Nat. Commun., 6 (2015), 8737.

79. D.E. Fullenkamp, J.G. Rivera, Y. Gong, K.H.A. Lau, L. He, R. Varshney, P.B. Messersmith "Mussel-inspired silver-releasing antibacterial hydrogels" Biomaterials, 33 (2012), 3783–3791.
80. J. Yang, M.A. Cohen Stuart, M. Kamperman "Jack of all trades: versatile catechol crosslinking mechanisms" Chem. Soc. Rev., 43 (2014), 8271–8298.
81. D.E. Fullenkamp, D.G. Barrett, D.R. Miller, J.W. Kurutz, P.B. Messersmith "pH-dependent cross-linking of catechols through oxidation via Fe^{3+} and potential implications for mussel adhesion" RSC Adv., 4 (2014), 25127–25134.
82. K.J. Kramer, M.R. Kanost, T.L. Hopkins, H. Jiang, Y.C. Zhu, R. Xu, J.L. Kerwin, F. Turecek "Oxidative conjugation of catechols with proteins in insect skeletal systems" Tetrahedron, 57 (2001), 385–392.
83. D. Montroni, F. Valle, S. Rapino, S. Fermani, M. Calvaresi, M.J. Harrington, G. Falini "Functional biocompatible matrices from mussel byssus waste" ACS Biomaterials Science & Engineering, 4 (2018), 57−65.
84. P.K. Forooshani, B.P. Lee "Recent approaches in designing bioadhesive materials inspired by mussel adhesive protein" J. Polym. Sci., Part A: Polym. Chem., 55 (2017), 9–33.
85. J.H. Waite, X. Qin "Polyphosphoprotein from the adhesive pads of Mytilus edulis" Biochemistry, 40 (2001), 2887–2893.
86. J.H. Waite "Mussel adhesion–essential footwork" Journal of Experimental Biology, 220 (2017), 517-530.
87. J. Sedõ, J. Saiz-Poseu, F. Busqué, D. Ruiz-Molina "Catechol-based biomimetic functional materials" Adv Mater., 25 (2013), 653–701.
88. V. Ball "Polydopamine nanomaterials: recent advances in synthesis methods and applications" Front Bioeng Biotechnol., 6 (2018), 109.

89. V. Ball, D. Del Frari, V. Toniazzo, D. Runch “Kinetics of polydopamine film deposition as a function of pH and dopamine concentration: insights in the polydopamine deposition mechanism” J. Colloid Interface Sci., 386 (2012), 366-372.
90. F. Bernsmann, V. Ball, F. Addiego, A. Ponche, M. Michel, J.J. Gracio, V. Toniazzo, D. Ruch “Dopamine-melanin film deposition depends on the used oxidant and buffer solution” Langmuir, 27 (2011), 2819-2825.
91. Q. Wei, F. Zhang, J. Li, B. Li, C. Zhao “Oxidant-induced dopamine polymerization for multifunctional coatings” Polym. Chem., 1 (2010), 1430-1433.
92. X. Du, L. Li, J. Li, C. Yang, N. Frenkel, A. Welle, S. Heissler, A. Nefedov, M. Grunze, P.A. Levkin “UV-triggered dopamine polymerization: control of polymerization, surface coating, and photopatterning” Adv. Mater., 26 (2014), 8029-8033.
93. F. Ponzio, J. Barthès, J. Bour, M. Michel, P. Bertani, J. Hemmerlé, M. d’Ischia, V. Ball “Oxidant control of polydopamine surface chemistry in acids: a mechanism-based entry to superhydrophilic-superoleophobic coatings” Chem. Mater., 28 (2016), 4697-4705.
94. M. Arzillo, A. Pezzella, O. Crescenzi, A. Napolitano, E. Land, V. Barone, M. d’Ischia “Cyclic structural motifs in 5,6-dihydroxyindole polymerization uncovered: biomimetic modular buildup of a unique five-membered macrocycle” Org. Lett., 12 (2010), 3250-3253.
95. O. Crescenzi, C. Kroesche, W. Hoffbauer, M. Jansen, A. Napolitano, G. Prota, M.G. Peter “Synthesis of dopamines labelled with ^{13}C in the α- or β-side chain position and their application to structural studies on melanins by solidstate NMR spectroscopy” Eur J Org Chem, 6 (1994), 563-567.
96. D.R. Dreyer, D.J. Miller, B.D. Freeman, D.R. Paul, C.W. Bielawski “Elucidating the structure of poly(dopamine)” Langmuir, 28 (2012), 6428-6435.

97. S. Hong, Y.S. Na, S. Choi, I.T. Song, W.Y. Kim, H. Lee “Non-covalent self-assembly and covalent polymerization co-contribute to polydopamine formation” Adv. Funct. Mater., 22 (2012), 4711-4717.
98. N.F. Della Vecchia, R. Avolio, M. Alfè, M.E. Errico, A. Napolitano, M. d’Ischia “Building-block diversity in polydopamine underpins a multifunctional eumelanin-type platform tunable through a quinone control point” Adv. Funct. Mater., 23 (2013), 1331-1340.
99. N.F. Della Vecchia, A. Luchini, A. Napolitano, G. D’Errico, G. Vitiello, N. Szekely, M. d’Ischia, L. Paduano “Tris buffer modulates polydopamine growth, aggregation, and paramagnetic properties” Langmuir, 30 (2014), 9811-9818.
100. J. Liebscher, R. Mrowczynski, H.A. Scheidt, C. Filip, N.D. Hadade, R. Turcu, A. Bende, S. Beck “Structure of polydopamine: a never-ending story?” Langmuir, 29 (2013), 10539–10548.
101. R.A. Zangmeister, T.A. Morris, M.J. Tarlov “Characterization of polydopamine thin films deposited at short times by autoxidation of dopamine” Langmuir, 29 (2013), 8619-8628.
102. Y. Ding, L.T. Weng, M. Yang, Z. Yang, X. Lu, N. Huang, Y. Leng “Insights into the aggregation/deposition and structure of a polydopamine film” Langmuir, 30 (2014), 12258-12269.
103. Y. Yang, P. Qi, Y. Ding, M.F. Maitz, Z. Yang, Q. Tu, K. Xiong, Y. Leng, N. Huang “A biocompatible and functional adhesive amine-rich coating based on dopamine polymerization.” J. Mater. Chem. B., 3 (2015), 72-81.
104. Q. Lyu, J. Zhang, K.G. Neoh, C.L. Lin Chai “A one step method for the functional and property modification of DOPA based nanocoatings” Nanoscale, 9 (2017), 12409-12415.
105. M. Salomäki, L. Marttila, H. Kivelä, T. Ouvinen, J.O. Lukkari “Effect of pH and oxidant on the first steps of polydopamine formation: a thermodynamic approach” J. Phys. Chem. B, 122 (2018), 631-6327.

106. H.W. Kim, B.D. McCloskey, T.H. Choi, C. Lee, M.J. Kim, B.D. Freeman, H.B. Park “Oxygen concentration control of dopamine-induced high uniformity surface coating chemistry” ACS Appl. Mater. Interfaces, 5 (2013), 233-238.
107. T. Shalev, A. Gopin, M. Bauer, R.W. Stark, S. Rahimipour “Non-leaching antimicrobial surfaces through polydopamine bio-Inspired coating of quaternary ammonium salts or an ultrashort antimicrobial lipopeptide” J. Mater. Chem. 22 (2012), 2026−2032.
108. S.H. Ku, J.S. Lee, C.B. Park “Spatial control of cell adhesion and patterning through mussel-inspired surface modification by polydopamine” Langmuir, 26 (2010), 15104−15108.
109. H. Fan, X. Yu, Y. Liu, Z. Shi, H. Liu, Z. Nie, D. Wu, Z. Jin “Folic acid−polydopamine nanofibers show enhanced ordered-stacking via π−π interactions” Soft Matter, 11 (2015), 4621−4629.
110. E. Kaxiras, A. Tsolakidis, G. Zonios, S. Meng “Structural model of eumelanin” Phys. Rev. Lett., 97 (2006), 218102.
111. C. Zhang, Y. Ou, W.X. Lei, L.S. Wan, J. Ji, Z.K. Xu “$CuSO_4/H_2O_2$-induced rapid deposition of polydopamine coatings with high uniformity and enhanced stability” Angew. Chem., 128 (2016), 3106-3109.
112. R. Edge, M. d’Ischia, E.J. Land, A. Napolitano, S. Navaratnam, L. Panzella, A. Pezzella, C.A. Ramsden, P.A. Riley “Dopaquinone redox exchange with dihydroxyindole and dihydroxyindole carboxylic acid” Pigm. Cell Res., 19 (2006), 443-450.
113. C.S. McKay, M.G. Finn “Click chemistry in complex mixtures: bioorthogonal bioconjugation” Chem Biol., 21 (2014), 1075–1101.
114. X. Ji, K. Ji, V. Chittavong, R.E. Aghoghovbia, M. Zhu, B. Wang “Click and fluoresce: a bioorthogonally activated smart probe for wash-free fluorescent labeling of biomolecules” J. Org. Chem., 82 (2017), 1471−1476.

115. J. Chan, S.C. Dodani, C.J. Chang "Reaction-based small-molecule fluorescent probes for chemoselective bioimaging" Nat. Chem., 4 (2012), 973–984.
116. M.E. Jun, B. Roy, K.H. Ahn, ""Turn-on" fluorescent sensing with "reactive" probes" Chem. Commun., 47 (2011), 7583-7601.
117. L. Liang, F. Lan, L. Li, M. Su, S. Ge, J. Yu, H. Liu, M. Yan "Fluorescence "turn-on" determination of H_2O_2 using multilayer porous SiO_2/NGQDs and PdAu mimetics enzymatic/oxidative cleavage of single-stranded DNA" Biosens. Bioelectron., 82 (2016), 204–211.
118. J.C. Jewett, C.R. Bertozzi "Synthesis of a fluorogenic cyclooctyne activated by Cu-free click Chemistry" Org. Lett., 13 (2011), 5937–5939.
119. M. Isik, T. Ozdemir, I.S. Turan, S. Kolemen, E.U. Akkaya "Chromogenic and fluorogenic sensing of biological thiols in aqueous solutions using BODIPY-based reagents" Org. Lett., 15 (2013), 216–219.
120. S. Gui, Y. Huang, F. Hu, Y. Jin, G. Zhang, L. Yan, D. Zhang, R. Zhao "Fluorescence turn-on chemosensor for highly selective and sensitive detection and bioimaging of $Al^{(3+)}$ in living cells based on ion-induced aggregation" Anal. Chem., 87 (2015), 1470–1474.
121. A. Loudet, K. Burgess "BODIPY dyes and their derivatives: synthesis and spectroscopic properties" Chem. Rev., 107 (2007), 4891–4932.
122. D. Li, Y. Zhang, Z. Fan, J. Yu, "AIE luminogen-functionalised mesoporous nanomaterials for efficient detection of volatile gases" Chem. Commun., 51 (2015), 13830-13833.
123. K. Liu, C. Shang, Z. Wang, Y. Qi, R. Miao, K. Liu, T. Liu, Y. Fang "Non-contact identification and differentiation of illicit drugs using fluorescent films" Nat. Commun., 9 (2018), 1-11.
124. Y. Feng, X. Li, H. Ma, Z. Zhang, M. Zhang, S. Hao "A simple fluorescent film probe for the detection of fluoride anion in organic solution" Dyes Pigm., 153 (2018), 200-205.

125. O. Crescenzi, A. Napolitano, G. Prota, M.G. Peter “Oxidative coupling of DOPA with resorcinol and phloroglucinol: isolation of adducts with an unusual tetrahydromethanobenzofuro[2,3-d]azocine skeleton” Tetrahedron, 47 (1991) 6243–6250.
126. A.U. Acuña, F. Amat-Guerri “Early history of solution fluorescence: the lignum nephriticum of Nicolás Monardes” Springer Series in Fluorescence, 4 (2008), 3–20.
127. A.U. Acuña, F. Amat-Guerri, P. Morcillo, M. Liras, B. Rodrìguez “Structure and formation of the fluorescent compound of lignum nephriticum” Org. Lett., 11 (2009) 3020–3023.
128. A.U.Acuña, M. Álvarez-Pérez, M. Liras, P.B. Coto, F. Amat-Guerri “Synthesis and photophysics of novel biocompatible fluorescent oxocines and azocines in aqueous solution” Phys. Chem. Chem. Phys., 15 (2013) 16704–16712.
129. F. Nador, F. Novio, D. Ruiz-Molina “Coordination polymer particles with ligand-centred pH-responses and spin transition” Chem. Commun., 50 (2014), 14570–14572.
130. A. Kamal-Eldin, A. Pouru, C. Eliasson, P. Åman “Alkylresorcinols as antioxidants: hydrogen donation and peroxyl radical-scavenging effects” J. Sci. Food Agric., 81 (2001), 353–356.
131. E. Bendary, R.R. Francis, H.M.G. Ali, M.I. Sarwat, S. El Hady “Antioxidant and structure–activity relationships (SARs) of some phenolic and anilines compounds” Ann. Agric. Sci., 58 (2013), 173–181.
132. N. Wells, D. Yusufu, A. Mills “Colourimetric plastic film indicator for the detection of the volatile basic nitrogen compounds associated with fish spoilage” Talanta, 194 (2019), 830-836.
133. L.H. Nguyen, S. Naficy, R. McConchie, F. Dehghani, R. Chandrawati “Polydiacetylene-based sensors to detect food spoilage at low temperatures” J. Mater. Chem. C, 7 (2019), 1919-1926.

134. Q. Ma, Y. Ren, Z. Gu, L. Wang “Developing an intelligent film containing *Vitis* amurensis husk extracts: the effects of pH value of the film-forming solution” J. Clean. Prod., 166 (2017), 851-859.
135. C. Xu, S. Liu, Z. Liu, F. Song, S. Liu “Superoxide generated by pyrogallol reduces highly water-soluble tetrazolium salt to produce a soluble formazan: a simple assay for measuring superoxide anion radical scavenging activities of biological and abiological samples” Anal. Chim. Acta, 793 (2013), 53–60.
136. L. Long, D. Zhang, X. Li, J. Zhang, C. Zhang, L. Zhou “A fluorescence ratiometric sensor for hypochlorite based on a novel dual-fluorophore response approach” Anal. Chim. Acta, 775 (2013), 100–105.
137. J. Fan, X. Chang, M. He, C. Shang, G. Wang, S. Yin, H. Peng “Functionality-oriented derivatization of naphthalene diimide: a molecular gel strategy-based fluorescent film for aniline vapor detection” ACS Appl. Mater. Interfaces, 8 (2016), 18584–18592.
138. M. He, H. Peng, G. Wang, X. Chang, R. Miao, W. Wang, Y. Fang “Fabrication of a new fluorescent film and its superior sensing performance to N-methamphetamine in vapor phase” Sensors Actuators B., 227 (2016), 255–262.
139. S. Philip “Organic solid-state fluorescence: strategies for generating switchable and tunable fluorescent materials” Chempluschem, 77 (2012), 518–531.
140. K. Liu, T. Liu, X. Chen, X. Sun, Y. Fang “Fluorescent films based on molecular-gel networks and their sensing performances” ACS Appl. Mater. Interfaces, 5 (2013), 9830-9836.
141. M.-J. Wu, H.-H. Hu, C.-Z. Siao, Y.-M. Liao, J.-H. Chen, M.-Y. Li, T.-Y. Lin, Y.-F. Chen “All organic label-like copper(II) ions fluorescent film sensors with high sensitivity and stretchability” ACS Sens., 3 (2018), 99–105.

142. S. Chen, J. Zhang, Y. Chen, S. Zhao, M. Chen, X. Li, M.F. Maitz, J. Wang, N. Huang “Application of phenol/amine copolymerized film modified magnesium alloys: anticorrosion and surface biofunctionalization” ACS Appl. Mater. Interfaces, 7 (2015), 24510-24522.
143. R.A. Heacock, L. Marion “The infrared spectra of secondary amines and their salts” Can. J. Chem., 34 (1956), 1782–1795.
144. D. Ruiz-Molina, J. Saiz Poseu, F. Busque, F. Nador, J. Mancebo “The chemistry behind catechol-based adhesion” Angew. Chem. Int. Ed., 58 (2019), 696-714.
145. M. Vatankhah-Varnoosfaderani, X. Hu, Q. Li, H. Adelnia, M. Ina, S.S. Sheiko “Universal coatings based on zwitterionic-dopamine copolymer microgels” ACS Appl. Mater. Interfaces, 10 (2018), 20869-20875.
146. J. Y. Kim, W. I. Kim, W. Youn, J. Seo, B. J. Kim, J. K. Lee, I. S. Choi “Enzymatic film formation of nature-derived phenolic amines” Nanoscale, 10 (2018), 13351-13355.
147. Q.Z. Zhong, J.J. Richardson, S. Li, W. Zhang, Y. Ju, J. Li, S. Pan, J. Chen, F. Caruso “Expanding the toolbox of metal–phenolic networks via enzyme-mediated assembly” Angew. Chem. Int. Ed., 58 (2019), 2-9.
148. S. Jus, V. Kokol, G.M. Guebitz “Tyrosinase-catalysed coating of wool fibres with different protein-based biomaterials” J Biomater Sci Polym Ed., 20 (2009), 253-269.
149. M. Richter, C. Schulenburg, D. Jankowska, T. Heck, G. Faccio “Novel materials through nature's catalysts” Materials Today, 18 (2015), 459-467.
150. M. Guazzaronia, C. Crestini, R. Saladino “Layer-by-layer coated tyrosinase: an efficient and selective synthesis of catechols” Bioorganic & Medicinal Chemistry, 20 (2012), 157-166.
151. G.Z. Sauerbrey “The use of quartz oscillators for weighing thin layers and for microweighing” Phys., 155 (1959), 206-222.

152. D. Huang, B. Ou, R.L. Prior “The chemistry behind antioxidant capacity assays” J. Agric. Food Chem, 53 (20053), 1841-1856.
153. I.F. Benzie, J.J. Strain “The ferric reducing ability of plasma (FRAP) as a measure of "antioxidant power": the FRAP assay” Anal. Biochem., 239 (1996), 70-76.
154. M. Gauden, A. Pezzella, L. Panzella, M.T. Neves-Petersen, E. Skovsen, S.B. Petersen, K.M. Mullen, A Napolitano, M. d’Ischia, V. Sundstrom “Role of solvent, pH, and molecular size in excited-state deactivation of key eumelanin building blocks: implications for melanin pigment photostability” J. Am. Chem. Soc., 130 (2008), 17038– 17043.
155. A. Corani, A. Huijser, T. Gustavsson, D. Markovitsi, P. Malmqvist, A. Pezzella, M. d’Ischia, V. Sundström “Superior photoprotective motifs and mechanisms in eumelanins uncovered” J. Am. Chem. Soc., 136 (2014), 11626–35.
156. L. Panzella, A. Napolitano, M. d’Ischia “Is DHICA the key to dopachrome tautomerase and melanocyte functions?” Pigment Cell Melanoma Res., 24 (2011), 248–249.
157. D. Kovacs, E. Flori, V. Maresca, M. Ottaviani, N. Aspite, M.L. Dell'Anna, L. Panzella, A. Napolitano, M. Picardo, M. d'Ischia “The eumelanin intermediate 5,6-dihydroxyindole-2-carboxylic acid is a messenger in the cross-talk among epidermal cells” J. Invest. Dermatol, 132 (2012), 1196-1205.
158. G. Prota, Melanins and melanogenesis, Academic Press, (1992)
159. S. Ito, K. Wakamatsu “Chemistry of mixed melanogenesis-pivotal roles of dopaquinone” Photochem. Photobiol., 84 (2008), 582–592.
160. S. Ito “The IFPCS presidential lecture: a chemist’s view of melanogenesis” Pigment Cell Res., 16 (2003), 230–236.

161. A. Palumbo, M. d'Ischia, G. Misuraca, G. Prota, T.M. Schultz. "Structural modifications in biosynthetic melanins induced by metal ions" Biochim. Biophys. Acta, 964 (1988), 193–199.
162. S. Ito, M. Kikuta, S. Koike, G. Szewczyk, M. Sarna, A. Zadlo, T. Sarna, K. Wakamatsu "Roles of reactive oxygen species in UVA-induced oxidation of 5,6-dihydroxyindole-2-carboxylic acid-melanin as studied by differential spectrophotometric method" Pigment Cell Melanoma Res., 29 (2016), 340-51.
163. R. Micillo, M. Iacomino, M. Perfetti, L. Panzella, K. Koike, G. D'Errico, M. d'Ischia, A. Napolitano "Unexpected impact of esterification on the antioxidant activity and (photo)stability of a eumelanin from 5,6-dihydroxyindole-2-carboxylic acid" Pigment Cell Melanoma Res., 31 (2018), 475-483.
164. A. Napolitano, A. Palumbo, M. d'Ischia, G. Prota "Mechanism of selective incorporation of the melanoma seeker 2-thiouracil into growing melanin" J. Med. Chem., 39 (1996), 5191–5201.
165. T. Ling-Hsien, T. Ning-Hsuan, T. Ya-R, L. Tien-We, L. Yi-Wei, C. Jien-Lin, H. Hua-Ting, C. Yu-Sheng, C. Rong-Jie, W. Ying-Ta, C. Yi-Tsu, C. Chang-Shi, F. Jim-Min, C. Yun-Ru "Rationally designed divalent caffeic amides inhibit amyloid-β fibrillization, induce fibril dissociation, and ameliorate cytotoxicity" European Journal of Medicinal Chemistry, 158 (2018), 393-404.
166. M.C. Sheikh, S. Takagi, T. Yoshimura, H. Morita "Mechanistic studies of DCC/HOBt-mediated reaction of 3-phenylpropionic acid with benzyl alcohol and studies on the reactivities of 'active ester' and the related derivatives with nucleophiles" Tetrahedron, 66 (2010), 7272-7278.
167. S. Ghiani, S. Baroni, D. Burgio, G. Digilio, M. Fukuhara, P. Martino, K. Monda, C. Nervi, A. Kiyomine, S. Aime, "Characterization of human hair

melanin and its degradation products by means of magnetic resonance techniques" Magn Reson Chem, 46 (2008), 471–479.

168. A. Pezzella, L. Panzella, A. Natangelo, M. Arzillo, A. Napolitano, M. d'Ischia "5,6-dihydroxyindole tetramers with "anomalous" interunit bonding patterns by oxidative coupling of 5,5',6,6'-tetrahydroxy-2,7'-biindolyl: emerging complexities on the way toward an improved model of eumelanin buildup" J. Org. Chem., 72 (2007), 9225–9230.
169. K.B. Stark, J.M. Gallas, G.W. Zajac, J.T. Golab, S. Gidanian, T. McIntire, P.J. Farmer "Effect of stacking and redox state on optical absorption spectra of melanins-comparison of theoretical and experimental results" Journal of Physical Chemistry B, 109 (2005), 1970-1977.
170. A. Slominski, D.J. Tobin, S. Shibahara, J. Wortsman "Melanin pigmentation in mammalian skin and its hormonal regulation" Physiol. Rev., 84 (2004), 1155-1228.
171. J.D. Simon, D.N. Peles "The red and the black" Acc. Chem. Res., 43 (2010), 1452-1460.
172. M.S. Blois, A.B. Zahalan, J.E. Maling "Electron spin resonance studies on melanin" Biophys. J., 4 (1964), 471-490.
173. J. Borovanský, P.A. Riley, A. Patrick "Melanins and melanosomes : biosynthesis, biogenesis, physiological, and pathological functions" Wiley-Blackwell, (2011).
174. M.L. Tran, B.J. Powell, P. Meredith "Chemical and structural disorder in eumelanins: a possible explanation for broadband absorbance" Biophys. J., 90 (2006), 743–52.
175. M. d'Ischia, O. Crescenzi, A. Pezzella, M. Arzillo, L. Panzella, A. Napolitano, V. Barone "Structural effects on the electronic absorption properties of 5,6-dihydroxyindole oligomers: the potential of an integrated experimental and DFT approach to model eumelanin optical properties" Photochem. Photobiol., 84 (2008), 600–607.

176. D. Tuna, A. Udvarhelyi, A.L. Sobolewski, W. Domcke, T. Domratcheva "Onset of the electronic absorption spectra of isolated and π-stacked oligomers of 5,6-dihydroxyindole: an ab initio study of the building blocks of eumelanin" J. Phys. Chem. B, 120 (2016), 3493–3502.

177. A. Pezzella, O. Crescenzi, L. Panzella, A. Napolitano, E.J. Land, V. Barone, M. d'Ischia "Free radical coupling of o-semiquinones uncovered" J. Am. Chem. Soc., 135 (2013), 12142–12149.

178. L. Ascione, A. Pezzella, V. Ambrogi, C. Carfagna, M. d'Ischia "Intermolecular π-electron perturbations generate extrinsic visible contributions to eumelanin black chromophore in model polymers with interrupted interring conjugation" Photochem. Photobiol., 89 (2013), 314–318.

179. M. d'Ischia, A. Napolitano, A. Pezzella, E.J. Land, C.A. Ramsden, P.A. Riley "5,6-dihydroxyindoles and indole-5,6-diones" Adv. Heterocycl. Chem., 89 (2005), 1–63.

180. M. d'Ischia, A. Napolitano, A. Pezzella "5,6-dihydroxyindole chemistry: unexplored opportunities beyond eumelanin" Eur. J. Org. Chem., 28 (2011), 5501–5516.

181. L. Panzella, A. Pezzella, A. Napolitano, M. d'Ischia "The first 5,6-dihydroxyindole tetramer by oxidation of 5,5',6,6'-tetrahydroxy-2,4'-biindolyl and an unexpected issue of positional reactivity en route to eumelanin-related polymers" Org. Lett., 72 (2007), 9225–9230.

182. K.B. Stark, J.M. Gallas, G.W. Zajac, M. Eisner, J.T. Golab "Spectroscopic study and simulation from recent structural models for eumelanin: I. monomer, dimers" J. Phys. Chem. B, 107 (2003), 3061-3067.

183. A. Pezzella, D. Vogna, G. Prota "Synthesis of optically active tetrameric melanin intermediates by oxidation of the melanogenic precursor 5,6-dihydroxyindole-2-carboxylic acid under biomimetic conditions" Tetrahedron Asymmetry, 14 (2003), 1133–1140.

184. A. Pezzella, L. Panzella, O. Crescenzi, A. Napolitano, S. Navaratnam, R. Edge, E.J. Land, V. Barone, M. d'Ischia "Short-lived quinonoid species from 5,6-dihydroxyindole dimers en route to eumelanin polymers: integrated chemical, pulse radiolytic, and quantum mechanical investigation" J. Am. Chem. Soc., 128 (2006), 15490–15498.
185. A. Pezzella, L. Panzella, O. Crescenzi, A. Napolitano, S. Navaratnam, R. Edge, E.J. Land, V. Barone, M. d'Ischia "Lack of visible chromophore development in the pulse radiolysis oxidation of 5,6-dihydroxyindole-2-carboxylic acid oligomers: DFT investigation and implications for eumelanin absorption properties" J. Org. Chem., 74 (2009), 3727–3734.
186. C.T. Chen, C. Chuang, J. Cao, V. Ball, D. Ruch, M.J. Buehler "Excitonic effects from geometric order and disorder explain broadband optical absorption in eumelanin" Nat. Commun., 5 (2014), 3859.
187. R. Micillo, L. Panzella, M. Iacomino, G. Prampolini, I. Cacelli, A. Ferretti, O. Crescenzi, K. Koike, A. Napolitano, M. d'Ischia "Eumelanin broadband absorption develops from aggregation-modulated chromophore interactions under structural and redox control" Sci. Rep., 7 (2017), 41532.
188. G. Prota "The role of peroxidase in melanogenesis revisited" Pigment cell Res. Suppl 2, 189 (1992), 25-31.
189. C. Olivares, F. Solano "New insights into the active site structure and catalytic mechanism of tyrosinase and its related proteins" Pigment Cell Melanoma Res., 22 (2009), 750-760.
190. J.D. Simon, D. Peles, K. Wakamatsu, S. Ito "Current challenges in understanding melanogenesis: bridging chemistry, biological control, morphology, and function" Pigment Cell Melanoma Res., 22 (2009), 563-579.
191. H. Hara, N. Walsh, K. Yamada, K. Jimbow "High plasma level of a eumelanin precursor, 6-hydroxy-5-methoxyindole-2-carboxylic acid as a

prognostic marker for malignant melanoma" J. Invest. Dermatol., 102 (1994), 501-505.

192. S. Memoli, A. Napolitano, M. d'Ischia, G. Misuraca, A. Palumbo, G. Prota "Diffusible melanin-related metabolites are potent inhibitors of lipid peroxidation" Biochim Biophys Acta, 1346 (1997), 61-68.
193. L. Novellino, M. d'Ischia, G. Prota "Nitric oxide-induced oxidation of 5,6-dihydroxyindole and 5,6-dihydroxyindole-2-carboxylic acid under aerobic conditions: non-enzymatic route to melanin pigments of potential relevance to skin (photo)protection" Biochim Biophys Acta, 1425 (1998), 27-35.
194. L. Novellino, A. Napolitano, G. Prota "5,6-Dihydroxyindoles in the fenton reaction: a model study of the role of melanin precursors in oxidative stress and hyperpigmentary processes" Chem Res Toxicol, 12 (1999), 985-992.
195. D.R. Bickers, M. Athar "Oxidative stress in the pathogenesis of skin disease" J. Invest. Dermatol., 126 (2006), 2565-2575.
196. M.L. Immordino, F. Dosio, L. Cattel "Stealth liposomes: review of the basic science, rationale, and clinical applications, existing and potential" Int J Nanomedicine, 1 (2006), 297-315.
197. M. Schäfer-Korting, W. Mehnert, H.C. Korting "Lipid nanoparticles for improved topical application of drugs for skin diseases" Adv Drug Deliv Rev, 59 (2007), 427-443.
198. K. Jores, W. Mehnert, M. Drechsler, H. Bunjes, C. Johann, K. Mäder "Investigations on the structure of solid lipid nanoparticles (SLN) and oil-loaded solid lipid nanoparticles by photon correlation spectroscopy, field-flow fractionation and transmission electron microscopy" J Control Release, 95 (2004), 217-227.
199. Z. Zhang, Y. Wo, Y. Zhang, D. Wang, R. He, H. Chen, D. Cui "In vitro study of ethosome penetration in human skin and hypertrophic scar tissue" Nanomedicine, 8 (2012), 1026-1033.

200. Y.A. Shchipunov “Lecithin organogel: a micellar system with unique properties” Colloids Surf A Physicochem Eng Asp, 185 (2001), 541-554.
201. M. Foox, M. Zilberman “Drug delivery from gelatin-based systems” Expert Opin. Drug Deliv., 12 (2015), 1547-1563.
202. A. Sgambato, L. Cipolla, L. Russo “Bioresponsive hydrogels: chemical strategies and perspectives in tissue engineering” Gels, 2 (2016), 2, 28.
203. A.H. Nguyen, J. McKinney, T. Miller, T. Bongiorno, T.C. McDevitt “Gelatin methacrylate microspheres for controlled growth factor release” Acta Biomaterialia, 13 (2014), 101-110.
204. J.P.D. Garcia, M.-F. Hsieh, B.T. Doma, D.C. Peruelo, I.-H. Chen, H.-M. Lee “Synthesis of gelatin-γ-polyglutamic acid-based hydrogel for the in vitro controlled release of epigallocatechin gallate (EGCG) from Camellia sinensis” Polymers, 6 (2014), 39-58.
205. B. Manickam, R. Sreedharan, M. Elumalai “'Genipin' - the natural water soluble cross-linking agent and its importance in the modified drug delivery systems: an overview” Curr Drug Deliv., 11 (2014), 139-145.
206. F. Liu, J. Antoniou, Y. Li, J. Yi, W. Yokoyama, J. Ma, F. Zhong “Preparation of gelatin films incorporated with tea polyphenol nanoparticles for enhancing controlled-release antioxidant properties” J. Agric. Food Chem., 63 (2015), 3987-3995.
207. C.Y. Huang, T.C. Wu, Y.H. Hong, S.L. Hsieh, H.R. Guo, R.H. Huang “Enhancement of cell adhesion, cell growth, wound healing, and oxidative protection by gelatins extracted from extrusion-pretreated Tilapia (Oreochromis sp.) fish scale” Molecules, 23 (2018), 2406.
208. M.K. Satapathy, B. Nyambat, C.W. Chiang, C.H. Chen, P.C. Wong, P.H. Ho, P.R. Jheng, T. Burnouf, C.L. Tseng, E.Y. Chuang “A gelatin hydrogel-containing nano-organic PEI-Ppy with a photothermal responsive effect for tissue engineering applications” Molecules, 23 (2018), 1256.

209. Y. Di Iorio, M.A. Brusa, A. Feldhoff, M.A. Grela “Electron transfer from photoexcited TiO_2 to chelating alizarin molecules: reversible photochromic effect in alizarin-TiO_2 under UV irradiation” Chem Phys Chem, 10 (2009), 1077-1083.

210. L.M. Zimmermann-Dimer, D.C. Reis, C. Machado, V.G. Machado “Chromogenic anionic chemosensors based on protonated merocyanine solvatochromic dyes in trichloromethane and in trichloromethane-water biphasic system” Tetrahedron, 65 (2009), 239-248.

211. W. Sun, S. Guo, C. Hu, J. Fan, X. Peng “Recent development of chemosensors based on cyanine platforms” Chem. Rev., 116 (2016), 7768-7817.

212. C. Schwechheimer, F. Rönicke, U. Schepersb, H.-A. Wagenknecht "A new structure-activity relationship for cyanine dyes to improve photostability and fluorescence properties for live cell imaging" Chem. Sci., 9 (2018), 6557-6563.

213. L. Leone, O. Crescenzi, A. Napolitano, V. Barone, M. d'Ischia “The $\Delta^{2,2'}$-bi(2H-1,4-benzothiazine) structural motif of red hair pigments revisited: photochromism and acidichromism in a unique four-state system” Eur. J. Org. Chem., 27 (2012), 5136-5140.

214. A. Napolitano, L. Panzella, L. Leone, M. d'Ischia “Red hair benzothiazines and benzothiazoles: mutation-inspired chemistry in the quest for functionality” Acc. Chem. Res., 46 (2013), 519-528.

215. L. Leone, O. Crescenzi, R. Amorati, L. Valgimigli, A. Napolitano, V. Barone, M. d'Ischia “Red-hair-inspired chromogenic system based on a proton-switched dehydrogenative free-radical coupling” Org. Lett., 15 (2013), 4944-4947.

216. R. H. Thomson “The pigments of reddish hair and feathers” Angew. Chem. Int. Ed. Engl., 13 (1974), 305-12.

217. C. Santacroce, D. Sica, R.A. Nicolaus “Sintesi di 1,4-benzotiazine” Gazz. Chim. Ital., 98 (1968), 85-96.

218. G. Prota, F. Giordano, L. Mazzarella, C. Santacroce, D. Sica “Synthesis and stereochemistry of $\Delta^{2,2'}$-bi(2H-1,4-benzothiazine) derivatives. Crystal structures of cis- and trans- $\Delta^{2,2'}$-bi(3-p-bromophenyl)-2H-1,4-benzothiazines” J. Chem. Soc., 15 (1971), 2610.

219. L. Leone, A. Pezzella, O. Crescenzi, A. Napolitano, V. Barone, M. d'Ischia “Trichocyanines: a red-hair-inspired modular platform for dye-based one-time-pad molecular cryptography” Chemistry Open, 4 (2015), 370-377.

220. P.K. Feng, Q. Fernando “Stabilities of divalent metal complexes of 4-hydroxybenzothiazole” J. Org. Chem., 82 (1960), 2115.

221. S. Ito, G. Prota “A facile one-step synthesis of cysteinyldopas using mushroom tyrosinase” Experientia, 33 (1977), 1118–1119.

222. Y. Miyamura, S.G. Coelho, R. Wolber, S.A. Miller, K. Wakamatsu, B.Z. Zmudzka, S. Ito, C. Smuda, T. Passeron, W. Choi, J. Batzer, Y. Yamaguchi, J.Z. Beer, V.J. Hearing “Regulation of human skin pigmentation and responses to ultraviolet radiation” Pigment Cell Res., 20 (2007), 2–13.

223. C. M. Olsen, H.J. Carroll, D.C. Whiteman “Estimating the attributable fraction for melanoma: a meta-analysis of pigmentary characteristics and freckling” Int. J. Cancer, 127 (2010), 2430–2445.

224. T. Sarna, I.A. Menon, R.C. Sealy “Photosensitization of melanins: a comparative study” Photochem. Photobiol., 42 (1985), 529–532.

225. A.M. Morgan, J. Lo, D.E. Fisher “How does pheomelanin synthesis contribute to melanomagenesis? Two distinct mechanisms could explain the carcinogenicity of pheomelanin synthesis” Bioessays, 35 (2013), 672–676.

226. L. Panzella, L. Leone, G. Greco, G. Vitiello, G. D'Errico, A. Napolitano, M. d'Ischia “Red human hair pheomelanin is a potent pro-oxidant mediating UV-independent contributory mechanisms of melanomagenesis” Pigment Cell Melanoma Res. 27 (2014), 244–252.

227. P.A. Kilmartin, C.F. Hsu “Characterisation of polyphenols in green, oolong, and black teas, and in coffee, using cyclic voltammetry” Food Chem., 82(2003), 501−512.
228. R. Prehn, J. Gonzalo-Ruiz, M. Cortina-Puig “Electrochemical detection of polyphenolic compounds in foods and beverages” Curr. Anal. Chem., 8(2012), 472−484.
229. F.T.G. van den Brink, L. Buter, M. Odijk, W. Olthuis, U. Karst, A. van den Berg “Mass spectrometric detection of short-lived drug metabolites generated in an electrochemical microfluidic chip” Anal. Chem. 87 (2015), 1527−1535.
230. M.L. Lavaggi, M. Nieves, M. Cabrera, C. Olea-Azar, A.L. de Cerain, A. Monge, H. Cerecetto, M. Gonzalez “Structural modifications on the phenazine N,N′-dioxide-scaffold looking for new selective hypoxic cytotoxins” Eur. J. Med. Chem., 45 (2010), 5362−5369.
231. E. Zamir, P.I.H. Bastiaens “Reverse engineering intracellular biochemical networks” Nat. Chem. Biol., 4 (2008), 643–647.
232. G. Tarabella, A. Pezzella, A. Romeo, P. D'Angelo, N. Coppedè, M. Calicchio, M. d'Ischia, R. Mosca, S. Iannotta “Irreversible evolution of eumelanin redox states detected by an organic electrochemical transistor: en route to bioelectronics and biosensing” J. Mater. Chem. B, 1(2013), 3843–3849.
233. E. Kim, L. Panzella, R. Micillo, W.E. Bentley, A. Napolitano, G.F. Payne “Reverse engineering applied to red human hair pheomelanin reveals redox-buffering as a pro-oxidant mechanism” Sci Rep., 5 (2015), 18447.
234. E. Kim, Y. Liu, W.T. Leverage, J.J. Yin, I.M. White, W.E. Bentley, G.F. Payne “Context-dependent redox properties of natural phenolic materials” Biomacromolecules, 15 (2014), 1653−1662.

235. R.L. Schroeder, K.L. Double, J.P. Gerber “Using Sepia melanin as a PD model to describe the binding characteristics of neuromelanin − a critical review. J. Chem. Neuroanat., 64(2015), 20−32.
236. S. Ito, K. Wakamatsu “Chemical degradation of melanins: application to identification of dopamine-melanin” Pigment Cell Res., 11 (1998), 120-126.
237. G. Greco, L. Panzella, G. Gentile, M.E. Errico, C. Carfagna, A., Napolitano, M. d'Ischia “A melanin-inspired pro-oxidant system for dopa(mine) polymerization: mimicking the natural casing process” Chem Commun, 47 (2011), 10308-10310.
238. Y. Liu, L. Hong, V.R. Kempf, K. Wakamatsu, S. Ito, J.D. Simon “Ion-exchange and adsorption of Fe(III) by Sepia Melanin” Pigment Cell Res., 17(2004), 262−269.
239. S. Ito “Encapsulation of a reactive core in neuromelanin” Proc. Natl. Acad. Sci. U. S. A., 103(2006), 14647−14648.
240. W.D. Bush, J. Garguilo, F.A. Zucca, A. Albertini, L. Zecca, G.S. Edwards, R.J. Nemanich, J.D. Simon “The surface oxidation potential of human neuromelanin reveals a spherical architecture with a pheomelanin core and a eumelanin surface” Proc. Natl. Acad. Sci. U. S. A. 103 (2006), 14785−14789.
241. A. Bertolini, A. Ferrari, A. Ottani, S. Guerzoni, R. Tacchi, S. Leone “Paracetamol: new vistas of an old drug” CNS Drug Rev., 12 (2006), 250−275.
242. C.I. Ghanem, M.J. Perez, J.E. Manautou, A.D. Mottino “Acetaminophen from liver to brain: new insights into drug pharmacological action and toxicity” Pharmacol. Res., 109 (2016), 119−131.
243. W.-X. Zhao, J.-H. Zhang, J.-B. Cao, W. Wang, D.-X. Wang, X.-Y. Zhang, J. Yu, Y.-Y. Zhang, Y.-Z. Zhang, W.-D. Mi “Acetaminophen attenuates lipopolysaccharide-induced cognitive impairment through antioxidant activity” J. Neuroinflammation, 14 (2017), 17.

244. A. Crozier, I. B. Jaganath, M. N. Clifford “Dietary phenolics: chemistry, bioavailability and effects on health” Nat. Prod. Rep., 26 (2009), 1001 – 1043.
245. D. Treutter “Significance of flavonoids in plant resistance: a review” Environ. Chem. Lett., 4 (2006), 147-157.
246. G.F. Payne, P.B. Smith “Renewable and sustainable polymers” Eds. ACS Symposium Series American Chemical Society: Washington, DC, 1063 (2011).
247. H.A. Meylemans, B.G. Harvey, J.T. Reams, A.J. Guenthner, L.R. Cambrea, T.J. Groshens, L.C. Baldwin, M.D. Garrison, J.M. Mabry “Synthesis, characterization, and cure chemistry of renewable bis(cyanate) esters derived from 2-methoxy-4-methylphenol” Biomacromolecules, 14 (2013), 771–780.
248. J. Shin, Y. Lee, W.B. Tolman, M.A. Hillmyer “Thermoplastic elastomers derived from menthide and tulipalin A” Biomacromolecules, 13 (2012), 3833–3840.
249. X. Li, P. Gao, J. Tan, K. Xiong, M.F. Maitz, C. Pan, H. Wu, Y. Chen, Z. Yang, N. Huang “Assembly of metal-phenolic/catecholamine networks for synergistically anti-inflammatory, antimicrobial, and anticoagulant coatings” ACS App. Mater. Interfaces, 10 (2018), 40844-40853.
250. J. Ciurana, C.A. Rodríguez “Trends in nanomaterials and processing for drug delivery of polyphenols in the treatment of cancer and other therapies” Curr. Drug Targets, 18 (2017), 135–146.
251. V. Ambrogi, L. Panzella, P. Persico, P. Cerruti, C.A. Lonz, C. Carfagna, L. Verotta, E. Caneva, A. Napolitano, M. D’Ischia “An antioxidant bioinspired phenolic polymer for efficient stabilization of polyethylene” Biomacromolecules, 15 (2014), 302–310.
252. K. Zheng, H. Tang, Q. Chen, L. Zhang, Y. Wu, Y. Cui “Enzymatic synthesis of a polymeric antioxidant for efficient stabilization of polypropylene” Polym. Degrad. Stab., 112 (2015), 27–34.

253. C. Colín-Chávez, H. Soto-Valdez, E. Peralta, J. Lizardi-Mendoza, R.R. Balandrán-Quintana "Fabrication and properties of antioxidant polyethylene-based films containing marigold (Tagetes erecta) extract and application on soybean oil stability" Packag. Technol. Sci., 26 (2012), 267–280.
254. M.S. Kamath, S.S.S.J. Ahmed, M. Dhanasekaran, S.W. Santosh "Polycaprolactone scaffold engineered for sustained release of resveratrol: therapeutic enhancement in bone tissue engineering" Int. J. Nanomedicine, 9 (2014), 183–195.
255. S.D. Sommerfeld, Z. Zhang, M.C. Costache, S.L. Vega, J. Kohn "Enzymatic surface erosion of high tensile strength polycarbonates based on natural phenols" Biomacromolecules, 15 (2014), 830–836.
256. D. Monti, G. Ottolina, G. Carrea and S. Riva "Redox reactions catalyzed by isolated enzymes" Chem. Rev., 111 (2011), 4111–4140.
257. T.S. Sileika, D.G. Barrett, R. Zhang, K.H.A. Lau, P.B. Messersmith "Colorless multifunctional coatings inspired by polyphenols found in tea, chocolate, and wine" Angew. Chem., Int. Ed. 52 (2013), 10766−10770.
258. M.N. Nadagouda, R.S. Varma "Green synthesis of silver and palladium nanoparticles at room temperature using coffee and tea extract" Green Chem., 10 (2008), 859−862.
259. J.A. Ross, C.M. Kasum "Dietary flavonoids: bioavailability, metabolic effects, and safety" Annu. Rev. Nutr. 22 (2002), 19−34.
260. H. Wu, C. Wu, Q. He, X. Liao, B. Shi "Collagen fiber with surface-grafted polyphenol as a novel support for Pd (0) nanoparticles: synthesis, characterization and catalytic application" Mater. Sci. Eng. C, 30 (2010), 770−776.
261. S. Antenucci, L. Panzella, H. Farina, M.A. Ortenzi, E. Caneva, S. Martinotti, E. Ranzato, B. Burlando, M. D'Ischia, A. Napolitano, L. Verotta "Powering

tyrosol antioxidant capacity and osteogenic activity by biocatalytic polymerization" L. RSC Adv., 6 (2015), 2993–3002.

262. K. Zheng, L. Zhang, Y. Gao, Y. Wu, W. Zhao, Y. Cui "Enzymatic oxidative polymerization of pyrogallic acid for preparation of hindered phenol antioxidant" J. Appl. Polym. Sci., 132 (2015), 41591.

263. L. Panzella, A. Napolitano "Natural phenol polymers: recent advances in food and health applications" Antioxidants, 6 (2017), E30.

264. C. Liégeois, G. Lermusieau S. Collin "Measuring antioxidant efficiency of wort, malt, and hops against the 2,2'-azobis(2-amidinopropane) dihydrochloride-induced oxidation of an aqueous dispersion of linoleic acid" J. Agric. Food Chem., 48 (2000), 1129–1134.

265. L. Marcocci, J. J. Maguire, M.T. Droy-Lefaix, L. Packer "The nitric oxide-scavenging properties of Ginkgo biloba extract EGb 761" Biochem.Biophys. Res. Commun., 201 (1994), 748–755.

266. L. Binet, D. Gourier, S. Derenne, F. Robert "Heterogeneous distribution of paramagnetic radicals in insoluble organic matter from the Orgueil and Murchison meteorites" Geochim. Cosmochim.Acta, 66 (2002), 4177–4186.

267. S. Bulotta , M. Celano , S.M. Lepore , T. Montalcini , A. Pujia, D. Russo "Beneficial effects of the olive oil phenolic components oleuropein and hydroxytyrosol: focus on protection against cardiovascular and metabolic diseases" J. Transl. Med., 12 (2014), 219.

268. A. Cárdeno, M. Sánchez-Hidalgo, C. Alarcón-de-la-Lastra "An up-date of olive oil phenols in inflammation and cancer: molecular mechanisms and clinical implications" Curr. Med. Chem., 20 (2013), 4758 —4776.

269. J.P. De La Cruz, M.I. Ruiz-Moreno, A. Guerrero, J.J. Reyes, A. Benitez-Guerrero, J.L. Espartero, J.A. González-Correa "Differences in the neuroprotective effect of orally administered virgin olive oil (Olea europaea) polyphenols tyrosol and hydroxytyrosol" Rats. J. Agric. Food Chem., 63 (2015), 5957-5963.

270. R. Fabiani “Anti-cancer properties of olive oil secoiridoid phenols: a systematic review of in vivo studies” Food & Function, 7 (2016), 4145–4159.
271. E. Bigagli, L. Cinci, S. Paccosi, A. Parenti, M. D’Ambrosio C. Luceri “Nutritionally relevant concentrations of resveratrol and hydroxytyrosol mitigate oxidative burst of human granulocytes and monocytes and the production of pro-inflammatory mediators in LPS-stimulated RAW 264.7 macrophages” International Immunopharmacology, 43 (2017), 147–155.
272. I. Medina, M.T. Satue-Gracia, J.B. German, E.N. Frankel “Comparison of natural polyphenol antioxidants from extra virgin olive oil with synthetic antioxidants in tuna lipids during thermal oxidation” J. Agric. Food Chem., 47 (1999), 4873−4879.
273. A. Napolitano, M. De Lucia, L. Panzella, M. d’Ischia “The chemistry of tyrosol and hydroxytyrosol: implications for oxidative stress” in Olives and Olive Oil In Health and Disease Prevention, Preedy, V. R., and Watson, R. R., Eds., Academic Press, Oxford, (2010), 1225-1232.
274. A. Napolitano, L. Panzella, M. Savarese, R. Sacchi, I. Giudicianni, L. Paolillo, M. d'Ischia “Acid-induced structural modifications of unsaturated fatty acids and phenolic olive oil constituents by nitrite ions: a chemical assessment” Chemical Research in Toxicology, 17 (2004), 1329–1337.
275. C. Manna, L. Tagliafierro, I. Scala, B. Granese, G. Andria, V. Zappia “The role of iron toxicity in oxidative stress-induced cellular degeneration in down syndrome: protective effects of phenolic antioxidants” Curr. Nutr. Food Sci., 8 (2012), 206–212.
276. R. de la Puerta, M.E. Martinez Dominguez, V. Ruiz-Gutierrez, J.A. Flavill, R.S. Hoult “Effects of virgin olive oil phenolics on scavenging of reactive nitrogen species and upon nitrergic neurotransmission” Life Sci., 69 (2001), 1213−1222.

277. M. Deiana, O.I. Aruoma, M.L. Bianchi, J.P. Spencer, H. Kaur, B. Haliwell, R. Aeschbach, S. Banni, M.A. Dessí, F.P. Corongui "Inhibition of peroxynitrite dependent DNA base modification and tyrosine nitration by the extra virgin olive oil-derived antioxidant hydroxytyrosol" Free Radic. Biol. Med., 26 (1999), 762-769.
278. Z. Liu, L. Sun, L. Zhu, X. Jia, X. Li, H. Jia, Y. Wang, P. Weber, J. Long, J. Liu "Hydroxytyrosol protects retinal pigment epithelial cells from acrolein-induced oxidative stress and mitochondrial dysfunction" Journal of Neurochemistry, 103 (2007), 2690–2700.
279. X. Zhang, J. Cao, L. Jiang, C. Geng, L. Zhong "Protective effect of hydroxytyrosol against acrylamide-induced cytotoxicity and DNA damage in HepG2 cells" Mutation Research- Fundamental and Molecular Mechanisms of Mutagenesis, 664 (2009), 64–68.
280. Y.Y. Lee, C. Crauste, H. Wang, H.H. Leung, J. Vercauteren, J.M. Galano, C. Oger, T. Durand, J.M. Wan, J.C. Lee "Extra virgin olive oil reduced polyunsaturated fatty acid and cholesterol oxidation in rodent liver: is this accounted for hydroxytyrosol-fatty acid conjugation?" Chemical Research in Toxicology, 29 (2016), 1689–1698.
281. J. Rooney "Aplastic anemia, membranous nephropathy and mercury" Indian Journal of Nephrology, 23 (2013), 467–468.
282. G. I. Harisa, A. D. Mariee, O. M. Abo-Salem, S. M. Attiaa "Erythrocyte nitric oxide synthase as a surrogate marker for mercury-induced vascular damage: the modulatory effects of naringin" Environmental Toxicology, 29 (2014), 1314–1322.
283. J.K. Virtanen, T.H. Rissanen, S. Voutilainen, T.-P. Tuomainen "Mercury as a risk factor for cardiovascular diseases" The Journal of Nutritional Biochemistry, 18 (2007), 75–85.
284. C.O.R. Okpala, G. Sardo, S. Vitale, G. Bono, A. Arukwe "Hazardous properties and toxicological update of mercury: from fish food to human

health safety perspective" Critical Reviews in Food Science and Nutrition, 58 (2018), 1986-2001.

285. K. Sundseth, J.M. Pacyna, E.G. Pacyna, N. Pirrone, R. J. Thorne "Global sources and pathways of mercury in the context of human health" International Journal of Environmental Research and Public Health, 14 (2017), 481.

286. V. Branco, S. Caito, M. Farina, J. Teixeira da Rocha, M. Aschner, C. Carvalho "Biomarkers of mercury toxicity: past, present, and future trends" Journal of Toxicology and Environmental Health Part B, 20 (2017), 119–154.

287. S. Miller, S. Pallan, A.S. Gangji, D. Lukic, C.M. Clase "Mercury-associated nephrotic syndrome: a case report and systematic review of the literature" American Journal of Kidney Diseases, 62 (2013), 135–138.

288. A. Carocci, N. Rovito, M.S. Sinicropi, G. Genchi "Mercury toxicity and neurodegenerative effects" Reviews of Environmental Contamination and Toxicology, 229 (2014), 1–18.

289. M. Chin-Chan, J. Navarro-Yepes, B. Quintanilla-Vega "Environmental pollutants as risk factors for neurodegenerative disorders: alzheimer and parkinson diseases" Frontiers in Cellular Neuroscience, 9 (2015), 124.

290. Z. Chen, X. Wu, H. Luo, L. Zhao, X. Ji, X. Qiao, Y. Jin, W. Liu "Acute exposure of mercury chloride stimulates the tissue regeneration program and reactive oxygen species production in the Drosophila midgut" Environmental Toxicology and Pharmacology, 41 (2016), 32–38.

291. H. Ghizoni, V. de Souza, M.R. Straliotto, A.F. de Bem, M. Farina, M.A. Hort "Superoxide anion generation and oxidative stress in methylmercury-induced endothelial toxicity in vitro" Toxicology in Vitro, 38 (2017), 19–26.

292. J.P.K. Rooney "The role of thiols, dithiols, nutritional factors and interacting ligands in the toxicology of mercury" Toxicology, 234 (2007), 145–156.

293. L.E. Hernández, J. Sobrino-Plata, M.B. Montero-Palmero, S. Carrasco-Gil, M.L. Flores-Cáceres, C. Ortega-Villasante, C. Escobar "Contribution of glutathione to the control of cellular redox homeostasis under toxic metal and metalloid stress" Journal of Experimental Botany, 66 (2015), 2901–2911.
294. Y. Elseady, E. Zahran "Ameliorating effect of β-carotene on antioxidant response and hematological parameters of mercuric chloride toxicity in Nile tilapia (Oreochromis niloticus)" Fish Physiology and Biochemistry, 39 (2013), 1031–1041.
295. Y. Deng, Z. Xu, W. Liu, H. Yang, B. Xu, Y. Wei "Effects of lycopene and proanthocyanidins on hepatotoxicity induced by mercuric chloride in rats" Biological Trace Element Research, 146 (2012), 213–223.
296. W. R. García-Niño, J. Pedraza-Chaverrí "Protective effect of curcumin against heavy metals-induced liver damage" Food and Chemical Toxicology, 69 (2014), 182–201.
297. Y.J. Shin, J.J. Kim, Y.J. Kim, W.H. Kim, E.Y. Park, I.Y. Kim, H.-S. Shin, K.S. Kim, E.-K. Lee, K.H. Chung, B.M. Lee, H.S. Kim "Protective effects of quercetin against $HgCl_2$-induced nephrotoxicity in sprague-dawley rats" Journal of Medicinal Food, 18 (2015), 3242.
298. L. Tagliafierro, A. Officioso, S. Sorbo, A. Basile, C. Manna "The protective role of olive oil hydroxytyrosol against oxidative alterations induced by mercury in human erythrocytes" Food and Chemical Toxicology, 82 (2015), 59–63.
299. A. Officioso, K. Alzoubi, F. Lang, C. Manna "Hydroxytyrosol inhibits phosphatidylserine exposure and suicidal death induced by mercury in human erythrocytes: possible involvement of the glutathione pathway" Food and Chemical Toxicology, 89 (2016), 47–53.
300. V. Mohan, S. Das, S.B.S. Rao "Hydroxytyrosol, a dietary phenolic compound forestalls the toxic effects of methylmercury-induced toxicity in

IMR-32 human neuroblastoma cells" Environmental Toxicology, 31 (2016), 1264–1275.

301. R. Bernini, E. Mincione, M. Barontini, F. Crisante "Convenient synthesis of hydroxytyrosol and its lipophilic derivatives from tyrosol or homovanillyl alcohol" J. Agric. Food Chem., 56 (2008), 8897−8904.
302. S. Grasso, L. Siracusa, C. Spatafora, M. Renis, C. Tringali "Hydroxytyrosol lipophilic analogues: enzymatic synthesis, radical scavenging activity and DNA oxidative damage protection" Bioorg. Chem., 35 (2007), 137−152.
303. R. Bernini, F. Crisante, M. Barontini, D. Tofani, V. Balducci "Synthesis and structure/antioxidant activity relationship of novel catecholic antioxidants structurally analogues to hydroxytyrosol and its lipophilic esters" J. Agric. Food Chem., 60 (2012), 7408−7416.
304. R. Amorati, L. Valgimigli, L. Panzella, A. Napolitano, M. d'Ischia "5-S-lipoylhydroxytyrosol, a multidefense antioxidant featuring a solvent-tunable peroxyl radical-scavenging 3-thio-1,2-dihydroxybenzene motif" Journal of Organic Chemistry, 78 (2013), 9857–9864.
305. L. Panzella, L. Verotta, L. Goya, S. Ramos, M.A. Martín, L. Bravo, A. Napolitano, M. d'Ischia "Synthesis and bioactivity profile of 5-S-lipoylhydroxytyrosol-based multidefense antioxidants with a sizeable (poly)sulfide chain" Journal of Agricultural and Food Chemistry, 61 (2013), 1710–1717.
306. H.A. Guglielmone, A.M. Agnese, S.C. Núñez Montoya, J.L. Cabrera "Inhibitory effects of sulphated flavonoids isolated from Flaveria bidentis on platelet aggregation" Thromb. Res., 115 (2005), 495-502.
307. H.-W. Lin, M.-X- Sun, Y.-H. Wang, L.-M. Yang, Y.-R. Yang, N. Huang, L.-J. Xuan, Y.-M. Xu, D.-L. Bai, Y.-T. Zheng, K. Xiao "Anti-HIV activities of the compounds isolated from polygonum cuspidatum and polygonum multiflorum" Planta Med., 76 (2010), 889-892.

308. D.C. Rowley, M.S. Hansen, D. Rhodes, C.A. Sotriffer, H. Ni, J.A. McCammon, F.D. Bushman, W. Fenical "Thalassiolins A-C: new marine-derived inhibitors of HIV cDNA integrase" Bioorg. Med. Chem., 10 (2002), 3619-3625.

309. S.-H. Fang, Y.-C. Hou, W.-C. Chang, S.-L. Hsiu, P.-D.L. Chao, B.-L. Chiang "Morin sulfates/glucuronides exert anti-inflammatory activity on activated macrophages and decreased the incidence of septic shock" Life Sci., 74 (2003), 743-756.

310. S. de Pascual-Teresa, K.L. Johnston, M.S. DuPont, K.A. O'Leary, P.W. Needs, L.M. Morgan, M.N. Clifford, Y. Bao, G.J. Williamson "Quercetin metabolites downregulate cyclooxygenase-2 transcription in human lymphocytes ex vivo but not in vivo" J. Nutr., 134 (2004), 552-557.

311. C.-L. Hsieh, P.-D.L. Chao, S.-H. Fang "Morin sulphates/glucuronides enhance macrophage function in microgravity culture system" Eur. J. Clin. Invest., 35 (2005), 591-596.

312. H. Yang, P. Protiva, B. Cui, C. Ma, S. Baggett, V. Hequet, S. Mori, I.B. Weinstein, E.J. Kennelly "New bioactive polyphenols from Theobroma grandiflorum" J. Nat. Prod., 66 (2003), 1501-1504.

313. S. Takamatsu, A.M. Galal, S.A. Ross, D. Ferreira, M.A. ElSohly, A.-R.S. Ibrahim, F.S. El-Feraly "Antioxidant effect of flavonoids on DCF production in HL-60 cells" Phyther. Res., 17 (2003), 963-966.

314. H.A. Guglielmone, A.M. Agnese, S.C. Núñez Montoya, J.L. Cabrera "Anticoagulant effect and action mechanism of sulphated flavonoids from Flaveria bidentis" Thromb. Res., 105 (2002), 183-188.

315. M. Correia-da-Silva, E. Sousa, B. Duarte, F. Marques, F. Carvalho, L.M. Cunha-Ribeiro, M.M.M. Pinto “Flavonoids with an oligopolysulfated moiety: a new class of anticoagulant agents” J. Med. Chem., 54 (2011), 95-106.

316. M. Correia-da-Silva, E. Sousa, M.M.M. Pinto “Emerging sulfated flavonoids and other polyphenols as drugs: nature as an inspiration” Med. Res. Rev., 34 (2014), 223-279.
317. S.J. Paluck, T.H. Nguyen, H.D. Maynard “A heparin-mimicking block copolymer both stabilizes and increases the activity of fibroblast growth factor 2 (FGF2)” Biomacromolecules, 17 (2016), 3386-3395.
318. C. Bray, P. Gurnani, E.D.H. Mansfield, R. Peltier, S. Perrier “Sulfonated copolymers as heparin-mimicking stabilizer of fibroblast growth factor: size, architecture, and monomer distribution effects” Biomacromolecules, 20 (2019), 285-293.
319. S.T. Olson, B. Richard, G. Izaguirre, S. Schedin-Weiss, P.G.W. Gettins “Molecular mechanisms of antithrombin-heparin regulation of blood clotting proteinases. a paradigm for understanding proteinase regulation by serpin family protein proteinase inhibitors” Biochimie, 92 (2010), 1587–1596.
320. M. Guerrini, P.A.J. Mourier, G. Torri, C. Viskov “Antithrombin-binding oligosaccharides: structural diversities in a unique function?” Glycoconj J., 31 (2014), 409–416.
321. B.H. Monien, B.L. Henry, A. Raghuraman, M. Hindle, U.R. Desai “Novel chemo-enzymatic oligomers of cinnamic acids as direct and indirect inhibitors of coagulation proteinases” Bioorg. Med. Chem., 14 (2006), 7988–7998.
322. B.L. Henry, B.H. Monien, P.E. Bock, U.R. Desai “A novel allosteric pathway of thrombin inhibition: Exosite II mediated potent inhibition of thrombin by chemo-enzymatic, sulfated dehydropolymers of 4-hydroxycinnamic acids” J. Biol. Chem., 282 (2007), 31891–31899.
323. X. Lin, J. Brooks, M. Bronson, M. Ngu-Schwemlein "Evaluation of the association of mercury(II) with some dicysteinyl tripeptides" Bioorg. Chem., 44 (2012), 8-18.

324. M. Farid, H. Khan, H. Khan, R. Z. Paracha, G.M. Khan "Effect of mercuric chloride on glutathione (GSH) level in plasma and cytosolic fraction of human blood" J. J. Pharm. Science, 2 (2008), 22-31.

325. D. Vogna, A. Pezzella, L. Panzella, A. Napolitano, M. d'Ischia "Oxidative chemistry of hydroxytyrosol: isolation and characterisation of novel methanooxocinobenzodioxinone derivatives" Tetrahedron Lett., 44 (2003), 8289-8292.

326. M. De Lucia, L. Panzella, A. Pezzella, A. Napolitano, M. d'Ischia "Plant catechols and their S-glutathionyl conjugates as antinitrosating agents: expedient synthesis and remarkable potency of 5-S-glutathionylpiceatannol" Chem. Res.Toxicol., 21 (2008), 2407-2413.

327. E. Fragopoulou, T. Nomikos, H.C. Karantonis, C. Apostolakis, E. Pliakis, M. Samiotaki, G. Panayotou, S. Antonopoulou "Biological activity of acetylated phenolic compounds" J. Agric. Food Chem., 55 (2007), 80-89.

328. G.T. Gunnarsson, U.R. Desai "Exploring new non-sugar sulfated molecules as activators of antithrombin" Bioorganic Med. Chem. Lett., 13 (2003), 679-683.

329. J.J. van den Berg, J.A. Op den Kamp, B.H. Lubin, B. Roelofsen, F.A. Kuypers "Kinetics and site specificity of hydroperoxide-induced oxidative damage in red blood cells" Free Radicical Biology & Medicine, 12 (1992), 487-98.